NKS-410
ISBN 978-87-7893-499-4

Scenarios and Phenomena Affecting Risk of Containment Failure and Release Characteristics

Pavel Kudinov[1]
Sergey Galushin[1]
Dmitry Grishchenko[1]
Sergey Yakush[1]
Anders Riber Marklund[2]
Ola Bäckström[2]

[1]Division of Nuclear Power Safety (NPS)
Royal Institute of Technology (KTH)
Sweden

[2]Lloyd's Register Consulting – Energy AB
Sweden

October 2018

Abstract

The report summarizes results of the NKS-SPARC project. The ROAAM+ framework addresses accident progression from initial plant damage states to ex-vessel melt-coolant interactions and debris coolability. Detailed mechanistic full models (FM) have been developed. A set of computationally efficient surrogate models (SM) has been developed using the databases of FM solutions. Uncertainty in the containment failure probability has been quantified according. An approach has been developed and demonstrated for using obtained in ROPAAM+ data on the failure probability for different combinations of scenario parameters in a large scale PSA model. Results of the pilot study show clear benefits for PSA improvement in more realistic understanding and modeling of the risks. Main findings of the analysis of effectiveness of SAM strategy in Nordic BWRs using ROAAM+ framework and main results are presented using failure domain maps. The project outcomes enhance completeness and consistency of safety analysis and modelling methods for level 2 PSA; presentation of results in level 2 PSA, and related risk criteria.

Key words

ROAAM+, IDPSA, PSA, DSA, BWR, Severe accident, MELCOR, core degradation, steam explosion, debris coolability.

NKS-410
ISBN 978-87-7893-499-4
Electronic report, October 2018
NKS Secretariat
P.O. Box 49
DK - 4000 Roskilde, Denmark
Phone +45 4677 4041
www.nks.org
e-mail nks@nks.org

Scenarios and Phenomena
Affecting Risk of Containment Failure and
Release Characteristics

NKS-R SPARC project

(Contract: NKS_R_2016_122)

Pavel Kudinov[1], Sergey Galushin[1], Dmitry Grishchenko[1], Sergey Yakush[1],
Anders Riber Marklund[2], Ola Bäckström[2]

[1]Royal Institute of Technology (KTH)
[2]Lloyd's Register Consulting – Energy AB

June 2018

Contents

Introduction

This report summarizes the results achieved within the NKS-SPARC project. The project is motivated by apparently high sensitivity of effectiveness of severe accident management (SAM) strategy to the uncertainties in physical phenomena (deterministic) and accident scenarios (stochastic). Furthermore, scenarios, including timing of events, and physical phenomena are also important sources of uncertainty for estimation of the consequences of containment failure, i.e. characteristics of the fission product release. Adequate approaches are necessary in order to address both deterministic (epistemic) and stochastic (aleatory) sources of uncertainty for a consistent assessment of the effectiveness of the accident mitigation strategy and environmental impact.

The project aims at integrating probabilistic and deterministic methods to improve risk analyses. Ideally, a risk analysis would at all point consider all challenges that can occur at that particular point in time. The process could be thought of like a dynamic event tree covering all possible failures (aleatory) and uncertainties associated with the lack of knowledge about system response (epistemic uncertainty). As much this is an appealing approach, the state space that would need to be analyzed to cover all possible scenarios and epistemic uncertainties is enormous and it will not be feasible to perform this analysis.

To make it possible to analyze the problem in a PSA framework, the problem can be viewed upon from two angles: deterministic and probabilistic viewpoints. From a deterministic analysis point of view a few simultaneous failures are considered during a sequence and the failures may be represented by “super components”. This would allow for a simplified process like the dynamic event tree. The merit would be that the approach would consider all possible effects, known and unknown, of the represented failures. To further limit the state space, consideration needs to be taken to the probability of failures, in such a way that negligible failure combinations are omitted. This approach would hence give a complete picture of the scenarios studied, and not only a few defined scenarios as in the current deterministic calculations.

From a probabilistic point of view all possible failure combinations should be covered by the PSA model. The simplifications therefore need to be regarding grouping of sequences (failure combinations that have similar effect) and simplified treatment of timing of failure combinations. The dynamic approach would give enhanced input about which scenarios that should be studied separately (where epistemic uncertainty can be quantified and eventually reduced), and also information about timing of events of importance. This information is expected especially relevant regarding PSA-L2. The enhanced information requires improvements in the PSA quantification methods to include the information in the PSA model. The project employs the two above mentioned concepts in order to provide consistent treatment of the uncertainties.

The report is organized as follows: In paragraph Chapter 1 the state of the art review of the Probabilistic, Deterministic and Integrated Safety Analyses is presented. We mainly focus on

Risk Oriented Accident Methodology (ROAAM+) as a tool for quantifying conditional threats to containment integrity, with emphasis on a Nordic type BWR.
The framework addresses all stages of the accident progression from initial plant damage states (defined in PSA level 1), through core degradation (paragraph 3.3) and vessel failure (paragraphs 3.3.5, 3.4), melt ejection mode (paragraph 3.6) to ex-vessel melt-coolant interactions (paragraph 3.8) and debris coolability, which is presented in Chapter 3, together with implementation details of ROAAM+ framework itself.

In Chapter 4 we present main findings of the analysis of effectiveness of SAM strategy in Nordic BWRs using ROAAM+ framework, considering threats of ex-vessel steam explosion and ex-vessel debris coolability. We present main results as failure domain maps in terms of the most influential parameters (based on full and surrogate model sensitivity analysis results).

In Chapter 5 we outline a conceptual approach for combined use of Probabilistic Safety Assessment (PSA) and Integrated Probabilistic Deterministic Safety Assessment (IDPSA), considering Nordic BWR severe accident issues for illustration. Methodological enhancements of PSA analysis, based on PSA and DSA integration are proposed, in particular – improved sequence definitions for PSA L2 analysis, estimation of probabilities of phenomena and consequences and improved method for integration of timing in the normally static fault tree method.

Main conclusions and suggestions for future research are presented in Chapter 6.
The main benefits of the project are:

- Better understanding of the modelling pre-requisites in current PSA (level 1 input to level 2 and level 2 design).
- New methods for combined deterministic-probabilistic analysis and
- Practical experience in using them in combination with existing PSA models.

The project outcome will allow the end users to enhance understanding, completeness and consistency of safety analysis dealing with risk analysis in:

- management of severe accident issues;
- improved reliability analysis modelling methods for level 2 PSA;
- presentation of results in level 2 PSA, and related risk criteria;
- handling of modelling uncertainties.

Not being the main focus of the proposed project, but the methodology could also be used for (for example): identify safety vulnerabilities (scenarios of safety importance which can threaten safety barriers) in active and passive safety systems.

Experiences from performed studies are summarized in the report as well as suggestions of areas which need further investigations.

Chapter 1. State of the Art Review of the Probabilistic, Deterministic and Integrated Safety Analysis.

Over the past decades, methods of Probabilistic Safety/Risk Analysis (PSA/PRA) have emerged as important tools to examine safety of complex, potentially hazardous, engineered systems such as Nuclear Power Plants (NPP). As safety requirements become increasingly stringent, requirements for quality and completeness of PSA models also increase. However further increase of the PSA models complexity is not necessarily an effective way to increase accuracy of PSA methods.

Deterministic analyses are the basis for construction of a nuclear power plant. The analyses are based on the single failure criterion and a number of conservative assumptions such as loss of offsite power and no credit for non-safety systems. The initiating events considered in the analyses are divided in different event categories, ranging from likely events (once or several times/year) down to residual risks. The more likely the event category is the higher the margins (conservatisms) against core damage must be. Thus, there are already some probabilistic considerations in the deterministic analyses.

The core damage frequency for both existing and advanced future plants is calculated to be in the range from 10^{-5}/reactor year to 10^{-8}/reactor year. However, the plant operation is sometimes hit by "improbable" (defined in PSA as very low probability) events, which can surprise, revealing a potential vulnerability in the complex plant system. We recognize that state of the art PSA methods provide numbers to quantify probability of what is already known as an "issue", but are not capable of revealing what, and to what extent, is not known (i.e. scenarios that are not prescribed in the PSA input). PSA is based on a set of assumptions about possible accident scenarios believed to be conservative. Such "decomposition" of a complex problem into a set of pre-defined sequences can be prone to false conservatism in the PSA or deterministic analysis, rendering possibility of potentially dangerous scenarios being missed or underestimated.

Standard PSA and deterministic approach has fundamental problems with resolving the dynamic nature of mutual interactions between (i) stochastic disturbances (e.g. failures of the equipment), (ii) deterministic response of the plant (i.e. transients), (iii) control logic and (iv) operator actions. Passive safety systems, severe accident and containment phenomena are examples of the cases when such dependencies of the accident progression on timing and order of events are especially important.

Since the late eighties, realistic deterministic-dynamic models, commonly referred to as best-estimate methods, received recognition as safety analysis tools. However, the best estimate codes are still used in a largely decoupled manner from the PSA. That hinders their application to risk analysis and identification of plant vulnerabilities.

In making predictions regarding the response of a system to disturbances, both the uncertainties arising from the stochastic nature of events (aleatory uncertainties) as well as those arising from lack of knowledge about the processes relevant to the system (epistemic uncertainties) have to be taken into account. Often, it is difficult to distinguish between epistemic and aleatory uncertainties [331]. Dynamic PSA methodologies allow a unified framework to account for the joint effects of both types of uncertainties simultaneously in predicting the distribution of risk associated with the system response.

Dynamic PSA methodologies can be divided into three main categories [332]: (i) continuous-time methods, (ii) discrete-time methods, and (iii) methods with graphical interfaces. While the methods with graphical interfaces are also either continuous or discrete time methods, they are listed as a separate category because the availability of a graphical interface is usually regarded as rendering them more user friendly. IDPSA tools usually employ (i) system simulation codes and models with explicit consideration of the effect of timing on the interactions between epistemic (modeling) and aleatory (scenario) uncertainties, (ii) a method for exploration of the uncertainty space. A review of the IDPSA methods for nuclear power plant applications can be found in [332, 157]. The inputs for all dynamic methodologies are:

- a time-dependent system model (such as RELAP5 [333] or MELCOR [334] codes);
- possible normal and abnormal system configurations which may need to be determined using a failure-modes-and-effects (FMAE) analysis;
- transition probabilities (or rates) among these configurations.

1.1.1 IDPSA methods and the decision making process

It was mentioned previously [336] that the readiness of a tool is difficult to determine if there are no clear criteria for success or goal for the analyses. In terms of decision making, quantification of consequences into figures of merit is necessary (i.e. to establish safety goals and success criteria).

IDPSA methods are capable of quantifying aleatory uncertainties in time dependent scenarios. It was emphasized (during the IDPSA meeting 2012 [336]) that this mostly had an effect within the context of academia whereas it did not do much for deployment into the industry. Therefore, focus must be directed towards what the decision makers need and what they regard as important.

Credibility, uncertainty quantification (robustness of decision), comprehensiveness (risk profile instead of one number) and understanding were outlined as important factors in terms of what kind of data to be provided for the decision makers. Consistency was also emphasized as important since different kinds of decisions (e.g. for industry or regulators) put different requirements on the data provided.

The Risk Oriented Accident Analysis Methodology (ROAAM) [270], [122] can be considered as an example of a decision support method. The focus of ROAAM is upon reducing the uncertainty to the extent that a defense-in-depth is considered as achieved. When the whole community of experts in a given problem area is convinced that the demonstration is effected and regarded successful the problem may be considered solved (in a robust and final way). Eventually the complete reaching of all experts is effected by publication in the technical literature, with additional iterations thereof if necessary. ROAAM provides guidelines for development of framework for bounding of epistemic (modelling) and aleatory (scenario) uncertainties in a transparent and verifiable manner that enables convergence of experts opinions on the outcome of the analysis (not necessarily on the uncertainties in the input information). ROAAM integrates risk assessment (analysis) and risk management (modifications in the design, procedures, etc.) in an effective manner in order to resolve safety issues.

1.2 Risk Orineted Accident Approach and Nordic BWR Severe Accident Management Strategy

The Risk Oriented Accident Analysis Methodology (ROAAM) [270], [122] can be considered as an example of a decision support method. The ROAAM marries probabilistic and deterministic approaches. This methodology developed by Professor Theofanous [270] has been applied to successfully resolve different severe accident issues in LWR plants, and severe accident treatments in ALWR designs e.g., [122].

The focus of ROAAM is upon reducing the uncertainty to the extent that a defense-in-depth is considered as achieved. When the whole community of experts in a given problem area is convinced that the demonstration is effected and regarded successful the problem may be considered solved (in a robust and final way). Eventually the complete reaching of all experts is effected by publication in the technical literature, with additional iterations thereof if necessary. ROAAM provides guidelines for development of framework for bounding of epistemic (modelling) and aleatory (scenario) uncertainties in a transparent and verifiable manner that enables convergence of experts' opinions on the outcome of the analysis (not necessarily on the uncertainties in the input information). ROAAM integrates risk assessment (analysis) and risk management (modifications in the design, procedures, etc.) in an effective manner in order to resolve safety issues.

When applied to the Nordic BWR plants, the tight coupling between severe accident threats (steam explosion and basemat melt-through due to debris un-coolability) and high sensitivity of the SAM effectiveness to timing of event (e.g., vessel failure) and characteristics (e.g., melt release conditions) present new challenges in decomposition, analysis and integration.

It is instructive to note that discussion of approaches to risk management regulatory framework has been initiated at US NRC [6]. Risk Management Task Force provided recommendation that NRC should implement a consistent process that includes both deterministic and probabilistic methods. It is acknowledged that Risk assessments provide valuable and realistic insights into potential exposure scenarios. In combination with other technical analyses, risk assessments can inform decisions about appropriate defense-in-depth measures.

ROAAM+ framework employs a two-level coarse-fine iterative analysis. First, fine-resolution but computationally expensive methods are used in order (i) to provide better understanding of key phenomena and their interdependencies, (ii) to identify transitions between qualitatively different regimes and failure modes, and (iii) to generate reference data. The fine-resolution codes are run independently, assuming wider possible ranges of the input parameters. Second, a set of coupled modular frameworks is developed connecting initial plant damage states with respective containment failure modes. Deterministic processes are treated using surrogate models based on the data obtained from the fine-resolution models. The surrogate models are computationally efficient and preserve the importance of scenario and timing. Systematic statistical analysis carried out with the complete frameworks helps to identify risk significant and unimportant regimes and scenarios, as well as ranges of the uncertain parameters where fine-resolution data is missing. This information is used in the next iteration of analysis with fine-resolution models, and then refinement of (i) overall structure of the frameworks, (ii) surrogate models, and (iii) their interconnections. Such iterative approach helps identify areas where additional data may significantly reduce uncertainty in the fine- and coarse-resolution methods, and increase confidence and transparency in the risk assessment results. The overall modular structure of the frameworks and the refinement process are discussed in the paper in detail [157].

1.2.1 Background: Quantitative Definition of Risk and ROAAM Basics

According to quantitative definition of risk ([123] by Kaplan and Garrick), the risk R_i associated with associated with specific scenario s_i can be characterized by its frequency f_i and consequences c_i. Consequences are obtained from predictions that are subject to epistemic uncertainty due to incomplete knowledge. The degree of uncertainty in the prediction of the future course of events can be quantified as "probability" P_i or "likelihood" of c_i. Such probability is evaluated by an expert based on the available evidences (data and experience with similar courses of action in the past). Therefore, two rational beings given the identical evidence must assess the probability identically [123]. "Frequency" is the outcome of an experiment involving repeated trials. Aleatory uncertainty is expressed in terms of frequency.

$$R_i = \{s_i, f_i, P_i(c_i)\} \tag{1-1}$$

Consequences c_i of scenario s_i can be presented as joint probability density function $\mathrm{pdf}_{C_iL_i}(L_i, C_i)$, which accounts for the epistemic uncertainty and possible dependencies between the loads (L_i) on the system in question and its capacity (C_i) to withstand such loads. Thus, failure probability P_{Fi} for scenario s_i can be evaluated as

$$P_{Fi} = P(L_i \geq C_i) = P(C_i - L_i = Z_i \leq 0) = \iint_{Z_i \leq 0} \mathrm{pdf}_{C_iL_i}(c, l)dcdl \tag{1-2}$$

or, in case when load and capacity are independent

$$P_{Fi} = P(L_i \geq C_i) = \int_{-\infty}^{\infty}\int_{-\infty}^{l\geq c} \mathrm{pdf}_{L_i}(l)\,\mathrm{pdf}_{C_i}(c)dc\,dl = \int_{-\infty}^{\infty} \mathrm{CDF}_{C_i}(l)\,\mathrm{pdf}_{L_i}(l)dl \tag{1-3}$$

where CDF_{C_i} is the cumulative probability density function for the capacity. Unacceptability of containment failure is equivalent to requirement that all P_{Fi} should be below "physically unreasonable" level P_s.

The idea of characterizing risk as a set of triplets (scenario, its frequency, and probability of consequences) was further developed and practically applied to assessment of severe accident risks in ROAAM [270]. According to ROAAM, the use of Risk for effective management and regulation of rare, high-consequence hazards requires the simultaneous (coherent) consideration of (i) safety goal, (ii) assessment methodology, and (iii) application specifics. ROAAM provides guidelines for development of frameworks for bounding the epistemic (modeling), and aleatory (scenario) uncertainties in a transparent and verifiable manner that should enable convergence of experts' opinions in the review process.

Important premise of ROAAM is that safety goals can be defined only qualitatively when epistemic uncertainty is significant. The goal should effectively communicate the idea that the perceived hazard is "physically unreasonable" under "any circumstances" leading up to it in a "physically meaningful" context. More specifically, for severe accident analysis the safety goal can be defined as: "containment failure is a physically unreasonable event for any accident sequence that is not remote and speculative" [270].

In order to achieve the transparency and verifiability, ROAAM employs its principal ingredients: (i) identification, separate treatment, and maintenance of separation (to the end results) of aleatory and epistemic uncertainties; (ii) identification and bounding/conservative treatment of uncertainties (in parameters and scenarios, respectively) that are beyond the reach of any reasonably verifiable quantification; and (iii) the use of external experts in a review, rather than in a primary quantification capacity.

Separation of epistemic and aleatory uncertainties stems from the work of Kaplan and Garrick [123]. Separate treatment of screening frequency for aleatory, and the physically unreasonable concept for epistemic uncertainties is a must for clarity and consistency of the ROAAM result.

An arbitrary scale for probability is introduced which defines a physically unreasonable process as one involving the independent combination of an end-of-spectrum with one expected to be outside but cannot be positively excluded [270]:
1/10 Behavior is within known trends but obtainable only at the edge-of-spectrum parameters.
1/100 Behavior cannot be positively excluded, but it is outside the spectrum of reason.
1/1000 Behavior is physically unreasonable and violates well-known reality. Its occurrence can be argued against positively.

The starting point of ROAAM is an interest in the "likelihood" (L_j) of different containment failure modes (hazards H_k) given a set of initial plant damage states ($\{D_j\}$)

$$L_j(H_k) = G(p_1, p_2, \dots, p_l), \quad \text{given } \{D_j\} \tag{1-4}$$

where damage states have frequency higher than selected screening frequency f_s and lower than target frequency f_t achieved as the prevention goal, that is, $f_s < f_j(D_j) < f_t$.

The approach employed in ROAAM is not to realize a defensible approximation to function G, and seeking the likelihood L_j, but to establish that it is (or can be made by appropriate decisions) low enough as to regard the hazard H_k as physically unreasonable, avoiding excess conservatism while still remaining convincing [270].

A separation must be made between the aspects of systems response that can be stated as well-posed physical problems or "causal relations", and other aspects which are subject to inherently variable behavior and called "intangibles". The structure of separation synthesis is called "probabilistic framework". Each framework refers to a particular "scenario" s_i. The art in the decomposition is to envelop the behavior through the coherent use of "intangibles" and respective "scenarios" such that it will be understandable (and scrutable). Each "causal relation" requires an in-depth and demonstrable understanding of the controlling physics; "scenarios" and "intangibles" are to fill in the gaps whenever this is not possible. Uncertainty in causal relations can be reduced. Uncertainty in intangibles can only be qualitatively approached, but it can always be bounded. The adequacy of scenarios can be determined according to the completeness of the logical structures used in deriving them. The process of integration through the probabilistic framework is effected by introducing a scale for the temporary quantification of intangibles, and the results are rendered in qualitative terms by applying this scale in reverse.

The problem is decomposed into framework and stochastic scenarios $\{s_i\}$, such that:

$$L_{ji}(H_k) < P_{ji}(H_k), \quad P_{ji}(H_k) = F(d_1, d_2, \dots, i_1, i_2, \dots) \tag{1-5}$$

where $\{d_i\}$ is a set of "deterministic" parameters, $\{i_i\}$ is a set of "intangible" parameters, $P_{ji}(H_k)$ is based on arbitrary probability scale. The goal of analysis is to show that

$$P_{ji}(H_k) < P_s \text{ given } \{D_j\} \text{ for all } \{s_i\} \tag{1-6}$$

where P_s is the "physically unreasonable" level. The above structure separates out epistemic from aleatory uncertainty which is also motivated by the distinct approaches to judge residual risk: with screening frequency for aleatory, and with physically unreasonable concept for epistemic. Any stochastic behavior not already included in the definition of the severe accident window (the plant damage states to be considered) can be taken up in the definition of scenarios and intangibles, since they would be expected to dominate the uncertainty in any case. A similar separation can be effected in this case, too, by simply finding the total probability in each frequency range, and applying the same criteria for judging the results – but now these frequencies should be combined with the respective plant damage state frequencies [270].

1.3 Nordic BWR Challenges for ROAAM Application

Severe accident management (SAM) strategy in Nordic boiling water reactors (BWRs) employs ex-vessel core debris coolability. Molten core is released form the vessel into a deep pool of water in the lower drywell. The melt is expected to fragment, quench, and form a debris bed that is coolable by natural circulation of water. Formation of non-coolable debris bed and energetic interactions between hot liquid melt and volatile coolant (steam explosion) pose credible threats to containment integrity. Conditions of melt release from the vessel determine (i) debris bed properties and thus coolability, and (ii) steam explosion energetics.

While conceptually simple, the strategy involves complex physical phenomena affected by the transient accident scenarios. The multistage path of severe accident progression and effect of the earlier stages on the later ones is another important source of complexity and uncertainty.

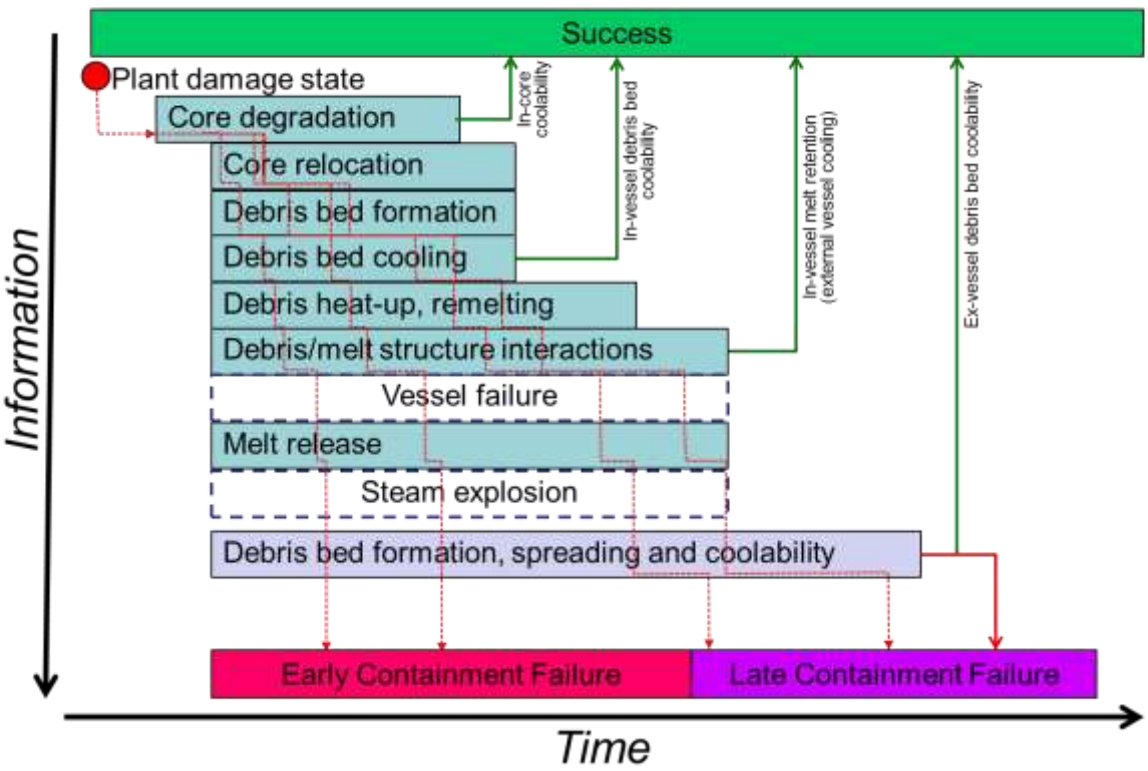

Figure 1-1: Severe accident progression in Nordic BWR.

Timing of event, with the same order of the stages, can affect accident progression. For instance, late recovery of core cooling affect core degradation and relocation processes, and thus formation of the debris bed in lower head, reheating and re-melting of multi-component corium debris, thermo-mechanical interactions between melt and vessel structures and penetrations, vessel failure, melt release mode, respective jet fragmentation in the pool, debris solidification, energetic melt-coolant interactions, two-phase flow in porous media, spreading of debris in the pool, spreading of particulate debris bed, etc. Decay heat is decreasing with time providing better chances for coolability of the debris bed if melt is released from the vessel later [310]. However, later release leads to higher temperature of the melt, which increase the risk of debris agglomeration [168], [145], [142] hindering coolability of the debris bed [316], [311] and creating a potential for an energetic steam explosion which can threaten containment integrity [92].

Interdependencies between non-coolable debris and steam explosion is another source of uncertainty. For instance, if lower drywell flooding is not activated, then steam explosion risk is eliminated, but hot corium melt will attack cable penetrations in the containment floor leading to almost immediate containment failure. If flooding is timely activated, then even a mild steam explosion might lead to degradation of debris bed cooling function, e.g. by destroying protective covers for cable penetrations in the containment floor and exposing them to hot debris, or by creating a leak of coolant from the lower drywell, or by activating filtered containment venting, releasing fraction of nitrogen which can potentially lead to drop of containment pressure well below atmospheric level, etc.

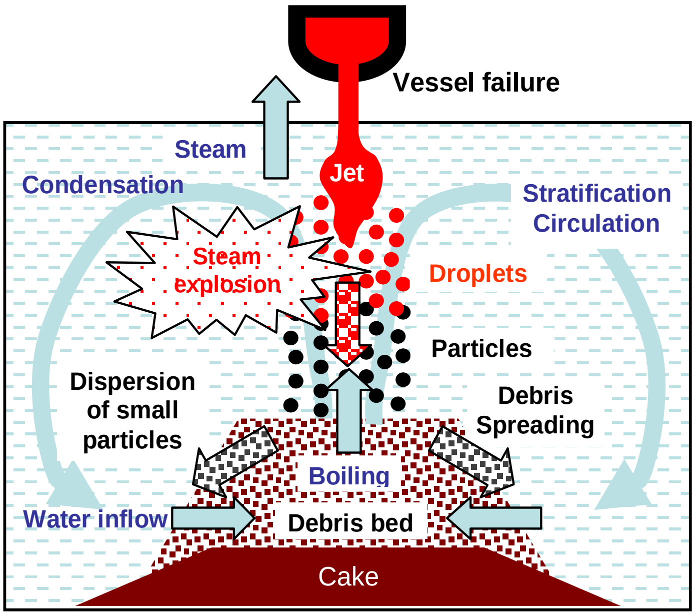

Figure 1-2: Severe accident phenomena in Nordic BWR.

Significant progress, that has been made in understanding and predicting MSWI physical phenomena during the last few decades, was not sufficient to make a firm conclusion on the robustness of the SAM strategy. Severe accident issues in Nordic BWR design are intractable for separate probabilistic or deterministic analysis due to the uncertainty stemming from interactions between (i) stochastic scenarios of time dependent accident progression, and (ii) deterministic phenomena.

Enter the Risk Oriented Accident Analysis Methodology (ROAAM) that marries probabilistic and deterministic approaches. This methodology developed by Professor Theofanous and co-workers [270], [243] has been applied to successfully resolve several severe accident issues and to develop new severe accident management strategies in different designs of light water reactors (e.g. [60]). When applied to the Nordic BWR plants, the tight coupling between severe accident threats (steam explosion and basemat melt-through due to debris un-coolability) and high sensitivity of the SAM effectiveness to timing of event (e.g., vessel failure) and characteristics (e.g., melt release conditions) present new challenges in decomposition, analysis and integration.

1.3.1 Complexity of Phenomenology and Scenarios

While ROAAM is logically sound and has been successfully applied in several practical cases to resolve severe accident issues, there are some challenges for application of ROAAM to Nordic BWR case. Typical phenomenological stages of severe accident progression in Nordic BWR are shown in Figure 1-1.

The multistage path from the initial plant damage state to the containment threats is an important source of complexity and uncertainty. Phenomena and scenarios including operator actions are tightly coupled in their mutual interactions and eventual impact on the possibility of different containment failure modes. Conditions created at the earlier stages can significantly affect configurations and problem statements at later stages. For instance, if there is no activation of lower drywell flooding, then steam explosion risk is eliminated, but hot corium melt will attack cable penetrations in the containment floor leading to almost immediate containment failure.

Timing of transition between different stages is also important. Different time-dependent trajectories of the accident scenarios with the same logical sequence of the stages can result in different outcomes. For instance, decay heat is decreasing with time providing much better chances for coolability of the debris bed if melt is released from the vessel later [310]. However, if melt is released from the vessel later, it will have higher temperature, which could increase the risk of debris agglomeration [168], [145], [142] hindering coolability of the debris bed [316], and creating a potential for an energetic steam explosion which can threaten containment integrity.

Combination of (at least) two threats (non-coolable debris and steam explosion) is another source of uncertainty. On one hand, there is a possibility that stem explosion might contribute to spreading of the debris over containment floor. On the other hand, even a mild steam explosion might lead to degradation of debris bed cooling function, e.g. by destroying protective covers for cable penetrations in the containment floor and exposing them to hot debris, or by creating a leak of coolant from the lower drywell, or by activating filtered containment venting, releasing fraction of nitrogen which can potentially lead to drop of containment pressure below atmospheric level, etc.

The major challenge for application of ROAAM to Nordic BWR is the complexity of tightly coupled transient phenomena and scenarios which limit the effectiveness of heuristic approaches in (i) problem decomposition and (ii) a priori judgment about importance and impact of coupled and time dependent phenomena and scenarios on the accident progression and outcome.

1.3.2 Decision Making Context

Conditional containment failure probability is considered in this work as an indicator of severe accident management effectiveness for Nordic BWR. It is instructive to note that different modes of failure (assumed to be equivalent to loss of containment integrity) can potentially lead to quite different consequences in terms of fission products release. At this point we consider any failure mode as unacceptable for the sake of conservatism.

The ultimate goal of classical ROAAM process [270] is to provide a scrutable process and framework for achieving convergence of experts' opinions on the question: whether containment failure is "possible" (physically unreasonable), for a given SAM and current state-of-the-art knowledge. If safety margins are large, then containment failure being physically unreasonable, can be demonstrated through consistent conservative treatment of uncertainties in risk assessment and improving necessary knowledge and data. If inherent margins are small or negative, improvement of knowledge is ineffective. Risk management (through appropriate modifications of the system e.g. safety design, SAMGs, etc.) should be undertaken in order to achieve the safety goal [270].

However, for complex systems, uncertainty can create a space for "hope" that the system is safe due to yet incompletely understood phenomena, scenarios and interactions, and thus acquiring further knowledge about the system is justified. Conservative treatment of uncertainty is not very helpful to address such "hope". Instead, the assessment should be focused on the necessity of containment failure (in other words, how unavoidable it the failure) using "optimistic" treatment of uncertainty.

The risk assessment framework should be capable of providing assessments in support for both possible decisions: (i) current strategy is sufficiently reliable (according to a "conservative" analysis); (ii) strategy is not sufficiently reliable (according to an "optimistic" analysis) and thus changes are necessary.

A difficulty arises when bounding "conservative" (or "optimistic") approaches become inadequate. E.g. if success domain is in a middle of the uncertainty space and only "optimal" combinations of the uncertain factors lead to success, while limiting values of the uncertain parameters result in failure. This is often the case when there are competing phenomena or threats, when positive or negative effect on the possibility of failure from some parameters or events changes depending on other parameters or events. For instance, in case of successful attempt of in-vessel debris cooling using control rode guide tube (CRGT) flow, melt release from the vessel can be prevented. However, if corium retention is not successful, CRGT cooling can lead to delay of vessel failure, formation of a larger melt pool with higher superheat. Melt release from the vessel with such conditions can significantly increase potential energetics of steam explosion and the risk of formation of agglomerated, non-coolable debris bed.

Using "risk informed" approach in case with large irreducible uncertainties and competing threats can be at best inconclusive. If dependencies between uncertain factors are strong, then risk quantification can be polluted with uncertainty to the point where "everything is possible". Such outcome is a clear sign that the system is complex, i.e. understanding and control of the system is beyond our reach. Changes in the system are necessary in order to make its behavior predictable with sufficient confidence.

The costs of improving the knowledge, changes the system, and consequences should be weighted in the decision making process. In order to reduce uncertainty in estimations of potential losses consequences of release have to be investigated in greater detail.

In order to address the difficulties a structured process is needed for coherent (i) development of risk assessment framework, (ii) collection of necessary data and knowledge. This process should be guided by extensive sensitivity and uncertainty analysis and eventually result in a robust and scrutable assessment of either "possibility" or "necessity" of containment failure in order to support decision making. In the next section we discuss some important aspects of development of such process for Nordic BWR SAM.

1.3.3 Connection to PSA

The work on connection between ROAAM+ to PSA is motivated by apparently high sensitivity of effectiveness of severe accident management (SAM) strategy to the uncertainties in physical phenomena (deterministic) and accident scenarios (stochastic). Furthermore, scenarios, including timing of events, and physical phenomena are also important sources of uncertainty for estimation of the consequences of containment failure, i.e. characteristics of the fission product release. Adequate approaches are necessary in order to address both deterministic (epistemic) and stochastic (aleatory) sources of uncertainty for a consistent assessment of the effectiveness of the accident mitigation strategy and environmental impact.

The project aims at integrating probabilistic and deterministic methods to improve risk analyses. Ideally, a risk analysis would at all point consider all challenges that can occur at that particular point in time. The process could be thought of like a dynamic event tree covering all possible failures (aleatory) and uncertainties associated with the lack of knowledge about system response (epistemic uncertainty). As much this is an appealing approach, the state space that would need to be analyzed to cover all possible scenarios and epistemic uncertainties is enormous and it will not be feasible to perform this analysis.

To make it possible to analyze the problem in a PSA-like framework, the problem can be viewed upon from two angles: deterministic and probabilistic viewpoints. From a deterministic analysis point of view a few simultaneous failures are considered during a sequence and the failures may be represented by "super components". This would allow for a simplified process like the dynamic event tree. The merit would be that the approach would consider all possible effects, known and unknown, of the represented failures. To further limit the state space, consideration needs to be taken to the probability of failures, in such a way that negligible failure combinations are omitted. This approach would hence give a complete picture of the scenarios studied, and not only a few defined scenarios as in the current deterministic calculations.

From a probabilistic point of view all possible failure combinations should be covered by the PSA model. The simplifications therefore need to be regarding grouping of sequences (failure combinations that have similar effect) and simplified treatment of timing of failure combinations. The dynamic approach would give enhanced input about which scenarios that should be studied separately (where epistemic uncertainty can be quantified and eventually reduced), and also information about timing of events of importance. This information is expected especially relevant regarding PSA-L2. The enhanced information requires improvements in the PSA quantification methods to include the information in the PSA model. The project employs the two above mentioned concepts in order to provide consistent treatment of the uncertainties.

The main benefits of the project are:

- Better understanding of the modelling pre-requisites in current PSA (level 1 input to level 2 and level 2 design).
- New methods for combined deterministic-probabilistic analysis and
- Practical experience in using them in combination with existing PSA models.

The project outcome will allow the end users to enhance understanding, completeness and consistency of safety analysis dealing with risk analysis in:

- management of severe accident issues;
- improved reliability analysis modelling methods for level 2 PSA;
- presentation of results in level 2 PSA, and related risk criteria;
- handling of modelling uncertainties.

Not being the main focus of the proposed project, but the methodology could also be used for (for example): identify safety vulnerabilities (scenarios of safety importance which can threaten safety barriers) in active and passive safety systems.

Experiences from performed studies are summarized in the report as well as suggestions of areas which need further investigations.

Chapter 2. Development of ROAAM+ Framework for Integration of Knowledge and Treatment of Uncertainty

It is clear that key ingredients of ROAAM such as:

- Separation of aleatory and epistemic uncertainties through
  - o Consideration of risk as a set of the triplets (scenario, its frequency, and probability of consequences),
  - o Decomposition of the problem into stochastic "scenarios" and deterministic "frameworks",
- Arbitrary scale of probability for epistemic uncertainty,
- Qualitative definition of safety goal,

are critical for consistency of assessment and transparency of review and must be preserved. However, the challenges presented by Nordic BWR SAM strategy require further development of the approach. In this section we discuss the basic ideas and examples of development of such an approach which we call ROAAM+.

The goal of the ROAAM+ approach is to provide sufficient information for a decision to:

I. Keep SAM strategy: "Possibility" of containment failure is low even with "conservative" treatment of uncertainty, thus current strategy is reliable.
II. Modify SAM strategy: "Necessity" of containment failure in the course of accident is high (i.e. "possibility" that containment doesn't fail is low) even with "optimistic" treatment of uncertainty, thus the current strategy is unreliable and changes should be considered.

In order to achieve the goal, ROAAM+ process is developed for construction and adaptive refinement of the risk assessment framework, models, and data. The process is aiming to refine the resolution of the framework in order to bound the influence of the largest contributors to the uncertainty in risk assessment.

2.1 Iterative Adaptive Refinement Process for Development of Risk Assessment Framework: Two-Level "Coarse-Fine", "Forward" and "Reverse" Analysis.

System complexity limits effectiveness of heuristic approach (based on expert judgment) to identification of the key physics and system behavior. There is a need for an iterative process for identifying and evaluating importance of different contributors to the risk. Thus at each stage of the process, a framework for risk assessment should exist, providing a means for sensitivity and uncertainty analysis of "possibility" and "necessity" of containment failure with respect to the uncertain factors. Such analysis points to the necessary improvement of the framework and data and provides assessment of potential impact of such improvements at the next iteration of the framework development or effectiveness of the system modifications.

The framework is used to carry out (i) Conservative assessment of containment failure possibility; (ii) Optimistic assessment of containment failure necessity; (iii) Sensitivity and uncertainty analysis to guide development and refinement of the risk assessment framework itself. In practice, different analysis types are implemented through consistent use of assumptions on uncertainty in (i) scenarios and (ii) ranges and probability distributions of the uncertain parameters. Sensitivity and uncertainty analysis is employed for both (i) optimal refinement of the data, knowledge and risk analysis framework, and (ii) optimization and assessment of effectiveness of potential system modifications.

Complex phenomena require adequate complexity of the models. Adequately complex “full models” (FMs) are implemented for each stage of the accident progression using multidimensional codes for severe accident, thermal hydraulics, and structural analysis. Application of such FMs in extensive sensitivity and especially uncertainty analysis is often unaffordable due to extreme computational costs and difficulties in establishing direct coupling between the codes. Therefore, we employ a two-level coarse-fine modeling approach. At the first (bottom) level we use loosely coupled fine resolution FMs and available experimental evidences in order to generate relevant data and develop understanding of key physics. Then coarse-resolution computationally efficient “surrogate models” (SMs) are developed to approximate the most important parameters of the FM solutions. The SMs provide computationally efficient approximations for the most important parameters of the FM solutions. The SMs are used at the second (top) level of the framework for sensitivity, uncertainty analysis and risk quantification. Risk quantification starts from initiating event and propagates information through the framework in what we call “forward analysis”.

When complexity is high, it is difficult to identify a priori what is more important and what is missing from our knowledge of each individual stage of the accident progression. Such information can be obtained when all stages are coupled and a connection between uncertainties at each individual stage and resulting uncertainty in containment failure probability can be established. Until such connection is established, it is not possible to assess if FMs and SMs provide sufficient resolution for all important phenomena. In fact, some of the FMs might not be available yet. In such case FMs should be designed according to the requirements which can be inferred from the results of the reverse analysis. Accuracy of the FM should be sufficiently qualified through scaling, calibration, verification, validation and uncertainty quantification process using relevant experimental data. The need for new data stems from the model validation needs. Therefore, there is a need for iterative refinement process of the FMs, SMs, experimental data and structure of the framework. Criteria for the need of refinement can be established based on consideration of the failure domain. Failure domain (FD) is a domain in the space of the uncertain parameters where probability of containment failure is larger than a “physically unreasonable” threshold. The refinement is needed when there are (i) large uncertainty in resolving the boundaries of the failure domain with existing FM and SM, and (ii) physical phenomena or scenarios not taken into account yet that can significantly change FD boundaries. Naturally, the FD identification and refinement starts from the last stages of the accident progression analysis and propagates failure domains "upstream" to the earlier stages of the accident progression. We call this process "reverse" analysis.

The two-level coarse-fine approach to development and iterative adaptive refinement of the risk assessment frameworks is summarized below:

1) *Development and refinement:* of models, frameworks and data based on the results of the forward and reverse analyses in order to reduce uncertainty in the failure probability and resolution of failure domain boundary.

Experimental evidences and fine-resolution but computationally expensive methods (FMs) are used in order to:

i. Develop hypothesis about key phenomena and provide better understanding of their possible interdependencies,
ii. Identify transitions between qualitatively different regimes and failure modes, and
iii. Generate reference databases for development calibration and verification of coarse-resolution but computationally efficient surrogate models (SMs).

FMs are run in "exploratory" mode, loosely coupled or independently from each other, assuming bounding ranges for model input parameters. Scaling analysis is employed for the experimental evidences.

2) *Forward analysis:* quantification of major contributors to the uncertainty in the failure probability at each stage of the modeling of accident progression.

A probabilistic framework is developed based on coupled SMs in order to connect the initial plant damage states with respective containment failure modes.

i. Deterministic processes are treated using the developed and verified SMs preserving importance of scenarios and timing.
ii. Sensitivity and uncertainty analysis is carried out using the framework to:
    a. Identify significant and unimportant parameters, regimes and scenarios.
    b. Quantify the risk and contribution to the overall uncertainty for the most influencing factors.

3) *Reverse analysis:* identification of failure domains and their boundaries at each stage of the modeling of accident progression.

Failure domains and their boundaries are identified in the spaces of uncertain input parameters for each SM (representing different stages of the accident progression) in order to identify the needs for improvement of:

i. Experimental data and scaling.
ii. FMs and their validation metrices.
iii. SMs, calibration and verification databases (based on FMs and experimental data), interconnections and databases of solutions.
iv. Overall structure of the problem decomposition into scenarios and frameworks.

Such iterative process is designed to develop state of the art knowledge, confidence and transparency in the risk assessment results, to the point when convergence of experts' opinion on the possibility or necessity of containment failure can be achieved. Such convergence is a stopping criterion for the refinement process.

Adaptive decomposition (into scenarios and phenomena) depends largely on the knowledge base (relevant data, code capability, etc.). Employment of the fine resolution FMs in the process of risk quantification and uncertainty reduction is justified when appropriate evidences of the models' validation are provided. Failure domain (reverse) analysis points to the domains of parameters and scenarios where evidences of detailed validation are most needed and improvement of the validation database has the largest impact on the uncertainty reduction. Proper scaling of experimental data is important for establishing consistency between modeling and experimentation in the iterative process of uncertainty reduction. In this light, a list of phenomena and corresponding experiments that can be used for validation of FMs and calibration of SMs should be provided along with the assessment of the data quality (relevance, scaling, and uncertainty). Such information is a basis for the decisions on decomposition and the needs for improvements of the evidence database.

2.2 Failure Probability

Quantification of failure probability is the ultimate goal of the analysis. Illustration of the failure probability quantification determined by forward propagation of the uncertainties through a single stage framework is illustrated in Figure 2-1.

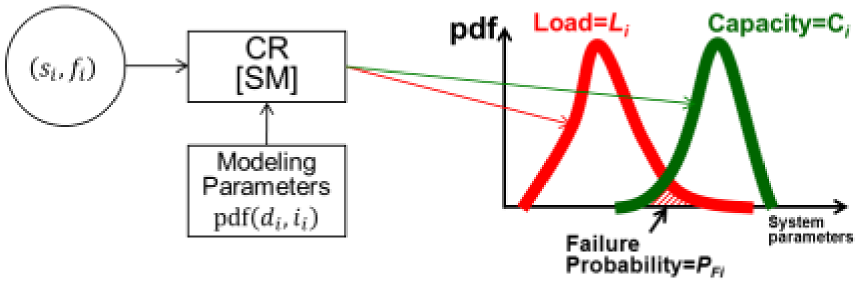

Figure 2-1: Failure probability in a single stage framework.

For each plant damage state $\{D_i\}$ there is a set of respective scenarios $\{s_{ij}\}$, are characterized by frequencies (f_{ij}). For the sake of brevity, in the future we will omit second index when referring to scenarios (s_i) and their probabilities (f_i) considering them as a whole set of all scenarios relevant to all initial damage states. Scenarios (s_i) introduce specific combinations of initial and boundary conditions for causal relationships (CR) and structure of the probabilistic framework. The CR provides "bounding" assessment of the load and the capacity which can provide optimistic and conservative estimates. If bounding assumptions in modeling approaches are not obvious "a priori", sensitivity analysis is required. A set of surrogate models (SM) is used to approximate the CR. Epistemic uncertainty in prediction of the failure probability is introduced by multidimensional probability density function $(\mathrm{pdf}(d_i, i_i))$ of intangible (i_i) and deterministic (d_i) modeling parameters. These distributions determine the probability of the consequences $(P_i(c_i))$ or, more specifically, probability of containment failure (P_{Fi}) of scenario (s_i). It is instructive to note that Figure 2-1 provides a simplified view on the problem, where space of system parameters is generally multidimensional and different types of loads and capacities correspond to different threats and failure modes.

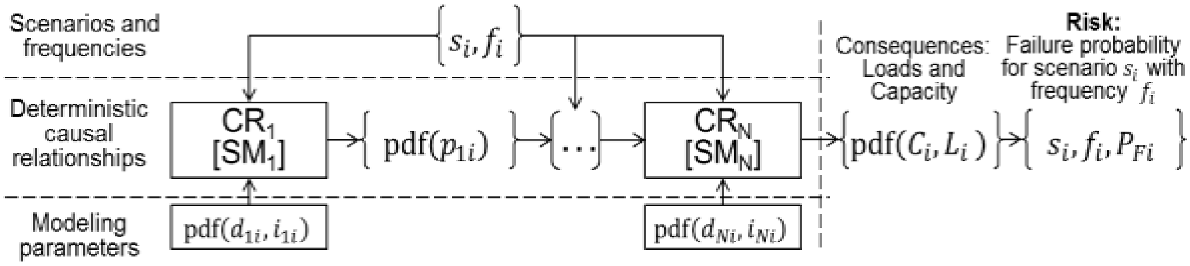

Figure 2-2: Failure probability in a multistage framework.

Similarly to the single stage process, the probability of failure (P_{Fi}) in scenario (s_i) can be introduced for a multistage framework where CR is a set of N models connected through initial conditions (p_{ki}), as illustrated in Figure 2-2. Simulations are carried out for each individual scenario s_i separately, which enables maintaining of transparent separation of aleatory (characterized by frequency f_i of scenario s_i) and epistemic uncertainties. Note that scenario parameters can affect modeling at any intermediate stage. Respective timing should also be provided as a part of scenario s_i, e.g. timing of activation, failure or recovery of specific safety systems. Different scenarios might require different chains of CRs, or "phenomenological event trees". Splinters should be used to ensure consistent bounding approaches in addressing intangible characteristics of such event trees. Output of CR_k is determined as multidimensional probability density function {pdf(p_{ki})} and provides an initial input conditions for model CR_{k+1}. Timing is explicitly included as one of the p_{ki} parameters.

In the conservative assessment we are seeking for a confirmation that $P_{Fi} < P_S$, or, in other words, that containment failure in scenario s_i can be positively excluded as physically unreasonable according to current state of knowledge. This conclusion would support the proposition that current SAM is reliable and no changes are necessary.

In the optimistic assessment we are looking for confirmation that $P_{Fi} > P_S$ which can be interpreted as: containment failure cannot be excluded as physically unreasonable even with optimistic bounding assumptions and state of the art knowledge. In other words "necessity" of containment failure is unacceptably high and the SAM has to be changed through modifications of the SAMGs or design.

The state of knowledge is expressed in terms of the ranges and probability distributions for the uncertain input parameters. Selection of the models, ranges and distributions is based on evidences (experimental data, scaling, synthesis of fine resolution simulation results, etc.).

Failure probability is used not only as the final results of the assessment, but also as a research instrument in the adaptive process. Sensitivity analysis of P_{Fi} to ranges and distributions of the uncertain parameters is used to identify (i) major sources of the uncertainty and possible unreasonable conservatism in the risk assessment, (ii) the needs for refinement of the evidence database.

Joint consideration of sensitivity of failure probability P_{Fi} to (i) possible improvement of knowledge necessary to reduce conservatism in the framework, and (ii) possible changes in the accident management strategy necessary to decrease failure probability with given state of knowledge, and associated costs for both options can provide a quantitative measure for selection of the most efficient approaches in both (a) risk assessment, and (b) risk management.

In the forward analysis, information is propagated from the initial plant damage state through the sequences of phenomena, determined by specific scenarios, towards the failure probability for each scenario, estimated at the very end. Such process provides limited information for inferring about adequacy of selected framework structure and generated data for the assessment of the failure possibility. Forward propagation of the uncertainties, especially in the multistage modeling framework, often amplifies uncertainties at each stage, unless there are clear limiting physical mechanisms. As a result of such amplification, there is a risk of "phenomenological explosion" (analogous to combinatorial explosion) when epistemic uncertainty becomes so large that success and failures become equally possible and nothing can be positively excluded as physically unreasonable. Therefore, there is a need for another kind of analysis where adequacy and consistency of the modeling framework and data can be evaluated.

2.3 Treatment of the Intangible Uncertain Parameters in Forward and Reverse Analyses

While ranges of the intangible parameters can be always (conservatively) bounded, the knowledge about distributions within the ranges is usually missing. In classical ROAMM, uncertainty in the intangibles can only be qualitatively approached, but it can always be bounded [270]. Such bounding approach is, in fact, similar to the interval analysis [104]. If inherent safety margins are sufficiently large, then bounding approach to the intangibles does not affect conclusions from the risk analysis. For some systems, however, bounding approach to quantification of the influence of intangible parameters might be insufficient. If failure probability P_f is sensitive not only to the ranges but also to the distributions, then uncertainty in prediction of P_f with "conservative" or "optimistic" bounding assumptions might be too large and, therefore, not suitable for a robust decision making process.

In order to assess the importance of the missing information about the distributions we can consider distributions as uncertain parameters. A space of possible probability distributions of the intangible parameters can be introduced. Each randomly selected set of distributions for the intangible parameters will result in a single value of failure probability P_f. Sampling in the space of the distributions for model intangible parameters will result in calculation of different possible values of P_f, including the bounding ones. A cumulative distribution function of $cdf(P_f)$ can be used to characterize confidence in prediction of P_f.

Let's assume that risk acceptance criterion is $P_f < 0.01$. From the interval analysis (resulting P-box shown in Figure 2-3), we can only notice that P_f is between 0 and 1. Such information is not very helpful for making conclusions on the risk acceptance. If we consider cumulative distribution of P_f, we can conclude that:

- For green curve: 95% of the cases the value of P_f is in the acceptable region.
  - It is possible to identify a subset of distributions of the model intangible parameters that result in P_f exceeding acceptability value. Once identified, those distributions can be a subject to further research and quantification.
- For red curve: 95% of the cases the value of P_f is in the unacceptable region.
  - This would mean that the system is not safe with most of the distributions belonging to the space of the possible distributions.

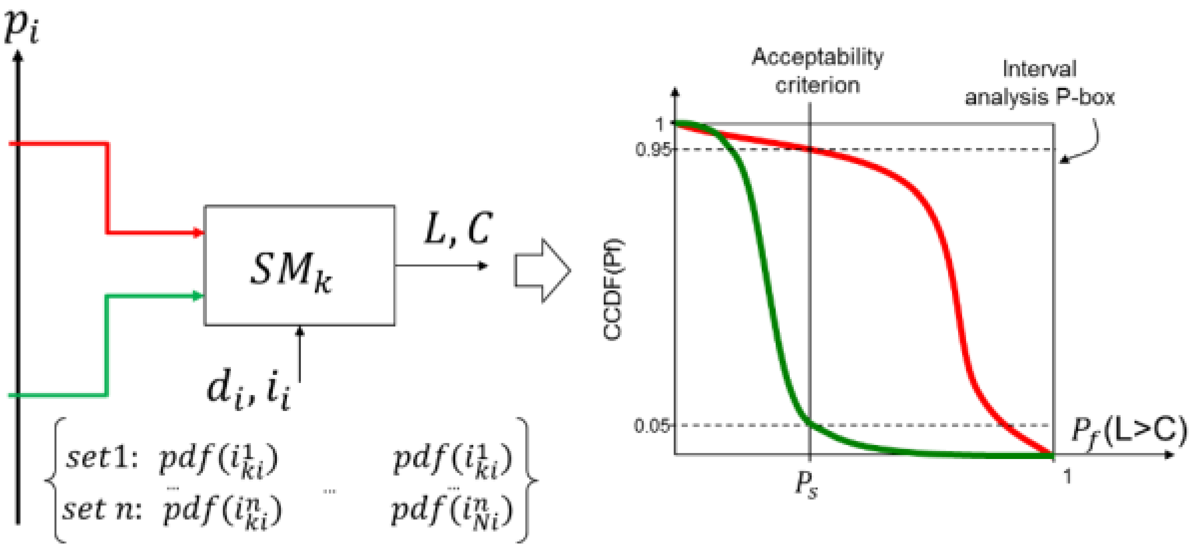

Figure 2-3: The influence of the distributions of intangible parameters on the failure probability.

Mathematical implementation:

Let us assume a model intangible parameter $i_{N,i}$, where we have no knowledge about its probability distribution, but we have knowledge about its range. To evaluate the effect of probability distribution for this parameter the sampling is made in space of possible distributions of this parameter. Each selected distribution out of randomly selected set of distributions will result in a single value of failure probability P_f calculated by

$$P_F(s_i,p_{k-1i}) = \int_{-\infty}^{\infty} P_F(s_i,p_{ki})\mathrm{pdf}\big(p_{ki}(s_i,p_{k-1i})\big)\,dp_{ki} \qquad (2\text{-}1)$$

then, confidence in prediction of P_f or $\overline{CDF}\left(P_F\big(s_i,p_{N-1,i}\big)\right) = 1 - CDF\left(P_F\big(s_i,p_{N-1,i}\big)\right)$ can be obtained as follows

$$CDF\left(P_F\big(s_i,p_{N-1,i}\big)\right) = \int_{-\infty}^{\infty}\left[\int_{0}^{P_F} pdf\big(P_F(s_i,p_{Ni})\big)\,dP_F\right] pdf\big(p_{Ni}(s_i,p_{N-1i})\big)dp_{Ni} \qquad (2\text{-}2)$$

where $\mathrm{pdf}\big(P_F(s_i,p_{Ni})\big)$ probability distribution function of P_f is obtained by sampling in space of possible distributions of $i_{N,i}$ and $pdf\big(p_{Ni}(s_i,p_{N-1i})\big)$ – probability distribution function of model output parameters p_{Ni} is obtained by sampling in space of model intangible parameters $i_{N,i}$.

Propagation of the failure domain in ROAAM+ framework reverse analysis:

If we consider multistage framework, the sampling of probability distributions and the calculation of the values of P_F in reverse analysis will be done for every selected set of distributions of model intangible parameters for every surrogate model.

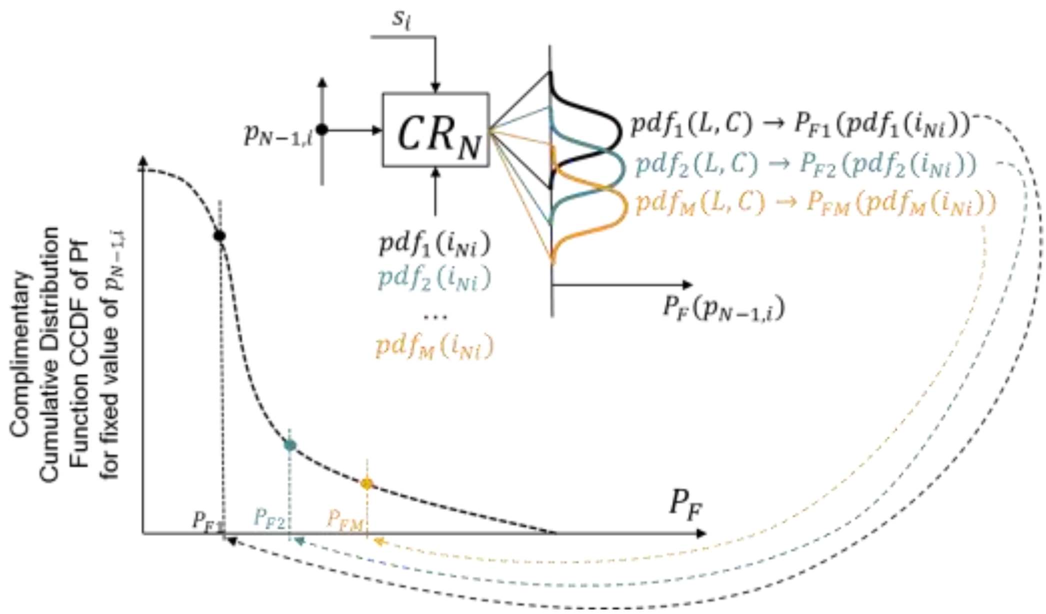

Figure 2-4: Treatment of model intangible parameters in ROAAM+ framework for Nordic BWR.

At the last stage of the framework (CR_N), from the domain of possible distribution of model intangible parameters ($i_{N,i}$) we select a set of probability distributions calculate the value of P_F for selected combination of model input ($p_{N-1,i}$) and scenario parameters (s_i). Repeating this process for every possible set of distributions will yield probability distributions of P_F and $CCDF\left(P_F(s_i, p_{N-1,i})\right)$ (Figure 2-4). Repeating the same process for each stage of the framework in the reverse analysis provides distributions of the failure probability for all possible combination of model input p_{ki} and scenario parameters s_i.

2.4 Characterization of Evidence and consideration of SM uncertainty for Integrated Assessment and FM Validation

Each FM represents a complex, often multi-physics and multi-scale phenomenon/processes. Multiple models are then brought together. To reduce uncertainty in model forms and model parameters, e.g., narrowing their distributions (pdf or applicability intervals), models and simulation codes are benchmarked and calibrated against relevant experiments. This requires identification, processing, qualification, and appropriate integration of a necessarily substantial and large body of heterogeneous data. Generally, effectiveness of model calibration depends on (a) availability (quantity, reproducibility) of applicable experiments; (b) degree of applicability of experiments (material scaling, geometric similarity, physics scaling); (c) quality of experimentation: characterization of uncertainty in experimental (initial, boundary) conditions;

(d) diversity of diagnostics, number of measuring channels, temporal and spatial resolutions; and (e) characterization of uncertainty of measured data [54] .

Subject to a broad range of above-listed characteristics, data sets obtained in experimental programs vary greatly by their format and validation and uncertainty quantification (VUQ) quality. In order to evaluate the impact of the uncertainty on predicted quantity of interest (QOI), it requires that the uncertainty be quantified, integrated and propagated toward QOIs. In an assessment framework such as one developed in this study, characterization and harmonization of evidence are ever more instrumental for the integration. For example, information value (weight) of evidence (dataset) can be computed through a function of global accuracy (relevance/applicability/scaling): Reactor Prototypicality Parameter, and local precision e.g. Experimental Measurement Uncertainty [54].

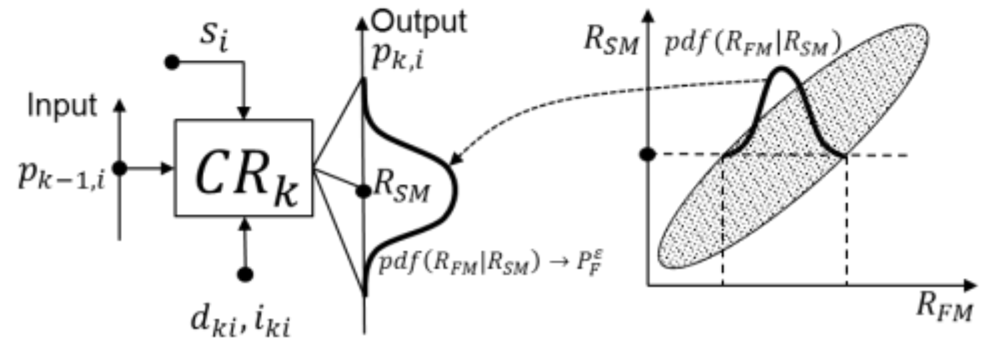

Figure 2-5: Treatment uncertainty in SM approximation of the FM response.

For each fixed point in the space of input p_{k-1} and modeling parameters d_i, i_i the uncertainty in the SM approximation of the FM can be characterized by the distribution $pdf(R_{FM}|R_{SM})$ of possible values of full model response (R_{FM}) given response of the SM (R_{SM}). Respective failure probability P_F^{ε} which takes into account the uncertainty in the SM approximation of the FM can be calculated (Figure 2-5).

Similar approach can be used for taking into account uncertainty in the FM prediction on the failure probability. The uncertainty in prediction of the FM should be characterized in the validation process. The aim of the validation is to assess a distribution of possible values of actual system response (R_A) given predicted full model response (R_{FM})

$$pdf(R_A|R_{FM}) \tag{2-3}$$

Combining information about full model uncertainty with SM uncertainty ($pdf(R_{FM}|R_{SM})$) one can obtain a distribution of possible actual system response given SM response

$$pdf(R_A|R_{SM}) \tag{2-4}$$

Obtained failure probability P_F^{ε} will take into account uncertainty in both SM approximation of FM and uncertainty in FM prediction. It is instructive to note that data about full scale system behavior at prototypic conditions is rarely available. A challenge for validation is to develop relevant scaling approaches along with separate and integral effect test data for robust assessment of the $pdf(R_A|R_{FM})$.

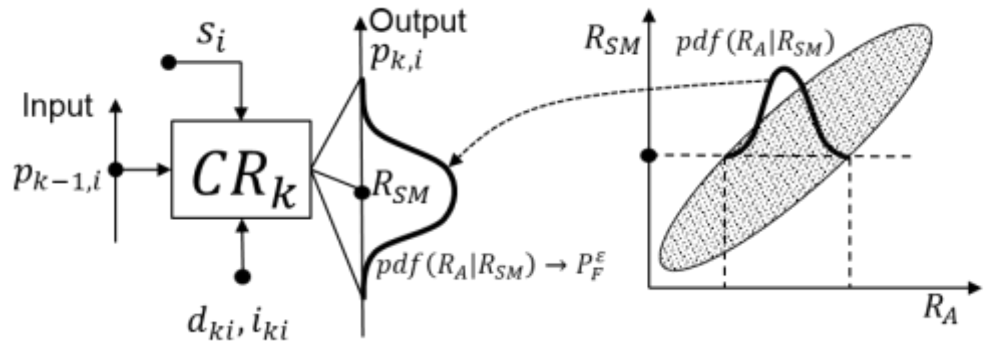

Figure 2-6: Treatment of uncertainty in SM approximation of the actual system behavior.

Figure 2-7a illustrates an example of possible CDFs (or CCDFs) of P_f that is color-coded as follows:

- CCDF $\{P_F(p_{N-1,i}) \geq P_s\} \leq 0.05$: "Green" – at most 5% of the cases exceed P_s, or there is 95% confidence that the probability of failure P_F will not exceed selected screening probability P_s.
- CCDF $\{P_F(p_{N-1,i}) \geq P_s\} > 0.95$: "Red" – at least 95% of the cases exceed P_s, or there 95% confidence the probability of failure P_F will exceed selected screening probability P_s.
- CCDF $\{P_F(p_{N-1,i}) \geq P_s\} \in (0.05 - 0.5]$: "Blue" – P_F exceed P_s in 5-45% of the cases.
- CCDF $\{P_F(p_{N-1,i}) \geq P_s\} \in (0.5 - 0.95]$: "Purple" – P_F exceed P_s in 50-95% of the cases. These are the cases where failure can be neither positively excluded nor assumed as imminent.

Figure 2-7b shows an example of the failure domain map calculated for the containment hatch door (with structural capacity limit 6 kPa*s) due to steam explosion loads as a function of jet size, melt velocity and water level. The failure domain is constructed in the space of the input parameters. The SM is sampled in each cell to obtain a distribution of the failure probability. Each cell on the map is colored according to the $\text{CCDF}(P_f)$ as described above.

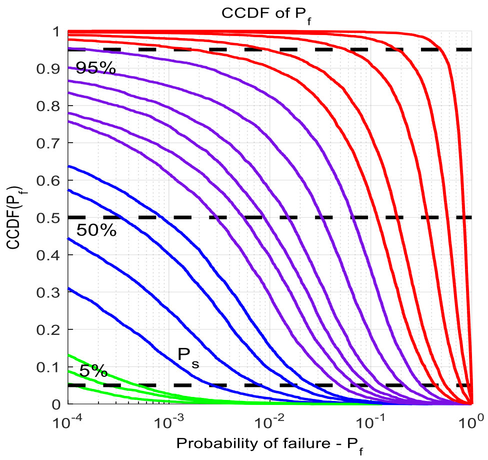

a

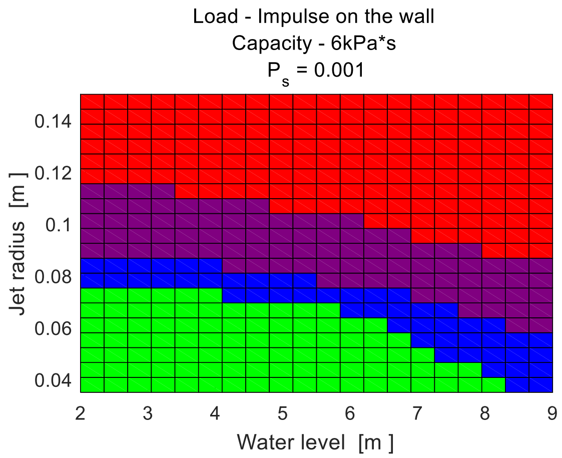

b

Figure 2-7. Complimentary cumulative distribution function of probability of failure $\mathbf{CCDF(P_f)}$ (a) and an example of the failure domain map (b)

Chapter 3. Development and Implementation of the ROAAM+ Framework and Models

3.1 Approach to Development and Refinement of the ROAAM+ Framework, Models and Data for Nordic BWRs

The top layer of the ROAAM+ framework for Nordic BWR (Figure 3-1) decomposes severe accident progression (Figure 1-1) into a set of causal relationships (CR) represented by respective surrogate models (SM) connected through initial conditions. While decomposed, the framework SMs still can be used for an end-to-end transient analysis if necessary.

Computational efficiency of the top layer of the framework allows for extensive sensitivity and uncertainty analysis in the forward and reverse analyses. Forward analysis defines conditional containment failure probability for each scenario $\{s_i\}$. Reverse analysis identifies failure domains in the space of scenarios $\{s_i\}$, and "deterministic" $\{d_i\}$ and "intangible" $\{i_i\}$ parameters specific to each model. Grouping and classification of failure scenarios corresponding to specific initial plant damage states helps to identify plant vulnerabilities and provides insights into possible efficient mitigation actions by operator. Failure domain in the space of deterministic and intangible modeling parameters $\{d_{ki}, i_{ki}\}$ identifies the need for improvement of knowledge, modeling and data.

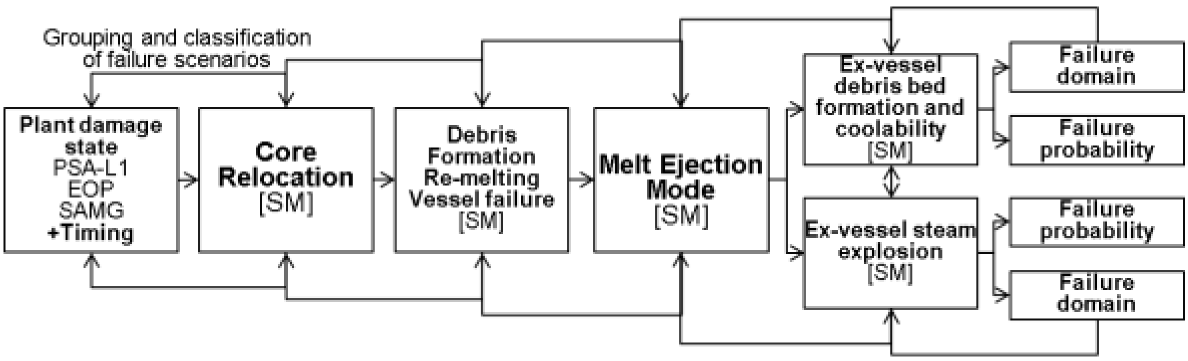

Figure 3-1: ROAAM+ framework for Nordic BWR.

The process of development and validation of the individual surrogate models is most important for completeness, consistency, and transparency of the results. General ideas of the process are illustrated in Figure 3-2. Initial conditions come from the SM analysis at the previous stages of the framework. Experimental and other evidences provide a knowledge base for validation of the FMs and calibration of SMs. Full Model (FM) is implemented as detailed fine resolution (computationally expensive) simulation approach. Database of the FM transient solutions is developed in order to provide better understanding of basic physical processes and typical behavior of the target parameters. The target parameters are the input conditions for the next model in the framework. Simplified modeling approaches and data mining techniques are used in order to develop a surrogate model. Surrogate model (SM) is an approximation of the FM model prediction of the target parameters which employ simplified (coarse resolution) physical modeling, calibratable closures, or approximations to the response surface of FM.

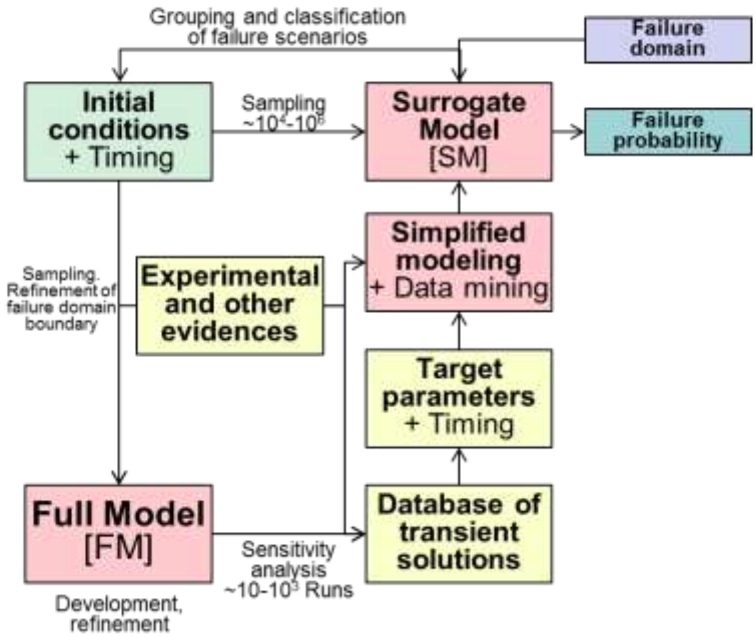

Figure 3-2: Full and Surrogate model development, integration with evidences, refinement, prediction of failure probability and failure domain identification.

Detailed discussion of the FM and SM development are presented in a series of publications (see Table 3-1). Four techniques were used for implementation of the SMs: (i) mapping (based on mapping of the FM solution to a grid in the space of the input parameters); (ii) polynomial (scaling analysis and data fitting); (iii) physics based uses simplified modelling of the phenomena; (iv) Artificial Neural Networks (ANN is based on complex regression analysis). Failure criteria are determined for SEIM and DECO.

Table 3-1. Summary of full and surrogate models developed for the ROAAM+ framework

SM	FM, experiments and SM purpose	References
CORE	FM: MELCOR model of the Nordic BWR containment. SM Type: Mapping. Given timing of ADS and ECCS activation provides time, composition and mass of core relocation and conditions in the lower drywall: pressure, pool temperature and depth.	[151], [82], [83], [84], [85], [86], [87]
Vessel failure	FM: coupled thermos-mechanical analysis (PECM/ANSYS, DECOSIM code) of the vessel lover head and debris. SM Type: Polynomial. Given mass and composition of the debris SM computes timings of the IGT, CRGT and vessel wall failure and corresponding mass and composition of liquid melt available for release.	[96], [97], [276], [277], [279], [280], [281], [282], [283], [284], [285], [293], [294], [295], [296], [297], [298], [316], [314], [313], [324]
Melt release	FM: parametric model of the melt release rate and vessel wall ablation. Experiment: remelting of multi-component debris and interaction with the vessel. SM Type: Physics based. Given timings and mode of lower head failure SM computes conditions of melt release, i.e. ablation of the breach, rate and duration of the release, thermal properties of the melt.	[163], [162], [152], [154], [160], [151]
SEIM	Steam Explosion Impact Map. FM: TEXAS-V code. SM Type: ANN. Given conditions of melt release and LDW characteristics SM returns a distribution of possible explosion impulses.	[92], [93], [94], [158], [95]
DECO	Debris Coolability. FMs: DECOSIM code for coolability of the debris, debris bed spreading model, debris agglomeration models. Series of experiments on debris bed formation, agglomeration and particulate debris spreading are carried out. SMs Type: Physics based. Given conditions of melt release and pool, respective SMs return dryout heat flux and max debris bed heat flux, the effect of debris spreading and agglomerated debris are taken into account.	[10], [11], [12], [13], [14], [15], [134], [135], [61], [62], [142], [143], [144], [145], [146], [147], [148], [149], [150], [153], [160], [164], [165], [166], [167], [168], [169] [170], [171], [172], [307], [309], [310], [311], [315], [316], [317], [318], [319], [320], [321], [322], [323]

3.2 ROAAM+ Framework Architecture

In this section we focus on some implementation aspects of the ROAAM+ framework. The ROAAM+ framework architecture has two levels (Figure 3-1). The first (top) level is based on SMs, all procedures at this level are unified and standardized. The second (bottom) level employs data mining techniques to establish connections between full models, experimental data and evidences, databases of full model solutions and surrogate models (Figure 3-2).

Implementation of ROAAM+ top level framework.

1. *Definition of the initial plant damage states and scenario space.*

Initial plant damage states $\{D_j\}$ (determined by availability of safety systems) and their frequencies $\{f_j\}$ are determined based on PSA L1 data [151]. The states are determined aiming at completeness of the analysis.

For each plant damage state, a full set of possible events (such as different recovery and mitigation actions) which can affect further accident progression is considered. The events, their order and timing create a space of scenarios $\{s_i\}$. Timing of events is an important factor. For instance, ECCS failed to start and ECCS failed after 2 hours after an initiating event will result in quite different initial conditions for the further analysis of the accident, e.g. decay heat, water pool level and temperature, etc. Possible ranges for timing of different events are considered based on EOPs and SAMGs.

It is instructive to note that there is a difference between (i) timing of random evens which is a part of scenario description (e.g. recovery of safety systems in MELCOR modeling) and is not predictable by the available deterministic models (aleatory), and (ii) timing of events predicted by the models (epistemic). We treat these two kinds of time differently. Aleatory timing is used in grouping of different scenarios according to their effect (failure domains). Epistemic timing is treated as any other dependent (i.e. obtained in the process of calculations) deterministic modeling parameters (p_{ki}).

The scenarios are used (i) to set specific initial conditions for deterministic analysis of the accident progression and for calculating respective failure probabilities in forward analysis; and (ii) to identify which conditions lead to high probability of containment failure in the reverse analysis. Grouping of scenarios is an iterative process which should aim at adequate resolution of the initial plant damage states which lead to similar consequences with respect to the containment failure.

2. *Specification of the input data and establishing connections between frameworks.*

Lists of input/output parameters are determined for each SM:

- Scenario specific data (e.g. water level and temperature in the lower drywell, possible mitigating actions and their timing, etc.).
- Initial conditions (p_{ki}), that connects SMs between each other through SM input/output.
- Deterministic and intangible parameters $\{d_{ki}, i_{ki}\}$ specific to each SM.

Ranges and respective multidimensional probability density functions are determined for all $\{d_{ki}, i_{ki}\}$.

3. *Implementation of the forward and reverse analysis algorithms for the whole framework.*

Each framework is implemented as a set of functions in MATLAB, with respective I/O structure for forward and reverse analysis. Implementation of the reverse analysis in ROAAM+ framework for Nordic BWR starts from SEIM and DECO frameworks failure domain analysis, then, information about the failure domain is propagated through their input parameters (output of MEM frameworks) in reverse mode towards the space of scenario parameters.

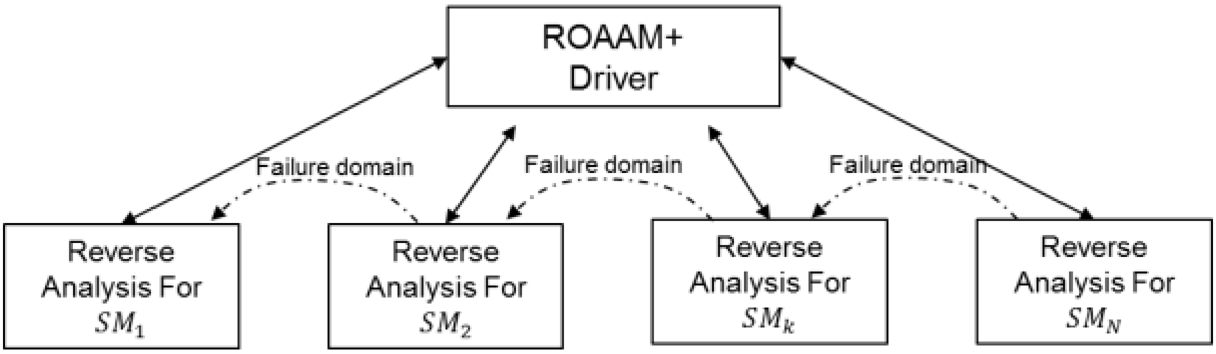

Figure 3-3: ROAAM+ framework reverse analysis implementation

Figure 3-4 represents data flow and connections between different blocks in ROAAM+ reverse analysis. The analysis and the connection between different models in ROAAM+ framework (see Figure 3-1) is driven by ROAAM+ Driver. The main functions of ROAAM+ Driver is to:

- Establish connections between user defined SM (e.g. failure domain information from SEIM SM will be propagated back to MEM SM).
- Based on connections between SM, establish hierarchy of SM execution (including splinter scenario and different failure modes, for example 3 failure modes in MEM SM (IGT, CRGT, vessel wall) will create three parallel threads of analysis in consequent SMs (SEIM,DECO).
- Provide information about Input/Output structure, ranges and distributions (where applicable) for every surrogate model to Reverse Analysis Object.
- Perform partitioning with n – dimensional grid (binning) of scenario space (scenario space is unique for all surrogate models in the analysis).

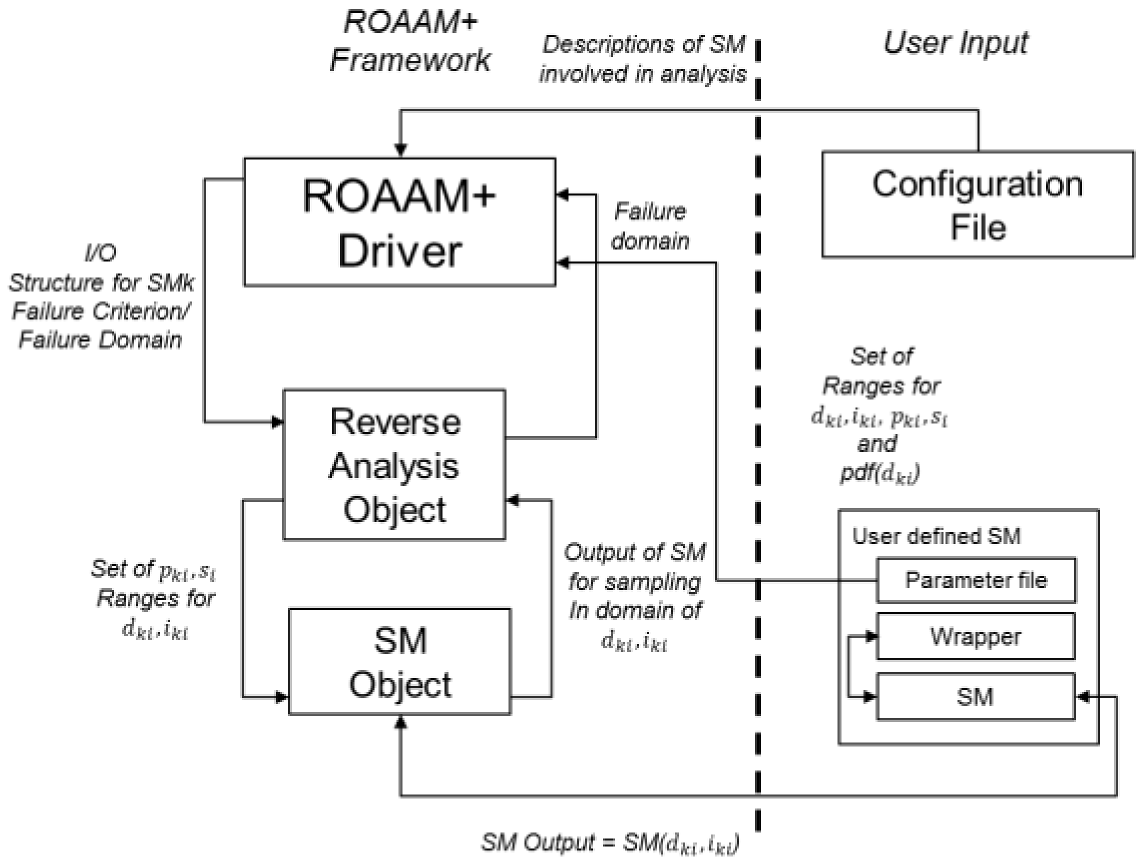

Figure 3-4: ROAAM+ framework reverse analysis implementation

In reverse analysis characterization and propagation of the failure domain is performed by Reverse Analysis Object. Based on the I/O information, ranges of the parameters involved in the analysis Reverse Analysis Object performs:

- Partitioning (binning) of model input - p_{ki} with static/adaptive grid.
- Generation of the sampling set for the analysis in space of model input and scenario parameters.
- For every possible combination Reverse Analysis Object calls SM Object to generate sampling in model deterministic/intangible parameters and calculate SM response for fixed p_{ki} and s_i.
- Calculate probability of failure P_f – for every cell in domain of model input parameters.

Partitioning (binning) of the input space is performed with adaptive mesh grid [180], then, the influence of model deterministic and intangible parameters is evaluated using SM Object. The main functions of SM object are:

- Iterative generation of the sampling sets in domains of model deterministic and intangible parameters.
- Generate set of input vectors for SM execution
- Execution of the SM (through the SM wrapper, SM wrapper is a user defined intermediate link between ROAAM+ framework and SM)
- Preliminary analysis of the results for each iteration to establish output convergence.

- Reporting of the results to Reverse Analysis Object for calculation of P_f.

4. *Implementation of sampling in ROAAM+ reverse analysis*

The general approach for reverse analysis for failure domain identification in ROAAM+ framework includes:

- Generation of the data base of surrogate model solutions at each step of multistage process, using respective SM, connecting plant damage states to the potential threats for containment integrity.
- Probabilistic evaluation and failure domain analysis, which include
  - Sampling of probability distributions (PDFs)
  - Calculation of probability of failure for selected sets of PDFs.
  - Calculation of cumulative distribution function of probability of failure for selected sets of PDFs.

Generation of the data base of SM solutions involves sampling in domains of:

- Model input parameters $\{p_i\}$
  - Grid based sampling is used in order to get good coverage of the uncertainty space and good knowledge about failure domain location.
- Model deterministic and intangible parameters $\{d_i, i_i\}$
  - Quasi-random Halton sequence is used to generate sampling in multidimensional space of $\{d_i, i_i\}$ parameters.
  - The amount of samples in space of $\{d_i, i_i\}$ parameters depends on the convergence of the SM output between two consecutive generation of samples.

For each combination of parameters $\{p_i\}$ and $\{d_i, i_i\}$ ROAAM+ framework runs SM and stores output in the database of SM solutions for further probabilistic evaluation and failure domain analysis.
Sampling in the space of model input parameters $\{p_i\}$ is performed on the regular (static) grid (in the future Adaptive Mesh Refinement of the boundary of the failure domain will be implemented). Application of grid based sampling techniques, in general, is quite computationally expensive, thus, in order to make failure domain analysis in space of model input parameters feasible, it is necessary to perform model sensitivity analysis with respect to a) Individual models; b) Grouped models.

Model sensitivity analysis is performed for:

- Individual models
  - To identify the most influential parameters with respect to:
    - Model output.
    - Probability of failure (P(L>C)).
- Grouped models:
  - To identify the most influential parameters in the "down-stream" models with respect to
    - Grouped (connected) models output

- Probability of failure (P(L>C))

Model sensitivity analysis allows to improve our understanding of the impact of each step in multi-stage analysis process on the final outcome and on the probability of failure (e.g. Jet diameter – is the most influential parameter for steam explosion, on the other hand Jet diameter is predicted by Melt-Ejection SM and defined by the properties of relocated debris in LP that depend on the accident scenario and recovery time of safety systems.
Sensitivity analysis of probability of failure currently require an approach that will include parameters that characterize distributions of model intangible parameters, together with model input parameters in the analysis.

5. Implementation of PDF sampling

In order to assess the importance of the missing information about the distributions we can consider distributions as uncertain parameters (see chapter 2.3). A space of possible probability distributions of the intangible parameters can be introduced. Each randomly selected set of distributions for the intangible parameters will result in a single value of failure probability P_f. Sampling in the space of the distributions for model intangible parameters will result in calculation of different possible values of P_f, including the bounding ones. A cumulative distribution function of $cdf(P_f)$ can be used to characterize confidence in prediction of P_f (see Figure 2-3).

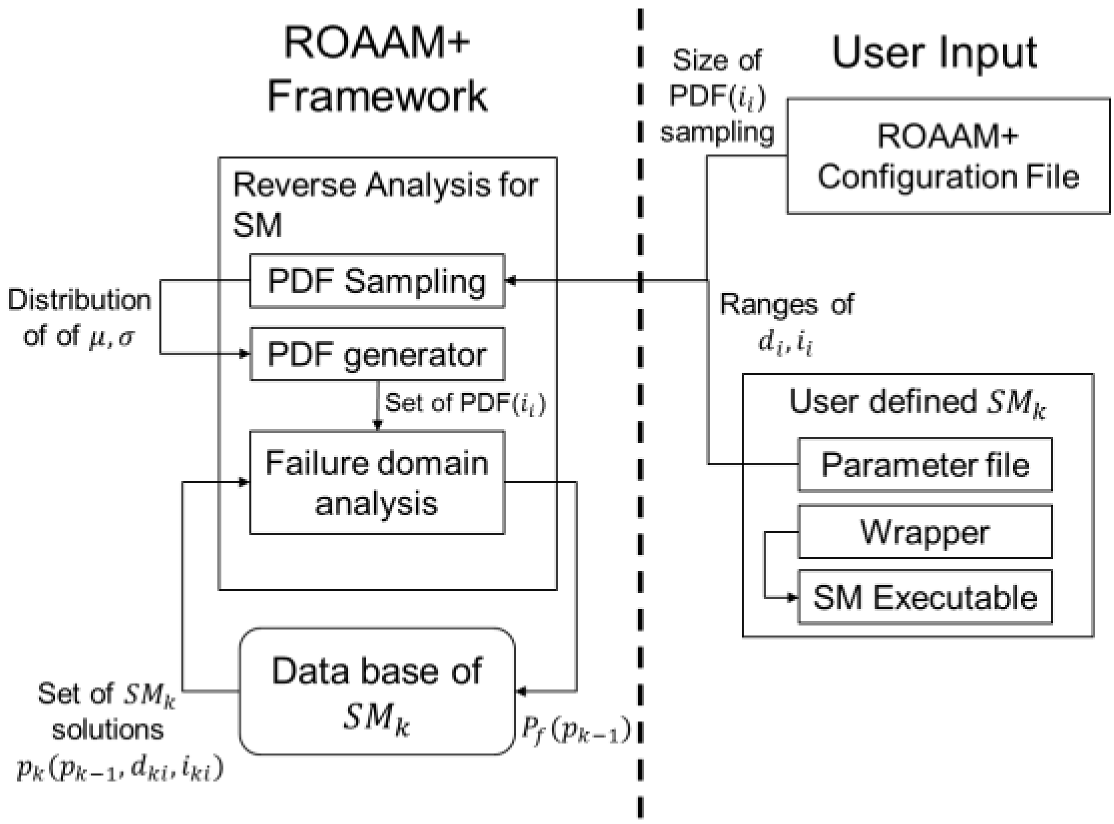

Figure 3-5: Implementation of PDF sampling of intangible parameters in ROAAM+ framework.

Figure 3-5 illustrates algorithmic implementation of PDF sampling of intangible parameters in ROAAM+ framework. The process of PDF sampling is implemented in following steps:

- Based on the user input in ROAAM+ configuration a set of parameters that characterize PDF for every intangible parameter in SM_k is generated (μ, σ – in current implementation we use different variations of normal distributions).
- Function "PDF generator" generates a set of discrete PDFs for every intangible parameter based on the set of μ, σ on the range between [0,1] (see Figure 3-6) and then scales each PDF to specific ranges correspondent to each intangible parameter.
    - μ_i, σ_i – are sampled from the prior distribution of the mean and standard deviation.

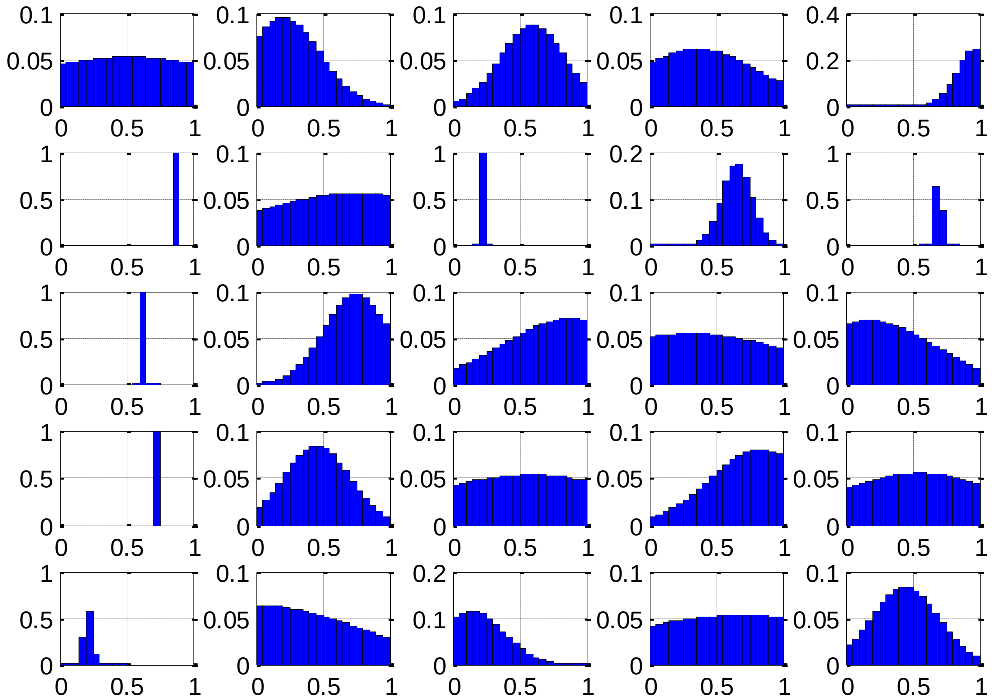

Figure 3-6: Example of randomly generated PDFs for model intangible parameters.

- The value of P_f is calculated for each combination of model input ($p_{k-1,i}$) and selected distribution $pdf(d_{ki}, i_{ki})$.
- For every model input ($p_{k-1,i}$) - $CDF\left(P_F\left(s_i, p_{k-1,i}\right)\right)$ is obtained using equation (3-31) and can be characterized by exceedance frequency of screening probability P_s.

Figure 3-7 illustrate an example of possible CDFs (or CCDFs) of P_f that can be obtained in ROAAM+ failure domain analysis. These resultant CDFs can be interpreted as follows:

- $CCDF(P_F)$ – where at most 5% of the cases exceed P_s are colored green – it means that with 95% confidence the probability of failure P_F will not exceed selected screening probability P_s. – which is considered as "failure is physically unreasonable".

- $CCDF(P_F)$ – where at least 95% of the cases exceed P_s are colored red – it means that with 95% confidence the probability of failure P_F will exceed selected screening probability P_s. – which is considered as "failure is imminent"
- $CCDF(P_F)$ – where P_F exceed P_s in 5-45% of the cases are colored blue, and – where P_F exceed P_s in 50-95% of the cases are colored purple. These are the cases where we can neither positively exclude failure nor conclude that the failure is imminent at given screening frequency P_s, due to the uncertainties coming from the model deterministic and intangible parameters and their distributions.

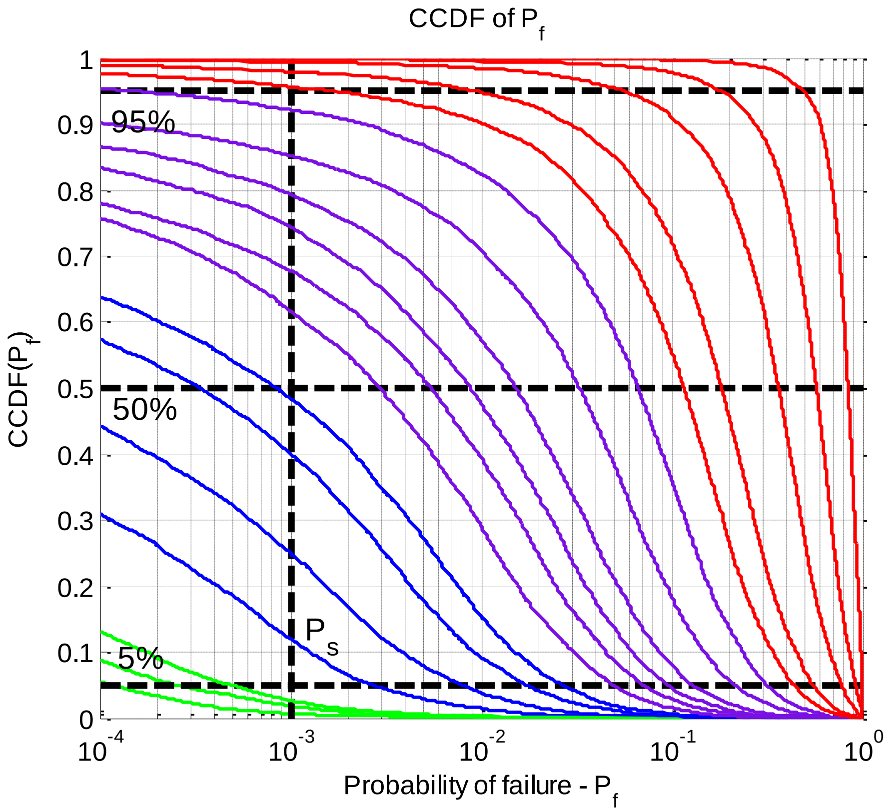

Figure 3-7: Complimentary cumulative distribution function of probability of failure $CCDF(P_f)$

6. Calculation of probability of failure - P_f

In reverse analysis failure domain characterization can be done using clustering and classification approach [185], with application of decision trees for visualization of the failure domain in multidimensional space in each step of multistage process.

For each cell in space of model input and scenario parameters sampling in space of the model deterministic and intangible parameters d_{ki}, i_{ki} generates a set of points in the load/capacity domain (L,C). Then the values P_f in each cell are calculated. Numerical implementation is done by binning in space of Load and Capacity as in Figure 3-8. Then for every cell (i,j) in domain of (L,C) the value of $P_{f(i,j)}$ is obtained by

$$P_{f(i,j)} = \frac{1}{N}\sum_{i,j} p(L > C) \tag{3-1}$$

then the value for the whole domain (L,C) equals

$$P_f = \sum_{\forall i,j} P_{f(i,j)} \tag{3-2}$$

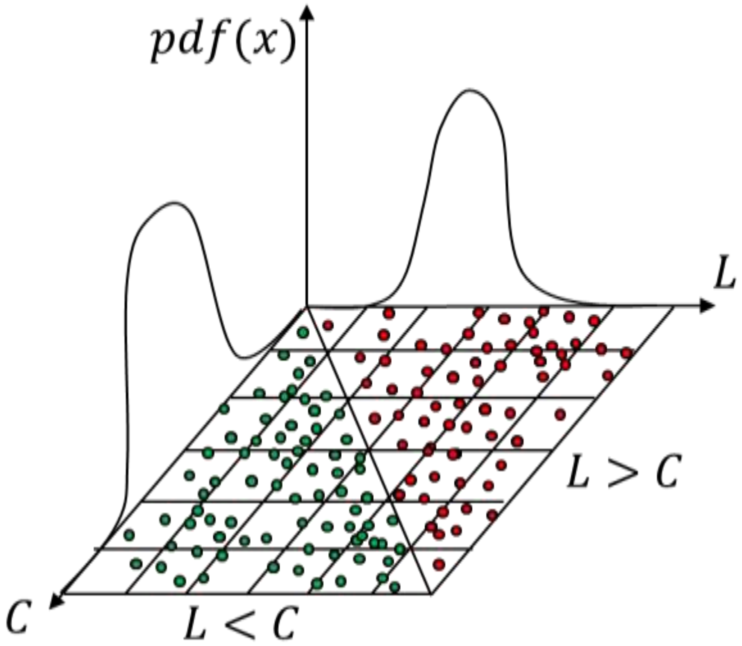

Figure 3-8: Output in Load/Capacity domain.

3.3 Core Relocation SM

Core relocation in BWR is a complex process. It starts when core melt accumulates on the lower core support plate and drips down to the vessel lower head. Large core relocation seems to occur when the melt accumulation leads to the failure of the lower core support plate and thus discharges large amount of melt resident in the bottom of the core into the lower head. Properties of relocated debris (mass, composition, configuration, etc.) determine the initial conditions for corium-structure interactions, vessel failure and melt release analyses.

Core relocation phenomenon in a reactor can be simulated using severe accident analysis computer codes such as MELCOR, MAAP. However, the calculations using these codes are relatively expensive, while scenario space needed to be sampled is extremely large when taking into account time to event trees in classic probability safety analysis (plant damage states and scenarios of severe accident management). The Core Relocation Surrogate Model (SM) can be constructed based on quite representative database of simulations (e.g. using MELCOR). The SM will provide a much more economical tool to approximately calculate the phenomenon with relatively good accuracy.

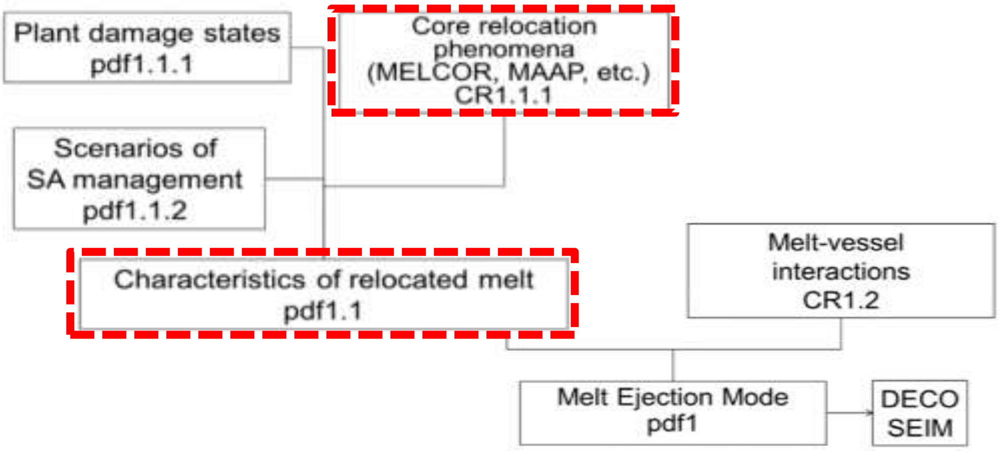

Figure 3-9: Core relocation framework

Figure 3-10 shows scheme of the development of the Core Relocation SM framework. Implementation of the framework bases on the following tasks:

1. Identification of the complete list of input and output parameters of the SM.

   a) The SM inputs can be divided into scenario, deterministic, and intangible parameters. Each input parameter is presented by a probability density function.
   For example:
   Scenario parameters:
      - Initial plant state,
      - Initiating events,
      - Timing and capacity of recovery of safety systems,
      - etc.

Deterministic parameters:

- Nodalization,
- Candling heat transfer coefficients,
- Component critical minimum thicknesses to maintain intact,
- In-vessel falling debris quench model parameters,
- etc.

Intangible parameters:

- Decay heat standard (ANS, Origen),
- Loading and failure rule for supporting structures (for example lower core support plate),
- Support rule for non-supporting structures,
- Pool heat transfer from bottom/top of structure support plates,
- Candling secondary material transport,
- etc.

b) The SM output (p_1) includes important physical parameters of debris bed in the vessel lower plenum which can be used for input of the next surrogate model of debris formation, re-melting and vessel failure in the ROAAM+ framework.
For example, p_1 will include:

- Composition and mass of debris.
- Other thermal properties of debris.
- Initial decay heat.
- Geometrical properties of debris bed.
- Timing of important events (e.g., start of large core relocation, end of core relocation, etc.).
- Other system parameters (e.g., pressure, water level in the vessel).
- etc.

2. Calculations of probability density function (pdf) of the scenario input parameters taking into account the timing. This defines the scenario space to be sampled later.

Due to complexity, utilization of pdf information can be divided into two stages:

a) consider only uncertainty range of parameters,
b) consider multidimensional pdf of parameters.

The pdf's can be achieved through calculations or based on experimental evidences. Sensitivity analysis is necessary to identify influential input parameters affecting the core relocation.

3. Analysis of plant damage states (PDS).

a) Analysis of initial plant damage states received from the standard PSA-L1 study, EOP and SAMG.
b) Selection of representative plant damage scenarios for MELCOR (Full model) calculations. The selection can be based on contribution of scenarios to total core damage frequency from the PSA-L1 study.

c) The analysis can iteratively get feedback information about failure possibility from CR_2 (vessel failure SM) following the reverse analysis. The boundary of the failure domain can be refined by an iterative process.

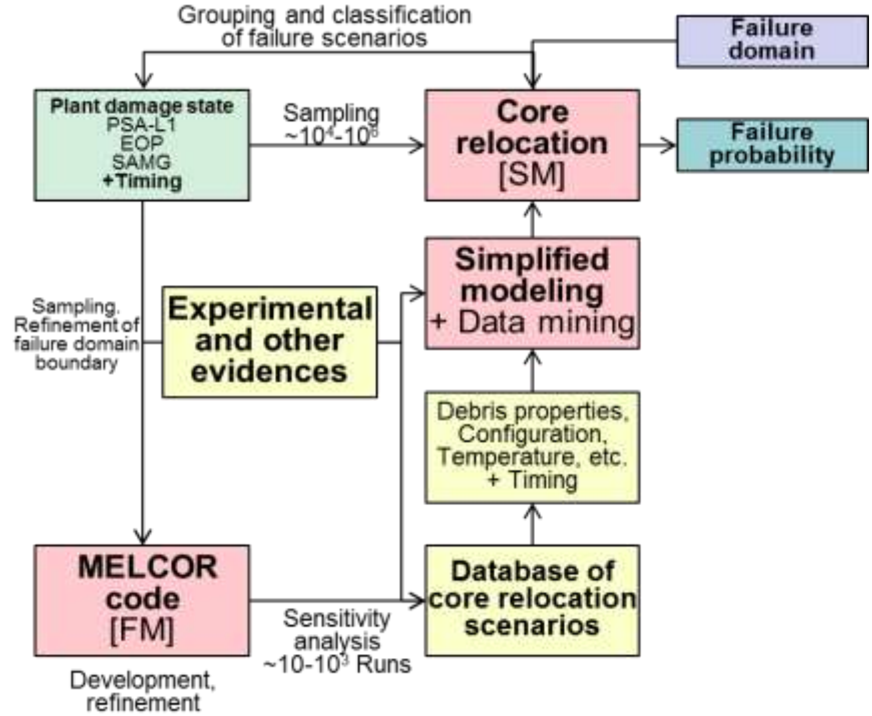

Figure 3-10: Core relocation surrogate model.

4. MELCOR (Full model) calculations of representative plant damage scenarios.

MELCOR is used to calculate accident progression of scenarios with concerned plant damage states.

a) Sampling of influential input parameters (mostly scenario parameters) is done in the order of ~10 - 10^3 runs (because the full model calculations are expensive) to get the response surface.
b) Sensitivity analysis can be done for other input parameters (such as deterministic, intangible parameters).
c) Plant input model can be continuously improved based on better understanding of the phenomenon modeling in the code and the plant systems.

5. Building database of core relocation scenarios.

a) The database is built from MELCOR simulation results. It stores data of output parameters of core relocation process, which are identified in task 1, and corresponding scenarios, input parameters.
b) Common formats for the code output data and the database should be agreed upon from the beginning. There will be many batches of calculations performed iteratively, possibly with significant input deck modifications.

6. Data mining and simplified modeling.

The process prepares data for building the core relocation SM.

a) Information from the database of core relocation scenarios, experimental and other evidences, or directly from MELCOR calculations is analyzed.
b) Classification, clustering, mapping can be applied to condense the data depending on type of the SM, which is describe in the next task.

7. Development of the core relocation SM.
   a) The SM is developed based on the knowledge gained through data mining, classification and grouping of failure scenarios.
   b) There are different options for the core relocation SM:
      i. Machine learning (neural network) approach
         - Different neural networks can be used for the SM (e.g., back propagation network, radial basis function network).
         - Full database is used to train the neural network.
         - The database can be preprocessed using different techniques to increase the accuracy of the network.
      ii. Simplified/approximated physical models of the process
         Condensed information of the database (for example from the classification, clustering, mapping) is used to build simplified physical models and correlations of the core relocation process.
      iii. Combination of both two previous methods.
         The SM can be divided into connected sub-models. Some sub-models can be in form of neural networks; others can be simplified physical models.

8. Sampling of the core relocation SM to get the failure probability.
   a) The sampling of input parameters through the SM can be done in the order of ~10^4-10^6 runs.
   b) Given the scenario (s_i) and multidimensional pdf of the intangible (i_i) and deterministic (d_i) parameters as input for the core relocation SM (CR_1), the failure probability can be obtained following the forward analysis.
   c) In the reverse analysis, information of the failure domain boundary is received from CR_2 (next stage vessel failure SM). An iterative process can resolve/refine the boundary of the failure domain.

3.3.1 Core Relocation Surrogate Model

The work is motivated by apparent sensitivity of the vessel failure phenomena to the characteristics of the debris in the lower plenum [298], [96]. The ultimate goal of this work is to develop Core Relocation full and surrogate models that can be used in the ROAAM+ framework [154] for prediction of the effect of core degradation and relocation processes on the debris bed properties in the lower head. General approach to the development of the Core relocation SM is illustrated in Figure 3-10. In order to achieve the goal and develop the SM according to the general approach, following tasks are addressed and discussed in this work: (i) definition of the plant damage states and respective frequencies from PSA-L1; (ii) definition of the scenario space including possible timing of system recovery and operator actions; (iii) development of the database of the core degradation transients using MELCOR code with regular and GA-IDPSA [299], [300], [301], [173], [219], [220], adaptive sampling techniques in the scenario space; (iv) establishing of connections with the other SMs in the ROAAM+ framework; (v) data mining and simplified modeling for development of the SM based on the database of the FM solutions.

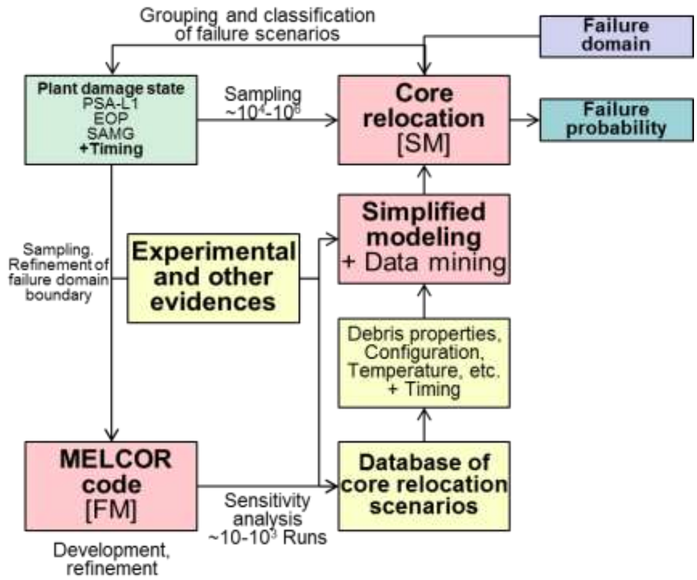

Figure 3-11: Core relocation surrogate model.

3.3.1.1 Definition of the plant damage states based on PSA-L1 data

This task includes (i) grouping of initial plant damage states based on PSA-L1, EOP and SAMG; (ii) selection of representative plant damage states (based on contribution to total core damage frequency) and scenarios for MELCOR (FM) analysis. It is important to identify (a) possible accident progression scenarios; (b) safety systems that can affect in-vessel/ex-vessel accident progression (e.g. ECCS, RHR, etc.); and (c) conditions for activation of these safety systems (e.g. lower drywell flooding condition – together with ECCS, RHR and depressurization history will identify water pool temperature in the cavity). In PSA L1 for Nordic BWR reference plant design the core damage states are grouped into 4 categories: HS1 (ATWS), HS2 (core damage due to inadequate core cooling), HS3 (core damage due to inadequate residual heat removal) and HS4 (rapid overpressure of the primary system). The categories (HS1, HS2, HS4) correspond to early core damage scenarios, HS3 corresponds to late core damage. In addressing ex-vessel behavior and consequences, the following physical phenomena can challenge containment integrity: direct containment heating (DCH), ex-vessel steam explosions (EVE) and basemat penetration (BMP) by non-coolable corium debris. DCH scenario corresponds to high pressure (HP) accident scenario, steam explosion in the containment (EVE) corresponds to low pressure (LP) scenario. Both HP and LP will lead to formation of ex-vessel debris bed and potential corium interaction with containment basemat. The core damage sequences can be grouped together based on the aforementioned challenges to the containment integrity as shown in Figure 3-12. Corresponding frequencies are obtained from PSA L1 data.

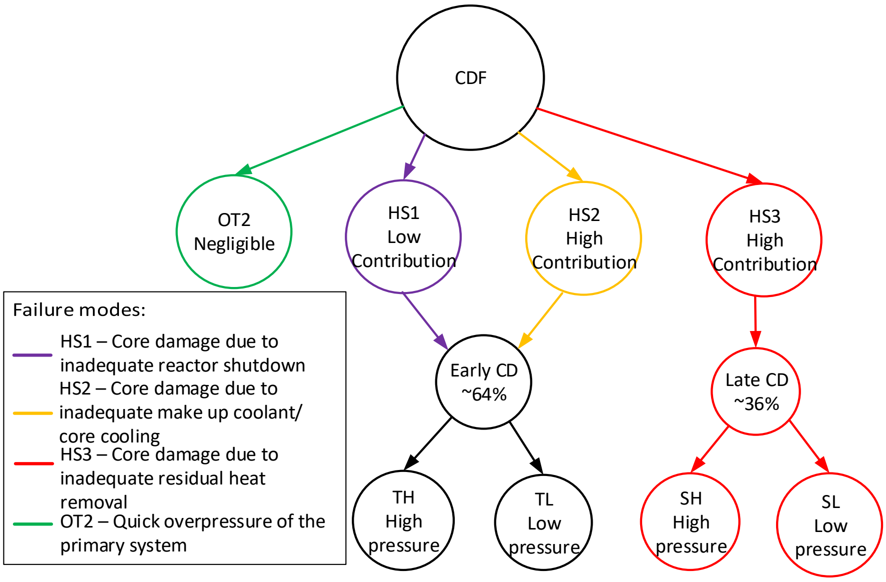

Figure 3-12: Core damage states classification.

3.3.1.2 Definition of the scenario space with possible recovery and operator actions

The station blackout (SBO) scenarios occurred in Fukushima-Daiichi accident [89] and is among the major contributors to the core damage frequency (CDF) for Nordic BWR according to PSA Level 1 analysis. In the Forsmark 2006 incident, an overvoltage in the 400 kV switchyard caused the failure of 2 (out of 4) of the Uninterruptable Power Supplies (UPS), including their 220 V batteries. It took about 30 minutes for the plant operators to restart all diesels. In this work we consider station blackout (SBO) scenario with a delayed power recovery. We consider a simultaneous loss of the offsite power (LOOP) and backup diesel generators. This results in the simultaneous loss of all water injection systems, including crud purge flow through the control rod drive tubes. We consider that the power (external grid or diesel generators) can be recovered after some time delay and emergency core cooling system (ECCS) system can be restarted. According to the considered scenario, the operator can delay activation of the depressurization system to keep coolant in the vessel. Yet, for injection of water with low pressure ECCS, depressurization has to be activated.

The timing of the safety systems recovery is as part of the accident scenario space. For instance, we consider a delay in activation of Reactor Pressure Vessel (RPV) depressurization systems which includes battery-powered ADS-Valves (System 314) and Water-Valves (System VX105, FL314 & FL330). Overpressure protection system (FL314) is spring-operated will open stepwise, starting at slightly above 70 bar and opening completely at 75 bar to protect the RPV from failure. The auxiliary Feedwater System (System 327, FL327) is considered non-functional. Other system like the Control Rod Guide Tube (CRGT) Cooling or the Residual Heat Removal (RHR) Systems are also considered non-functional. The capacity and timing of activation of the Emergency Core Cooling System (ECCS System 323, FL323) is another element of the scenario. Necessary condition for activation of the ECCS is low pressure in the RPV. Mass flow begins at pressure difference of 12.5 bars between down comer (DC) and wet well (WW) and will reach its maximum value at 2 bars above the wetwell pressure.

3.3.2 Nordic BWR Reference Plant Design and its Modeling in Core Relocation FM

MELCOR input model for Nordic BWR was originally developed for accidents analysis in the power uprated plants [337]. Current MELCOR input deck has total thermal power output of 3900 MW. The core consists of 700 fuel assemblies of SVEA-96 Optima2 type – which is divided into five non-uniform radial rings and eight axial levels. The primary coolant system is represented by 27 control volumes (CV), connected with 45 flow paths (FL) and 73 heat structures (HS). The vessel is represented by a 6-ring, 14/19 (for MELCOR 1.86 and 2.1/2.2 correspondingly)-axial level control volume geometry.

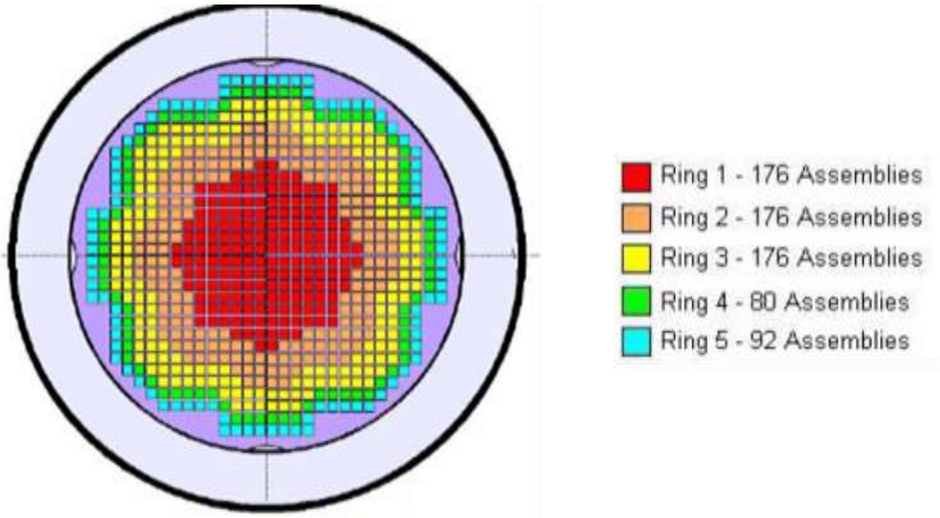

Figure 3-13: Nordic BWR MELCOR Model Core Radial Nodalization (MELCOR 1.86/2.1/2.2)

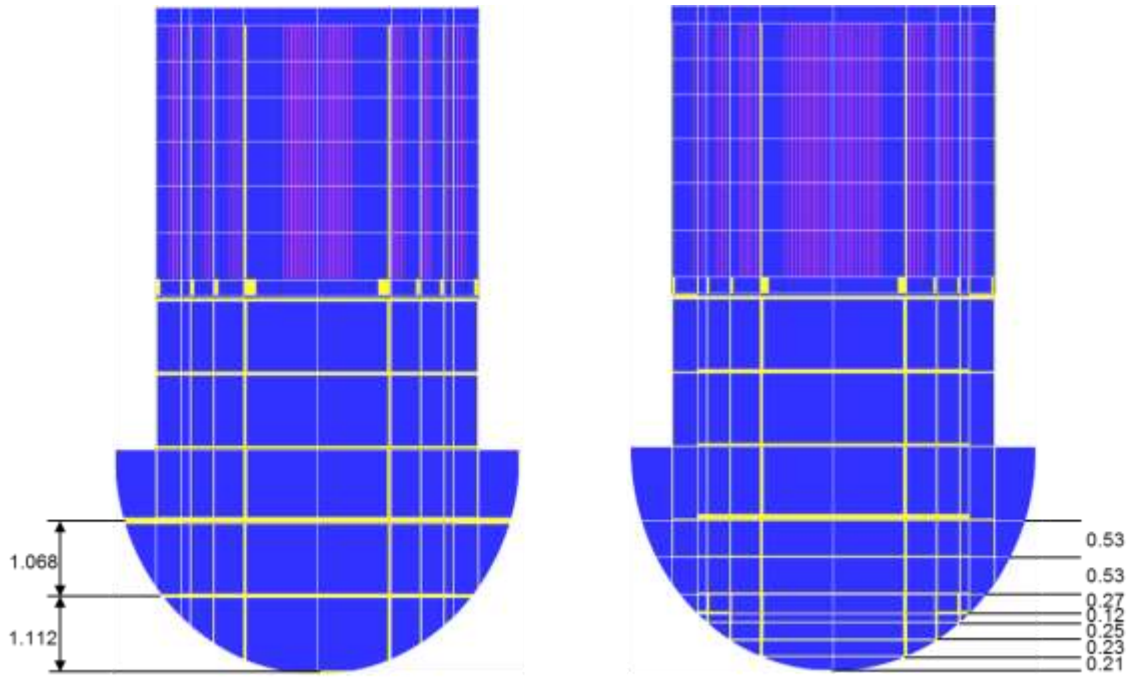

Figure 3-14: Nordic BWR MELCOR Model Core Axial Nodalization (MELCOR 1.86 (LHS) and 2.1/2.2 (RHS))

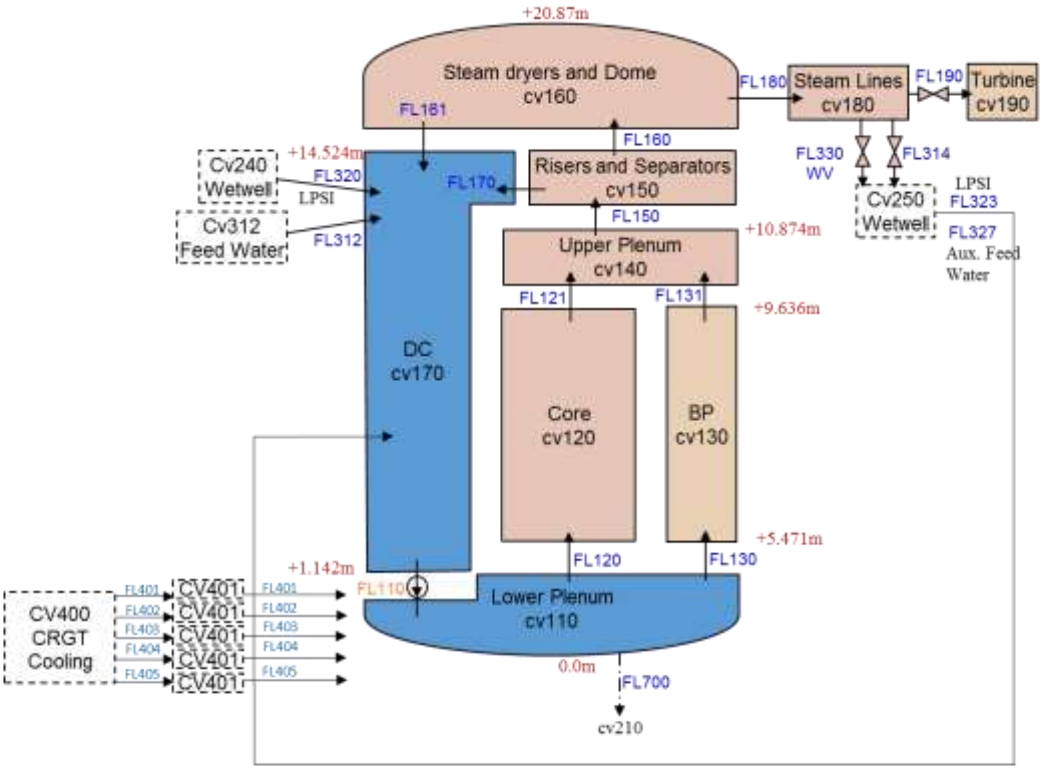

Figure 3-15: Nordic BWR MELCOR Model Vessel Nodalization

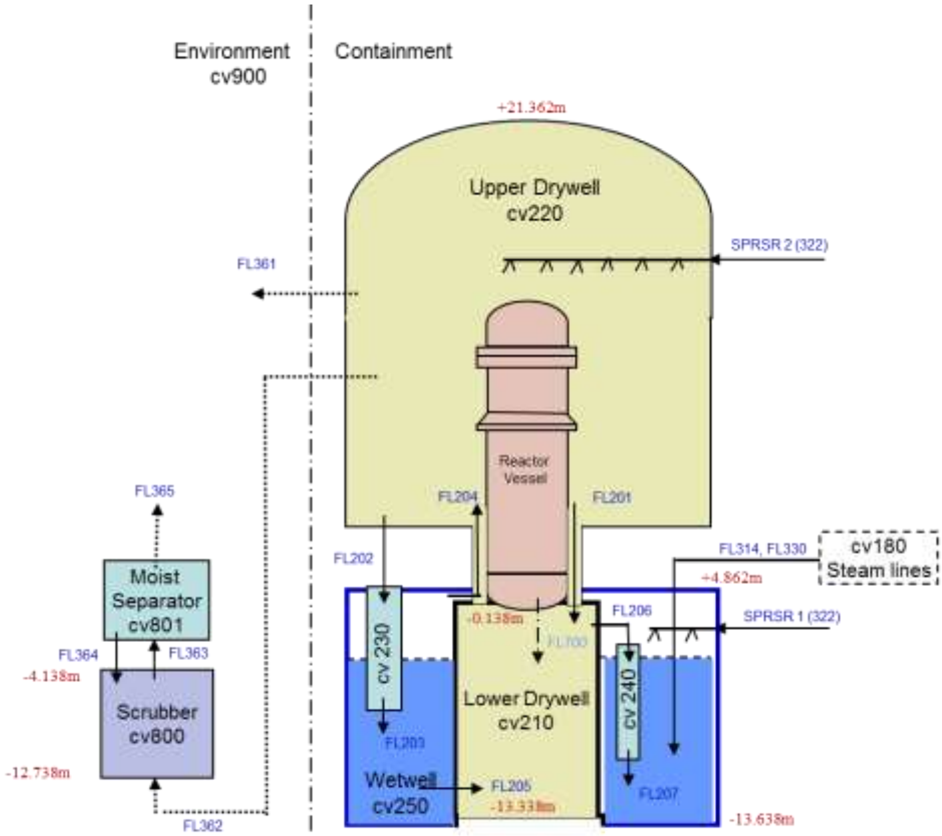

Figure 3-16: Nordic BWR MELCOR Model Containment Nodalization

Description of safety systems used in Analysis:

- System 354: Scram, the hydraulic actuating power shut-off system gives fully insertion of all control rods within a few seconds after initiation. The effect of this system is modeled in MELCOR by fission power decrease (during 3.5 s) according to a tabular function and scram conditions. In this case loss of power, is applied as a control function.
- System 314: Pressure control and relieve system (ADS) has several functionalities and is able to operate with only battery backups:
    - 314 TA Function: The spring-operated part of the overpressure protection system will open valves stepwise, starting at slightly above 70 bar and opening completely at 75 bar, to release steam and protect the Reactor Pressure Vessel (RPV) from a catastrophic failure.
    - 314 TB Function: Activation of 314TB initiates steam discharge into the wet well (WW) on low water level signal L6 (1 m below the core top). The pressure is reduced by ADS to a level sufficient for activation of the low pressure emergency core cooling system (ECCS). At the same time the coolant is lost from the primary system quite rapidly, which leads to core uncover. It is assumed that the actuation of the system can be delayed by the operator.
- System 323: The low pressure coolant injection (LPCI) system is the part of the ECCS, which provides water injection into the downcomer. In station blackout conditions it is not available. The system is activated on L3 level signal (+2m). However, the water injection starts when pressure difference between wet well (WW) and down comer (DC) is below 12.5bar. Maximum injection capacity of ECCS is reached at 2 bar difference between WW and DC and equals to 4 trains x 366 kg/s = 1464 kg/s.
    - It is assumed that the system can activated if power source is recovered after some time delay. Simultaneous recovery of all 4 trains is assumed in this paper. The results for mass flow of 25,50,75% of the designed capacity that corresponds to 1,2,3 injection trains is a subject of the future work.
- System 358: Flooding of LDW from the WW is initiated to provide the water pool for melt fragmentation and debris cooling in case of melt release from the vessel.
- System 361: Non-filtered containment venting system (CVS) is the pressure relief directly to the ambient atmosphere. It is activated when the internal containment pressure reaches to a setpoint that is below containment failure pressure.
- System 362: Filtered containment venting with multi venturi scrubbing system (CVS MVVS) provides pressure relief and scrubbing the radioactive aerosols.

3.3.3 Sampling of FM Solutions

Sampling, i.e. MELCOR code execution and data extraction processes, is run by a simulation driver, implemented in MATLAB (see Figure 3-17), which performs: (i) sampling generation (uniform sampling, DAKOTA interface to generate sampling for sensitivity and uncertainty analysis [2]); (ii) MELCOR Input file generation; (iii) execution of the MELCOR code on distributed computing network, which allows performing up to 60 simultaneous threads of calculations; (iv) adaptive refinement of the maximum time step and restarting in case of crashed calculations; (v) extraction of the data to the database of solutions and post-processing of the results.

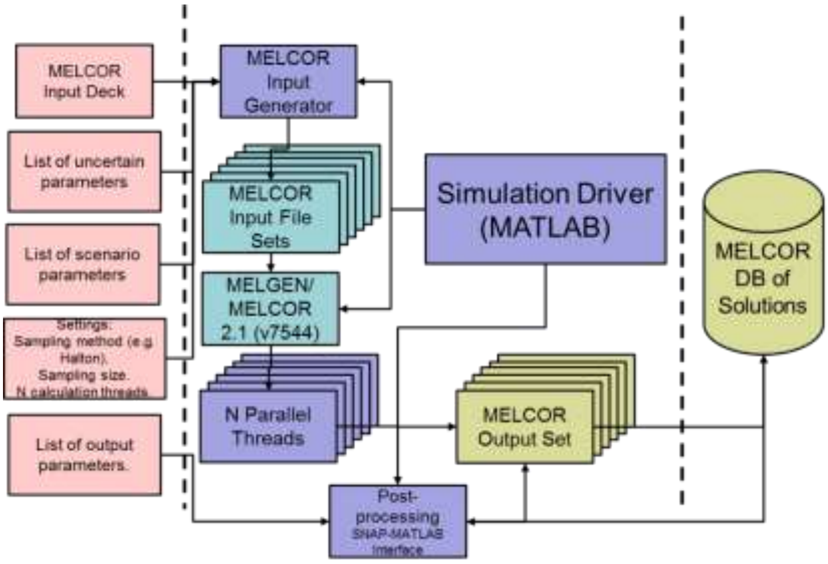

Figure 3-17: Simulation Driver Information Flow

3.3.4 Core Relocation Analysis Results Using MELCOR code

3.3.4.1 The Effect of Severe Accident Scenario on the Properties of Relocated Debris in LP

The analysis of the effect of severe accident scenario and possible recovery actions using different MELCOR code versions has been performed [83],[86]. A data base of full model solutions has been generated using MELCOR code versions 1.86 (rev2911), 2.1(rev7544) and 2.2(rev9541). Summary of the results are presented in this section.

3.3.4.1.1 Properties of Relocated Debris in LP

Figure 3-18 - 3-20, 3-26 and 3-27 present the summary of the results obtained with MELCOR versions 1.86 rev2911 [85], [83],[374], MELCOR 2.1 rev7544 and MELCOR 2.2 rev9544 [86],[87].

The results show that the total amount of the debris in LP and its properties are highly sensitive to the timing of safety systems activation, e.g. if the recovery of onsite or external grid can be provided within ~5000 seconds after the initiating event then the massive relocation into the LP can be avoided by a latter activation of ADS system. A delay in activation of ADS can significantly delay massive core relocation into the LP, and results in a greater extent of core oxidation (see Figure 3-26a,b); ECCS is effective in preventing massive core relocation only within a relatively small time window after activation of ADS.

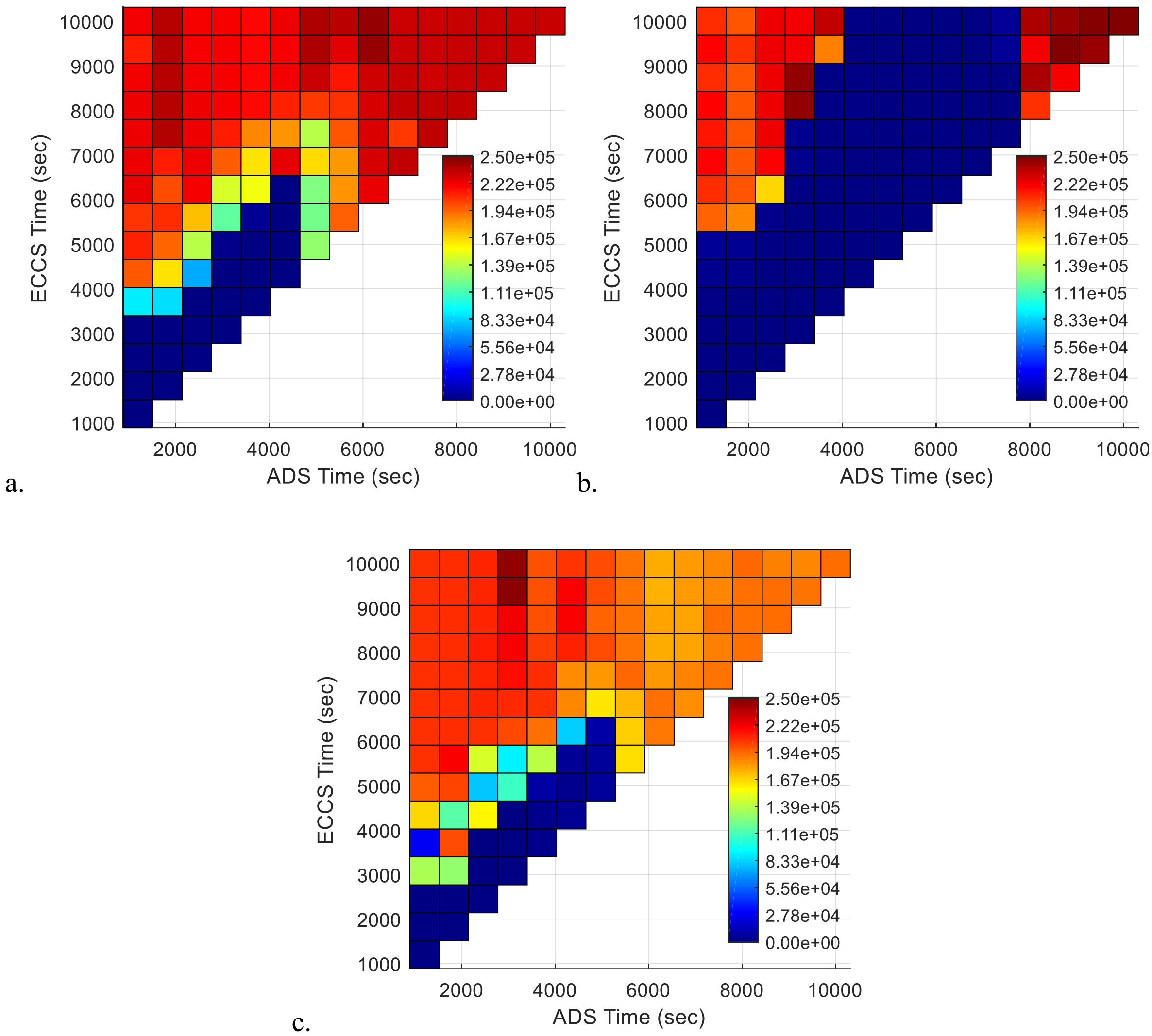

Figure 3-18. Debris Mass in Nordic BWR Lower Plenum at T_{tr} as a function of ADS time and ECCS time obtained with (a). MELCOR 2.1. (b). MELCOR 2.2. (c) MELCOR 1.86.

The results also show that there is significant difference between MELCOR code version 2.2 rev9541, compared to MELCOR 2.1 rev7544 and MELCOR 1.86 rev2911. The results obtained with MELCOR code versions 1.86 and 2.1 look very consistent between each other and the small differences in predictions can be explained by the different values of sensitivity coefficients being used and the differences in fuel failure modelling [339],[338],[342].

MELCOR 2.2 (see Figure 3-18b) predicts a very small mass of the debris in LP for the scenarios with late depressurization (ADS time in the range of ~4500-9000sec) and late reflooding, in these scenarios the accident progression is stopped in the core region, and the debris are retained above the core support plate (see Figure 3-19b). The results presented in Figure 3-19 show that there is significant difference in predictions of the time of core support plate failure between MELCOR code versions 2.2 compared to 2.1, 1.86. The fraction of scenarios with core support failure is significantly lower in MELCOR 2.2 (~30% of the cases,) compared to MELCOR 1.86/2.1, which is also reflected in the fraction of scenarios with large debris mass in the LP –

predicted by the MELCOR code versions 2.1 and 1.86 in comparison to version 2.2 (see Figure 3-20a).

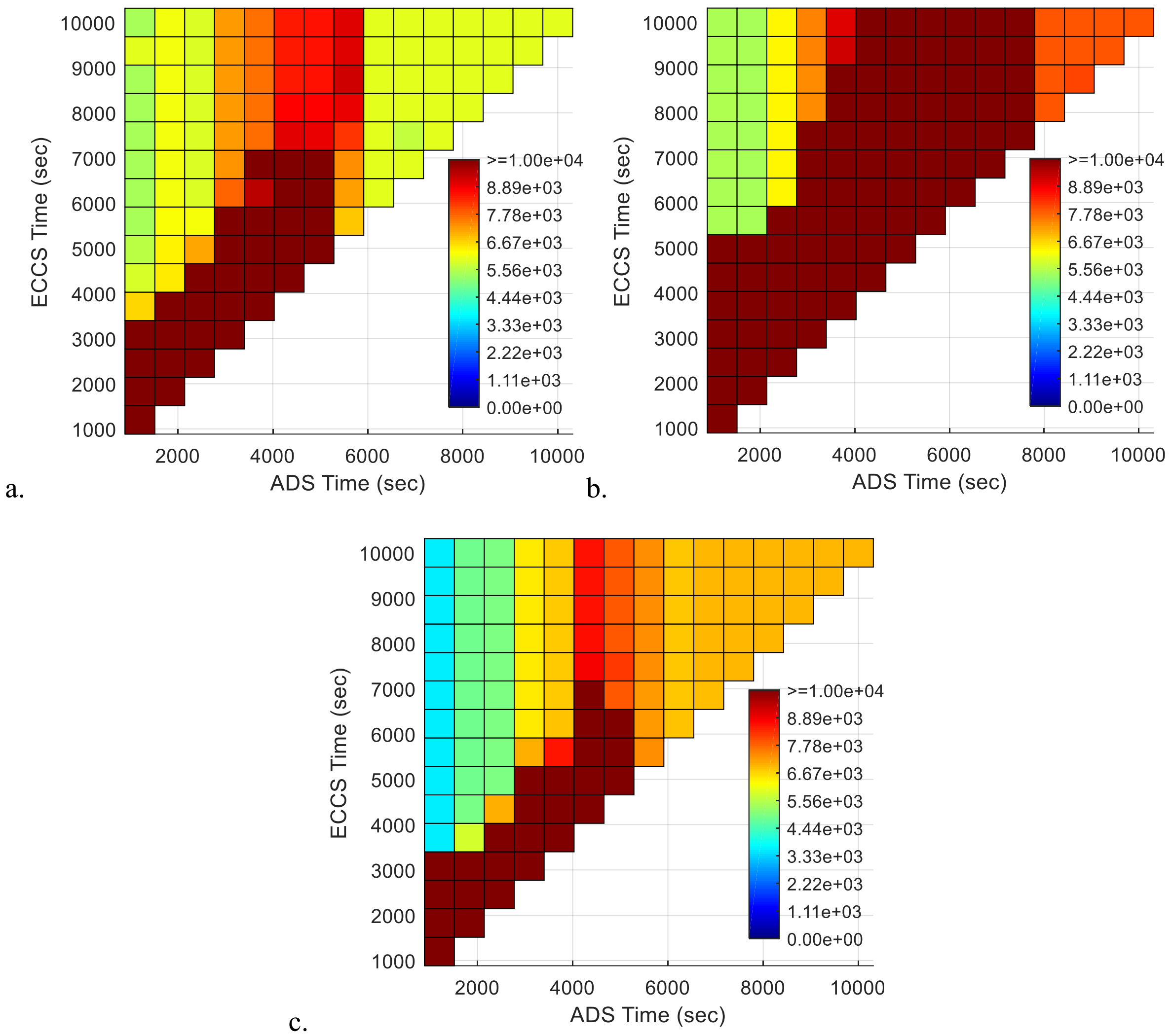

Figure 3-19. Time of core support plate failure as a function of ADS time and ECCS time obtained with (a). MELCOR 2.1. (b). MELCOR 2.2. (c) MELCOR 1.86.

MELCOR 2.2 predicts that in the scenarios with late depressurization (in the range of ~4000-7000 sec, see Figure 3-19b) and reflooding it is possible to stop the accident progression in the core region, and prevent relocation into the LP. We performed a comparison of two identical cases with MELCOR 2.2 and 2.1. Figure 3-24a taken from the domain where the discrepancy in the results between MELCOR 2.1 and 2.2 is observed. We have found that one of the possible explanations is a change in the process of early core degradation between the MELCOR code versions 1.86/2.1 compared to 2.2. In particular, it is assumed in MELCOR 1.86/2.1(rev prior to 7864) that when a canister fails and forms particulate debris (PD) in a cell and it melts and tries to candle to the cell below where PD may not exist, it will candle onto fuel rods, which freezes metallic Zr onto fuel rods which then oxidizes and leads to earlier failure of fuel rods. In MELCOR 2.2 (in revisions after 7864), it is assumed that it is more physical to expect candling of the canisters onto canisters (canisters facing channel (CN) and/or canisters facing bypass (CB)) located below (if they exist). This assumption reduces the cliff-edge effect in the rod failure due to canister failure and respectively reduces variance in solutions due to numerical effects (see reference [373] for details). Figure 3-21 shows the difference in the mass of Zr conglomerate on fuel cladding (CL) and canister (CN+CB) as predicted by MELCOR 2.1 rev7544 and MELCOR 2.2 rev9541.

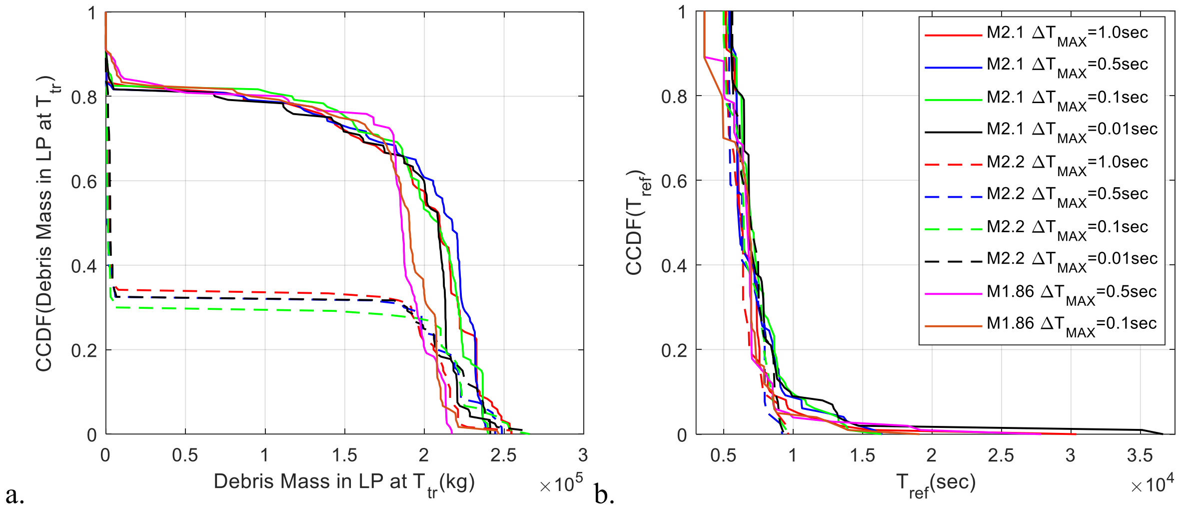

Figure 3-20. Complimentary Cumulative Distribution Function of (a) Debris Mass in LP at T_{tr}; (b) T_{tef} – Time of the core support plate failure.

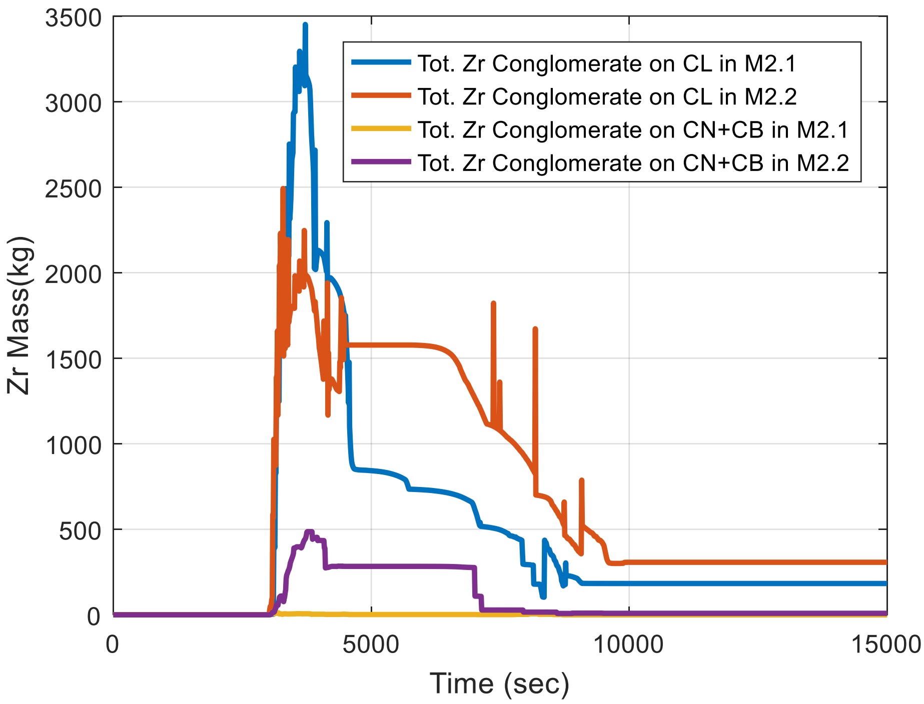

Figure 3-21. Total mass of Zr conglomerate on cladding (CL) and canister (CN+CB) in MELCOR 2.1 and MELCOR 2.2.

Another possible reason that can contribute to the discrepancy in the results is the change in the Lipinski dryout model, that is not used above the core support plate in MELCOR 2.2 (all revisions after 7874, see [373] for details), which may result in higher convective heat removal rate from the core in MELCOR 2.2 compared to MELCOR 1.86/2.1 (see Figure 3-22 and Figure 3-23). However, additional analysis is necessary to confirm this hypothesis.

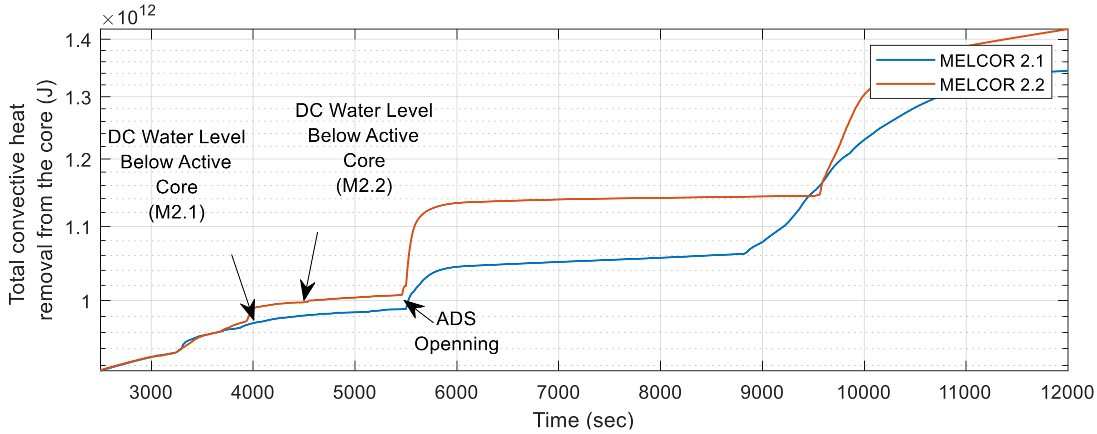

a.

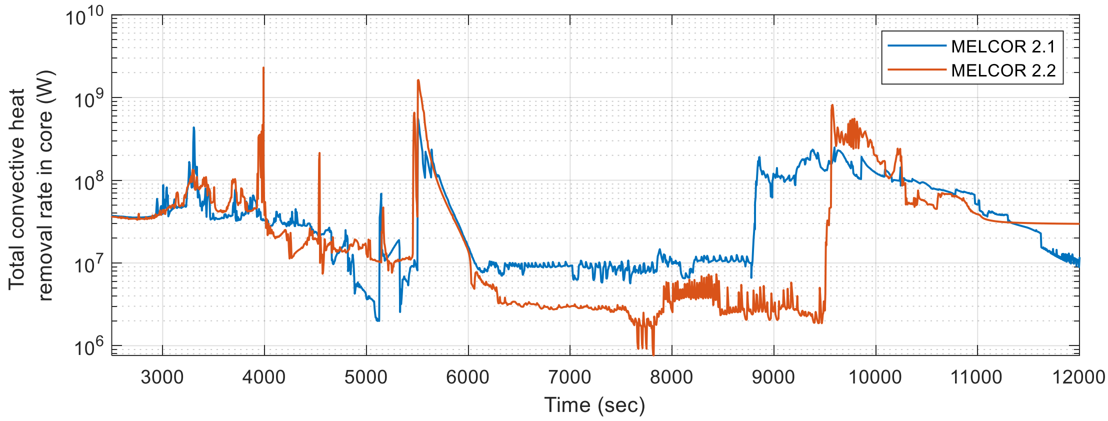

b.

Figure 3-22. MELCOR 2.1 and 2.2 predictions of (a) Total convective heat removal from the core (J); (b) Total convective hear removal rate in core (W).

Figure 3-24a shows the core damage state at 8800sec (time of core support plate failure in MELCOR 2.1) as predicted by MELCOR 2.2 and Figure 3-24b as predicted by MELCOR 2.1. Furthermore, there is considerably larger mass of the debris resting on the top of the core support plate in the latter case predicted by MELCOR 2.1. Larger mass of the debris results in significantly higher structural and thermal loads on the core support plate.

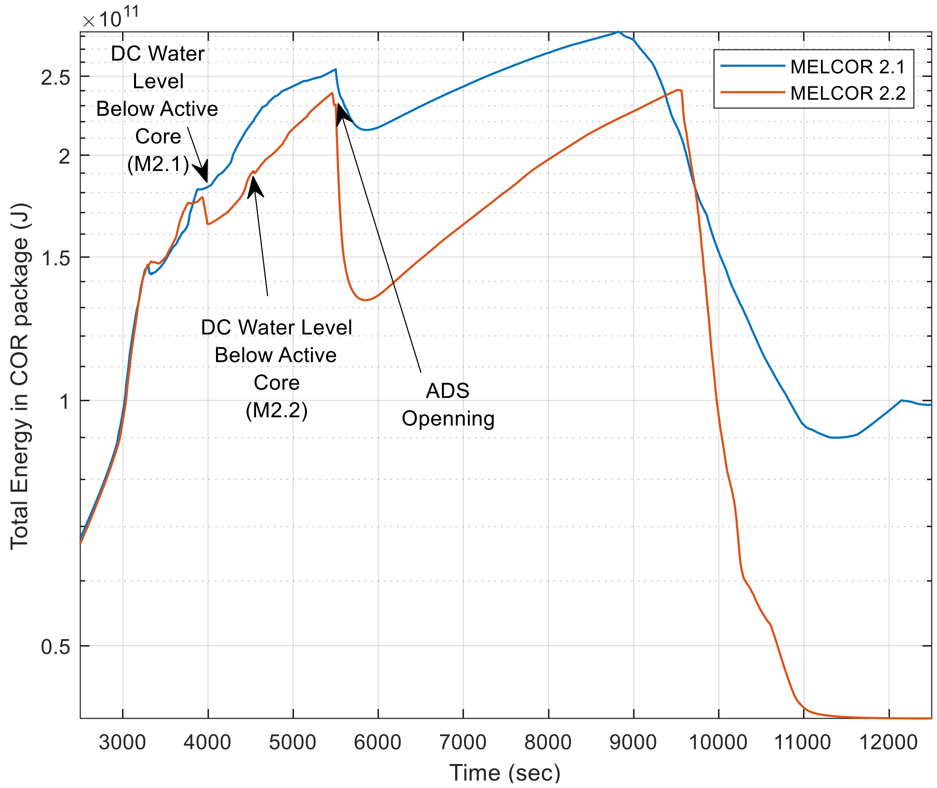

Figure 3-23. MELCOR 2.1 and 2.2 predictions of Total Energy in COR package (J)

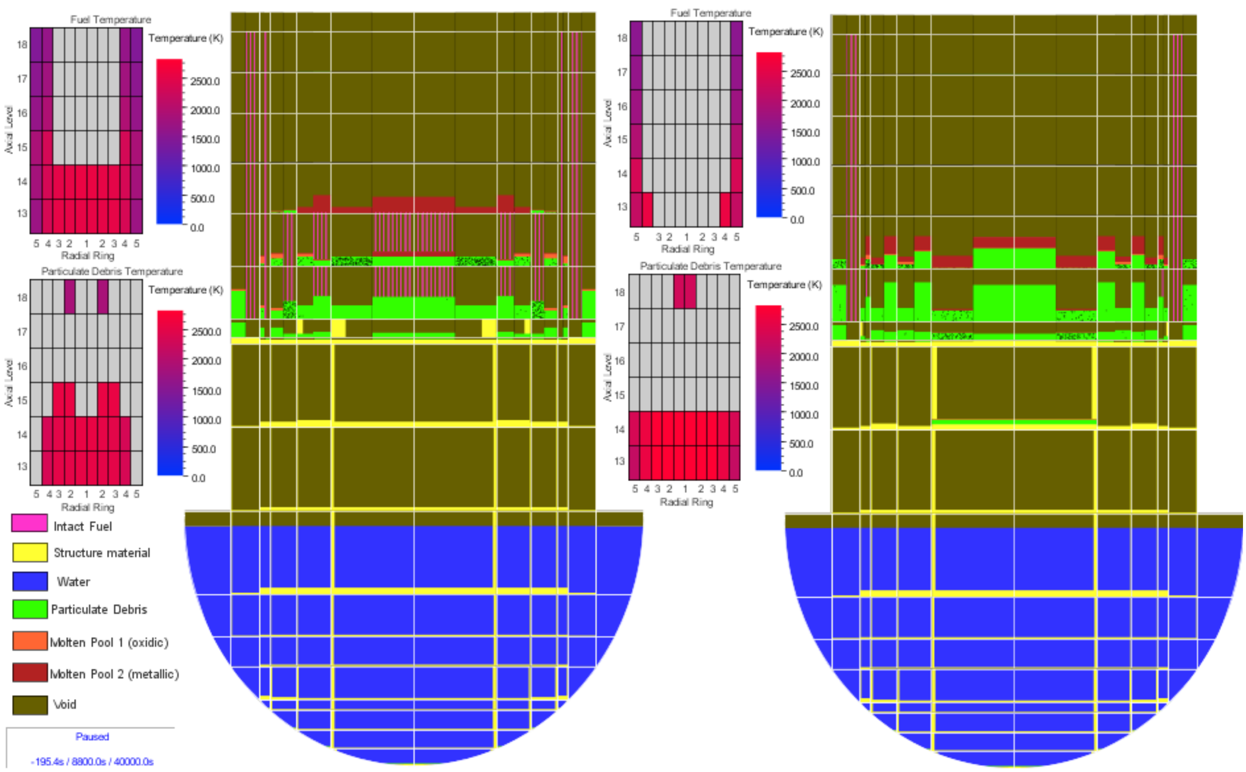

Figure 3-24. Core damage state for scenario with ADS Time = 5500 sec, ECCS Time = 9500sec at 8800sec with (a) MELCOR 2.2; (b) MELCOR 2.1;

Figure 3-25a,b – illustrate the core damage state as predicted by (a) MELCOR 2.2 (b) MELCOR 2.1 at 12400sec (i.e. 3600sec after initial core support plate failure in case (b)). Fuel and particulate debris temperature plots in Figure 3-25a – show that after reflooding, the debris resting on core support plate are quenched and accident progression is stopped in the core region - which indicates the effect of Lipinski dryout model (debris are in coolable configuration), while in Figure 3-25b the major part of core materials has relocated into the LP.

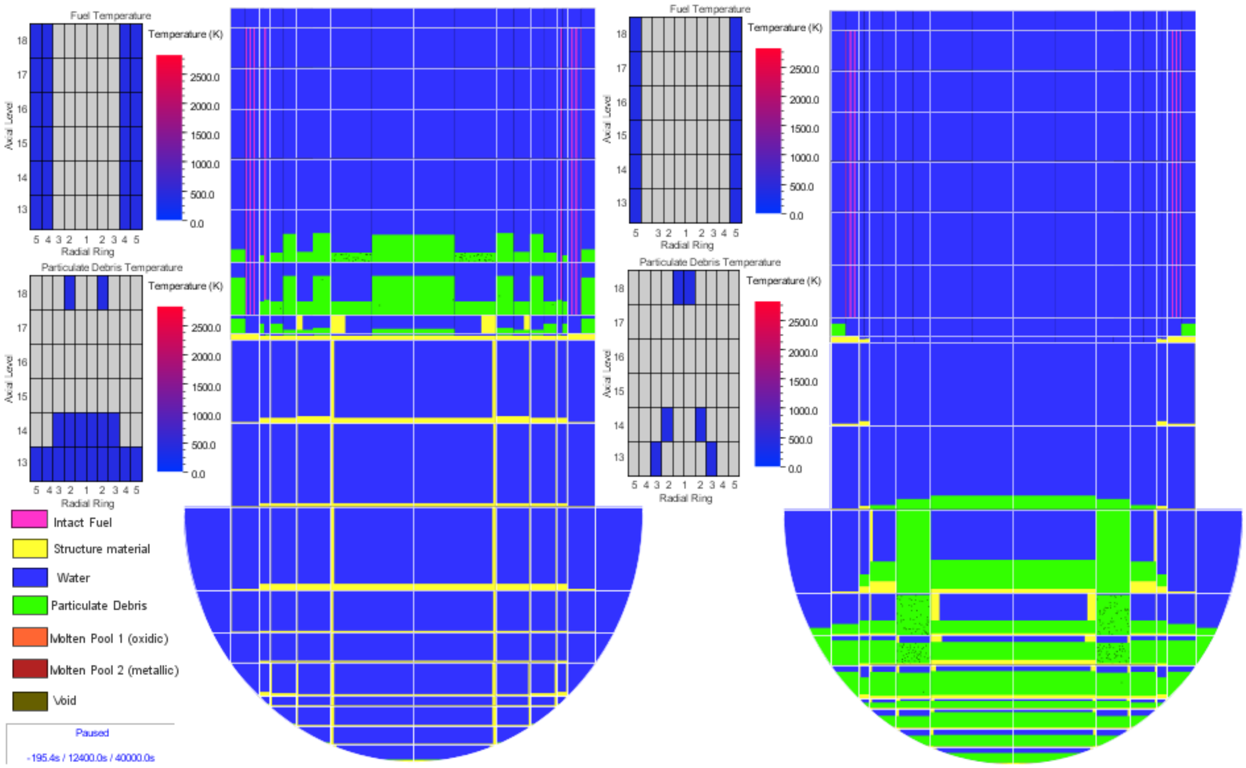

a. b.

Figure 3-25. Core damage state for scenario with ADS Time = 5500 sec, ECCS Time = 9500sec at 12400sec with (a) MELCOR 2.2; (b) MELCOR 2.1;

Figure 3-27 presents the complimentary cumulative distribution function of the hydrogen mass generated during the accident for the whole scenario domain. The results obtained with different code versions and different time steps are, in general, consistent between each other. The differences in predictions of the hydrogen mass between MELCOR 1.86 and 2.1/2.2 can be explained by the differences in the modelling of fuel failure. MELCOR 2.1/2.2 uses more advanced “time-at-temperature” fuel rod collapse model. It was developed in SOARCA studies to address cliff-edge behavior in fuel rod collapse that used fixed failure temperature threshold. “Time-at-temperature” model assumes that fuel assemblies collapse when they have been exposed to a temperature for a fixed amount of time. The period of time required to collapse a fuel assembly decreases with increasing temperature [342],[347]. Thus, “time-at-temperature” model results in longer periods of time during which the intact core structures are exposed to oxidation, which result in larger values of hydrogen mass generated.

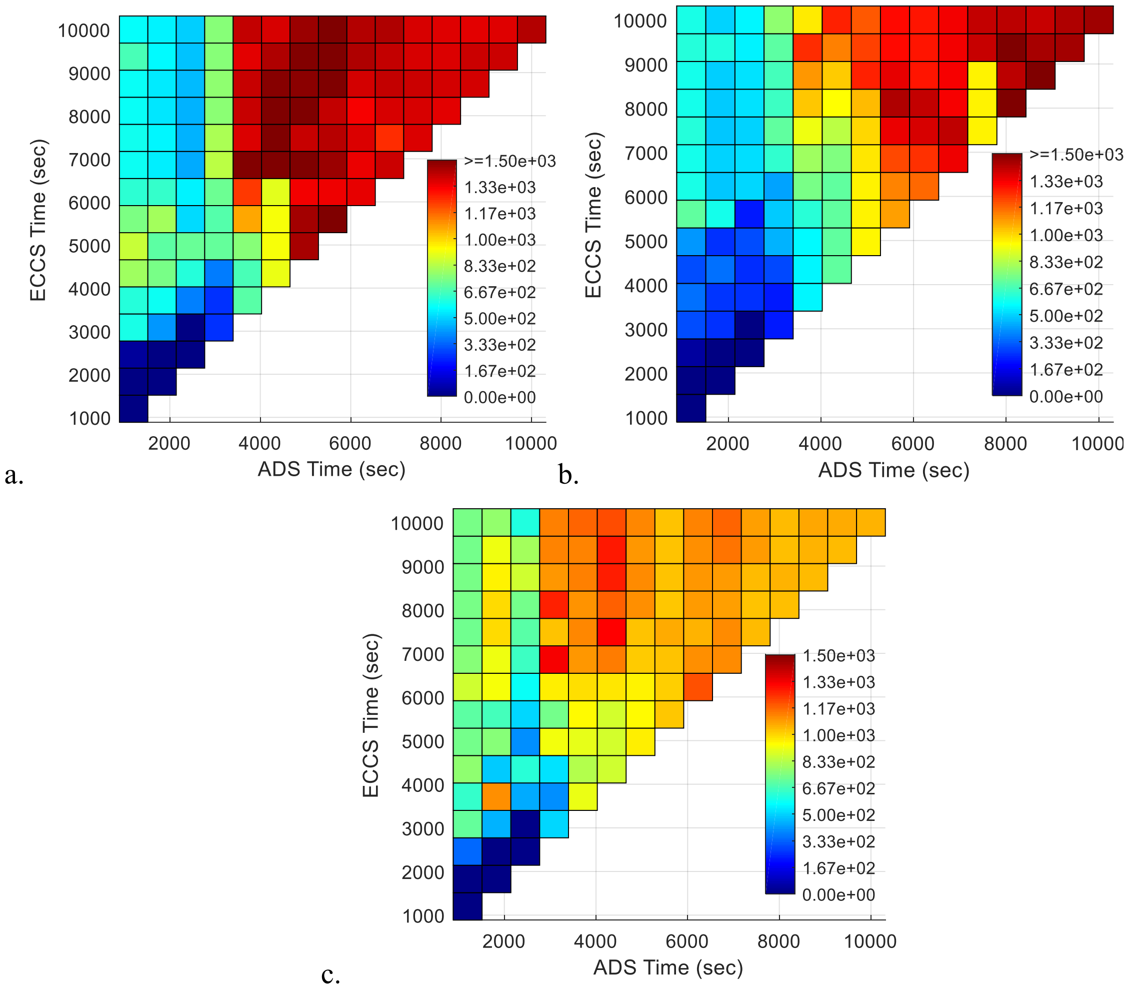

Figure 3-26. Hydrogen mass generated during the accident as a function of ADS time and ECCS time obtained with (a). MELCOR 2.1. (b). MELCOR 2.2. (c) MELCOR 1.86.

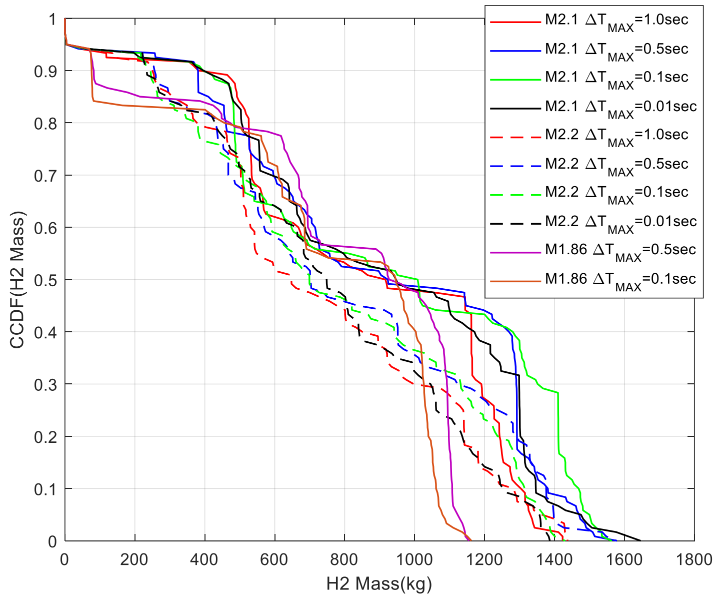

Figure 3-27. Complimentary Cumulative Distribution Function of Hydrogen Mass Generated During the Accident.

3.3.4.1.2 Debris Composition

Figure 3-28 shows the metallic debris fraction in the LP as a function of ADS and ECCS activation time. The timing of ADS activation has a major apparent effect on the fraction of metallic debris and the amount of hydrogen produced in the scenarios with large mass of relocated debris. In scenarios with late ADS activation the major amount of hydrogen is generated during slow recession of water level in the core region. The process of core degradation follows the TMI-like "wet-core" scenario in which the core is exposed to oxidation for a longer period, resulting in higher oxide fraction in the debris (see Figure 3-26).

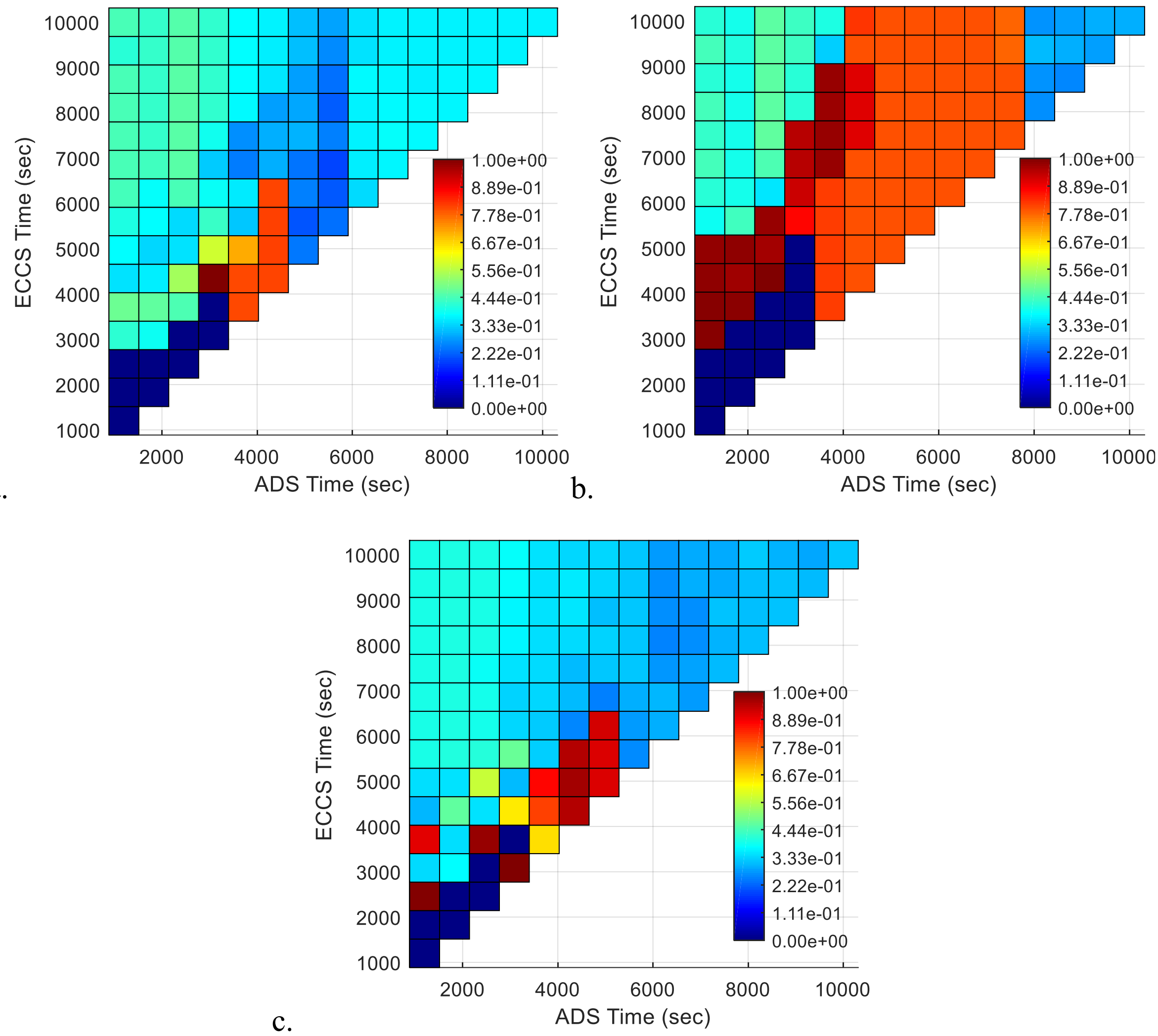

Figure 3-28. Metallic Debris Fraction in LP as a function of ADS time and ECCS time obtained with (a). MELCOR 2.1 rev7544. (b). MELCOR 2.2. (c) MELCOR 1.86.

In Figure 3-28b MELCOR2.2 predicts the domain with very large metallic fraction (red domain - over 70%) which corresponds to scenarios with very small debris mass (below 20 tons). In such scenarios molten materials (mostly metallic), e.g. control rode blades, drain from the core through the openings in the core support plate. The temperature of LP debris in such scenarios gradually decreases with time, since there is no heat generating materials. In the scenarios with late depressurization (in the range of ~4000-7000 sec.) and late reflooding MELCOR 2.2 predicts that the accident progression is stopped in the core region without massive relocation into the LP, the debris in these scenarios are resting on the top of the core support plate and in coolable configuration (see Figure 3-25a).

3.3.4.2 Sensitivity Analysis for Severe Accident Progression and LP Debris Properties

Sensitivity analysis using Morris method [195] has been performed for a couple of representative cases that represent typical behavior for scenarios with early and late depressurization and late water injection [83], [87]. Morris method is a method for global sensitivity analysis. The guiding philosophy of the Morris method [195] is to determine which factors may be considered to have effect, on model outputs, which can be considered as either negligible, linear or non-linear with other factors. The experimental plan proposed by Morris is composed of randomized experiments evaluating the impact of changing "one-factor-at-a-time" [235] (see references [195], [235] for more details).

Full model sensitivity analysis has been performed for a couple of representative scenarios for large relocation domain with a) small metallic debris fraction (Case B (ADS Time – 8000sec, ECCS Time – 8500sec) – 246 cases have been simulated) b) high metallic debris fraction (Case A (ADS Time – 2500sec, ECCS Time - 8500 sec) – 246 cases have been simulated) (see Figure 3-29, 3-31, 3-32, 3-34 – Pearson and Spearman correlation coefficients, scaled Morris μ - $\bar{\mu}$ and Morris σ - $\bar{\sigma_i} = {}^{\sigma_i}/_{\mu_i}$ [235], and – descriptive statistics in Table 3-3).

Sensitivity Analysis Results with MELCOR 1.86

For the analysis with MELCOR 1.86 we selected 5 parameters that can affect the properties of relocated debris in LP. The list with names and correspondent ranges of the parameters selected for MELCOR sensitivity study is presented in the Table 3-2. Total debris mass, hydrogen mass in containment, metallic fractions in the first and second axial levels and time of onset of massive relocation to LP were taken as response functions in this analysis.

Table 3-2: Selected MELCOR parameters and their ranges.

Parameter name	Range	Units
Maximum Time Step (MTS)	[0.001-2.0]	sec
Particulate Debris Porosity (PDPor)	[0.3-0.5]	-
Velocity of falling debris (VFALL)	[0.01-1.0]	m/s
LP Particulate debris equivalent diameter (DHYPDLP)	[0.002-0.005]	m
Oxidized fuel rod collapse temperature (TRDFAI)	[2500-2650]	K

- Maximum time step (MTS) – specified in executive (EXEC) package, MELCOR calculates its system time step based on directives from the packages, but it cannot take time steps greater than the maximum time and smaller than the minimum time step specified in EXEC package. It has been previously shown in [340],[341], that the MELCOR time step has quite significant effect on the results and lack of time step convergence of the solution with reduction of maximum time step. For the analysis we selected the range [0.001-2.0]sec, however this time step can be reduced by the simulation driver in case of crashed calculations.

- Particulate debris porosity (PDPor) – Porosity of particulate debris for all cells in specified axial level.
- Lower Plenum Particulate debris equivalent diameter (DHYPDLP) - MELCOR idealizes particulate debris beds as fixed-diameter particulate spheres.
  - The extent of debris coolability depends among others on the space between the particles. The porosity of randomly packed spheres is found to be approximately 40 % independent of particle size both by experiments and sophisticated computational methods [344]. The range of entrained particle size is considered to be 1-5 mm based on TMI-2 data [343].
  - Based on [342], [185] – the following ranges for porosity of particulate debris [0.3-0.5] and LP particulate debris equivalent diameter [0.002-0.005]m were selected.
- Velocity of falling debris (VFALL) - the debris is assumed to fall with a user-specified velocity. This allows the debris to lose heat to surrounding water in the lower plenum as it falls to the lower head, following failure of the core support plate in each radial ring. Based on [342] and [345], [346] the following range for this parameter has been selected – [0.01-1.0](m/s).
- Oxidized fuel rod collapse temperature (TRDFAI) - The temperature at which intact fuel rods are assumed to transition from rod-like geometry to a rubble form can affect the core degradation progression. MELCOR 1.86 default value is 2500K [345], [346], which represents the combined effects of eutectic interactions and fractured nature of irradiated fuel pellets. In MELCOR Best Practices as Applied in the State-of-the-Art Reactor Consequence Analyses (SOARCA) Project [342] it is suggested to use a new model for time to fuel rod collapse versus cladding oxide temperature, which range from 2500K(time to failure 1 hour) to 2600K(5 min). Within the scope of this work, the following range was used [2500-2650K].

Table 3-3: Descriptive statistics for the Case A and B.

	Mean value μ		Standard deviation σ		Min/Max Case A	Min/Max Case B
	Case A	Case B	Case A	Case B		
Debris mass (kg)	212930	134900	20690	36585	155940-264100	18752-215190
Hydrogen mass (kg)	851	1148	217	126	501-1545	969-1649
T_{ref}(sec)	5251	7515	234	2678	4510-5870	0-31000
Metallic debris fraction in 1st axial lvl.	0.48	0.35	0.12	0.12	0.25-0.79	0.13-0.97
Metallic debris fraction in 2nd axial lvl.	0.33	0.25	0.05	0.13	0.19-0.45	0.02-0.99
LDW Pool Temperature (K)	327.1	324	0.47	3.4	326.1-328.1	321-370
Containment Pressure (Bar)	2.6	3.46	0.14	0.25	2.21-3.08	3.17-3.75
LDW Pool Depth (m)	7.71	7.02	0.37	0.1	6.59-8.0	6.56-7.23

Figure 3-29 shows the sensitivity indices of the amount of relocated debris in LP to the modelling parameters in MELCOR. In most cases correlation coefficients are quite small indicating non-linear and non-monotonic dependencies. The results indicate that for the Case B, LP debris mass is largely influenced by TRDFAI (oxidized fuel rod collapse temperature), where larger values of TRDFAI will yield smaller debris mass (e.g. for TRDFAI = 2650K MELCOR predicts approximately 18 tons of debris in LP, while for TRDFAI = 2500K debris mass can reach 215 tons). Also, judging by Morris $\bar{\sigma}$ and correlation coefficients, there is a closer to monotonic dependency between TRDFAI and the resultant mass than that for the other parameters. Debris mass in LP predicted by MELCOR for the Case B ranges from 18 to 215 tons with mean value – 135 tons and standard deviation – 36.5 tons. For the Case A, debris mass in LP is in the range from 155 to 264 tons, with mean value – 212.9 tons and standard deviation – 20 tons (see Figure 3-30a). In case A, according to Morris method sensitivity analysis results, the most influencing parameters are particulate debris porosity (PDPor), falling debris velocity (VFALL which also has noticeable correlation coefficients suggesting closer to monotonic dependency) and oxidized fuel rod collapse temperature (TRDFAI), and, judging by $\bar{\sigma}$ values, all involved in non-linear interaction with other parameters. Note apparent minor contribution of the numerical factors, indicated by the sensitivity to the maximum time step (MTS).

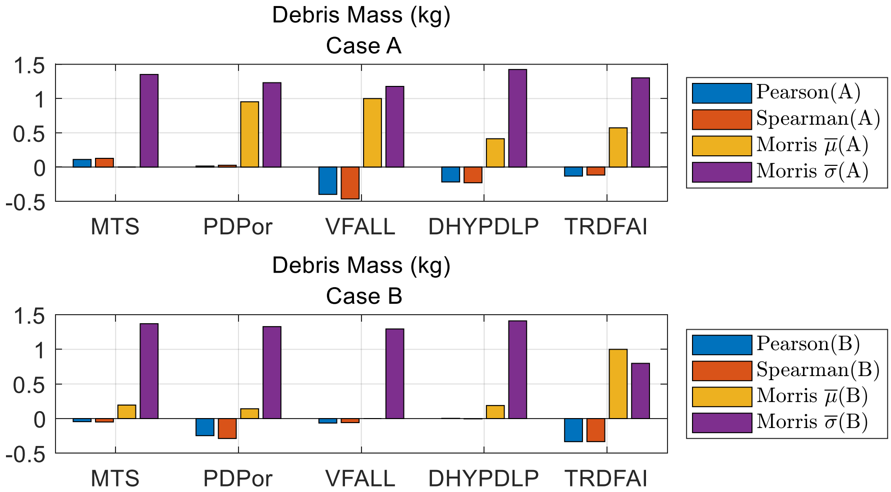

Figure 3-29: Sensitivity of debris mass in LP to modelling parameters in MELCOR.

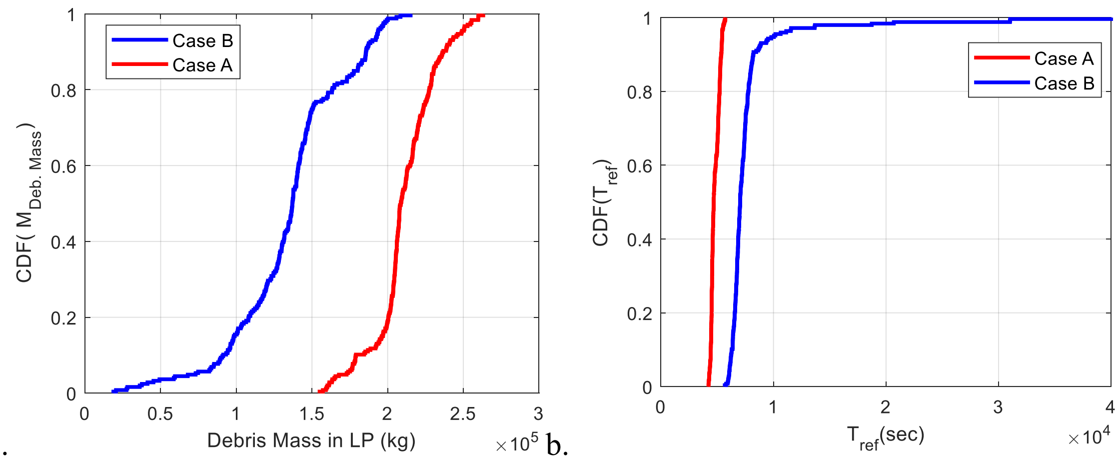

Figure 3-30: Cumulative distribution function (CDF) of (a) LP debris mass (kg) (b) T_{ref}- time of core support plate failure (sec).

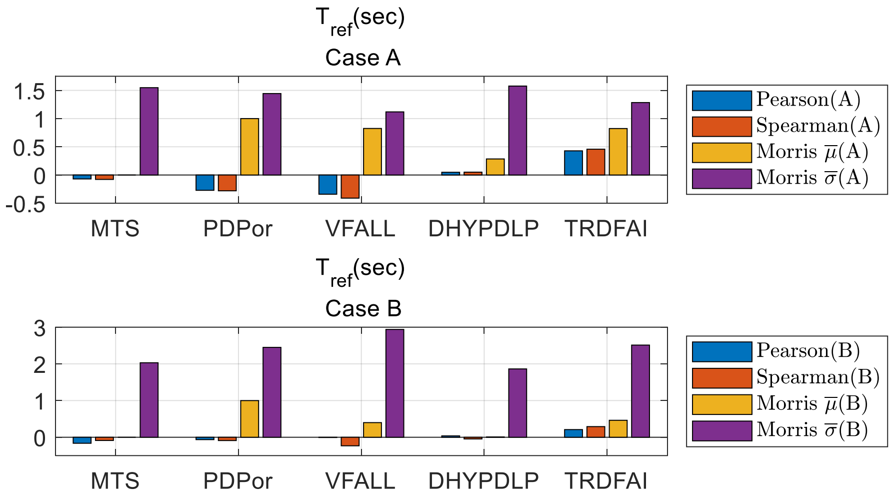

Figure 3-31: Sensitivity of timing of onset of massive core relocation to LP to modelling parameters in MELCOR.

Figure 3-31 shows the sensitivity indices of the time of massive relocation to LP (T_{ref}). For the Case B T_{ref} is largely influenced by particulate debris porosity (PDPor) and oxidized fuel rod collapse temperature (TRDFAI), as well as debris falling velocity (VFALL) – larger values of TRDFAI yield later fuel failure time, thus, delaying massive relocation to LP. It ranges from 40000 sec (i.e. no core support plate failure) to 5670 sec with mean value of ~7678sec and standard deviation of ~ 3350sec. For the Case A, T_{ref} lies within relatively small time window from 4510 to 5870 sec with mean value of 5251 sec and standard deviation 234 sec (see Figure 3-30b). The most influential factors are PDPor, TRDFAI and VFALL, however the overall uncertainty in T_{ref} is insignificant.

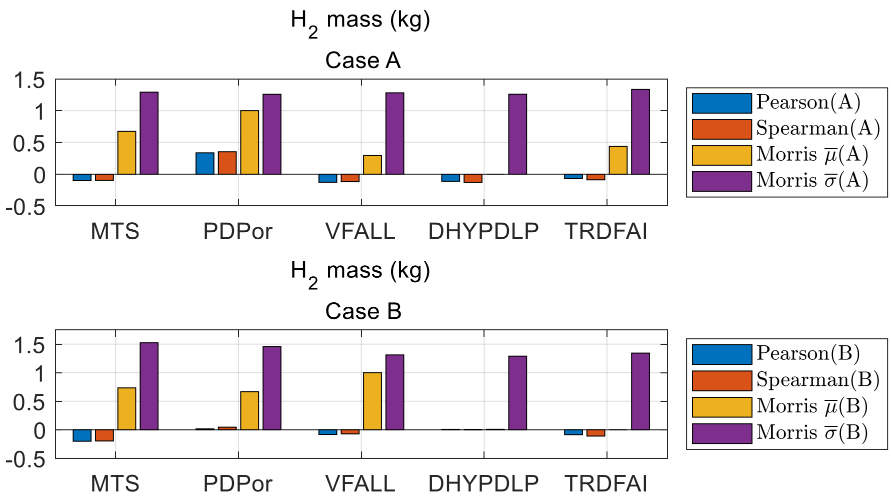

Figure 3-32: Sensitivity of hydrogen mass to modelling parameters in MELCOR.

Figure 3-32 shows the sensitivity indices of the amount of hydrogen produced during the accident to the modelling parameters in MELCOR. In Case B it ranges from 969 kg to 1649 kg, with mean value of 1148 kg and standard deviation 126 kg (see Figure 3-33a). The most important factors for hydrogen production are particulate debris porosity (PDPor) and debris falling velocity (VFALL). For the Case A, the hydrogen mass ranges from 501 to 1545 kg with mean value of 851 kg and standard deviation 218 kg (see Figure 3-33a). The most important factors for hydrogen production in Case A are PDPor, TRDFAI. Minimum time step (MTS) is among the influential factors in both cases. The results indicate that there is non-linear interaction between the parameters.

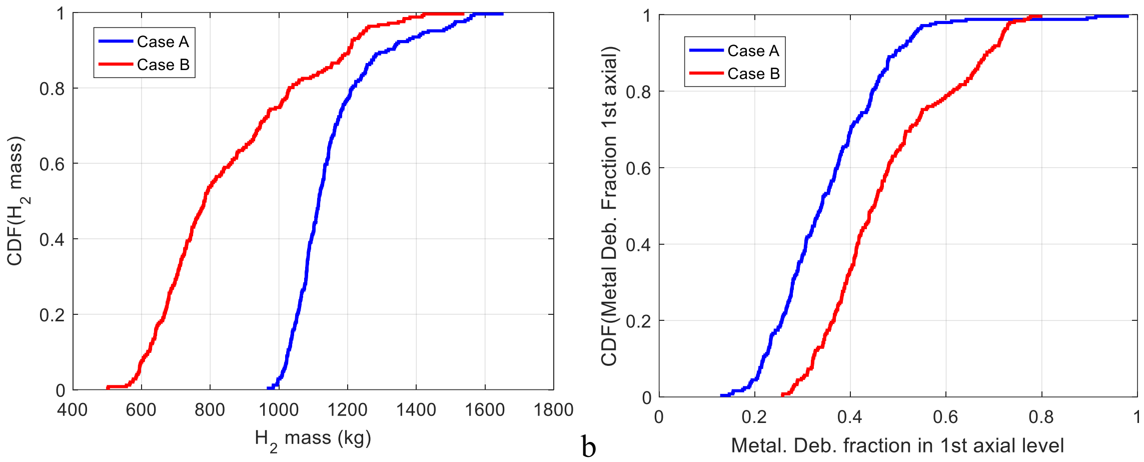

Figure 3-33: Cumulative distribution function (CDF) of (a) Hydrogen mass generated (kg) (b) Metallic debris fraction in the first axial level.

Figure 3-34 shows sensitivity indices of the metallic debris fraction in the first axial level to the modelling parameters in MELCOR. Metallic debris fraction in the 1st axial level ranges from 0.13-0.97 with mean value 0.35 and standard deviation 0.12 (scenarios with 0.97 metallic debris fraction corresponds to the cases where MELCOR does not predict core support plate failure and massive relocation to LP), and from 0.26 to 0.79 with mean value 0.48 and standard deviation 0.13 – for the Case B and A correspondingly. The most important factors for metallic debris fraction in the first axial level are VFALL for the Case A and VFALL, PDPor, DHYPDLP for the Case B.

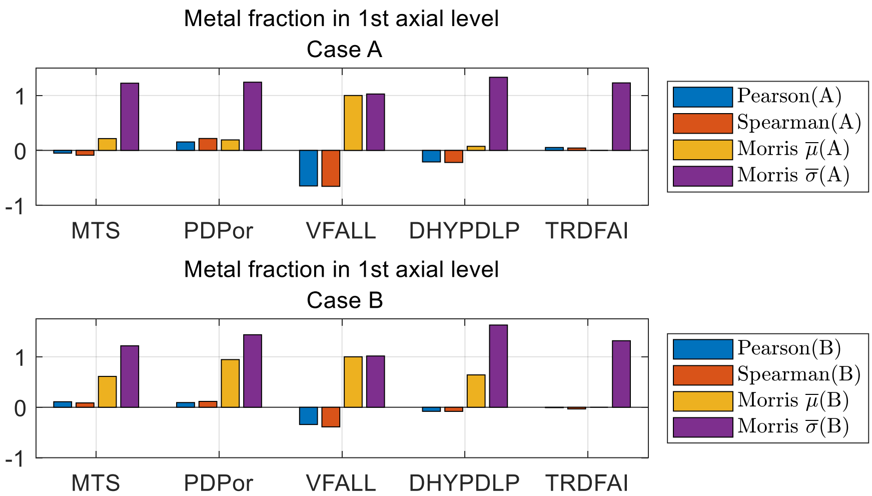

Figure 3-34: Sensitivity of metallic debris fraction in the 1st axial level to modelling parameters in MELCOR.

The results of sensitivity study can be summarized as follows:

- TRDFAI (oxidized fuel rod collapse temperature) – the temperature at which a transition from intact fuel rod geometry to a rubble form is assumed. There is quite significant influence of TRDFAI on the total amount of relocated debris (see Figure 3-29). This influence can be explained by the time (and respective generated heat) that is necessary to reach the fuel failure condition. With increase of TRDFAI it takes more time to heat up the fuel assemblies to the point at which they fail, convert into particulate debris, accumulate and cause support plate failure at certain time T_{ref} (as illustrated by the values of the correlations in Figure 3-29 and 3-31). The difference in relative importance of TRDFAI between Cases A and B (low and high pressure respectively) can be explained by different core heat up rates in these scenarios. The core heat up rate in Case A is higher (because there is no water in the core region) compared to Case B, therefore significance of TRDFAI is lower in Case A compared to Case B. TRDFAI has significant effect on the hydrogen production in Case A and B, where higher values of TRDFAI can result in longer periods of time during which the intact core structures are exposed to oxidation. However, the overall effect on the mass of hydrogen produced (see values of the correlation coefficients in Figure 3-32) is non-monotonic.
- PDPor (particulate debris porosity) – is defined for all cells in specified axial level. When structure failure criteria are reached the structures in the cell are converted into porous debris with the user defined porosity. Particulate debris in MELCOR are represented as spheres with an equivalent diameter. When debris relocates and joins a particulate debris bed in a computational cell, it is assumed that the volume of particulate debris increases and node porosity decreases [346], [345]. According to [346], the flow through the core node with particulate debris decreases along with the porosity, however MELCOR never completely blocks the flow. Reduced flow affects both, heat removal from the core and particulate debris by escaping steam, and core\debris oxidation rate (Figure 3-29, 3-31 and 3-32). Figure 3-29 indicates that PDPor has an important non-linear effect on LP debris bed formation, it might be due to: (i) steam flow through the core nodes with increased porosity increase oxidation (see Figure 3-32); (ii) additional steam generation in LP and cooling of outermost rings upon core support plate failure. The difference between Cases A and B can be explained by the effect of depressurization. In Case A, the water level after depressurization drops below the active core region, the uncovered core starts to heat up, eventually reaching the point where control rods\blades, canisters undergo degradation and relocate downwards to the core plate, where its either rest on top as PD, or refreezes as conglomerate, or flows through the openings into the lower plenum. The variation in PDPor, as a result will affect both, cooling of the core by escaping steam (see Figure 3-29 3-31) and core oxidation (see Figure 3-32). In Case B, the water level in core decreases gradually, so the relative importance of this parameter on steam flow rate through the core is lower, compared to the Case A, which can be observed in (Figure 3-29, 3-31 and 3-32). When it comes to core support plate failure (see Figure 3-31), it seems that larger PDPor values promote core cooling by escaping steam, but, on the other hand, enhance core oxidation and chemical heat production (especially for the Case A, where oxidation starts after water level dropped below active core bottom, so the results in Case A

are more sensitive to PDPor compared to the Case B), that may result in earlier degradation of the fuel assemblies and earlier failure of core support plate (T_{ref}), the extent of the effect of this parameter on core cooling\oxidation in different scenarios is also reflected in correlation coefficients in Figure 3-31. The effect of PDPor on the metallic debris fraction (see Figure 3-34) can be explained by the extent of core oxidation, since there is a clear distinction between Case A and Case B, which is quite evident in Table 3-3.

- DHYPD (Lower plenum particulate debris equivalent diameter) – MELCOR uses this parameter to calculate heat transfer surface area of the debris in LP, note that MELCOR equates the oxidation surface area to the heat transfer surface area of the node; so it should have an effect on the debris oxidation and steam generation rate. However, based on the results of sensitivity study the effect of this parameter within considered ranges on debris mass, hydrogen mass, time of core support plate failure was found to be smaller compared to the effect of the other parameters (Figure 3-29, 3-31 and 3-32). On the other hand, it might be involved in interaction with other parameters (e.g. PDPor and VFALL). Further analysis is necessary to determine the effect of particulate debris diameter and heat transfer coefficients in in-vessel debris quench model in MELCOR on the results. The effect of DHYPD on the metallic debris fraction in 1st axial level is yet to be explained.
- VFALL (velocity of falling debris) - MELCOR does not have a mechanistic model for debris dropping into the lower plenum. Instead a number user-specified parameters control the rate at which material relocates into the lower plenum and the effective heat transfer from and associated oxidation of the debris slumping into lower plenum water [346]. The effect of VFALL on the amount of the debris in LP (see Figure 3-29) can be explained by steam generation during core slumping that can affect both: steam cooling of core/core debris and enhanced oxidation. However, based on the results, it seems that the core slumping, together with its modelling parameters (such as VFALL, DHYPDLP and others) has different effect in different severe accident scenarios, e.g. in Case A the core heat up rate in the 1st, 2nd and 3rd radial rings is significantly higher compared to the periphery of the core (rings 4 and 5; ring 5 can also radiate a fraction of its decay heat to the shroud) – see Figure 3-35a, while in Case B, due to gradual coolant evaporation, the core heats up more evenly in all radial rings – see Figure 3-35b. Prior to core plate failure (T_{ref}) there is quite significant difference in fuel temperature in the 4th and 5th radial rings between Cases A and B (see Figure 3-35c, Figure 3-35d). The slumping of the core debris to lower plenum generates steam flow through the core, including outer rings, where it can i) provide steam cooling; ii) cause enhanced oxidation and chemical heat production, if the cladding temperature in the nodes exceeds oxidation cut-off threshold – 1100K. Further analysis of the effect of VFALL, PDPor, DHYPDLP on the flow and hydrogen generation in different radial rings and properties of relocated debris is necessary.

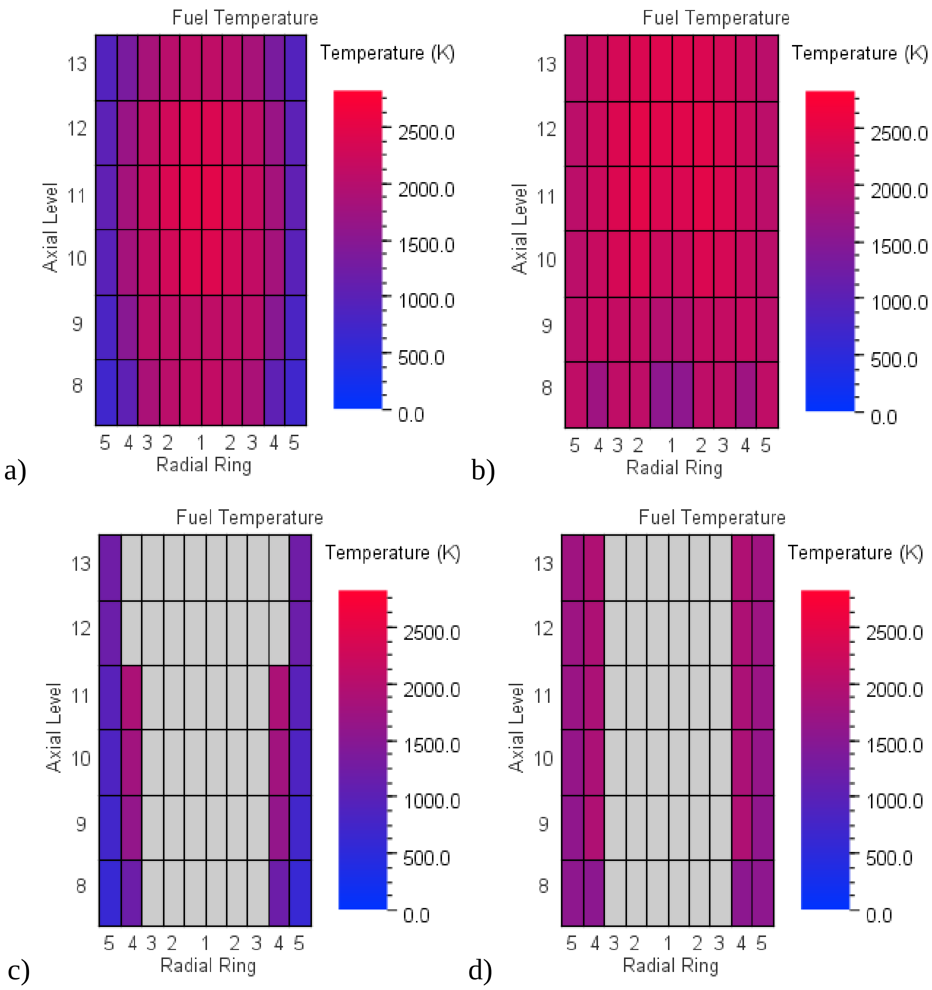

Figure 3-35: Core fuel temperature map prior to: onset of fuel rods failure for (TRDFAI equals to 2500K): a) Case A; b) Case B; core debris slumping to lower plenum (at T_{ref}) for c) Case A; d) Case B.

- MTS (Maximum time step) – based on the results of sensitivity study, MELCOR maximum time step has a very little impact on the mass of relocated debris and the time of core support plate failure, on the other hand, it has some non-negligible effect on the extent of core oxidation, which is linked to the amount of hydrogen produced (see Figure 3-32) and the metallic debris fraction (see Figure 3-34) – which can be caused by the complex non-linear interactions between physical models in MELCOR and their sensitivity to the time step.

Sensitivity Analysis Results with MELCOR 2.1 and 2.2

For the analysis with MELCOR 2.1/2.2 we selected 8 parameters that can affect the properties of relocated debris in LP. The list with names and correspondent ranges of the parameters selected for MELCOR sensitivity study is presented in the Table 3-4. Total debris mass, hydrogen mass in containment, metallic fractions in the different axial levels at the bottom of the vessel and time of onset of massive relocation to LP were taken as response functions in this analysis.

Table 3-4: Selected MELCOR parameters and their ranges.

Parameter name	Range	Units
Particulate Debris Porosity (PDPor)	[0.3-0.5]	-
Velocity of falling debris (VFALL)	[0.01-1.0]	m/s
LP Particulate debris equivalent diameter (DHYPDLP)	[0.002-0.005]	m
Molten Cladding (pool) drainage rate (SC11412)	[0.1-2.0]	kg/m-s
Molten Zircaloy melt break-through temperature (SC11312)	[2100-2540]	K
Time Constant for radial (solid) debris relocation (SC10201)	[180-720]	sec
Time Constant for radial (liquid) debris relocation (SC10202)	[30-120]	sec
Heat transfer coefficient from in-vessel falling debris to pool (CORCHTP)	[200-2000]	W/m2-K
Oxidized Fuel Rod Collapse Temperature (TRDFAI)	*	*

- Particulate debris porosity (PDPor) – Porosity of particulate debris for all cells in specified axial level.
- Lower Plenum Particulate debris equivalent diameter (DHYPDLP) - MELCOR idealizes particulate debris beds as fixed-diameter particulate spheres.
  - o The extent of debris coolability depends among others on the space between the particles. The porosity of randomly packed spheres is found to be approximately 40 % independent of particle size both by experiments and sophisticated computational methods [344]. The range of entrained particle size is considered to be 1-5 mm based on TMI-2 data [343].
  - o Based on [342], [185] – the following ranges for porosity of particulate debris [0.3-0.5] and LP particulate debris equivalent diameter [0.002-0.005]m were selected.
- Velocity of falling debris (VFALL) - the debris is assumed to fall with a user-specified velocity. This allows the debris to lose heat to surrounding water in the lower plenum as it falls to the lower head, following failure of the core support plate in each radial ring. Based on [342] and [339],[338] the following range for this parameter has been selected – [0.01-1.0](m/s).
- Heat transfer coefficient from in-vessel falling debris to pool (HDBH2O) – in MELCOR In-Vessel falling debris quench model, it is assumed that the debris fall with a user-specified velocity and heat transfer coefficient. This allows the debris to lose heat to surrounding water in the lower plenum as it falls to the lower head, following failure of the core support plate in each radial ring. Based on [342],[347] and [339],[338] the following range for this parameter has been selected – [200-2000](W/m2-K).
- Molten cladding (pool) drainage rate (SC11312) – used by candling model when molten material has just been released after holdup by an oxide shell or by a flow blockage (crust) [339],[338]. This sensitivity coefficient determine the maximum melt flow rate per unit width after breakthrough. In this study the following range was considered – (0.1-2.0 kg/m-s) [342],[347].
- Molten Zircaloy melt break-through temperature (SC11312) – this sensitivity coefficient is used to define the conditions for which molten material will be held up by an oxide shell. This sensitivity coefficient defined the maximum ZrO_2 temperature permitted to hold up molten Zr in cladding component (CL) in MELCOR code [339],[338]. In this study the following range was considered (2100-2500K) [342],[347].
- Time Constant for radial (solid\liquid) debris relocation (SC10201\SC10202) – Time constant for radial relocation of solid\liquid material.
  - o These parameters are responsible for leveling of particular debris and molten pools in Radial Relocation of Solid (SC1020-1) and Molten (SC1020-2)

materials. This model intended to simulate the gravitational leveling between adjacent core rings that tends to equalize the hydrostatic head in a fluid medium [339].

- In this study the following ranges were considered:
  - SC1020-1 - 180-720 sec [339],[338],[347].
  - SC1020-2 - 30-120 sec [339],[338],[347].

Oxidized fuel rod collapse temperature (TRDFAI) – the temperature at which intact fuel rods are assumed to transition from rod-like geometry to a rubble form [339],[338]. Results of the previous sensitivity study showed that the properties of relocated debris (total mass, time of the onset of core relocation to LP, etc.) are quite sensitive to the selection of the values of this parameter, especially in the cases with late depressurization [85]. Within this study more advanced "time-at-temperature" fuel rod collapse model has been used. It was developed in SOARCA studies to address cliff-edge behavior in fuel rod collapse that used fixed failure temperature threshold. "Time-at-temperature" model assumes that fuel assemblies collapse when they have been exposed to a temperature for a fixed amount of time. The period of time required to collapse a fuel assembly decreases with increasing temperature [342],[347].

The analysis of the effect of severe accident scenario and possible recovery actions [85],[83],[86] showed that the whole scenario domain consists of scenarios with (i) small relocation (below 20 tons) – characterized by small, mostly metallic debris mass, typically represented by scenarios with ADS activation within ~5000sec after initiating event and ECCS activation within relatively short time window after ADS); (ii) intermediate relocation – debris mass in LP is in the range of 20-100tons; (iii) large debris mass (>100 tons, debris composition and properties are highly influenced by severe accident scenario, typically represented by scenarios with late ECCS activation).

From the point of view of vessel failure mode analysis in ROAAM+ scenarios with large relocation mass contribute the most to the uncertainty in prediction of vessel failure mode [96], [293], [314].

Full model sensitivity analysis has been performed for a couple of representative scenarios for large relocation domain with a) early ADS (ADS Time – 1500sec) and late ECCS (ECCS Time – 10000sec) activation (Case A) b) late ADS (ADS Time (10000sec) and late ECCS (ECCS Time – 10000sec) activation (Case B). Table 3-5 and 3-6 present descriptive statistics of the results of sensitivity analysis for these representative cases from the large relocation domain with early (Case A) and late (Case B) ADS activation. In the analysis we used MELCOR 2.1 rev7544 (Table 3-5) and MELCOR 2.2 rev9541 (Table 3-6). Figures 3-36, 3-38, 3-40, 3-42 and 3-44 present Pearson and Spearman correlation coefficients, scaled Morris $\bar{\mu}$ (Morris μ values are scaled between 0 and 1, $\bar{\mu}$ – scaled separately for MELCOR 2.1 and 2.2; 3-37, 3-39, 3-41, 3-43 and 3-45 show $\bar{\mu}^*$ - scaled for combined results of MELCOR 2.1 and 2.2 to see relative importance of the parameters between two code versions) and Morris $\bar{\sigma_i} = {\sigma_i}/{\mu_i}$ [235]. Figure 3-36 shows the sensitivity indices of the amount of relocated debris in LP to the modelling parameters in MELCOR (2.1/2.2). Figure 3-37 indicates that relative importance of modelling parameters in MELCOR 2.2 is significantly higher compared to MELCOR 2.1. For example, particulate debris porosity (PDPor), molten zircaloy melt break-through temperature (SC1131-2), LP particulate debris equivalent diameter (DHYPDLP) – have almost twice as large values of $\bar{\mu}^*$ in MELCOR 2.2 compared to 2.1.

Table 3-5: Descriptive statistics for the Case A and B with MELCOR 2.1.

		Mean value μ **Standard deviation σ**		**Min** **Max**		**Skewness** **Kurtosis**	
		A	**B**	**A**	**B**	**A**	**B**
Debris mass (kg)		209773.36 19220.03	181655.64 37624.16	137373.20 261324.3	80772.82 260196.6	-0.31 4.26	-0.06 2.54
Metallic debris fraction		0.43 0.03	0.36 0.05	0.36 0.5	0.26 0.5	0.01 2.60	0.13 2.29
T_{ref}(sec)		5092.13 559.20	6882.19 905.14	3810.28 6050.1	4285.17 11050.1	-0.74 2.40	0.24 5.05
Hydrogen mass (kg)		583.47 135.83	1184.95 232.54	344.44 1008.1	792.49 1823.0	0.81 3.25	0.29 2.4
Metallic debris fraction in lvl	**1**	0.50 0.32	0.33 0.25	0.07 1.0	0.01 1.0	0.43 1.51	1.21 3.34
	2	0.01 0.02	0.01 0.01	0.00 0.2	0.00 0.1	4.68 33.2	6.65 61.7
	3	0.01 0.03	0.01 0.02	0.00 0.3	0.00 0.2	7.00 62.4	6.06 49.6
	4	0.36 0.12	0.29 0.13	0.11 0.8	0.10 0.8	1.06 4.78	1.14 4.43
	5	0.36 0.10	0.29 0.11	0.08 0.6	0.09 0.7	0.37 3.0	0.62 3.1
	6	0.36 0.10	0.32 0.13	0.12 0.6	0.06 0.7	0.15 2.44	0.37 2.68
	7	0.44 0.13	0.41 0.16	0.12 0.7	0.07 1.0	0.02 2.30	0.31 3.43

Table 3-6: Descriptive statistics for the Case A and B with MELCOR 2.2.

		Mean value μ **Standard deviation σ**		**Min** **Max**		**Skewness** **Kurtosis**	
		A	**B**	**A**	**B**	**A**	**B**
Debris mass (kg)		215722.44 26115.07	189982.17 52635.61	145404.72 278770.2	1171.99 290046.1	-0.25 3.56	-0.90 4.47
Metallic debris fraction		0.43 0.03	0.36 0.05	0.35 0.5	0.22 0.5	-0.08 2.81	0.00 2.50
T_{ref}(sec)		5186.08 797.30	7424.08 1304.18	3735.10 7025.0	0.00 9960.0	0.08 2.04	-2.97 18.44
Hydrogen mass (kg)		602.27 173.03	1231.48 263.86	315.45 1143.9	762.53 2115.4	0.89 3.22	0.28 2.57
Metallic debris fraction in lvl	**1**	0.52 0.32	0.29 0.22	0.0 1.0	0.0 1.0	0.18 1.46	1.40 4.46
	2	0.01 0.02	0.01 0.02	0.00 0.2	0.00 0.2	5.41 38.68	9.26 105.81
	3	0.02 0.04	0.01 0.03	0.00 0.3	0.00 0.3	6.08 45.52	5.77 43.43
	4	0.39 0.15	0.34 0.16	0.04 0.9	0.09 1.0	0.76 3.52	1.13 4.80
	5	0.36 0.10	0.31 0.13	0.14 0.7	0.12 1.0	0.71 4.06	1.81 8.30
	6	0.38 0.10	0.29 0.14	0.18 0.6	0.04 1.0	0.33 2.73	1.90 9.18
	7	0.45 0.13	0.37 0.18	0.18 0.9	0.09 1.0	0.41 2.93	1.12 4.66

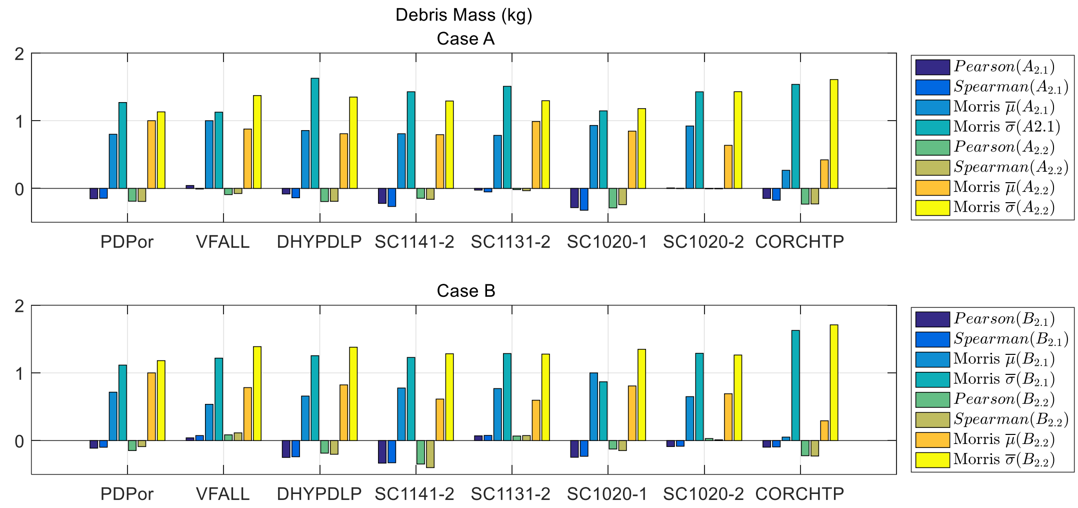

Figure 3-36: Sensitivity of debris mass in LP to modelling parameters in MELCOR (2.1,2.2)

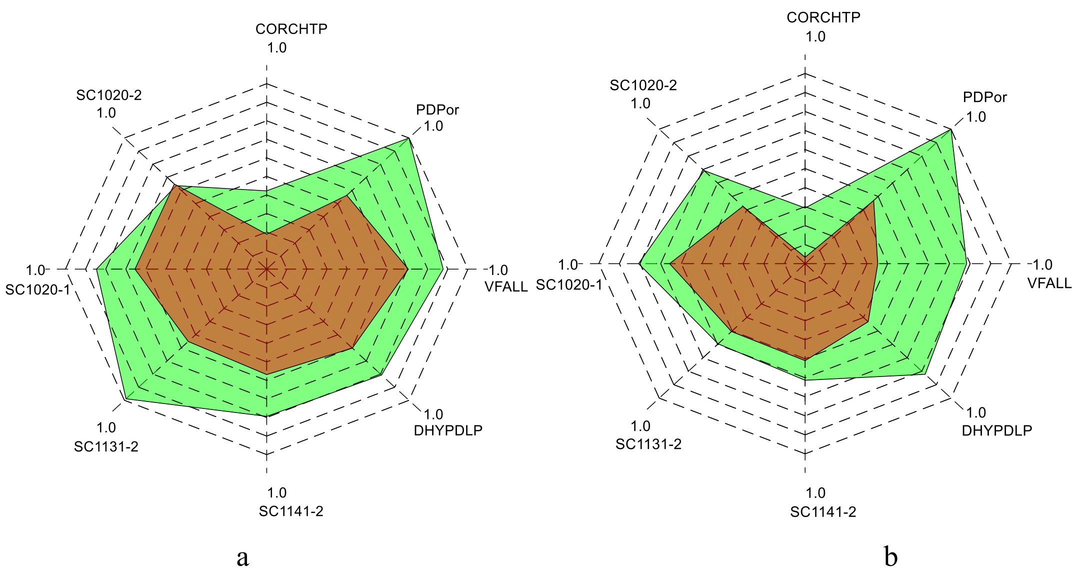

Figure 3-37: Scaled Morris $\bar{\mu}^*$ values for the Debris Mass in LP obtained with MELCOR 2.1(red) and MELCOR 2.2(green) (a) Case A; (b) Case B

The importance of modelling parameters also depends on severe accident scenario, e.g. in case A (with MELCOR 2.1) the most influential parameters are VFALL, SC1020-1 and SC1020-2, DHYPDLP; in MELCOR 2.2 the most influential parameters are PDPor, SC1131-2, VFALL. In scenario with late depressurization (case A) the parameters that affects LP debris mass are (i) in MELCOR 2.1 – SC1020-1, SC1131-2, SC1141-2; (ii) in MELCOR 2.2 – PDPor, SC1020-1; VFALL and DHYPDLP. In general, the results indicate that for the Case A all MELCOR modelling parameters (both versions 2.1/2.2), with exception to heat transfer coefficient from in-vessel falling debris to pool (CORCHTP), have relatively high values of scaled Morris $\bar{\mu}$, however, judging by standard deviation and kurtosis values (see Table 3-5 and 3-6) overall effect of these parameters on the variance is relatively small. In case B due to variability in MELCOR modelling parameters, the LP debris mass can change in the range 81-260 tons in

MELCOR 2.1, and 12-290tons in MELCOR 2.2; both distributions have negative skewness and slight excess kurtosis – which might indicate fatter tails of the distribution.

Figure 3-38 show the sensitivity indices for the metallic debris fraction in-vessel (core region and lower plenum). In case A and B most of the parameters have relatively high importance according to Morris $\bar{\mu}$ values, except heat transfer coefficient from in-vessel falling debris to pool (CORCHTP). Large Morris $\bar{\sigma_l}$ values indicate that parameters in this study involved in non-linear interactions between each other. It is important to note that in Case A, the fraction of metallic debris is distributed within relatively narrow range from ~0.35-0.5 for MELCOR 2.1 and 2.2. In case B the fraction of metallic debris is distributed in the range from 0.26-0.5 in MELCOR 2.1 and from 0.22-0.5 in MELCOR 2.2.

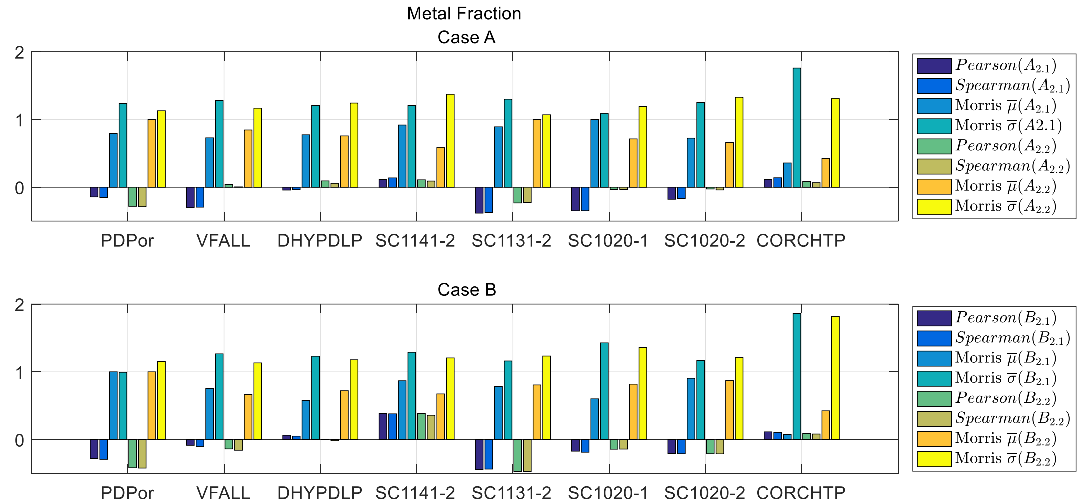

Figure 3-38: Sensitivity Metallic Debris Fraction to modelling parameters MELCOR 2.1,2.2

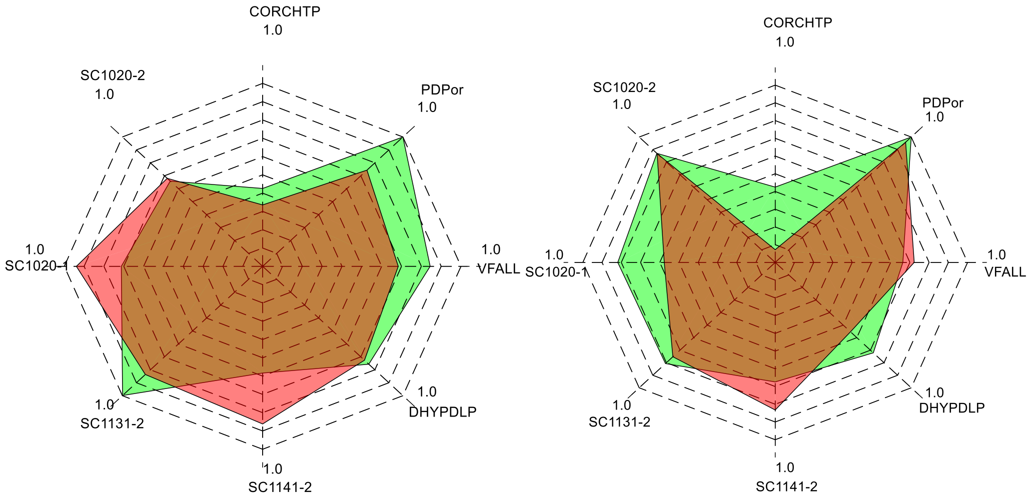

a b

Figure 3-39: Scaled Morris $\bar{\mu}^*$ values for the Metallic Debris Fraction obtained with MELCOR 2.1(red) and MELCOR 2.2(green) (a) Case A; (b) Case B.

The relative importance of MELCOR modelling parameters in MELCOR 2.1 and 2.2, according to Figure 3-39, is almost similar, with exception to the effect of PDPor, SC1141-2 and SC1131-2 in scenario with early depressurization.

Figure 3-40 and 3-41 presents the results of sensitivity of the time of core support plate failure to modelling options in MELCOR. The relative importance of modelling parameters depends on MELCOR code version being used and severe accident scenario. For example, in Case A with MELCOR 2.1 the most influential parameters are SC1141-2, SC1020-1, DHYPDLP; while in MELCOR 2.2 the most influential parameters are PDPor, SC1141-2, SC1131-2 – which is also reflected in Figure 3-41a. In Case B with MELCOR 2.1 – the most influential parameters are PDPor, SC1141-2, SC1131-2; while with MELCOR 2.2 the most influential parameters are DHYPDLP, SC1020-1, PDPor – however the overall impact on the results due to variability of these parameters is significantly higher in MELCOR 2.2 (see Figure 3-41b). Large Morris $\bar{\sigma_i}$ values indicate that parameters in this study involved in non-linear interactions between each other.

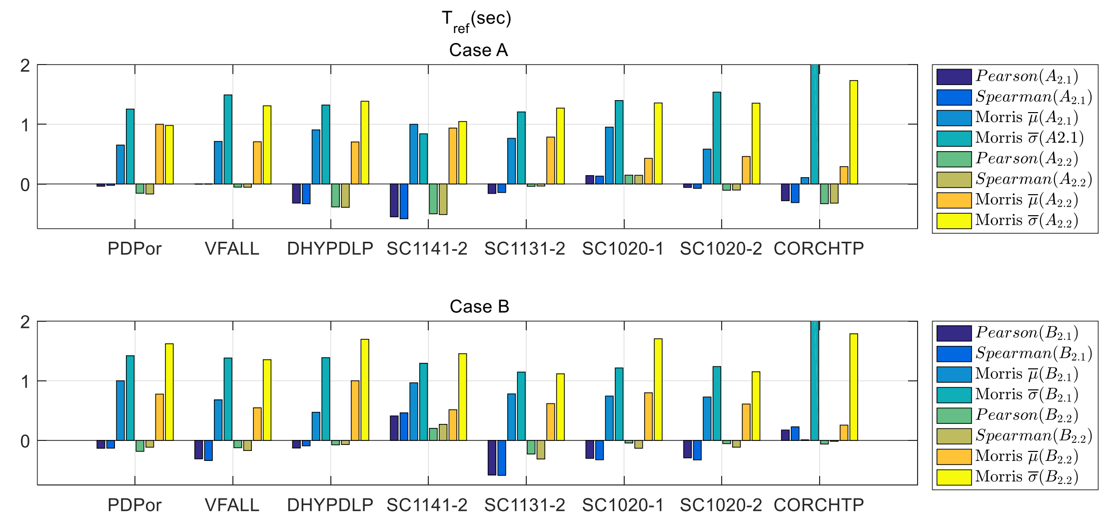

Figure 3-40: Sensitivity of Time of Core Support Plate Failure to modelling parameters in MELCOR (2.1, 2.2)

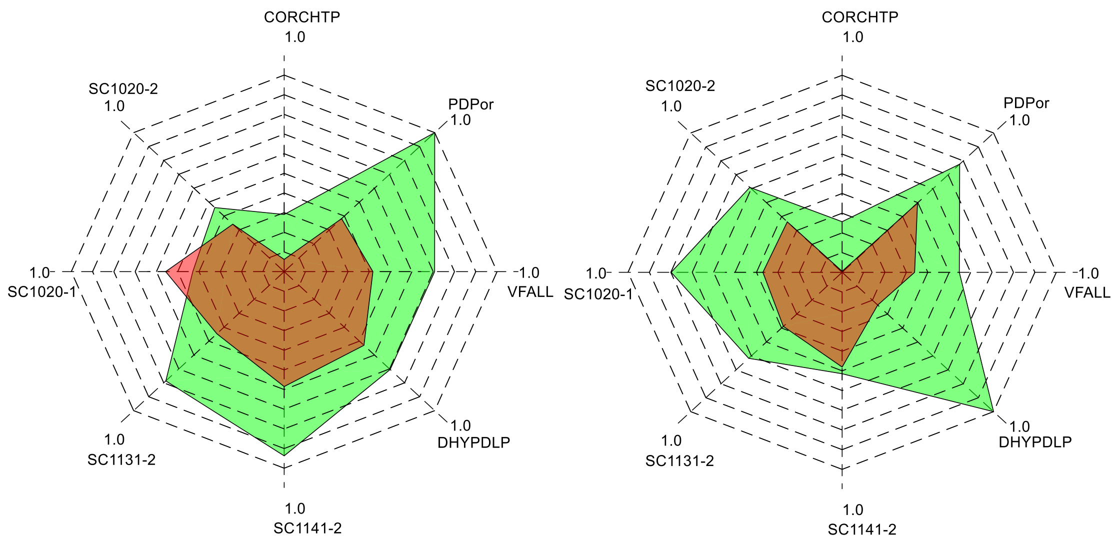

a b

Figure 3-41: Scaled Morris $\bar{\mu}^*$ values for the Time of Core Support Plate Failure obtained with MELCOR 2.1(red) and MELCOR 2.2(green) (a) Case A; (b) Case B

The time of core support plate failure in case A ranges from ~3700-6000sec and ~3800-7000sec in MELCOR 2.1 and 2.2 correspondingly. In case B it ranges from ~4200-11000sec in MELCOR 2.1 and from 0.0-10000sec (where $T_{ref} = 0$ indicates no core support plate failure, accident stopped in core region). The relative importance of the modelling options is very different in MELCOR 2.1 and 2.2.

Figure 3-42 show sensitivity indices of Hydrogen generated during the accident to modelling options in MELCOR 2.1/2.2. In case A the hydrogen mass is mostly influenced by PDPor in MELCOR 2.1, while in MELCOR 2.2 – the most influential parameters are SC1141-2, SC1131-2 and PDPor. In case B the most influential parameter is SC1131-2 in MELCOR 2.1 and 2.2 and, judging by Figure 3-43b the relative importance of this parameter in MELCOR 2.1 in slightly higher compared to MELCOR 2.2. The total amount of hydrogen generated during the accident in case A is distributed between ~300-1000kg in MELCOR 2.1 and 2.2; and between ~800-1800/2200kg in MELCOR 2.1/2.2.

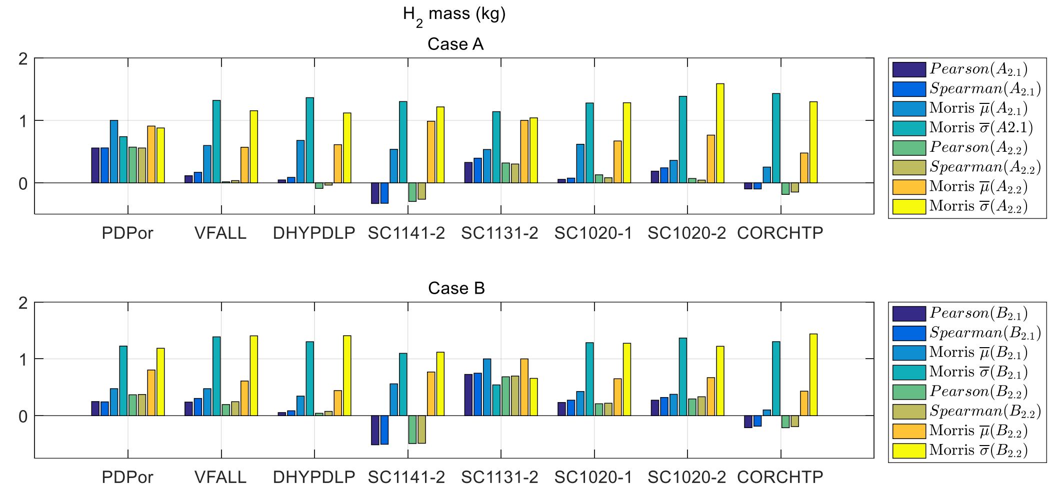

Figure 3-42: Sensitivity of Hydrogen Mass generate during the accident to modelling parameters in MELCOR (2.1, 2.2).

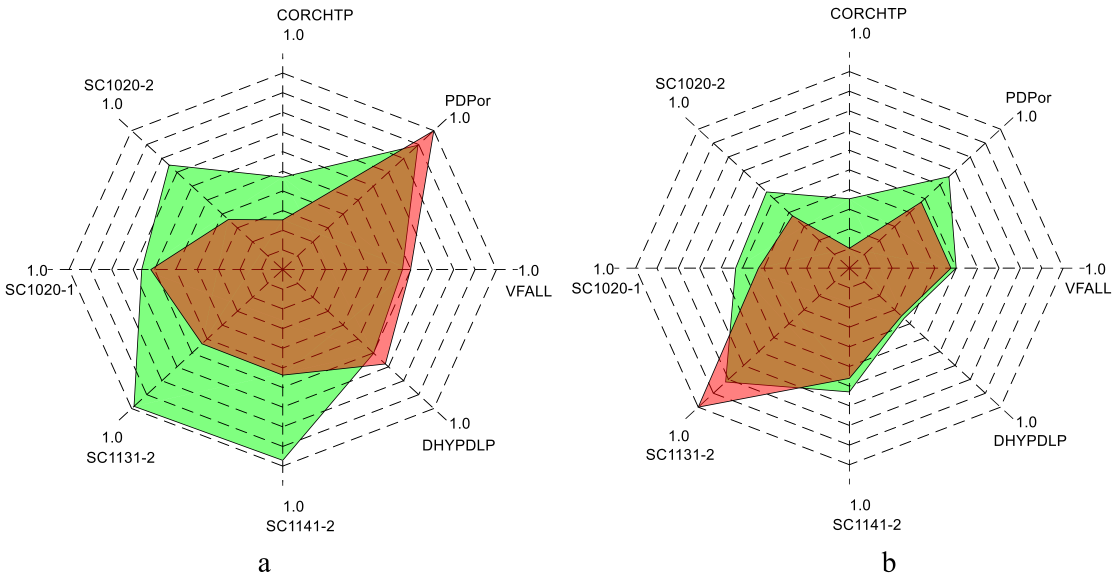

Figure 3-43: Scaled Morris $\bar{\mu}^*$ values for the Hydrogen mass generated obtained with MELCOR 2.1(red) and MELCOR 2.2(green) (a) Case A; (b) Case B

According to Figure 3-43b the relative importance of modelling parameters in MELCOR 2.1 and 2.2 are quite similar between MELCOR versions 2.1 and 2.2, while in case A (see Figure 3-43a) it differs significantly, both the most influential parameters and their contribution to the variance in hydrogen mass generated.

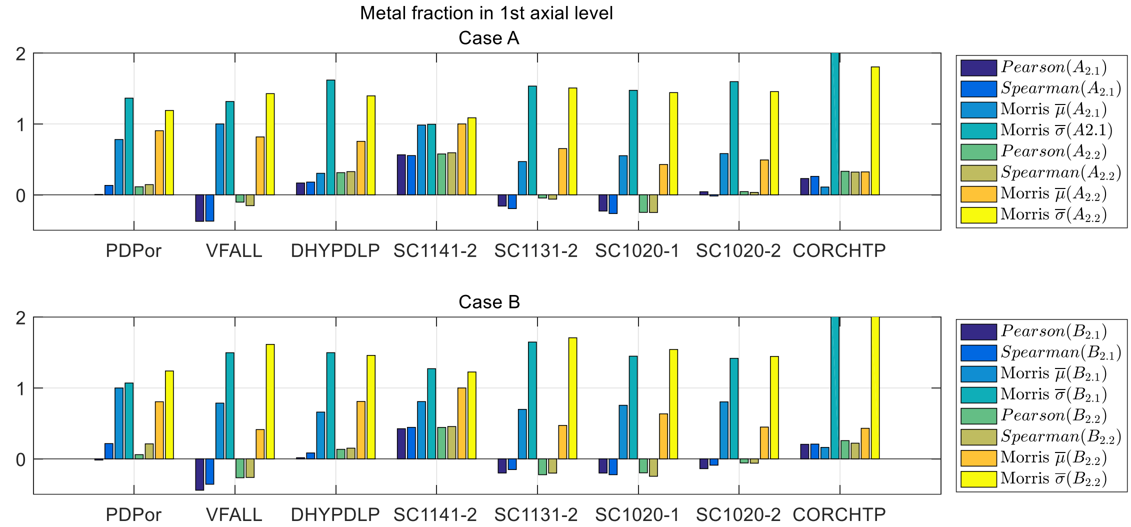

Figure 3-44: Sensitivity of Metallic Debris Fraction in the 1st axial level to modelling parameters in MELCOR (2.1, 2.2)

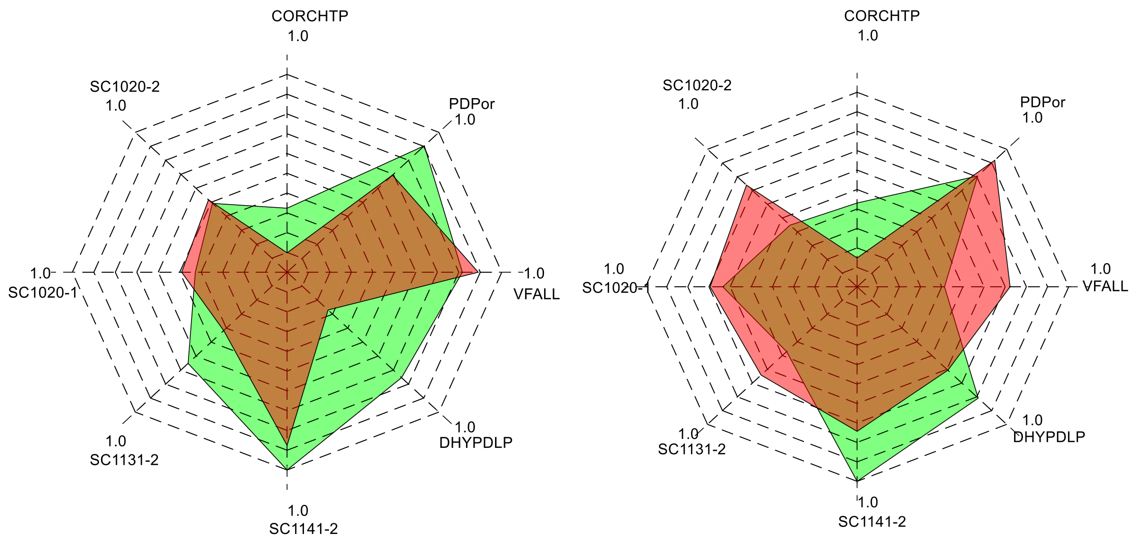

a b

Figure 3-45: Scaled Morris $\overline{\mu}^*$ values for the Metallic Debris Fraction in 1st axial level obtained with MELCOR 2.1(red) and MELCOR 2.2(green) (a) Case A; (b) Case B

Figure 3-44 shows the sensitivity indices of Metallic debris fraction at the 1st axial level (approximately 20cm from the bottom of the LP – corresponds to IGT nozzles welding points). In case A the most influential parameters are VFALL and SC1141-2 in MELCOR 2.1, and SC1141-2 and PDPor in MELCOR 2.2. In case B the most influential parameter are PDPor, SC1141-2 and SC1020-2 in MELCOR 2.1, and SC1141-2, DHYPDLP and PDPor in MELCOR

2.2. Metallic debris fraction in the 1st axial level is distributed from ~0.1-1.0 in MELCOR 2.1, and from 0.0-1.0 in MELCOR 2.2 for both cases with early and late depressurization. All distributions have positive skew (left-leaning) and positive excess kurtosis in case B – which might indicate fatter tails of the distribution; and negative excess kurtosis in case A, which indicate that the distribution have several peaks (e.g. beta distribution with $\alpha = \beta = 0.5$, kurtosis ~1.5).

Particulate Debris Porosity (PDPor) – is defined for all cells in specified axial level. When structure failure criteria are reached the structures in the cell are converted into porous debris with the user defined porosity. Particulate debris in MELCOR are represented as spheres with an equivalent diameter (DHYPDLP). When debris relocates and joins a particulate debris bed in a computational cell, it is assumed that the volume of particulate debris increases and node porosity decreases [339],[338]. According to [338], the flow through the core node with particulate debris decreases along with the porosity, however MELCOR never completely blocks the flow. Reduced flow affects both, heat removal from the core and particulate debris by escaping steam, and core\debris oxidation rate (see Figure 3-42). It is important to note that MELCOR 2.1 and 2.2 use different default values of SC1505-1 – minimum porosity to be used in calculation the flow resistance in the flow blockage model (0.05 vs 1.e-5 in 2.1/2.2 correspondingly) – which may cause differences between observations in MELCOR 2.1 and 2.2. The difference between cases A and B can be explained by the effect of depressurization. In Case A, the water level after depressurization drops below the active core region, the uncovered core starts to heat up, eventually reaching the point where control rods\blades, canisters undergo degradation and relocate downwards to the core plate, where its either rest on top as PD, or refreezes as conglomerate, or flows through the openings into the lower plenum. The variation in PDPor, as a result will affect both, cooling of the core by escaping steam and core oxidation.

Velocity of falling debris (VFALL) – MELCOR does not have a mechanistic model for debris dropping into the lower plenum. Instead a number user-specified parameters control the rate at which material relocates into the lower plenum and the effective heat transfer (Heat transfer coefficient from in-vessel falling debris to pool (CORCHTP)) from and associated oxidation of the debris slumping into lower plenum water. VFALL has significant effect, judging by Morris $\bar{\mu}$ values on debris mass in LP, metallic debris fraction and metallic debris fraction in the 1st axial level; VFALL has moderate effect on hydrogen mass and timing of core support plate failure. VFALL has also different effect in different severe accident scenarios and MELCOR code version being used. The effect of VFALL together with CORCHTP on the debris mass and other system response quantities can be explained by steam generation during core slumping to LP, that can affect both: core cooling and core oxidation\heat up due to oxidation, especially in the case with early depressurization, where water level dropped below the active core region, due to depressurization, long before the onset of core oxidation; which is also reflected by the difference in sensitivity coefficients between cases A and B. The difference of the effect of VFALL and CORCHTP in different code versions is yet to be explained.

Lower Plenum Particulate Debris Equivalent Diameter (DHYPDLP) – MELCOR uses this parameter to calculate heat transfer surface area of the debris in LP, note that MELCOR equates the oxidation surface area to the heat transfer surface area of the node; so it should have an effect on the debris oxidation and steam generation rate, however it is not supported by the results (see Figure 3-42). Further analysis is necessary to determine the effect of particulate debris diameter and heat transfer coefficients in in-vessel debris quench model in MELCOR on the results. The effect of DHYPD on the metallic debris fraction in 1st axial level and timing of core support plate failure predicted for case B with MELCOR 2.2 is yet to be explained.

Molten Zircaloy melt break-through temperature (SC1131-2) – defines critical temperature at which molten materials are released from an oxide shell or local blockage (crust). After oxide shell/crust break through MELCOR uses SC1141 array to control candling model, in particular CS1141-2 – Molten Cladding (pool) drainage rate represents a maximum flow rate (per unit surface width) of the molten pool after breakthrough; this coefficient also used to control the time step in candling model, when molten material has just released after hold up by an oxide shell or by a flow blockage (crust) [339],[338]. According the MELCOR manuals description [339],[338], these coefficients should have direct effect on the metallic debris fraction at the bottom of the LP, which can be observed in Figure 3-44 and 3-45, i.e. large values of Morris $\bar{\mu}$ and positive correlation coefficients(SC1141-2) in both versions of MELCOR code being used. SC1131-2 has smaller relative importance on the metallic debris fraction in the first axial level, however it is possible that it can be involved in non-linear interaction with other parameters in candling model (including SC1141-2), SC1131-2 has negative correlation coefficients with metallic debris fraction in the 1st axial level – which is opposite to what was initially expected, i.e. larger vales of SC1131-2 would result in larger metallic debris fraction at the bottom of the LP due to higher melt superheat. Sensitivity coefficients SC1141-2, SC1131-2 have significant effect on the processes of core oxidation and hydrogen generation with negative (SC1141-2) and positive (SC1131-2) correlation coefficients, which can be explained by the effect of this parameters to flow blockage formations and structures exposure to oxidation by steam – which is also evident in results for scenario with late depressurization (see Figure 3-42, 3-43b). The effect of these sensitivity coefficients on the amount of relocated debris in LP and timing of core support plate failure is most likely due to the formation of the flow blockages (cooling) and debris interaction with supporting structures (higher metallic debris fraction – higher thermal conductivity of the debris), however, more detailed analysis is necessary to confirm this hypothesis. The results also indicate that these sensitivity coefficients have higher relative importance in MELCOR 2.2 compared to MELCOR 2.1 – which still needs to be explained.

Time constant for radial solid/liquid debris relocation (SC1020-1/SC1020-2) – MELCOR uses particulate debris leveling (SC1020-1) and molten debris leveling (SC1020-2) models for radial relocation of solid and liquid(molten) materials. Sensitivity coefficients SC1020-1/SC1020-2 are used to calculate debris volume relocated during core time step, as follows $V_{rel} = V_{eq}(1 - \exp\left(-\frac{\Delta t_c}{\tau_{spr}}\right))$; where V_{eq} – volume of material that must be moved between the rings to balance the levels, $\frac{\Delta t_c}{\tau_{spr}}$ −COR package time step divided by sensitivity coefficient (SC1020-1/SC1020-2 – for solid/liquid debris correspondingly) [339],[338]. Radial relocation time constants have significant effect on the LP debris mass, metallic debris fraction (in-vessel) and timing of core support plate failure. Negative correlation coefficients in Figure 3-38, suggest that smaller values of sensitivity coefficients will yield larger debris mass in LP – which can be explained by larger debris relocation rate in-between rings in case of core support plate failure, especially in case A, where core support plate failure usually occurs early in one of the central rings (with higher power density) compared to rather gross core support plate failure (failure in several rings) in case B. These parameters have relatively small effect on the hydrogen production and metallic debris fraction in the 1st axial level, and the effect on the timing of core support plate failure and metallic debris fraction (in-vessel) is yet to be explained.

3.3.5 Vessel Failure Analysis with MELCOR Code

The primary focus of the analysis performed within core relocation framework was to investigate the effect of severe accident scenario and modeling options in MELCOR code on the process of core degradation and relocation (debris slumping) to LP.
The state of the debris in RPV LP have high impact on:

- Time of RPV breach.
- Type of RPV breach.
  - Vessel wall failure.
  - Penetration failure + location.
- The rate of the debris ejection (enthalpy) from the vessel, which can significantly affect containment behavior and corresponding loads on different safety functions.

Based on the results obtained in previous sections we performed preliminary analysis of the effect of severe accident scenario on the time and the mode of vessel failure and melt release conditions with MELCOR code.

3.3.5.1 Overview of MELCOR Modelling of Vessel Breach

MELCOR [345], [346] assumes that the vessel lower head can breach by following mechanisms (not mutually exclusive):

- Vessel wall failure:
  - Uses Creep-Rupture model (0D/1D options available)
    - Creep-rupture failure of a lower head segment occurs, in response to mechanical loading under conditions of material weakening at elevated temperatures.
- Penetration failure:
  - The temperature of a penetration (or the temperature of the innermost node of the lower head) reaches a failure temperature (TPFAIL) specified by the user.
  - Logical Control Function specified by user.

Whenever any failure condition is satisfied, an opening with an initial diameter defined by the user is established:

– Penetration diameter (e.g IGT – 0.07m, CRGT – 0.14m)
  - If there are no penetrations modeled, initial diameter will take default value of 0.1m.

After a failure has occurred, the mass of each material in the bottom axial level that is available for ejection (but not necessarily ejected) is calculated. Two simple options exist (Solid debris ejection switch)

- In the default option (ON), the masses of each material available for ejection are the total debris and molten pool material masses, regardless of whether or how much they are molten. Note, however, that this option has been observed to lead to ejection of much more solid debris with the melt than is realistic.
- In the second option (OFF),
  – The masses of steel, Zircaloy, and UO2 available for ejection are simply the masses of these materials that are molten;
  – The masses of steel oxide and control poison materials available for ejection are the masses of each of these materials multiplied by the steel melt fraction, based on an assumption of proportional mixing;
  – The mass of ZrO2 available for ejection is the ZrO2 mass multiplied by the Zircaloy melt fraction.
  – Additionally, the mass of solid UO2 available for ejection is the Zircaloy melt fraction times the mass of UO2 that could be relocated with the Zircaloy as calculated in the candling model using the secondary material transport model.

Additionally, MELCOR impose several constraints on the mass to be ejected at vessel failure:

- A total molten mass of at least 5000kg.
  – This value can be accessed through sensitivity coefficient SC1610(2). However, MELCOR still requires non-negative molten mass to be available for release in order to initiate debris ejection.
- A melt fraction of 0.1 (total molten mass divided by total debris mass) is necessary before debris ejection can begin to avoid calculation difficulties with the core-concrete interactions modeling.
  - This value can be accessed through sensitivity coefficient SC1610(1). However, MELCOR still requires non-negative molten mass to be available for release in order to initiate debris ejection.
- In case of gross failure all debris in the corresponding cell is discharged linearly over a 1s time step, regardless of the failure opening diameter and debris state.

After the total mass of all materials available for ejection has been determined, the fraction of this mass ejected during a single COR package subcycle is determined from hydrodynamic considerations. The velocity of material being ejected is calculated from the pressure difference between the lower-plenum control volume and the reactor cavity control volume, the gravitational head from the debris layer itself, and a user-specified flow discharge coefficient, using the Bernoulli equation [345], [346].

$$M_{ej} = \rho_m A_f v_{ej} \Delta t \tag{3-3}$$

$$v_{ej} = C_d \left(\frac{2\Delta P}{\rho_m} + 2g\Delta \mathrm{z_d} \right)^{1/2} \tag{3-4}$$

Where M_{ej} - maximum mass ejected, A_f - penetration failure area, Δt – time step, C_d - flow discharge coefficient, ΔP – pressure difference between LP and LDW, ρ_m - material density, g – gravitational acceleration, Δz_d - debris and molten pool height.

Ablation of the failure opening is modeled by calculating the heat transfer to the lower head by flowing molten debris. A simplified implementation of the ablation model by Pilch and Tarbell [375] is used, which gives the heat transfer coefficient for the flowing molten debris as the maximum of a tube correlation and a flat plate correlation [345], [346].

$$h_{abl,tube} = 0.023\ K_p v_{ej}^{0.8}/D_f^{0.2} \tag{3-5}$$

$$h_{abl,plate} = 0.0292\ K_p v_{ej}^{0.8}/\Delta z_h^{0.2} \tag{3-6}$$

where h_{abl} - ablation heat transfer coefficient, $K_p = \mathrm{k}\left(\frac{\rho}{\mu}\right)^{0.8} Pr^{1/3}$, calculated using average property vales from [376], D_f - failure diameter, Δz_h - lower head thickness.

The ablation rate is calculated using equation:

$$\frac{dD_f}{dt} = \frac{2h_{abl}(T_d - T_{m,s})}{\rho_s(c_{p,s}(T_{m,s} - T_{h,avg}) + h_{f,s})} \tag{3-7}$$

where ρ_s – density, $c_{p,s}$ - heat capacity, $h_{f,s}$ - latent heat of fusion, $T_{m,s}$ - melting temperature of LH steel, T_d - debris temperature, $T_{h,avg}$ - average LH temperature.

3.3.5.2 Analysis Results of Vessel Breach and Melt Release with MELCOR code.

The analysis of vessel breach and melt release conditions with MELCOR code was performed with MELCOR 2.1 (rev.7544) (see [377][378] for details). In the analysis we considered ADS and ECCS timing to be uniformly distributed within [1.e3-1.e4] (sec) (subject to ADS Timing < ECCS Timing constrain, i.e. water injection with ECCS(Low Pressure) cannot be initiated prior depressurization).

The analysis was performed for 4 sets of calculations:

- No penetration modelling, solid debris ejection.
    - Only vessel wall can failure due to creep-rupture.
    - Debris can be ejected regardless of its state.
- No penetration modelling, no solid debris ejection.
    - Only vessel wall can failure due to creep-rupture.
    - Molten debris (plus some fraction of solid debris, based on secondary material transport model [345], [346]) can be ejected.
- Penetration modelling, solid debris ejection.
    - Vessel can fail due to penetration failure and/or vessel wall failure (due to creep-rupture)
    - Debris can be ejected regardless of its state.
- Penetration modelling, no solid debris ejection.
    - Vessel can fail due to penetration failure and/or vessel wall failure (due to creep-rupture)

- Molten debris (plus some fraction of solid debris, based on secondary material transport model [345], [346]) can be ejected.

The analysis of the effect of severe accident scenario (ADS and ECCS Timing) on the process of core degradation, relocation to lower plenum, vessel failure and melt release has been performed using MELCOR 2.1 rev7544. In the analysis we considered different timing of activation of ADS and ECCS. Furthermore, the effect of maximum time step in MELCOR code was also considered in the analysis (6 different values), since it was previously show that MELCOR time step can have quite significant effect on the results and the lack of time step convergence of the solution with the reduction of the maximum time step [85],[374]. In the analysis presented in this paper we also consider the effect of MELCOR modelling of vessel failure (penetration failure vs. vessel wall failure) and modelling of melt release (solid debris ejection switch IDEJ).

The results presented as two-dimensional maps (120 accident scenarios (ADS – ECCS Timing combinations)), where different figures-of-merit are presented as expected values (as expected value of the results obtained with different time steps, 6 – MELCOR code runs with different max. time step were performed for every accident scenario, 2160 cases were simulated in total) color-coded according to the corresponding colorbar, as functions of accident scenario timings (ADS and ECCS Timing).
The results show that the effect of vessel failure modelling (i.e. penetration vs. vessel wall failure) has an effect on the amount of hydrogen produced in-vessel, however it can be considered as insignificant, since the major part of hydrogen is produced during in-core accident progression [83][86][87][374].

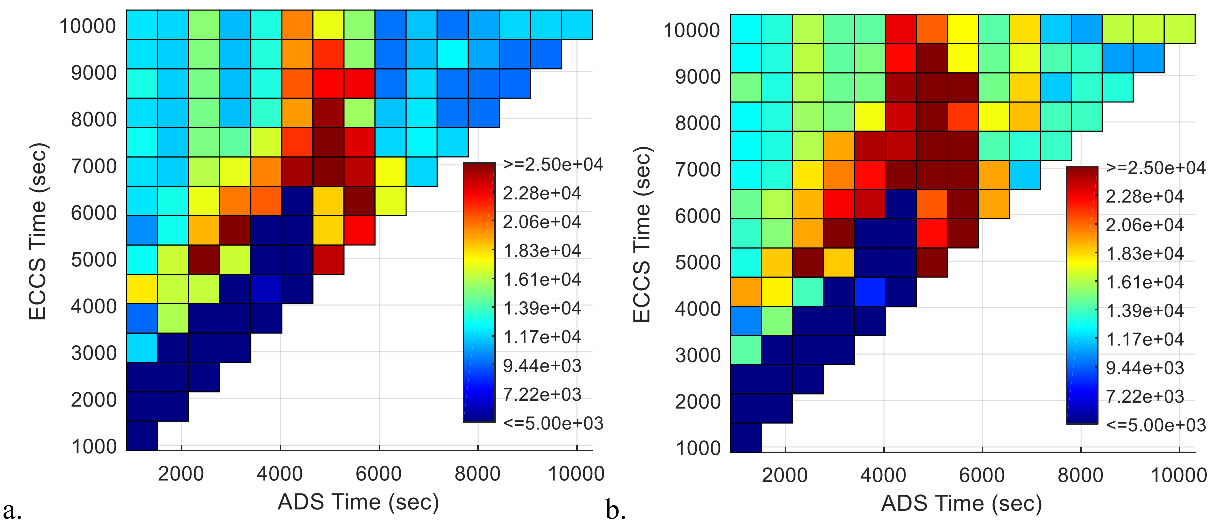

Figure 3-46. Expected value of (a) time of vessel failure (sec) (b) time of the onset of the release (sec), with penetration modelling; as a function of ADS and ECCS Timing (sec)

Figure 3-46a present the timing of vessel breach due to penetration failure (with penetration modelling) as a function of accident scenario. The results show that the penetration failure occurs at approximately 10000-15000sec in scenarios with early and late depressurization and late water injection (after 7000sec). Furthermore, apparently there is a domain of scenarios (with ADS timing in the range of 4000-6000sec) where vessel breach due to penetration failure can be delayed significantly. Figure 3-46b – shows the timing of melt release (melt release initiation, i.e. ejected mass from the vessel is > 0), according to the results, there is some time delay between the vessel breach and initiation of the debris ejection in the case with penetration modelling in MELCOR.

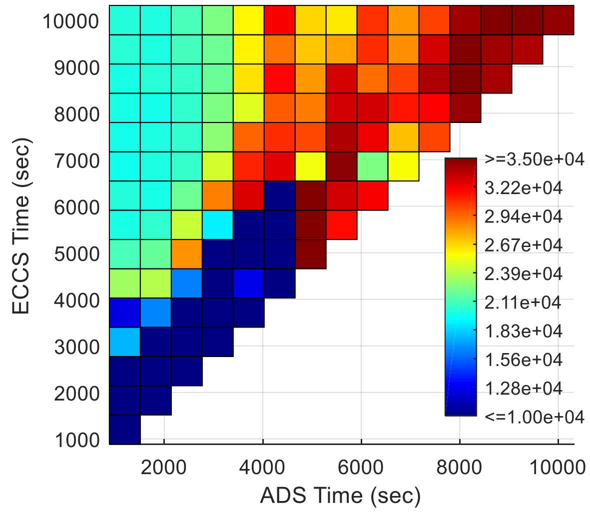

Figure 3-47. Expected value of the time of vessel failure and the onset of the release (sec), without penetration modelling; as a function of ADS and ECCS Timing (sec)

Figure 3-47 illustrates the timing of vessel failure and melt release in the case of vessel wall failure (without penetration modelling). The results show that in the scenarios with early depressurization, vessel failure occurs at approximately 20000sec, while in scenarios with late depressurization it occurs after 30000sec after initiating event. Moreover, in case of vessel wall failure, the ejection of the lower plenum debris starts at the time of vessel failure, without any delay.

The mass of lower plenum debris at the time of vessel breach is presented in Figure 3-48a in case of penetration modelling and Figure 3-48b in case without penetration modelling.

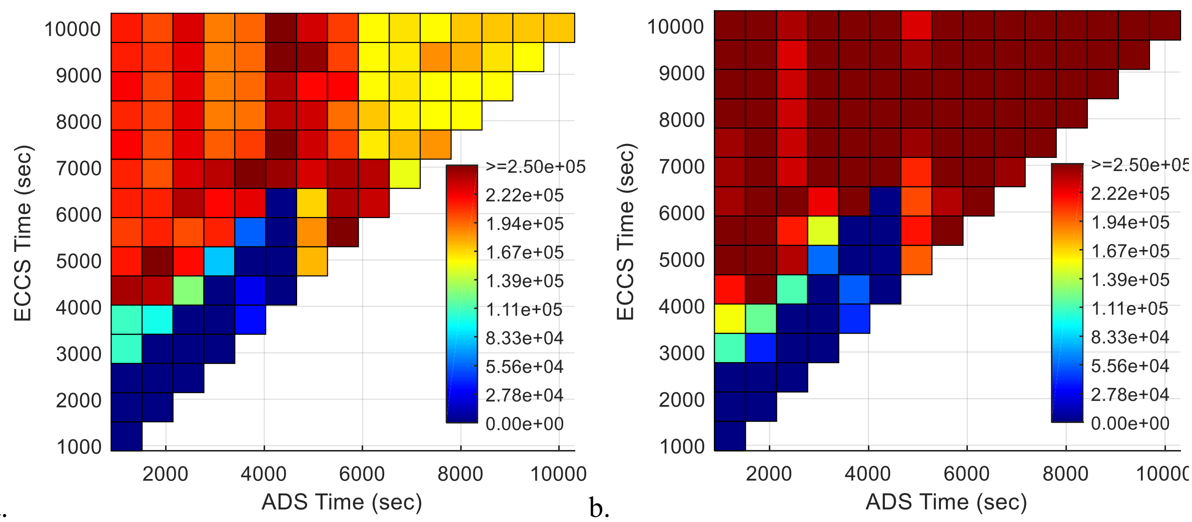

a. b.

Figure 3-48. Expected value of the debris mass (kg) in LP at the time of vessel failure (a)with penetration modelling (b) without penetration modelling; as a function of ADS and ECCS Timing (sec)

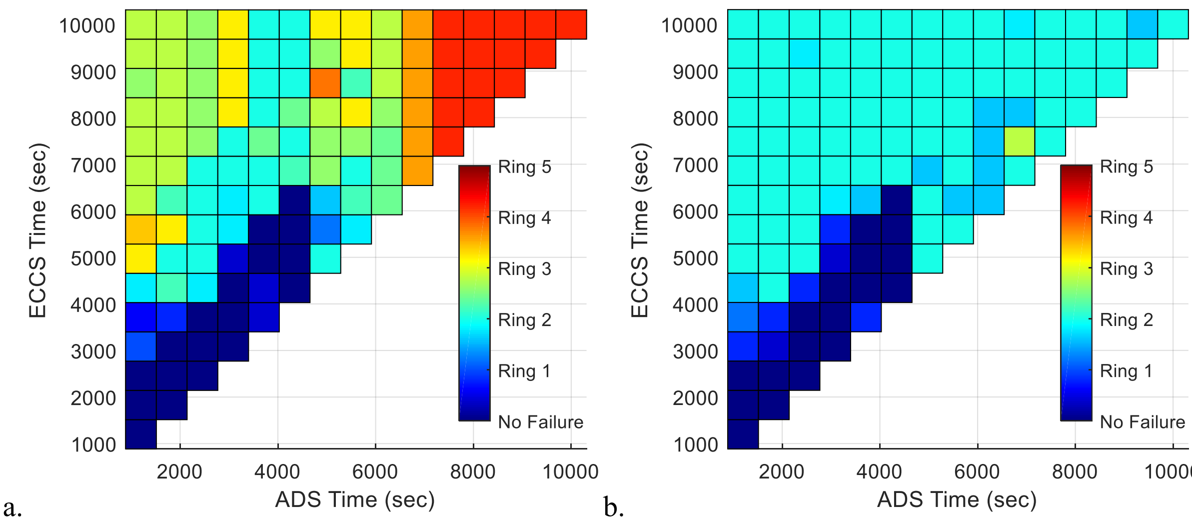

Figure 3-49. Expected Failure Location (Ring Number) (a) with penetration modelling (b) without penetration modelling; as a function of ADS and ECCS Timing (sec)

Figure 3-49a shows the expected location of penetration failure as a function of accident scenario, the results show that in the scenarios with ADS timing below 6000sec, penetration failure occurs in one of the central rings (most likely in the 2^{nd}-3^{rd} radial ring), while in the scenarios with ADS time above 6000 sec, penetration failure occurs in the 4^{th}-5^{th} radial rings. On the other hand, in the case without penetration modelling (see Figure 3-49b), vessel wall failure, in most of the cases, occurs in the 2^{nd} ring, regardless of the accident scenario.

3.3.5.3 Properties of the debris in LP

Figure 3-50a show the mass of molten metallic debris and Figure 3-50b shows the mass of molten oxidic debris at the time of vessel failure, with penetration modelling. The results show that the mass of molten metallic debris is significantly larger in scenarios with ADS timing below 4000sec, compared to the scenarios with ADS timing above 4000 sec (30-45tons vs. 10-15tons). The mass of molten oxidic debris is in the range of 0 to 7tons, without clear indication of the effect of accident scenario.

Figure 3-51 show the effect of accident scenario on the mass averaged superheat of the molten stainless steel debris in LP. The results suggest that in the scenarios with ADS timing below 6000sec, the mass averaged superheat of stainless steel debris can reach 1000-1100K, while in scenarios with ADS timing above 6000sec it is in the rage of 300-500K.

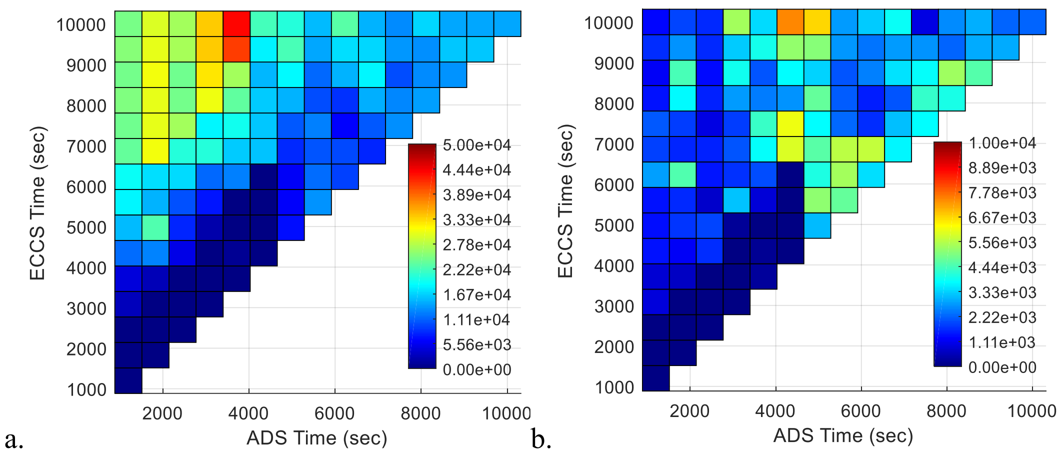

Figure 3-50. Expected value of (a) molten metallic debris mass (kg) (b) molten oxidic debris mass (kg), at the time of the release with penetration modelling; as a function of ADS and ECCS Timing (sec)

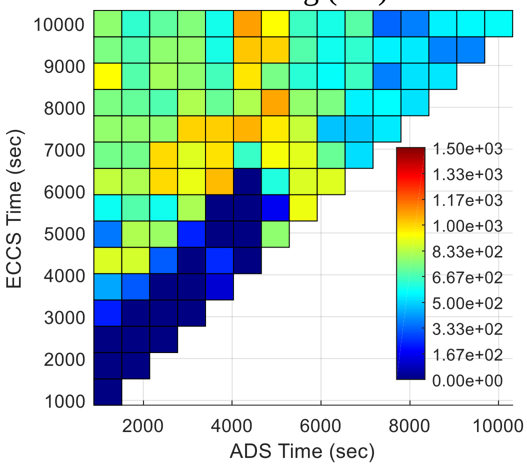

Figure 3-51. Expected value of LP molten stainless steel mass averaged superheat (K) at the time of the release with penetration modelling; as a function of ADS and ECCS Timing (sec)

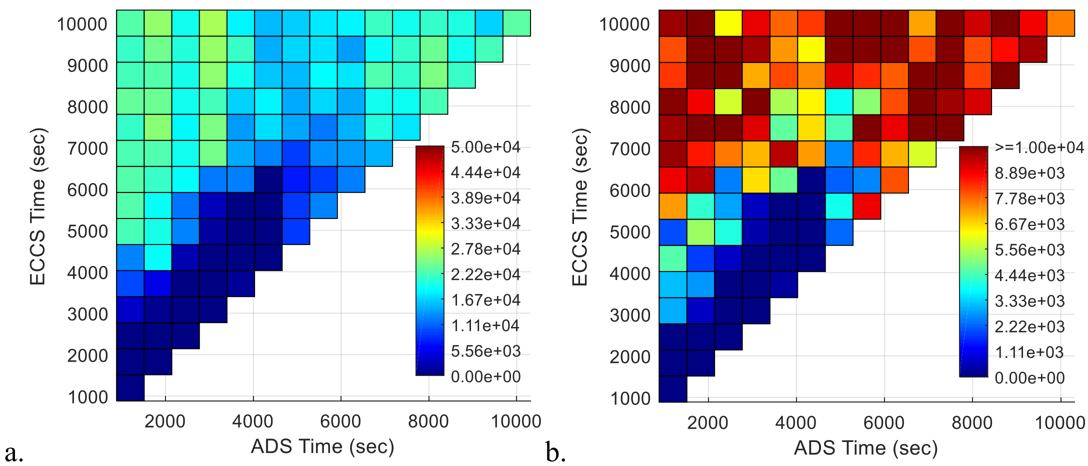

Figure 3-52. Expected value of (a) molten metallic debris mass (kg) (b) molten oxidic debris mass (kg), at the time of the release without penetration modelling; as a function of ADS and ECCS Timing (sec)

Figure 3-52a presents the mass of the molten metallic debris as a function of severe accident scenario, in the case of vessel wall failure without penetration modelling, the results show that the mass of molten metallic debris is in the range of 15-25 tons regardless of the accident scenario, with exception to the domain of scenarios with small relocated debris mass in the lower plenum see Figure 3-48. The mass of molten metallic debris at the time of vessel breach due to vessel wall failure (no penetration modelling) is significantly smaller compared to the scenarios with penetration modelling (see Figure 3-50a), even though the vessel breach in the case without penetration modelling occurs significantly later compared to the case with penetration modelling (e.g. 10000 to 20000 sec difference), and results in significantly larger values of the mass averaged superheat (see Figure 3-53, ~1200-1300K vs. ~1100K at most in case with penetration modelling, see Figure 3-51). This difference might be due to the effect of molten pool models in MELCOR code. It is assumed in MELCOR that particulate debris will sink into a molten pool, displacing the molten pool volume. Once solid debris components with lower melting point (such as stainless steel) start to melt, the volume occupied by solid debris decreases, the molten materials will occupy empty volume within the solid debris (reducing solid debris porosity). The remaining part will form a molten pool on top of the particulate debris, which will be displaced by the particulate debris from the cell located above, which eventually can result in stainless steel-rich layer on top of the solid debris.

Figure 3-52b shows the mass of molten oxidic debris as a function of accident scenario, the results show that the mass of molten oxides ranges from approximately 7000 to over 10000kg in the whole scenario domain (with exception to the domain with small debris mass in LP).

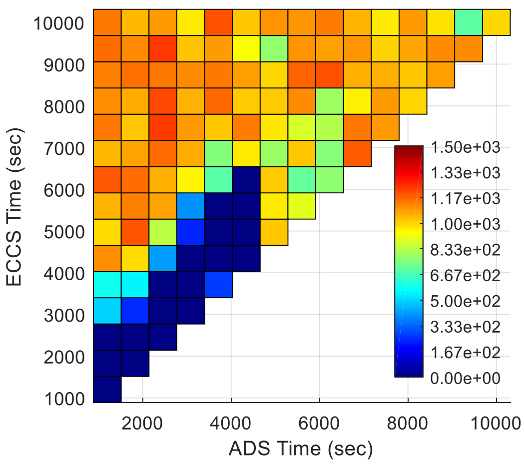

Figure 3-53. Expected value of Molten Stainless Steel in LP mass averaged superheat (K) at the time of the release without penetration modelling; as a function of ADS and ECCS Timing (sec)

3.3.5.4 Melt release from the vessel

Figure 3-54a show the effect of accident scenarios on the expected value of the maximum debris ejection rate from the vessel, in the case of penetration modelling with solid debris ejection (IDEJ = 0). The results show that the maximum debris ejection rate ranges from approximately 400kg/s, mostly in the domain of scenarios with ADS timing in the range of 4000-6000sec, up to approximately 1200kg/s, mostly in the scenarios with early depressurization (ADS time

<3000sec) and late depressurization (ADS time > 8000sec). The rate of enthalpy release, presented in Figure 3-54b, show that it is highly correlated with the debris ejection rate, however, some minor deviations can occur, due to the debris composition in LP. In scenarios with early depressurization ADS time < 3000sec, the maximum rate of enthalpy release range from approximately 1e9 to 1.5e9 (J/s), while in the rest of the scenario domain it stay below 1.0e9 (J/s).

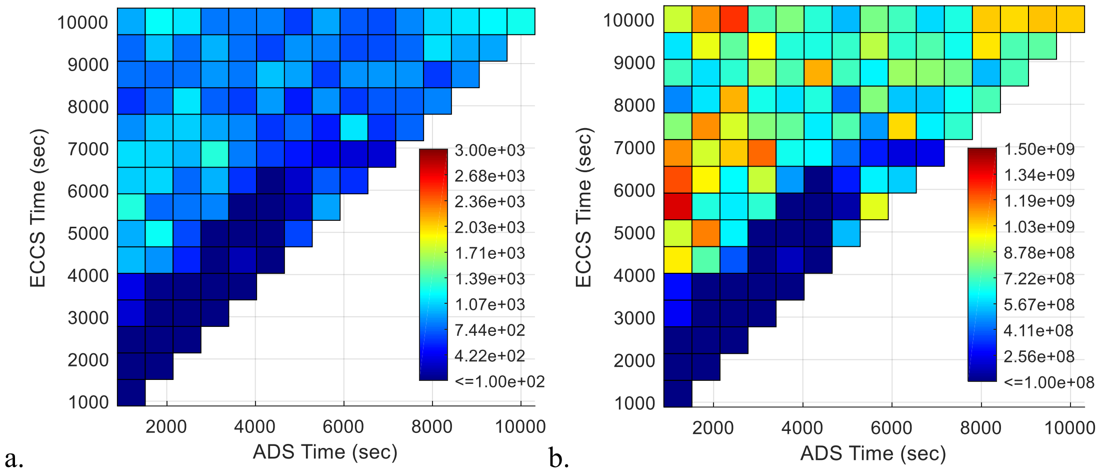

Figure 3-54. Expected Value of (a) Maximum debris ejection rate (kg/s) (b) Maximum enthalpy rate (J/s) with penetration modelling, solid debris ejection ON (IDEJ=0); as a function of ADS and ECCS Timing (sec)

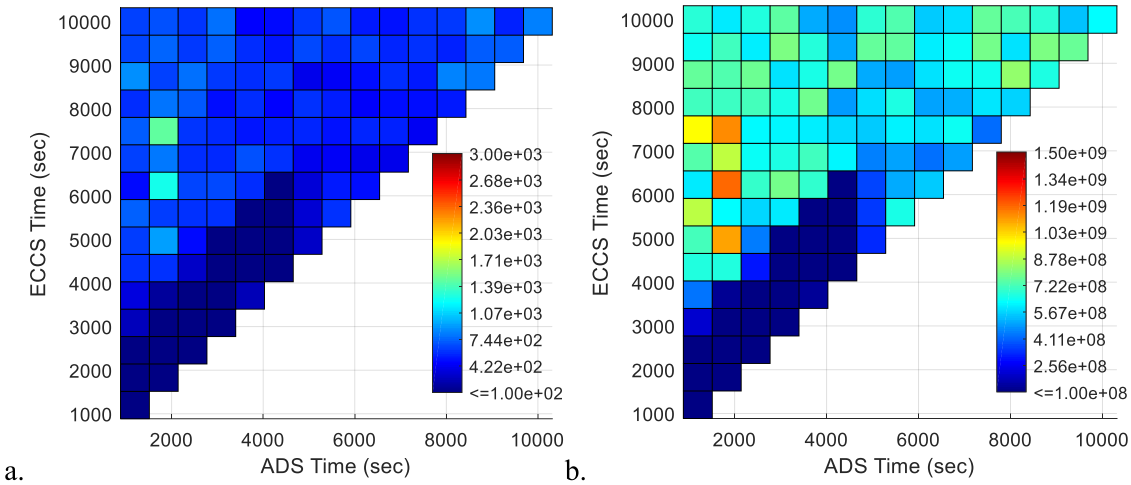

Figure 3-55. Expected Value of (a) Maximum debris ejection rate (kg/s) (b) Maximum enthalpy rate (J/s) with penetration modelling, solid debris ejection OFF (IDEJ=1); as a function of ADS and ECCS Timing (sec)

Figure 3-55a shows the debris ejection rate as a function of accident scenario in the case of vessel penetration modelling and with no solid debris ejection (IDEJ=1). The results show that the maximum debris ejection rate in case of IDEJ = 1 is significantly smaller (~400-500kg/s in most of the cases simulated) compared to IDEJ = 0 (see Figure 3-54a). This difference between the effect of solid debris ejection switch (IDEJ = 1 and IDEJ = 0) is also reflected in Figure 3-55b, where the maximum enthalpy release rate is approximately 5-8e8 (J/s), while in case of IDEJ=0 it is in the range of 8-15e8 (J/s).

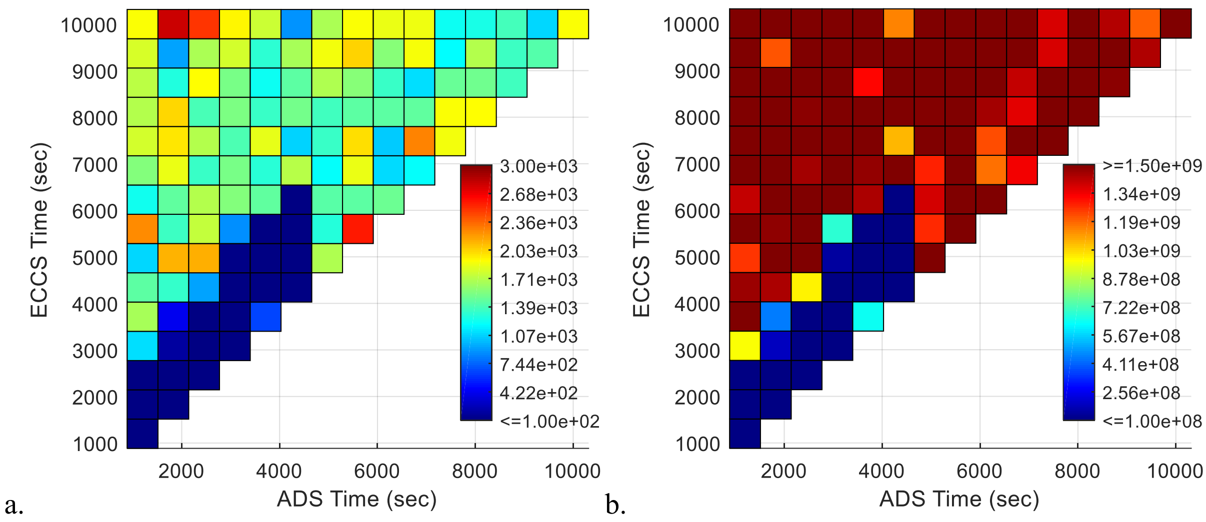

Figure 3-56. Expected Value of (a) Maximum debris ejection rate (kg/s) (b) Maximum enthalpy rate (J/s) without penetration modelling.; as a function of ADS and ECCS Timing (sec)

Figure 3-56a illustrate the effect of accident scenarios on the maximum debris ejection rate and enthalpy release rate (Figure 3-56b) in case of vessel wall failure (without penetration modelling). The results show that the maximum values for the debris ejection rate can vary in the range from 2000-3000kg/s, regardless of accident scenario, since in case of gross failure of the vessel wall, it is assumed that all debris in the bottom axial level of the corresponding ring, regardless its state, is discharged linearly over 1s time step without taking into account failure opening diameter [339],[338] this is also reflected in the values of enthalpy release rate, presented in the Figure 3-56b. Note that in figures 3-54 and 3-56 (penetration failure with solid debris ejection on (IDEJ=0) and vessel wall failure), solid and liquid debris are ejected.

3.3.6 Development of Core Relocation SM

Core relocation SM is of a “look-up table” type, where the properties of relocated debris (for every COR node and total) at the time of vessel failure and the time of the release, pool conditions (temperature, depth and pressure in LDW), melt release properties (expected or median values of: max. debris ejection rate, effective breach area at max. debris ejection rate, temperature of the ejected debris/mel at max. deris ejection rate) are perdicted as functions of severe accident scenario (in terms of ADS and ECCS Timings).

Table 3-7 shows the list of parameters predicted by core relocation SM. Core relocation SM predicts either expected or median value of the distribution of the properties of the debris, pool conditions, etc. Pool conditions are predicted at the time of the vessel breach and at the time of the onset of melt release. This is necessary since MELCOR predicts a time delay between the vessel breach and the onset of melt release in the case of penetration failure. Vessel failure results in opening of the flow path for water from the vessel lower plenum to the cavity, which can result in increased water level in the cavity (up to the level of the overflow pipes in lower drywell). Effective breach area, the temperature of the ejected debris are obtained at the time of max. debris ejection rate ($T_{EJRAT|\max(EJRAT)}$) (see Figure 3-58). This provides a conservative estimate of the melt release conditions for the analysis of ex-vessel steam explosion and coolability.

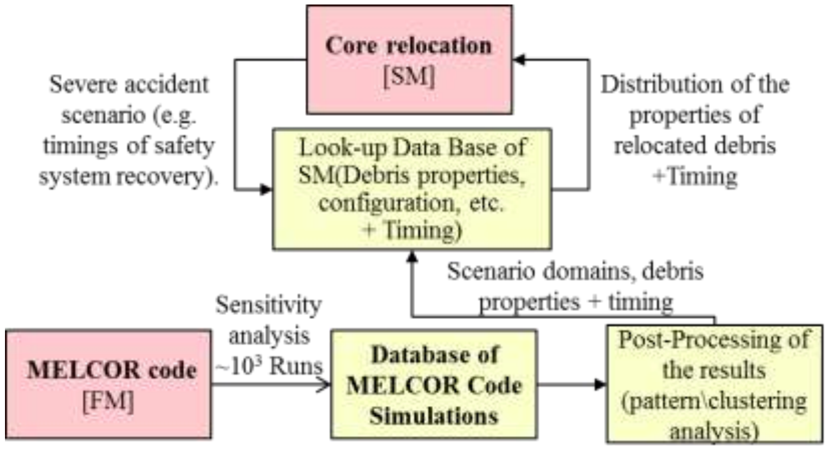

Figure 3-57: Structure of Core relocation SM.[85]

Table 3-7: Core relocation SM Outputs

Parameter name	Description	Units
XPW	Lower drywell pol depth	[m]
Po	LDW Pressure	[Pa]
Pv	Invessel Pressure	[Pa]
TLO	LDW water pool temp.	[K]
COR_ABRCH	Effective vessel breach area	[m^2]
TPIN	Ejected Debris Temperature	[K]
EJRAT	Debris Ejection Rate	[kg/s]
MDB	Total LP debris mass	[kg]

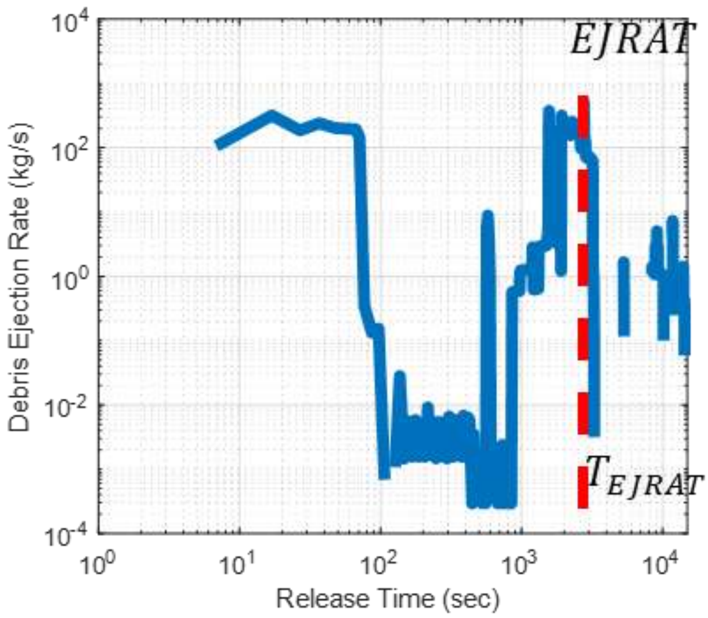

Figure 3-58: Debris ejection rate as a function of time (kg/s)

Furthermore, we consider metallic release (see section 3.8 for details) (debris properties such as debris thermal conductivity, specific heat, melting temperature, fusion heat, etc.) since MELCOR predicts the max temperature of ejected debris below 2900K (see Figure 3-59) and the mass of stainless steel oxide is insignificant.

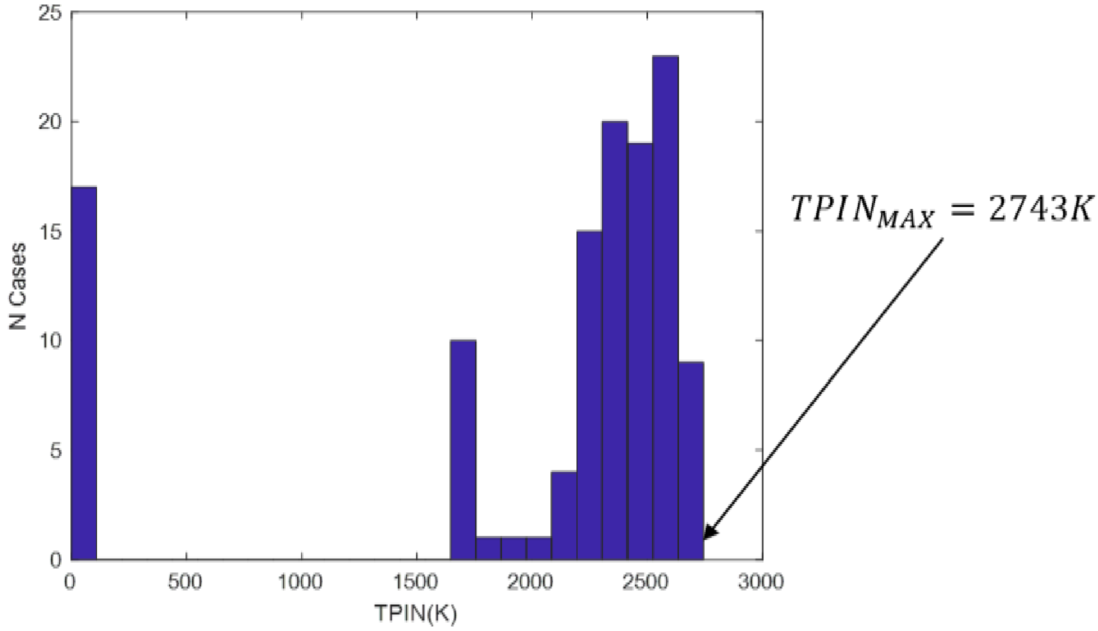

Figure 3-59: Distribution of the max. temperature of ejected debris (K) in different accident scenarios.

3.4 Vessel Failure SM

3.4.1 Approach

The modified system for depressurization of reactor vessel is highly reliable in Swedish plants. Therefore, we consider low-pressure scenario of core damage as most probable. Otherwise, the risks of High Pressure Melt Ejection and Direct Containment Heating are dominant. Figure 3-60 shows the schematic framework for the development of vessel failure surrogate model (SM). The goal of the vessel failure SM is to predict mode (IGT, CRGT, vessel wall), timing of the failure, amount, properties and superheat of the melt available for release. The process is iterative but initially starts with grouping and classification of failure scenarios. In particular, scenario parameter (s_i) are determined by the initial Plant Damage States (PDS) from PSA-L1, Emergency Operation Procedures (EOP), and Severe Accident Management Guidelines (SAMG), with the important element of timing and possible recovery actions. Application of the core relocation surrogate model (SM), generates the core debris properties and the relocation time which becomes the initial time for further calculations in the vessel failure SM. The switch from core relocation SM to vessel failure SM is carried out at the moment when core relocation SM is not adequate any more for further analysis of the accident progression. The criterion for the time to switch to the next model is based on significant mass relocation to the lower head with enough thermal load to inflict damage to the penetrations that can lead to penetration failure.

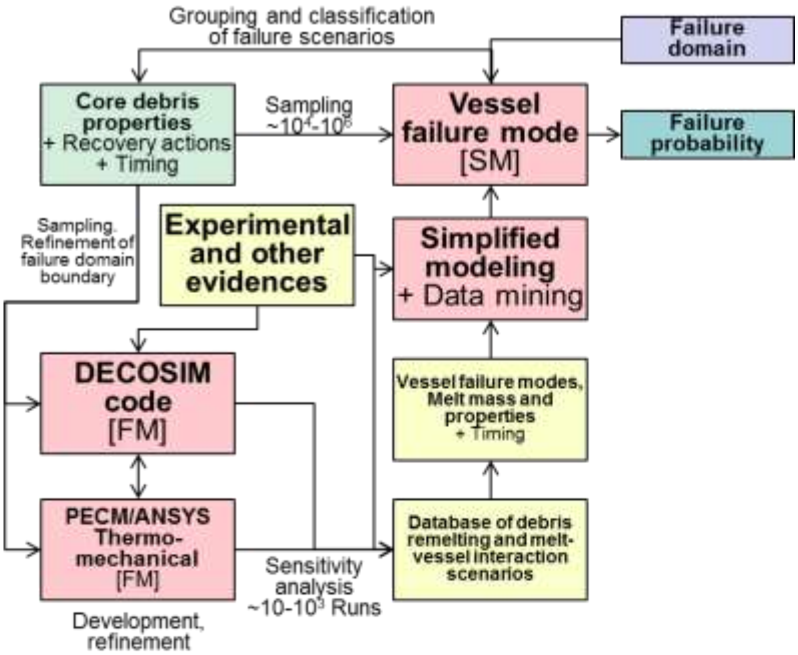

Figure 3-60: Debris re-melting Vessel failure surrogate model.

The uncertainties for the vessel failure SM can be classified into scenarios, initial and deterministic modeling parameters, and intangibles.

Scenario parameters:
- Initial plant damage state and its frequency,
- Order and timing of failures,
- Possible recovery actions and their timing,
- etc.

Initial conditions:
- Spatial distribution of solid debris thermal conductivity,
- Spatial distribution of decay heat,
- Debris initial temperature,
- Debris initial mass,
- Relocation time,
- etc.

Deterministic modeling parameters:
- Thermo-physical properties of the debris, vessel wall, and structures,
- Models of the heat transfer in porous media,
- Models of melt pool formation in heterogeneous (oxidic/metallic) debris,
- etc.

Intangible parameters:
- Heat generation due to corium oxidation,
- Debris bed shape,
- etc.

The development of the vessel failure SM includes following main steps:

1. Generate a complete list of required input parameters for each of the full models (DECOSIM, PECM/ANSYS).
2. Generate corresponding complete list of specific parameters from the sources where the input parameters are taken. These sources can be from the previous core relocation SM (initial P_1) or from experimental data (pdf(d_i)).
3. For transparency of review process, generate a complete list of assumptions, physical models, and numerical models for each of the full models.
4. Generate extensive simulation matrix for each of the full models. The matrix indicates the ranges of input parameters for sensitivity analysis.
5. Perform the FM calculations and identify domains of input parameter where FM solution cannot be obtained or unreliable with existing physical and numerical models.
6. Identify influential parameters from the FM calculations and update the complete list of input parameters indicating which ones are influential, relevant, and non-influential.
7. Characterize the data according to:
    - Failure mode,
    - Failure timing,
    - Melt mass available for release,
    - Melt superheat, and
    - Initial break size.

    as functions of initial debris properties.
8. Perform grouping, classification, or mapping of the characterized data.
9. Simplify the functional dependencies (in item #7) using experimental and other evidences.
10. Organize the database of results for an easy and efficient access (data mining). Standardize the call functions, output formats, and plots.
11. Develop the vessel failure Surrogate Model (FM) as a substitute for the FMs (DECOSIM, PECM/ANSYS). A couple of options can be pursued:
    - Neural Network Approach (Machine Learning) which makes full use of the database.
    - Simplified physical models, correlations, look-up tables, fitting curves, and maps can be generated. These submodels are expressed in the following output parameters that are needed as input parameters in the next stage of the ROAAM+, that is, melt ejection SM (see next section):
        - Melt mass available for release at the time of failure,
        - Corresponding melt superheat, and
        - Initial break size.
12. Given the scenario (s_i) and multidimensional probability density function (pdf(d_i, i_i)) of intangible (i_i) and deterministic (d_i) modeling parameters, sample the vessel failure SM in order to quantify the failure probability in the forward analysis. Feedback from the melt ejection SM following the reverse analysis can resolve the boundary of the failure domain and can be made more refined through an iterative process.

3.4.2 Conclusions

Debris bed configuration has significant influence on vessel failure mode and timing. There are several phenomena that can affect debris configuration: Multicomponent reheating and remelting; melt and water flow in a porous debris bed; debris configuration changes due to phase changes, oxidation, partial melt release; melting and collapse of IGT and CRGT pipes. MELCOR has models that address these phenomena, however, current approaches might be over-simplified and lacking necessary validation database due to the extreme complexity of the phenomena. Our approach is to focus on possible limiting factors in design, scenario, and phenomena that can simplify the analysis but still provide conservative coverage of possible scenarios.

Main findings from the analysis of MELCOR suggest that penetrations generally fail sooner than vessel wall, and, in some cases, amount of liquid melt can be relatively small at the time of failure. The ranges of vessel wall failure timing obtained in MELCOR is ~18000-37000 seconds after SCRAM. Melt superheat varies in MELCOR in wider ranges ~0-1200 K. MELCOR predicts that up to 60 tons of liquid metallic melt can be available at the time of penetration failure. MECLOR has models for considering non-homogeneous debris remelting and oxidation, which can affect local debris properties, thermal loads and allows to treat separately metallic and oxidic melt materials during melt ejection and the effect of partial melt release on the remelting of remaining debris. In summary, MELCOR, while lacking 3D features, provided ranges of possible scenarios of vessel failure and melt release, which can be taken as a reference for completeness of the analysis.

3.5 In-vessel Debris Coolability Analysis with DECOSIM

3.5.1 DECOSIM Code Modification for In-vessel Problems

The mathematical model implemented in DECOSIM code is based on multifluid equations, it is described in detail in [314], where all governing equations and closures are described. Here, we outline the approach and its numerical implementation, focusing on the specific features necessary to treat in-vessel coolability of porous debris bed. First, we take into account that in the presence of structural elements in the reactor vessel the space accessible by water and corium particles is reduced; therefore, we introduce an effective "porosity" $\varepsilon_c < 1$, assuming that a fraction $1 - \varepsilon_c$ of all volume is unavailable for the flow and debris due to space congestion by the structural elements. The effective "porosity" ε_c enters the phase flow and energy equations together with the "real" porosity ε of debris bed. This approach allows us to consider large-scale flowfields without resolving geometries of each individual CRGTs or IGTs. The volume fraction ε_c is assumed to be constant in time, but it can vary in space according to the availability and size of structural elements in the reactor pressure vessel. This simplification is justified before structural elements lose integrity (i.e., due to melting); we use it throughout the simulation because we are interested here in the conditions developing in the porous debris bed, rather than in detailed description of further melt propagation through the newly opened paths.

By occupying some space in the reactor vessel, the structural elements not only reduce the volume available to flow, but also change the effective heat capacity and effective conductivity of the medium. It is assumed here that the local temperature of structural elements is the same as that of surrounding porous medium (single-temperature model of solid material). Another simplification often used in the coolability studies is to consider the space above the debris bed as some effective low-drag porous medium (with high porosity and particle diameter), so that the same filtration equations could be applied to obtain the phase velocities in the whole computational domain. Note that in the drag laws, only the "real" porosity ε is taken into account.

Below we summarize the system of equations being solved in DECOSIM; relevant closures and description of numerical implementation can be found in [324]. Note that the same model formulation was applied in [310] to consider in-vessel porous debris bed under continuous water supply conditions. A simpler formulation (with $\varepsilon_c \equiv 1$) was used to model by DECOSIM the post-dryout behavior of ex-vessel debris beds where structural elements are absent [310].

3.5.1.1 Governing Equations

The multifluid three-phase model implemented in DECOSIM includes the mass, momentum, and energy conservation equations for liquid water (index $k = l$), vapor ($k = v$), and solid material (s); for the in-vessel problems we also take into account the congesting structures (index c):

$$\frac{\partial \alpha_k \rho_k \varepsilon \varepsilon_c}{\partial t} + \nabla \varepsilon_c \rho_k \boldsymbol{j}_k = \varepsilon_c \Gamma_k \tag{3-8}$$

$$\nabla P = \rho_k \boldsymbol{g} - \left(\frac{\mu_k}{K K_{rk}} \boldsymbol{j}_k + \frac{\rho_k}{\eta \eta_{rk}} |\boldsymbol{j}_k| \boldsymbol{j}_k\right) + \boldsymbol{F}_k \tag{3-9}$$

$$\alpha_k \rho_k \varepsilon \varepsilon_c \frac{d_k h_k}{dt} = \alpha_k \varepsilon \varepsilon_c \frac{d_k P}{dt} + \nabla(\alpha_k \lambda_k \varepsilon \varepsilon_c \nabla T_k) + \varepsilon_c \Gamma_k (h_k^I - h_k) + \gamma_k \varepsilon_c R_{sk} + \varepsilon_c R_k^I \tag{3-10}$$

$$[\varepsilon_c(1-\varepsilon)\rho_s C_s + (1-\varepsilon_c)(1-\varepsilon_{ci})\rho_c C_c] \frac{\partial T_s}{\partial t} = \nabla(\lambda_{\text{eff}} \nabla T_s) + \varepsilon_c (R_{dh} - R_{sl} - R_{sv}) \tag{3-11}$$

Here, ε is the "real" porosity, the phase volume fractions α_k satisfy the condition $\alpha_l + \alpha_v = 1$; $\boldsymbol{j}_k = \alpha_k \varepsilon \boldsymbol{u}_k$ are superficial phase velocities, $\boldsymbol{u}_k$ are actual phase velocities, the substantial derivatives are $d_i \ /dt = \partial/\partial t + (\boldsymbol{u}_i \nabla)$, $\boldsymbol{g}$ is the gravity acceleration. Water phase properties (densities ρ_k, specific enthalpies h_k, viscosities μ_k, thermal conductivities λ_k) as functions of pressure P and temperature T_k are approximated by polynomials according to IAPWS-IF97 formulation [117]. In the momentum equation (3-9), K, K_{rk}, η, and η_{rk} are absolute and relative permeabilities and passabilities, $\boldsymbol{F}_k$ is interphase friction force ($\boldsymbol{F}_l = -\boldsymbol{F}_v$), Γ_k is phase change rate ($\Gamma_v = -\Gamma_l$). Equations (3-8)–(3-11) are written in the operator form, with vector quantities typeset in boldface. In the current work, the problem is considered in the axisymmetric framework, with the gradient and divergence operators $\nabla \phi = \left(\frac{\partial \phi}{\partial r}, \frac{\partial \phi}{\partial z}\right)$, $\nabla \cdot \boldsymbol{v} = \frac{1}{r}\frac{\partial r v_r}{\partial r} + \frac{\partial v_z}{\partial z}$, where ϕ is a scalar, $\boldsymbol{v} = (v_r, v_z)$ is a vector quantity, r and z are the radial and vertical coordinate, respectively.

The phase energy equation (3-10) takes into account heat conduction, evaporation, heat exchange with solid particles material (source terms R_{sk} on the right-hand side), and interphase heat exchange (R_k^I); the superscript I denotes values pertaining to the liquid-vapor interface. In the solid material energy equation (3-11), T_s, ρ_s, and C_s are the temperature, density, and specific heat capacity of corium, ρ_c, and C_c are the density and specific heat capacity of the congesting structures, ε_{ci} is the internal porosity of congesting structures ($\varepsilon_{ci} > 0$ if the structures are not solid, e.g., in hollow pipes). Also, R_{dh} is the decay heat power per unit volume of porous medium, R_{sl} and R_{sv} describe heat exchange with liquid and vapor phases. The effective conductivity in the solid material is evaluated as

$$\lambda_{\text{eff}} = \varepsilon_c(1-\varepsilon)\lambda_s + (1-\varepsilon_c)(1-\varepsilon_{ci})\lambda_c \tag{3-12}$$

In this way, higher heat conductivity in the presence of metal structural elements is taken into account. Also, the properties of corium are taken as weighted between the values for solid (index sol) and molten (index m) states, the weighting factor being the mass fraction of melt χ:

$$\rho_s C_s = (1-\chi)\rho_{sol} C_{sol} + \chi \rho_m C_m, \quad \lambda_s = (1-\chi)\lambda_{sol} + \chi \lambda_m \tag{3-13}$$

The mass fraction of melt is obtained from energy balance in computational cell, taking into account the fusion heat. Two-phase drag in porous medium is modelled according to [286], with modifications introduced and validated in [242], [27]. Models for source terms are considered in details in [314].

Note finally that all porosities (ε, ε_c, ε_{ci}) and heat conductivities are considered in this work as scalars, i.e., isotropic values being constant for each porous region. More comprehensive treatment of porous media properties taking into account anisotropy due to vertical orientation of structural elements was outside the scope of the current study.

3.5.1.2 Numerical Implementation

The system of governing equations (3-8)–(3-11) is discretized in axisymmetric geometry on a staggered orthogonal grid in the 2D axisymmetric geometry. The grid was non-uniform in both radial and vertical directions in order to increase spatial resolution in the regions of high gradients. On each time step equation are solved by Newton iterations. On each time step, the momentum equations are solved first to find out the preliminary velocity components of each phase. The velocity corrections are expressed in terms of pressure and volume fraction corrections, with the phase change terms taken into account implicitly. They are then substituted into the phase continuity and energy equation which are solved in a fully coupled manner by an efficient ILUT-preconditioned PGMRES solver. Global iterations are performed on each time step until convergence with prescribed accuracy is reached. The time step is varied adaptively, depending on convergence success or failure [314].

3.5.2 Vessel and Debris Bed Geometry and Properties

Simulations are performed in the vessel geometry typical of Nordic-type BWRs, sketched in Figure 3-61a. In the reactor pressure vessel, there is a shroud which limits radial spreading of debris. The congested area containing CRGTs and IGTs is indicated by vertical dashed lines and hatching; in this zone, the structural elements are taken into account, as described above. The effective porosity due to congestion is set to $\varepsilon_c = 0.82$, the internal porosity of structural elements is $\varepsilon_{ci} = 0.02$; details of these can be found in [314]. The levels at which the welding points of CRGTs and IGTs are located (0.4 and 0.17 m above the vessel bottom surface) are shown by the dashed lined. The geometry coincides with that used in our previous works [314], except the vertical extent of computational domain was extended to 6 m, while the initial level of water was set to the height of 4 m, corresponding to the top of computational domain in simulations [314] where continuous water supply was assumed.

Formation of debris bed in severe accident conditions is a complex process, with substantial uncertainties involved with respect to fuel-coolant interaction. In terms of the problem considered, this translates into uncertainties both in properties of debris (porosity, mean particle diameter), debris bed shape (which depends on the formation process, including fuel melt fragmentation, fallout, interaction with boiling water flow in RPV, etc.), as well as the initial state of corium (particle temperature, fraction of quenched material) and water inventory in the reactor vessel. Since no mechanistic model addressing all these issues is available at the moment, we resort to setting the initial conditions *ad hoc*, mostly focusing on revealing the possible outcomes of different scenarios.

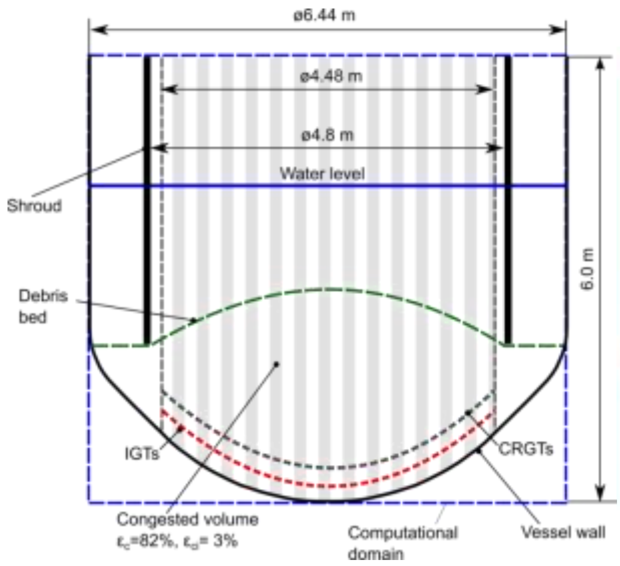

(a)

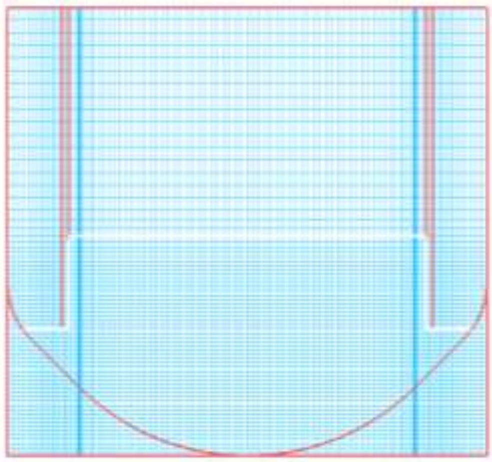

(b)

Figure 3-61: Sketch of reactor pressure vessel geometry and computational domain (a), numerical grid (b).

Two debris bed shapes are considered in this work: i) flat-top (corresponding to uniform dripping of core material through the core support plate, or intensive lateral redistribution of corium particles by convective flows); and ii) Gaussian-shaped heap, with the maximum on the axis of symmetry (corresponding to relocation of the large fraction of the core though the central part of the core support plate, e.g. see [83]). Note that some amount of melt can pass through the coolant inlets in the lower part of the shroud (see the horizontal "wings" of the schematic debris bed shape in Figure 3-61). The height of debris bed was determined by its mass M (100, 150, and 200 t), with the porosity taken equal to $\varepsilon = 0.4$. Simulations were performed for particle diameters $d_p = 1.5,\ 2.0$, and 3.0 mm, the specific decay heat power was varying in time, with the core relocation time chosen to be $t_r = 1.5$ h on the basis of MELCOR simulations for Nordic-type BWRs.

The physical properties of corium were taken from [250]: in the solid state $\rho_{sol} = 8285$ kg/m^3, $\lambda_{sol} = 1.9$ W/m·K, $C_{sol} = 566.2$ J/kg·K, for melt state $\rho_m = 7121.6$ kg/m^3, $\lambda_m = 3.6$ W/m·K, $C_m = 680.7$ J/kg·K, the melting temperature is $T_m = 2750$ K, specific fusion heat is $\Delta H_m = 428$ kJ/kg. The properties of the structural elements were taken constant and characteristic of stainless steel: $\rho_c = 7800$ kg/m^3, $\lambda_c = 15$ W/m·K, $C_s = 500$ J/kg·K.

Simulations were carried out on a Cartesian grid having 50×70 cells in the radial and vertical directions, respectively, see Figure 3-61b. The grid was refined in the debris bed and near the vessel walls and shroud: the minimum and maximum grid cell sizes in the radial direction were 4 and 8 cm, while in the vertical direction the grid cell sizes varied between 5.5 and 17 cm.

3.5.2.1 Effect of Decay Heat and Debris Property Inhomogeneity

Core degradation and relocation into the lower plenum can proceed in stages at which different materials are melted and relocated at different times. As a result, the properties of debris in different parts of debris bed can differ significantly. For example, a layer of mostly metallic materials with low decay power but high thermal conductivity can be formed near the vessel wall in the lower plenum. In order to study the effect of decay heat and property inhomogeneity on water cooling of porous debris bed, a set of simulations was performed.

Firstly, scoping simulations were carried out for water reflooding of an initially dry and hot (1000 K) debris bed; the decay heat power was reduced by 20% and 50% either in a lower half of the debris bed (by height), or in a 50 cm-thick spherical layer along the vessel wall. It was shown that a lower-power layer near RPV wall (metallic materials) promotes water penetration along the vessel wall in comparison with the homogeneous property case.

In order to reduce the uncertainty in the initial conditions and debris property distributions, a link to MELCOR simulation results was implemented:

- A snapshot of MELCOR simulations were taken as initial data for DECOSIM;
- Interface has been developed and implemented for data transfer (nodalization, materials, temperature, decay heat power per unit mass of UO2);
- Particulate debris (PD) volume fraction (COR_VOLF_PD) variable is used to determine the shape of debris bed;
- Parameters for each MELCOR cell are distributed evenly to all DECOSIM cells falling within it;
- Porosity of debris is assumed to be 40%, mean particle diameter is an input parameter;
- Where particulate temperature is above saturation, dry zone is assumed.

DECOSIM simulations were run for 3 hours in order to reveal the thermohydraulics of debris bed. For comparison, simulations were also run starting with quenched conditions where debris was initially at the saturation temperature, and debris bed was initially wet (filled with liquid water). As an example, consider the case which was started with MELCOR simulation snapshot at time 13000 s, see Figure 3-62.

In Figure 3-63, DECOSIM simulation of the reflooding of an initially dry debris bed with assumed particle diameter 1 mm is presented. It can be seen that, similar to the cases of homogeneous debris bed presented above, water penetration proceeds mainly along the bottom wall of reactor vessel lower plenum. By the time of 2 hours, water propagates about half of radial distance from the debris bed periphery to the axis. Also visible is water ingress in the top part of debris bed where the heat release rate is lower than in the bulk of debris.

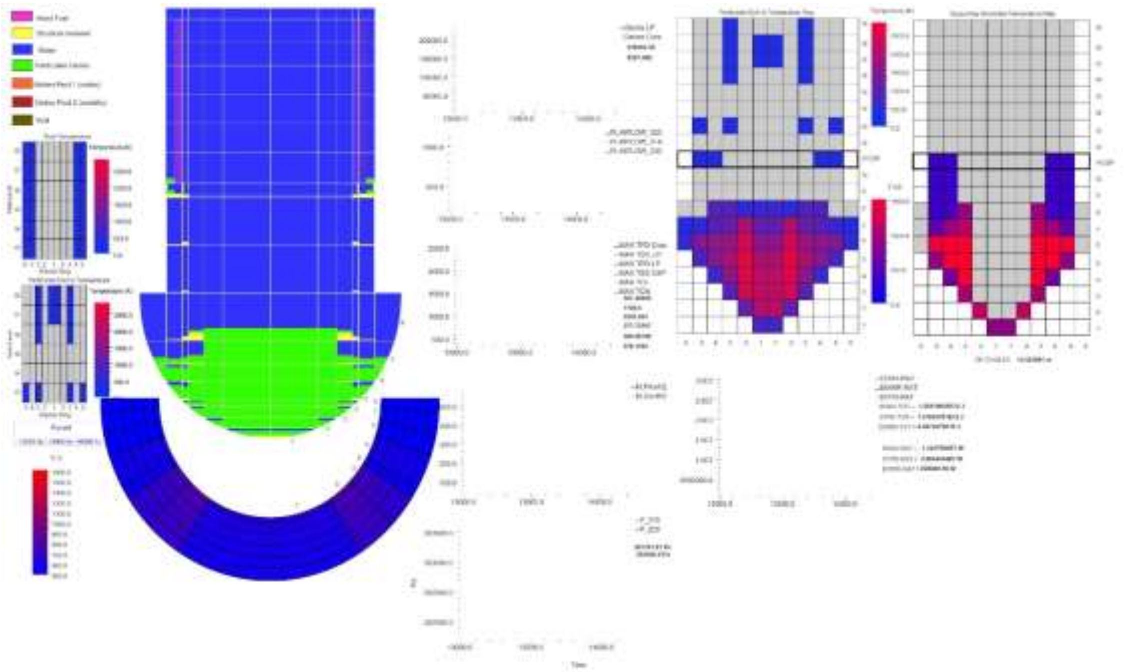

Figure 3-62: Snapshot of MELCOR simulation used for setting the initial conditions for DECOSIM simulation of water flooding of a porous debris bed.

t = 0 t = 30 min t = 2 hours

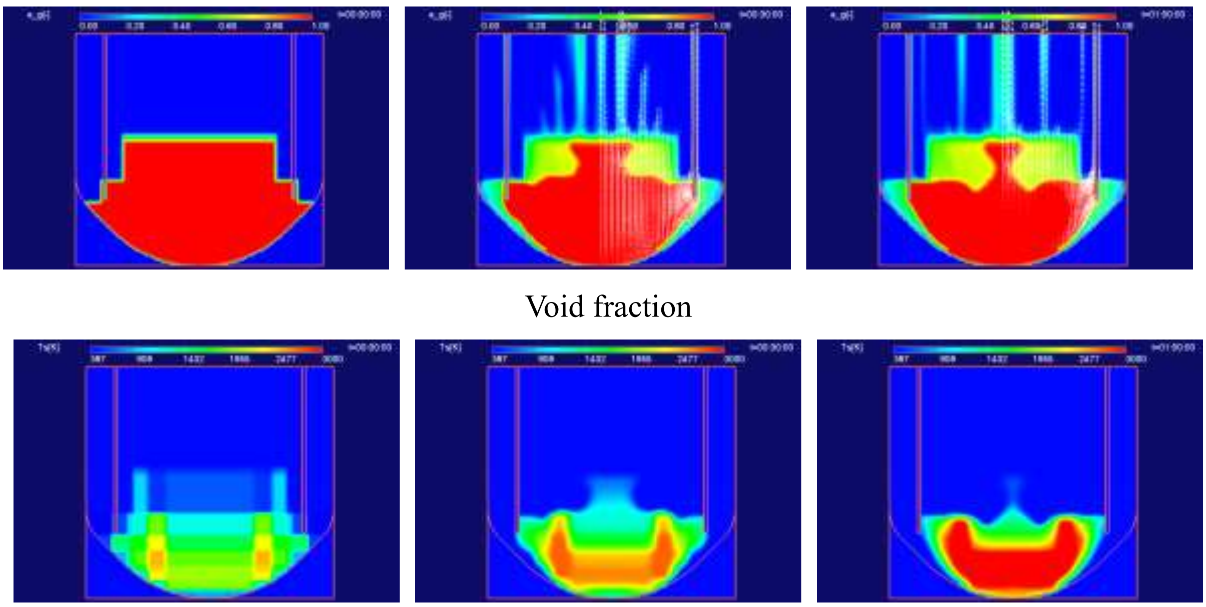

Void fraction

Temperature of porous debris

Figure 3-63: Reflooding of initially dry debris bed, 1 mm particles.

In Figure 3-64, similar results are shown for 2 mm particles, with the same initial conditions as in Figure 3-63. Evidently, water penetration proceeds much faster, leading to rapid cut-off of the hot zone from the vessel wall.

t = 0 t = 30 min t = 1.5 hours

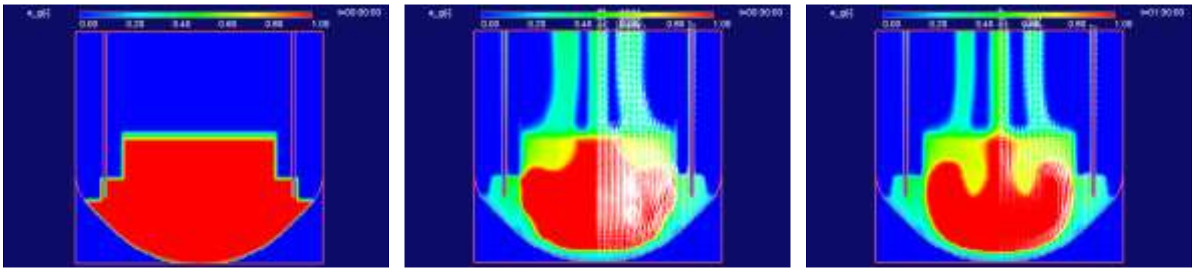

Void fraction

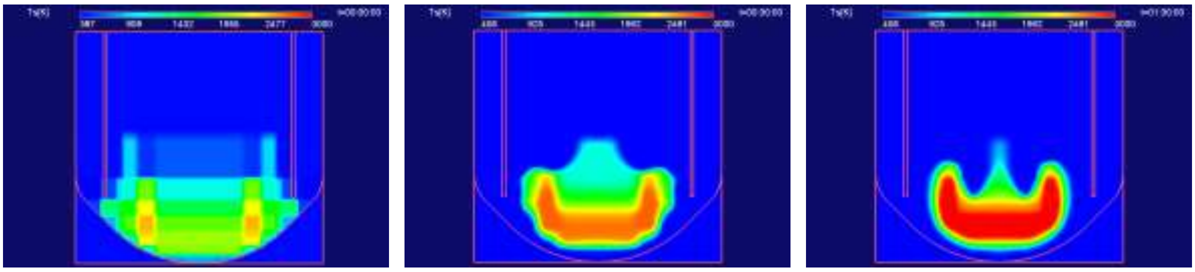

Temperature of porous debris

Figure 3-64: Reflooding of initially dry debris bed, 2 mm particles.

In Figure 3-65, the time histories of maximum particle temperatures are shown for different initial times (i.e., MELCOR snapshots at 7200 and 13000 s), particle diameters, and initial states (quenched or hot and dry). It can be seen that initially quenched debris bed is coolable for 2 mm particles, but non-coolable for 1 mm particles. Also, initially dry debris are heated up to remelting despite partial quenching of debris near vessel wall.

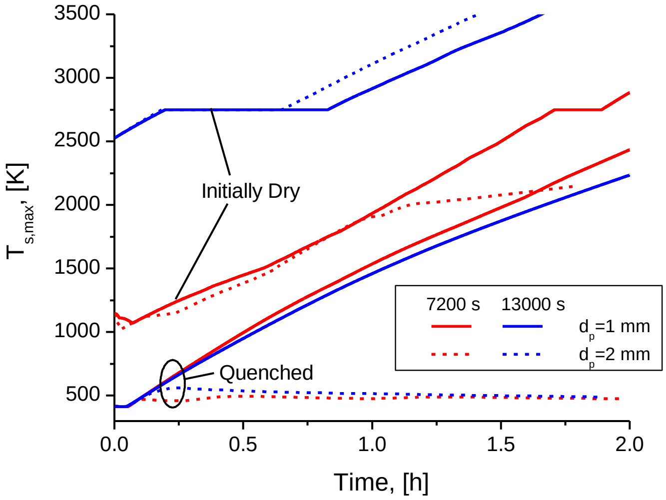

Figure 3-65: Time histories of the maximum particle temperature in debris bed.

3.5.3 Summary of Results on In-vessel Porous Debris Bed

The results obtained in APRI-9 on coolability of a porous in-vessel debris bed reveal several common features:

For large particles:

- The dry zone (if any) is located in the top part of the debris bed, where temperature escalation and remelting can occur;
- In this case, melt accumulation in a pool can be expected, with massive release to follow the RPV failure;
- Thermal attack on CRGT and IGT welding is likely to occur only after complete water evaporation.
-

For small particles:

- The debris bed remains mostly dry due to rapid evaporation of water in the bed and limited ingress of coolant due to high drag;
- CRGT and IGT wildings are likely to fail early, resulting in water drainage and melt release in dripping mode.

Inhomogeneity of debris bed affects its coolability:

- Low decay power and high-conductivity (metallic) layers promote water ingress into the debris bed, improving its coolability;
- Still, the effect of particle size on the outcome of porous debris bed formation in the RPV lower plenum is prevailing.

Thus, the uncertainty associated with porous debris bed behavior in the in-vessel conditions remains contingent upon the corium fragmentation processes.

3.6 Melt Ejection

Vessel failure mode provides initial conditions of lower head failure: (i) size of the opening (IGT, CRGT, pump, vessel wall) and (ii) amount, properties and superheat of the available melt. Note that these characteristics can change with time during melt release, e.g. due to ablation or plugging of the opening in the vessel. Quantification of breaching, ablation and plugging of the vessel opening is required to reduce uncertainty in the melt release mode.

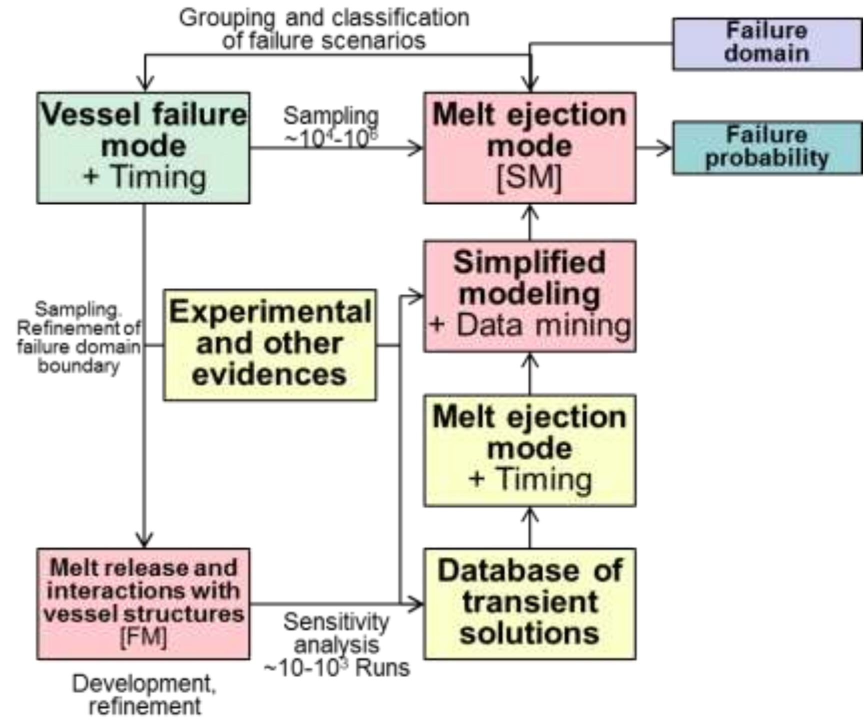

Figure 3-66: Melt ejection mode surrogate model.

There are two constitutive phenomena that should be addressed in the analysis of the melt ejection mode. The first is filtration of liquid melt through the solid porous debris. On one hand it can slow down the release, limiting the effective size of the melt jet; on the other hand, it can gradually increase the temperature of the melt jet, for example, in case of liquid metal filtration through decaying oxidic debris bed. The second is ablation / plugging of the initial breach during melt structure interaction. This is the key phenomena that alters jet diameter and therefore its modelling is paramount for ex-vessel scenario progression.

Currently, melt release mode is the least investigated element of the framework that lacks comprehensive modelling of melt structure interaction, melt filtration through porous debris bed and adequate experimental work necessary to collect the relevant evidences.

The goal of this work is to develop the numerical tool that for given initial conditions of vessel failure can predict transient parameters of melt ejection mode, i.e. jet diameter, melt thermal properties and duration of the release.

The development of MEM framework is depicted in the Figure 3-66. It relies on the MEM Full Model, which is still under development. Lack of complete FM and consequently a database of

FM solutions prevents development of the MEM surrogate model from the MEM FM. In order to make the whole framework operational a simplified model for vessel ablation and debris bed remelting has been implemented.

3.6.1 A 1D Modeling Approach to Plugging and Ablation

Previously we have performed extensive analysis of breach ablation relying on conservative 0D approach to calculate the transient rate of breach ablation given transient conditions of melt release rate and melt properties. In this iteration of MEM model development, we concentrate on the analysis of breach plugging, as a potentially limiting mechanism that can have important effect on the mode of melt release.

It is important to clarify if there is a possibility of whole core melt release in "dripping" mode i.e. avoiding "massive" release:

- no plugging of the breach,
- no extensive ablation of the breach.

Release in dripping mode can be defined as a mode of melt release that does not threaten the containment, i.e. green subdomain in the failure domain maps. Massive release can be defined as release that threatens the containment, i.e. red subdomain in the failure domain maps.

Previously we have demonstrated that definition of the dripping release can be based on estimated threshold value of

- jet enthalpy rate ($\dot{H}$) for steam explosion:

$$\pi \mathrm{U}_{\mathrm{rel}}(t)\rho_m R(t)^2\left(C_p \cdot (T - T_{water}) + H_f\right) < 30\,\frac{MJ}{s}$$

- ratio of the jet penetration depth (L) and the water pool depth (L_{wat}), which determines conditions for agglomeration:

$$\frac{L_{wat}}{L} = \frac{L_{wat}}{2.1D(t)\sqrt{Fr(t)}\sqrt{\frac{\rho_m}{\rho_w}}} < 1$$

where $Fr = U^2/gD$ is jet Froude number estimated at the water level.

Both criteria are dependent on the jet radius and therefore on the melt release scenario. Typical scenarios of melt release can be characterized by the amount of melt evaluable for release at the time of failure. Vessel (wall or penetration) fails when melt available for release is

- absent (all debris is solid) - probable scenario according to MELCOR predictions:
    - melt release rate will be limited by
        - debris remelting rate, i.e. decay heat and melt composition,
        - characteristics of vessel breach and driving pressure.
- relatively small (~10-30 tons) - most probable scenario according to MELCOR predictions:

- If melt accumulated at the time of failure can be released, then release of the remaining melt will be limited by:
  - debris remelting rate, i.e. decay heat and melt composition
  - characteristics of vessel breach and driving pressure
- If melt cannot be released (encapsulation by the crust or breach plugging) then it will accumulate as a melt pool and will lead to massive release

- relatively large (>100) - least probable scenario according to MELCOR predictions:
  - massive melt release.

Definition of the range of scenario parameters resulting in dripping release and characteristics of the dripping release are paramount for defining the possibility of melt accumulation in the lower head and possibility of massive releases.

The goal of this analysis is:

- Define conditions and assess amount of melt that can be released before onset of
  - plugging or,
  - ablation.
- Assess respective melt enthalpy release rates.
- Assess if decay heat can be a limiting factor for the enthalpy of melt release.

The main question of the analysis: in which conditions all melt can be released without significant ablation, i.e. in dripping mode?

In the following we develop steady state and transient analysis of the breach plugging, describe respective modelling and discuss the results. We then describe the implications of MEM FM and SM development and summarize the status of MEM in the conclusions and outlook.

3.6.1.1 Steady state analysis

The steady state model computes the thickness of the crust formed inside the breach given fixed conditions of melt release, constant vessel wall temperature T_{vw} and constant temperature T_m at the melt / crust interface. The model is axisymmetric with the axis of symmetry at $r = 0$ (see Figure 3-67).

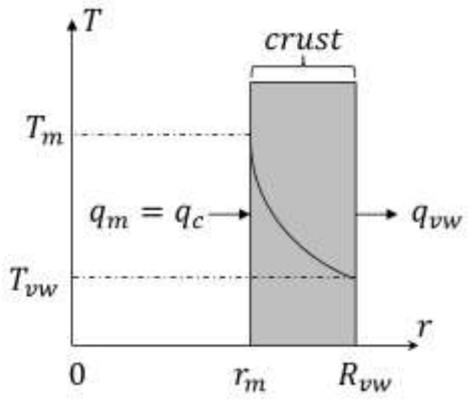

Figure 3-67: MEM: steady state model.

In steady state the heat flux from the melt is equal to the heat flux at the melt / crust interface:

$$q_m = q_c$$

The heat flux from the melt can be estimated as a function of Nusselt number Nu, melt thermal conductivity λ_m, melt superheat ΔT_{sup} and jet radius r_m:

$$q_m = Nu \frac{\lambda_m}{2r_m} \Delta T_{sup} \tag{3-14}$$

where $Nu = 0.5 \cdot Re^n \cdot Pr \cdot c_f,\ c_f = 0.005$ and

$$Re = 2\frac{\rho_m V_m r_m}{\mu_m}$$

$$Pr = \frac{\mu_m C_{p_m}}{\lambda_m}$$

Taking $n = 1$ makes q_m independent from the melt jet radius r_m.

The heat flux at the melt / crust interface is defined by crust thickness ($R_{vw} - r_m$), crust thermal conductivity λ_c and temperatures at its boundaries: T_{vw} and T_m:

$$q_c = \frac{T_m - T_{vw}}{r_m \cdot \ln(\frac{r_m}{R_{vw}})} \lambda_c \tag{3-15}$$

where R_{vw} is initial breasch radius (0.035 m in case of IGT failure and 0.075 m in case of CRGT failure).

Due to the cylindrical divergence, the steady state heat fluxes at different radiuses are not equal but related to each other through respective radiuses. For example, the steady state heat flux q_c at the melt / crust interface is related to the heat flux at the crust / wall interface q_{vw} as:

$$q_c \cdot r_m = q_{vw} \cdot R_{vw}$$

The implication of the cylindrical divergence is further demonstrated in the Figure 3-68. With increase of the crust thickness (decrease of the melt radius r_m) the heat flux at the vessel wall q_{vw} continuously decreases. However, below the critical melt radius $r_m < r_{crit}$ the heat flux at the melt / crust interface starts to increase reaching values exceeding $\sim 10^7 \frac{W}{m^2}$. The critical radius is only dependent on the initial breach radius:

$$r_{crit} = R_{vw} \cdot e^{-1}$$

The respective critical heat flux at the melt / crust interface q_{crit} is then given by

$$q_{crit} = -\frac{T_m - T_{vw}}{R_{vw} \cdot e^{-1}} \lambda_c \tag{3-16}$$

Depending on the value of the heat flux from the melt q_m three possible configurations can be established:

1. $q_m > q_{crit}$. There exist a stable equilirium crust thickness and constant melt release radius. The case when $q_m = 2 \cdot q_{crit}$ is demosntrated in the Figure 3-68, the respective jet radius $r_m \approx 0.0275\ m$. The solution is stable, meaning that small changes in the boundary conditions will result in small changes in the solution.
2. $q_m = q_{crit}$. There exist a steady state solution with $r_m = R_{vw} \cdot e^{-1}$. However, such solution is physically unstable: i.e. small changes in the boundary conditions (for example, reduction in melt release velocity or melt superheat) will lead to plugging of the breach.
3. $q_m < q_{crit}$. There is no steady state solution with melt flowing through the opening in the vessel, i.e. the breach will be plugged.

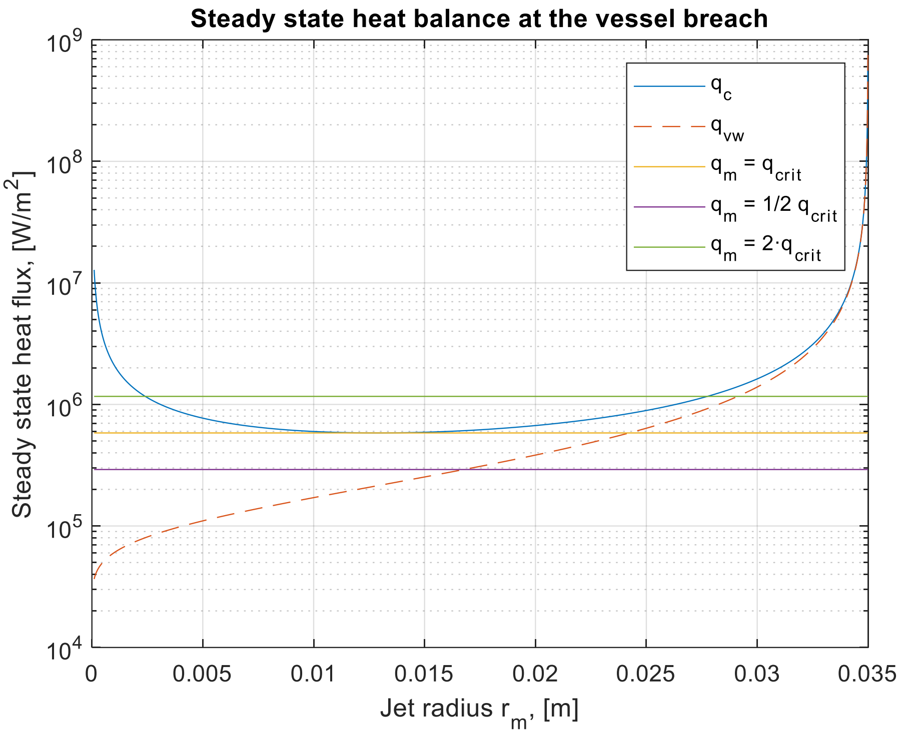

Figure 3-68: Steady state heat balance at the vessel breach.

An important finding from the steady state analysis is that *breach plugging* will occur if *heat flux from the melt* $q_m \leq q_{crit}$.

Given fixed (i) melt / crust thermophysical properties (specifically, T_m and λ_c) and (ii) initial breach size R_{vw}, the value of the:

- critical heat flux is only dependent on the vessel wall temperature T_{vw} (eq. (3-16)).

- heat flux from the melt is only dependent on the melt release velocity V_m and melt supereat T_{sup}.

Thus a steady state map of breach plugging and ablation can be built in terms of $\{T_{vw}, V_m, \Delta T_{sup}\}$, see Figure 3-69. The diagonal lines in the map correspond to a combination of $\{T_{vw}^{crit}, V_m^{crit}, \Delta T_{sup}^{crit}\}$ when critical heat flus is established. If melt release conditions $\{V_m, \Delta T_{sup}\}$ set a point below a critical line, then plugging of the breach could potentially occur; if melt release conditions define a point above a critical line then breach ablation will follow (given sufficient amount of melt).

Plugging conditions, i.e. combinations of the melt superheat ΔT_{sup} and melt release velocity V_{exit}, depend on the vessel wall temperature:

- In case of oxidic melt release (oxidic crust) vessel wall temperature has significantly smaller effect on the plugging conditions.
- In case of metallic release plugging conditions are lot more sensitive to vessel wall temperature.

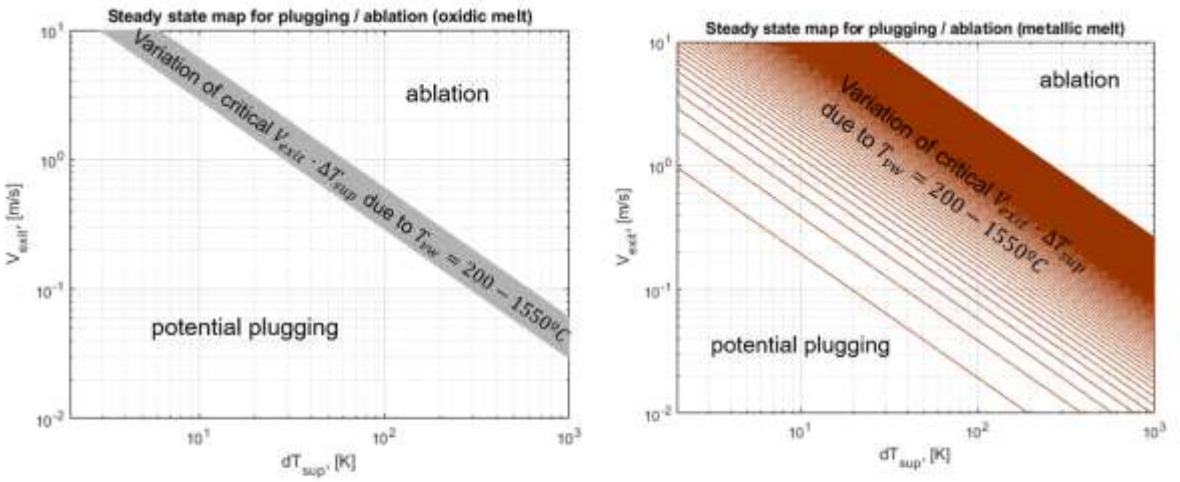

a b

Figure 3-69: Steady state map of plugging and ablation in terms of $\{T_{vw}, V_m, \Delta T_{sup}\}$ for $(R_{vw} = 0.035\ m)$ (a – oxidic melt, b – metallic melt)

The effect is due to significantly higher melting point of oxidic melt vs metallic melt: variation of the vessel wall temperature has mild effect on the temperature gradient and consequently heat flux in the oxidic crust compared to metallic crust.

The plots in the Figure 3-69 further suggest that for given vessel wall temperature the dependence of critical melt release velocity and melt superheat is linear in logarithmic scale and therefore the product $V_{exit}^{crit} \cdot \Delta T_{sup}^{crit}$ is constant.

Steady state map of plugging and ablation can then be expressed in terms of $\{V_{exit} \cdot \Delta T_{sup}, T_{vw}\}$, see Figure 3-70. The results suggest that:

- Domain of parameters where plugging is possible is limited but not physically impossible.
- The plugging domain is larger for the metallic release than for oxidic release.
- The size of the plugging domain for CRGT is smaller than for IGT.
    - Ablation of CRGT is consequently more likely to occur.

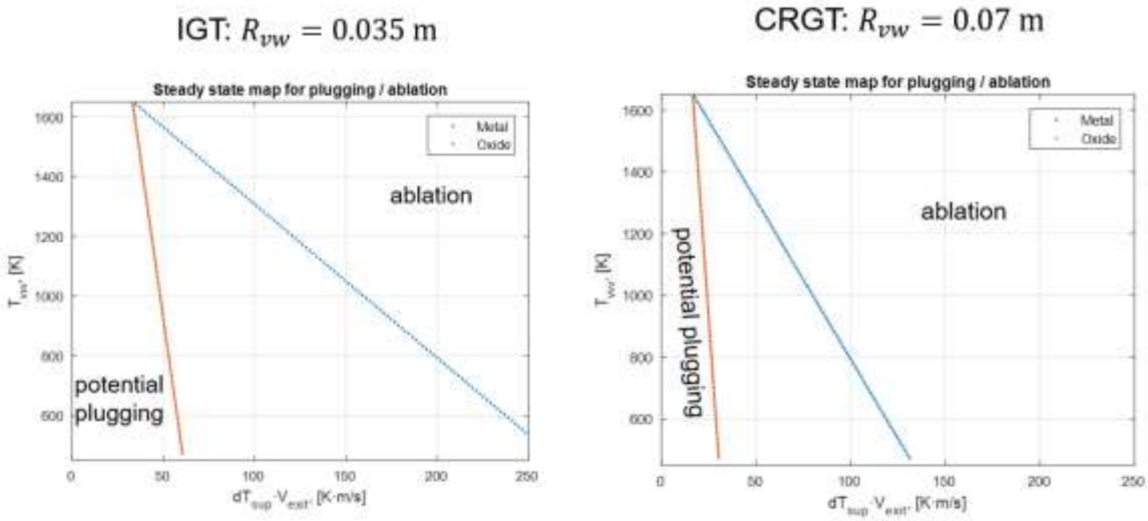

a b

Figure 3-70: Steady state map of plugging and ablation in terms of $\{\mathrm{T_{vw}}, \mathrm{V_m} \cdot \Delta\mathrm{T_{sup}}\}$. (a – IGT failure, b – CRGT failure)

Steady state analysis of breach plugging does not take into account transient reheating of the vessel wall. The results of the steady state analysis, therefore, should be considered only as qualitative (hence, "potential plugging" is used). Assessment of the mass of melt released before plugging or onset of ablation cannot be done without transient analysis.

3.6.2 Transient analysis

The transient model of breach plugging or ablation is schematically demonstrated in the Figure 3-71. It is 1D model with axis of symmetry located at $r_m = 0$ and separate meshing and solvers for temperature profile in the vessel wall and temperature profile in the crust. The heat flux from the melt and therefore at the melt/crust interface is resolved using the same as in the steady state analysis equation, providing a first boundary condition:

$$q_m = Nu \frac{\lambda_m}{2r_m} \Delta T_{sup}$$

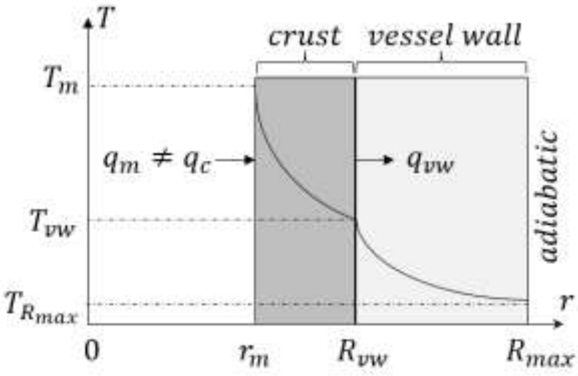

$$q_m = Nu\frac{\lambda_m}{2r_m}\Delta T_{sup}$$

Figure 3-71: Transient model.

Heat transfer equations are formulated in terms of enthalpy H instead of temperature for conservative modelling of transient crust front displacement:

- Temperature profile inside the vessel:

$$\frac{1}{r}\frac{\mathrm{d}H}{\mathrm{d}r} + \frac{\mathrm{d}^2 H}{\mathrm{d}r^2} = \frac{1}{\alpha_v}\frac{\mathrm{d}H}{\mathrm{d}t}$$

- Temperature profile inside crust:

$$\frac{1}{r}\frac{\mathrm{d}H}{\mathrm{d}r} + \frac{\mathrm{d}^2 H}{\mathrm{d}r^2} = \frac{1}{\alpha_c}\frac{\mathrm{d}H}{\mathrm{d}t}$$

where $\alpha_{v,c}$ is thermal diffusivity of the vessel steel and melt crust respectively.

The difference between the heat flux from the melt q_m and the heat flux into the crust at the melt / crust interface defines the rate of crust front displacement:

$$L\frac{dr_m}{dt} = \alpha_c\frac{dH}{dr} - \frac{Nu\,\lambda_m}{\rho_c Cp_m 2r_m}(H_m - H_{inf})$$

where H_m is melt enthalpy at melting temperature; H_{inf} is melt enthalpy at the temperature of the melt; ρ_c is melt density; Cp_m is melt heat capacity; L is the latent heat of solidification.

The second boundary conditions is adiabatic wall temperature at $r_m = R_{max}$:

$$\left.\frac{dH}{dr}\right|_{R_{max}} = 0$$

$R_{max} = 0.161\ m$ is the midpoint between two adjacent CRGTs.

The third boundary condition is equality of the heat fluxes in the crust and in the vessel wall at the crust / vessel interface:

$$\lambda_{vw} \frac{dT}{dr_{vw}}\bigg|_{R_{vw}} = \lambda_c \frac{dT}{dr_c}\bigg|_{R_{vw}}$$

The model has been verified for convergence to a steady state and to a known transient solution for breach plugging with zero melt superheat. Mesh size and time step convergence study has also been performed: 10x mesh and time step reduction resulted in less 3% change in the transient time of breach plugging. It should be notes that crust displacement is resolved continuously, i.e. independently from the mesh.

The model estimates time evolution of the breach radius for a combination of $\{T_{vw}, V_m \cdot \Delta T_{sup}\}$, melt and vessel wall thermal properties. The model predicts the time of the breach plugging or the time of the onset of the breach ablation. An example of transient model calculations is provided in the Figure 3-72. Every curve in the figure represents an individual transient solution. Those solutions that end at zero radius correspond to the cases of breach plugging; those that end at non-zero value characterize the last breach radius and time when start of the vessel wall ablation occurred.

In case of CRGT failure the time scale for plugging is in the order of several 100 or 1000 seconds. For the conditions with zero melt superheat (i.e. fasted possible plugging) the model predicts melt release time until plugging

- for oxidic melt: above 1000 sec;
- for metallic melt: above 200 sec.

Time scales for the onset of the ablation are sensitive to the melt release conditions and vary from 0 to few thousands of seconds. In cases of melt release with breach ablation the jet radius first reduces (suggesting crust growth), then increases (suggesting crust melting) and only after that ablation of the vessel wall starts.

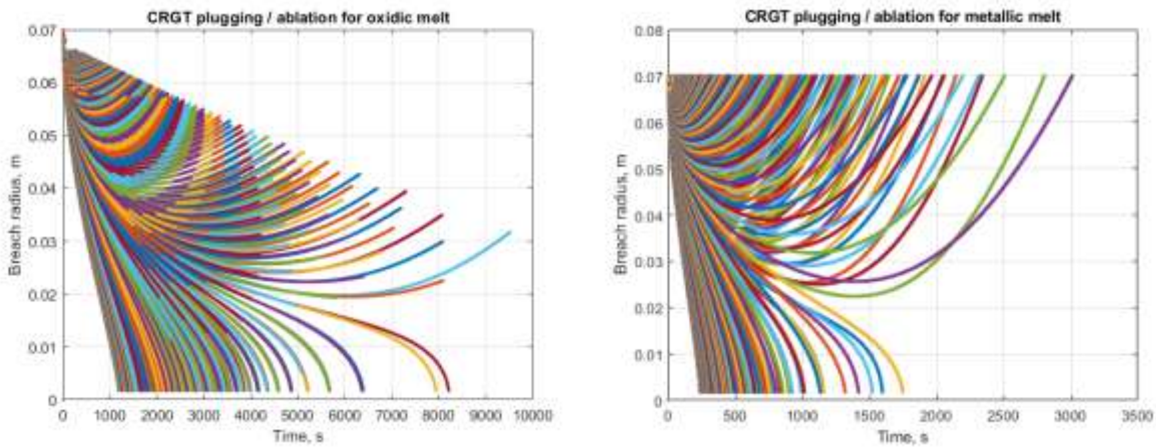

a b

Figure 3-72: Example of transient solution for CRGT failure.
(a – oxidic melt, b – metallic melt)

Similar to the steady state analysis, in the Figure 3-73 we provide the transient maps of breach plugging and ablation for IGT and CRGT failure. The size of the plugging domain is smaller compared to the steady state analysis. The lines separating plugging from ablation are not linear what can be seen from a more refined curve of oxidic boundary in case of CRGT failure (Figure 3-73b). Ranges of plugging conditions $\{V_{exit} \cdot \Delta T_{sup}, T_{vw}\}$ are larger for metallic release then for oxidic release. For example, at low vessel wall temperature 500K an IGT is expected to be plugged:

- in case of oxidic melt if $V_{exit} \cdot \Delta T_{sup} < 40$;
- in case of metallic melt if $V_{exit} \cdot \Delta T_{sup} < 90$.

Plugging of CRGT is less probable then plugging of IGT. For example, at low vessel wall temperature 500K in case of oxidic melt release:

- IGT will be plugged if $V_{exit} \cdot \Delta T_{sup} < 40$;
- CRGT will be plugged if $V_{exit} \cdot \Delta T_{sup} < 20$.

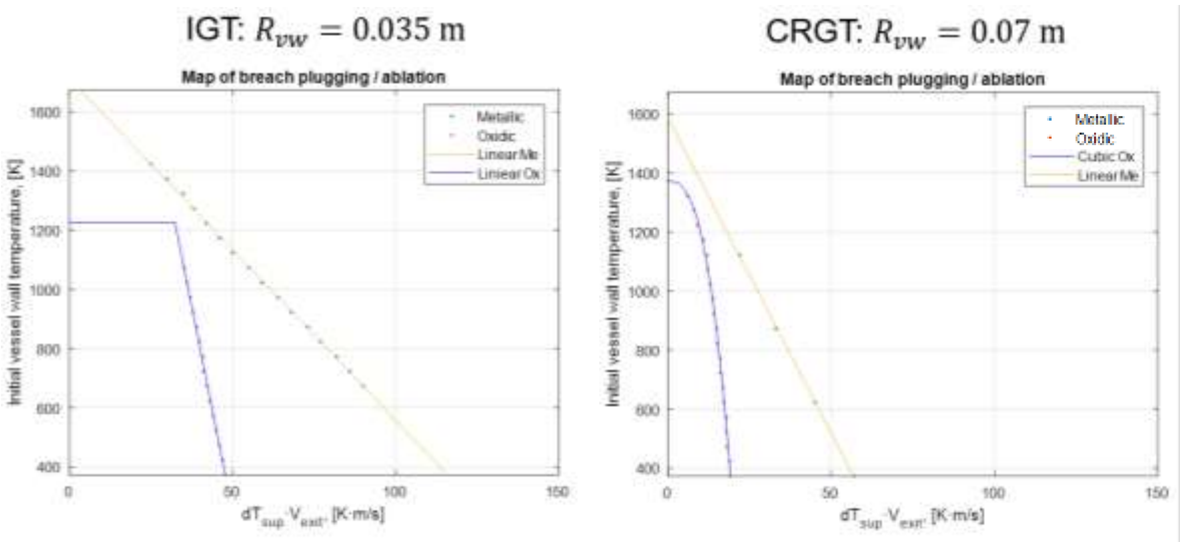

a b

Figure 3-73: Transient map of plugging and ablation in terms of $\{T_{vw}, V_m \cdot \Delta T_{sup}\}$.

(a – IGT failure, b – CRGT failure)

In general ablation is more likely to occur in case of failure of CRGT than IGT.

Given the currently established database of transient solutions (Figure 3-72) it became possible to calculate the mass of melt that can be released through a single breach before plugging or ablation. The results of calculations are provided in the Figure 3-74 and Figure 3-75 in terms of $\{V_{exit} \cdot \Delta T_{sup}, V_{exit}\}$ and a set of T_{vw}. All plots are in the rage from 0 to 250t. Note the database refinement is not yet sufficient and transition region from plugging to ablation (yellow triangle) is not fully resolved.

It should be noted that from the perspective of steam explosion melt release through IGT or CRGT before onset of ablation occurs in dripping regime, i.e. does not threaten the containment.

The results suggest that while significant masses of melt can be release through a single breach, large releases are possible in a limited range of $\{V_{exit} \cdot \Delta T_{sup}, V_{exit}\}$. In the Figure 3-74c-f we plot the statistical distribution of melt release conditions predicted by Vessel Failure SM for IGT failure. In case of oxidic release, the data indicate that less than 30% of scenarios (Figure 3-74d) fall into the range of $\{V_{exit} \cdot \Delta T_{sup}\}$ from 0 to 250, where for the provided upper and lower bound of melt release velocities (see green and black curves in the Figure 3-74c) the melt release mass may exceed 50t. In case of metallic release, the data indicate that less than 10% of scenarios (Figure 3-74f) fall into the range of $\{V_{exit} \cdot \Delta T_{sup}\}$ from 0 to 300, where for the provided upper and lower bound of melt release velocities (see green and black curves in the Figure 3-74c) the melt release mass may exceed 20t. It should be noted that the numbers provided are preliminary because direct coupling between the new MEM SM and Vessel Failure FM has not been implemented yet.

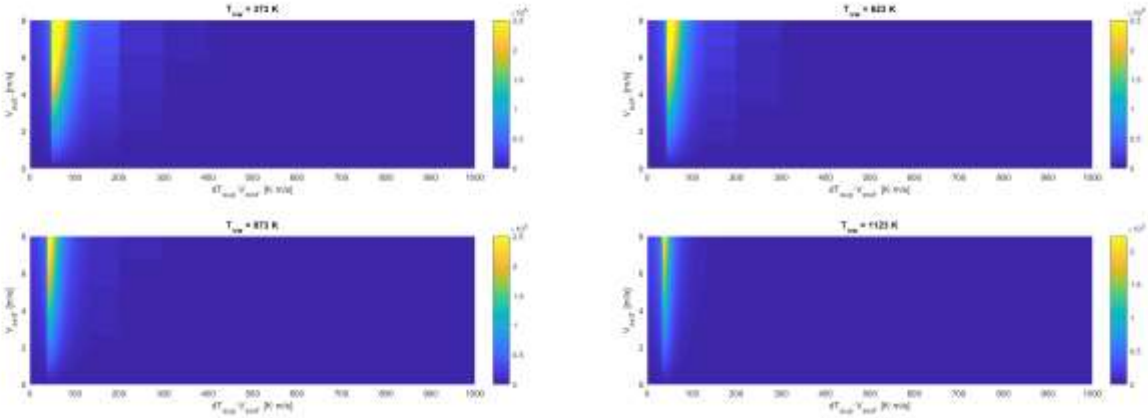

a

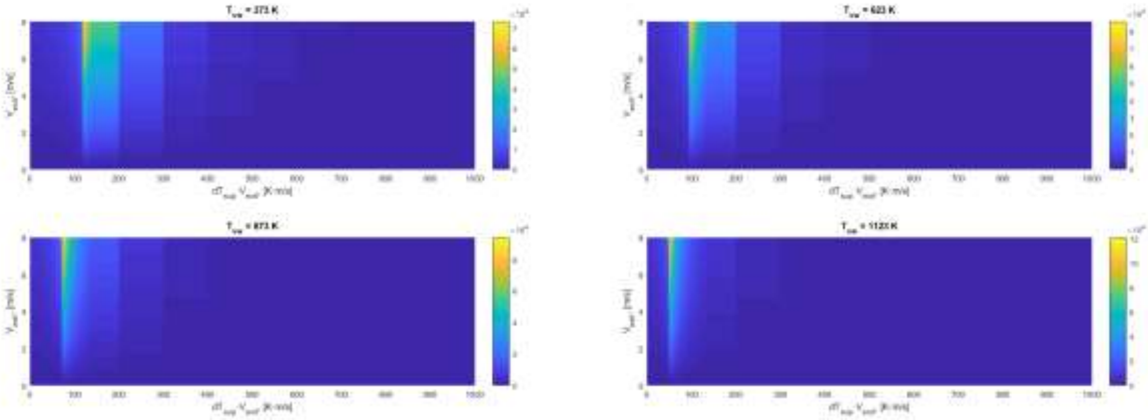

b

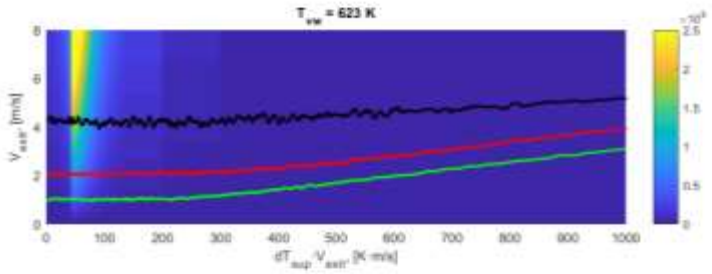

c

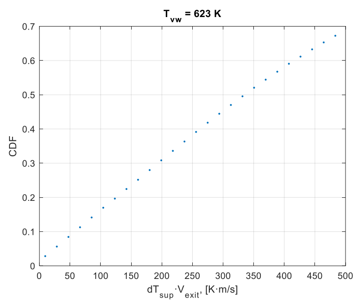

d

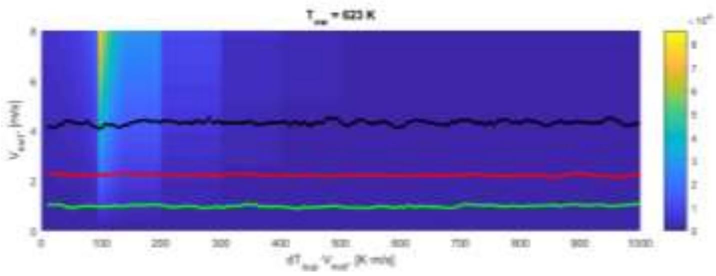

e

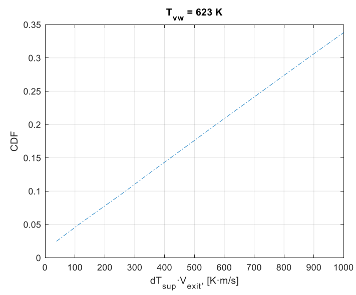

f

Figure 3-74: MEM: Mass of oxidic (a) and metallic (b) melt that can be released through a single IGT before plugging or ablation and expected domain of melt release conditions predicted by Vessel Failure SM for oxidic (c, d) and metallic (e, f) releases.

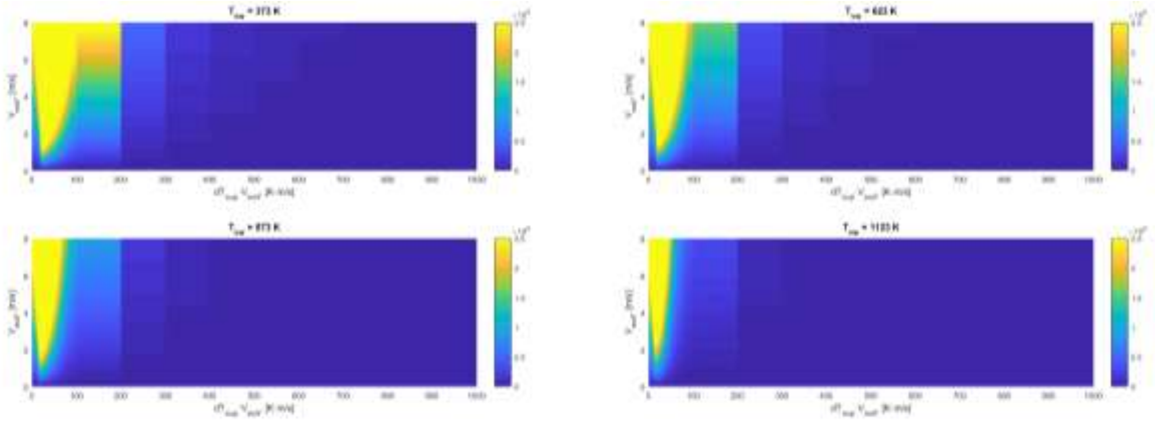

a

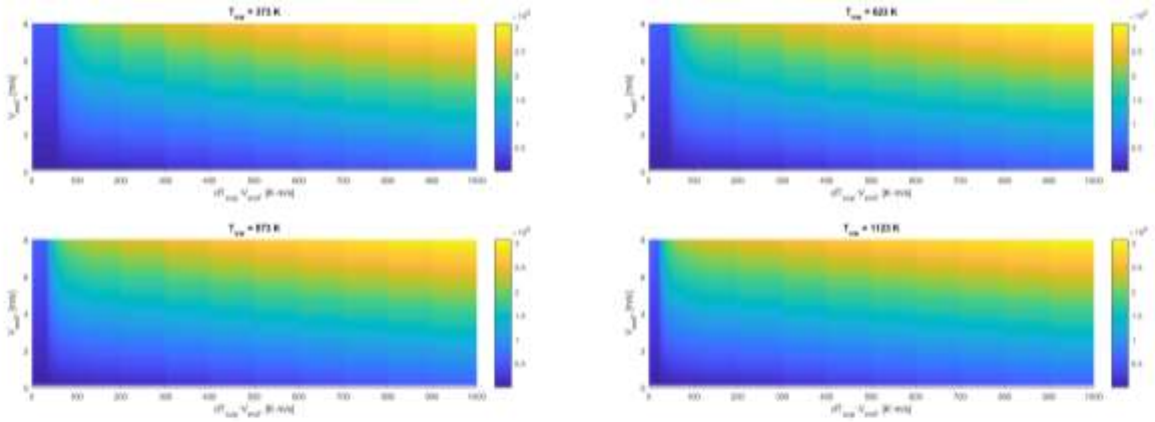

b

Figure 3-75: Mass of oxidic (a) and metallic (b) melt that can be released through a single CRGT before plugging or ablation

It is interesting to further consider the number of IGTs or CRGTs that should fail simultaneously to allow release of complete 250 t of melt before plugging or ablation. The results are given in the Figure 3-76 and Figure 3-77. All plots are provided in the range from 0 to 60 in case of IGT and from 0 to 140 in case of CRGT. While ranges of $\{V_{exit} \cdot \Delta T_{sup},\ V_{exit}\}$, where melt release is significant, can be increased due to multiple failures, especially in case of CRGT, the actual outcome is not straightforward. On one hand multiple failures might have a positive effect on more uniform debris spreading in the pool, on the other hand multiple jets increase the mass of melt premixture and thus of containment failure risks by steam explosion. In addition, failure and slip-off of CRGTs is questionable because they can be supported underneath the vessel.

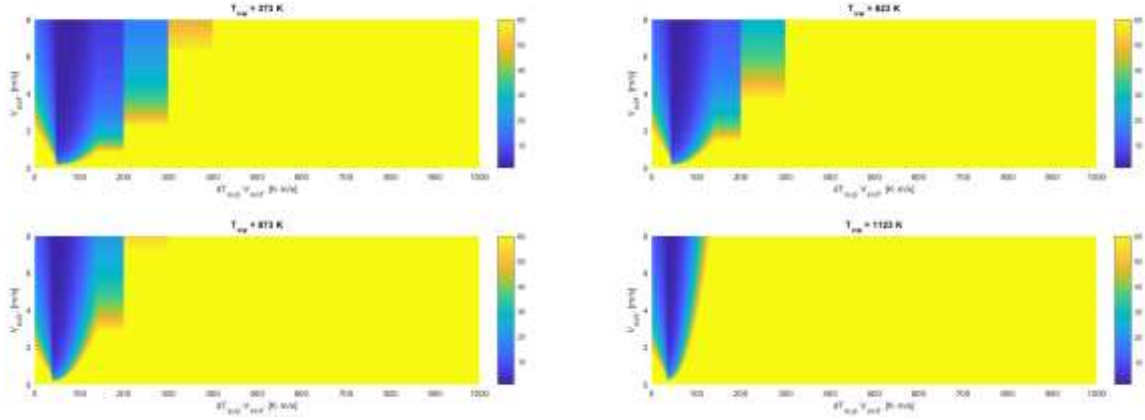

a

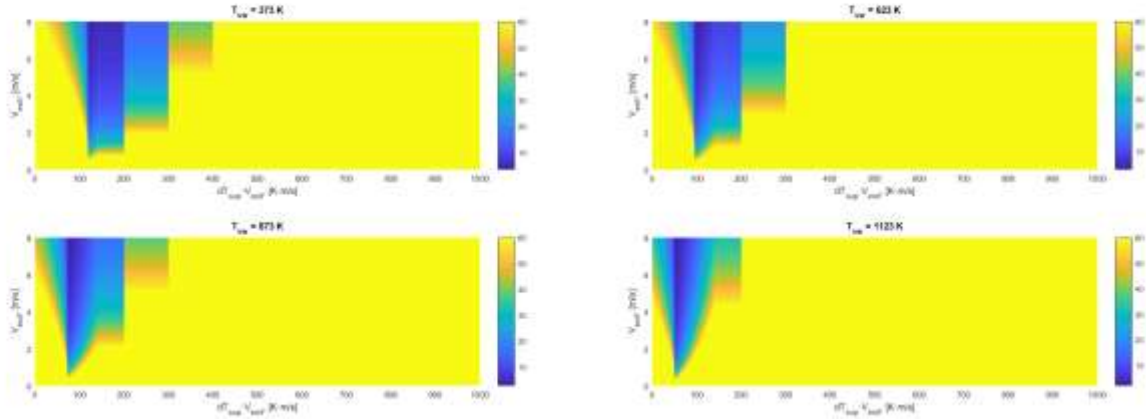

b

Figure 3-76: Number of failed IGTs required to release 250t of oxidic (a) and metallic (b) melt before plugging or ablation.

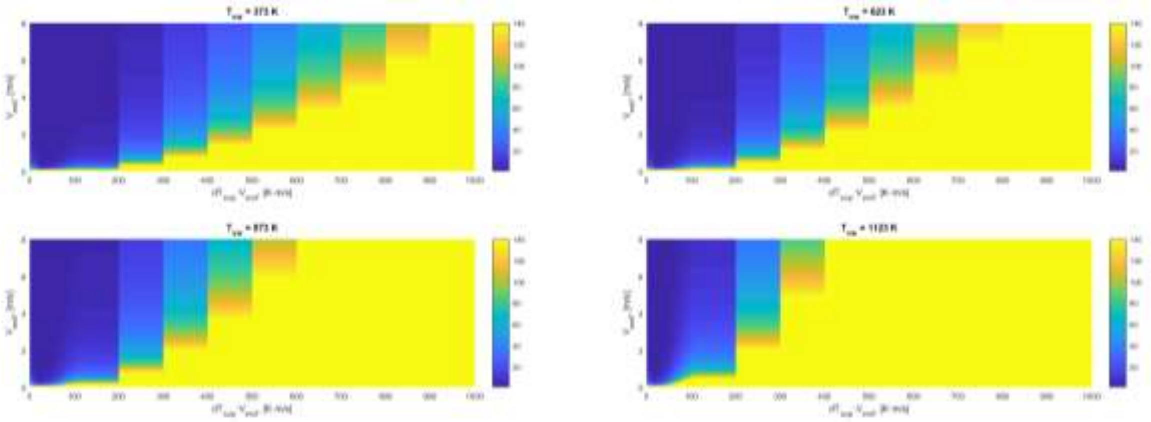

a

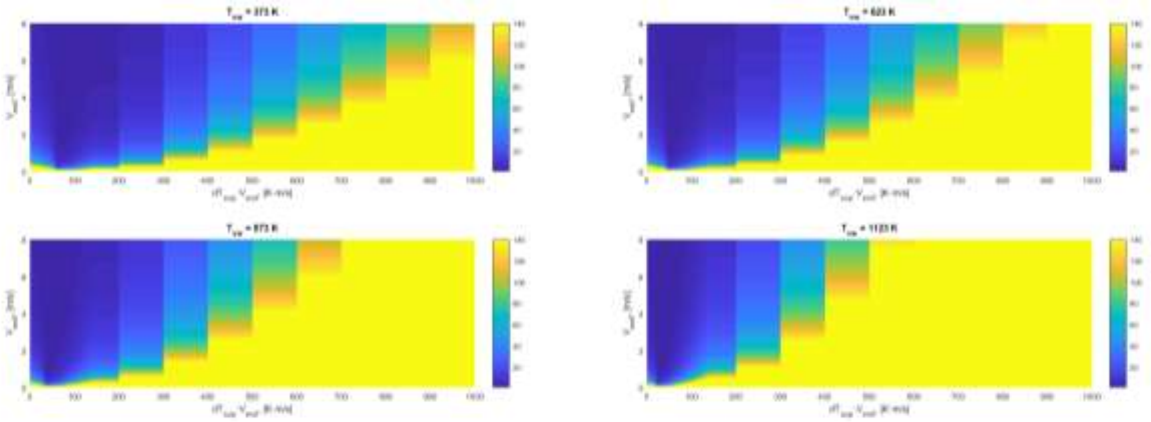

b

Figure 3-77: Number of failed CRGTs required to release 250t of oxidic (a) and metallic (b) melt before plugging or ablation.

3.7 Debris Coolability Map (DECO)

Non-coolable debris bed presents a credible threat to containment integrity. Phenomenology of ex-vessel debris bed formation and coolability includes coupled (i) jet breakup, (ii) melt droplet cooling and solidification; (iii) debris agglomeration; (iv) particle spreading in the pool; (v) debris bed self-levelling; (vi) debris bed coolability; (vii) post-dryout behavior with possible remelting, etc. Debris bed cools by evaporating water that is pushed into the bed by the hydrostatic pressure. Steam generated inside the debris bed is escaping predominantly upwards, generating convection flows in the pool and changing conditions for melt-coolant interactions. This changes particle properties (size distribution and morphology), packing, agglomeration, and bed formation phenomena. The large-scale circulation in the pool can spread effectively the falling corium particles over the basemat floor, distributing the sedimentation flux beyond the projection area of particle source (e.g., size of reactor vessel). Debris is gradually spread under the influence of steam production in the bed, resulting in self-leveling of the settled portion of the debris and changing the shape of debris bed with time. Relevant phenomena have been extensively studied in the past. Experiments (Figure 3-78) on debris bed and particle properties (DEFOR-S) [166], debris agglomeration (DEFOR-A) [168], porous media coolability (POMECO) [179], particulate debris spreading (PDS) [10] have been developed. A set of full and surrogate model has been developed and validated against produced experimental data for the debris formation [172], agglomeration ([146], [142]), coolability ([322], [310]) and spreading [11] of the debris.

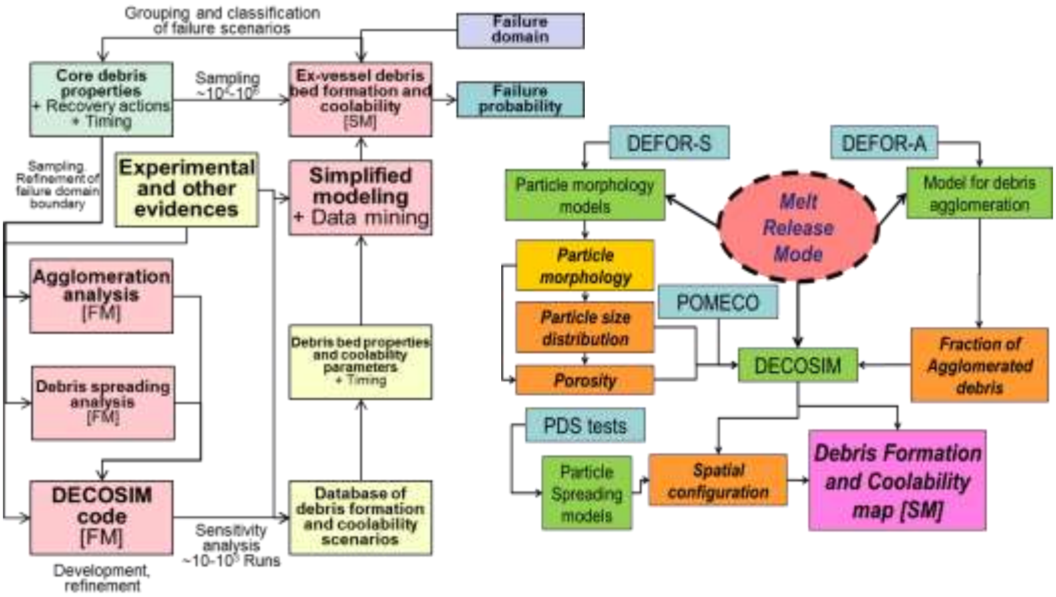

Figure 3-78. Ex-vessel debris bed formation and coolability framework.

The aim of the DECO framework is integration of knowledge about different phenomena in the models that can resolve important feedbacks and, possibly, identify limiting mechanisms that can reduce uncertainty in assessment of debris coolability.

3.7.1.1 DECOSIM Models for Debris Bed Coolability Analysis

The mathematical models implemented in DECOSIM code are based on multifluid formulation, they include a number of submodels describing two-phase pool flows, disperse particle sedimentation, as well as flows in heat-releasing porous media related to debris bed coolability in in-vessel and ex-vessel configurations. In this work, we concentrate on validation of the models relevant to modeling natural convection flows in the pool, spreading of particles and their fallout onto the bottom surface of the pool [308]. Air-water flow in the pool is described by the mass and momentum, and energy conservation equations for liquid water and gas; turbulence is taken into account only in continuous liquid and described by the $\boldsymbol{k-\varepsilon}$ model with additional terms for turbulence generation due to relative motion of liquid and gas phases [162]. Validity of $k-\varepsilon$ turbulence model in the context of two-fluid model has been addressed previously [140]. Flow-particle interaction due to drag depends on the diameter of the particle, relative velocity and phase composition of the ambient two-phase mixture. To account for turbulent dispersion of particles, the random walk model is applied. The effects of turbulence on particle dispersion are modeled by adding a fluctuating component to the liquid phase velocity. Note that PDS-P experiments [134], [135] were specifically designed to ensure that particle interaction and effect on the flow was negligible; therefore, their results are adequate for validation of the current DECOSIM model. Studies of high-concentration particle releases would require both different experimental conditions and model implementation with "two-way" particle-flow coupling; which is beyond the scope of the present work.

3.7.1.2 Experiment on Debris Formation and Agglomeration

First systematic study of the debris bed formation phenomena was carried out in the framework of DEFOR research program which includes experimental works [125], [126], [164], [165], [166], [167], [168], [169], [170], [189], [160], [136] and development of analytical models and approaches [143], [144], [145], [146], [148], [149], [150], [171], [172], [307]. The goal of DEFOR (debris bed formation) experiments is to provide data necessary for the development of analytical models and approaches for prediction of debris bed formation and agglomeration phenomena. DEFOR facility was developed for studies of melt fragmentation, particle and debris bed formation and agglomeration in deep water pool. The installation consists of (i) an induction furnace for melt generation, (ii) a funnel for melt deliver, (iii) a test section with optional metallic sample, and (iv) external water heating system. The scheme of the installation is given in Figure 3-79.

Each catcher is covering one of four quadrants of the test vessel cross section and collects melt fragments ejected from the jet. This allows assessment of the water pool depth on debris bed formation: agglomeration and local particle size distribution. Typical agglomerated debris and cake obtained in DEFOR-A (agglomeration) tests are presented in Figure 3-80.

More than 20 DEFOR-A tests have been carried (Table 3-8). In the first test series (A1-A9 [169], [168], [258]) Bi_2O_3-WO_3 (eutectic) melt with melting temperature 870°C was used. Second test series (A10-A21) was carried out using ZrO_2-WO_3 (eutectic) melt with melting temperature 1231°C. Debris bed topology, total porosity, agglomerated mass, and particle size distribution were measured in each test. Melt was released above or below the water surface in order to assess the effect of the jet velocity on the particle size distribution. Experiments with different melting temperature simulant materials and melt release conditions provided a database which can be used for assessment of different test parameters on the properties of the debris bed. While obtained DEFOR experimental database is quite extensive, the maximum size of the jet investigated in the tests was limited to 25 mm. Further investigation of the debris bed formation phenomena can help to clarify possible effects of larger size jets and higher water subcooling on the debris size distribution, agglomeration, porosity and shape. The main goal and focus of the new experimental studies is extension of the experimental database obtained in previous DEFOR tests ([164], [165], [166], [167], [168], [169], [170]) towards more prototypic conditions and covering ranges of important parameters. Conditions of the DEFOR tests carried out in the new test series are summarized in Table 3-9

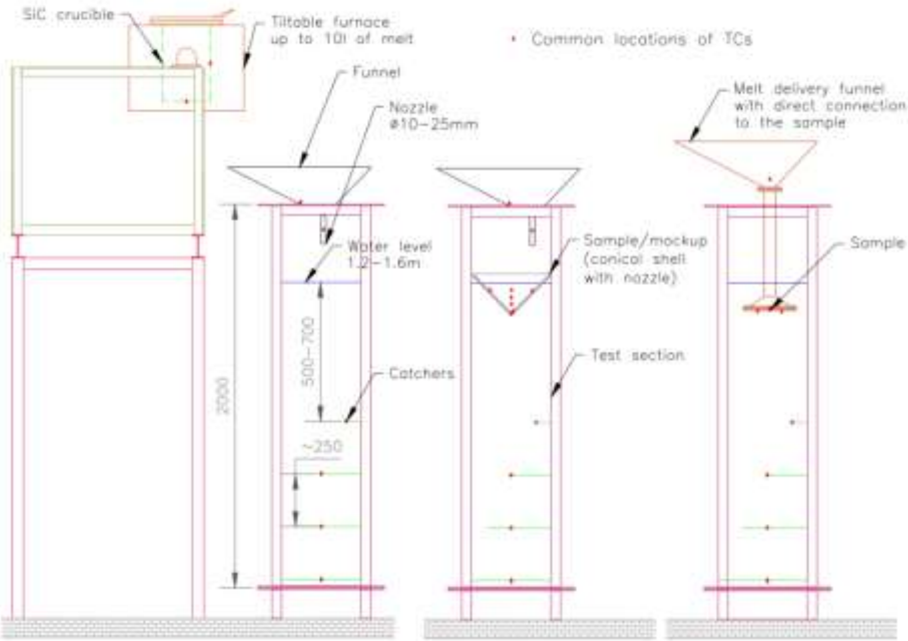

a. b. c.

Figure 3-79. DEFOR facility: for a) A01-11;15, b) A12-14;16 and c) A17-21. Inside the test section 4 debris catchers are positioned at different elevations

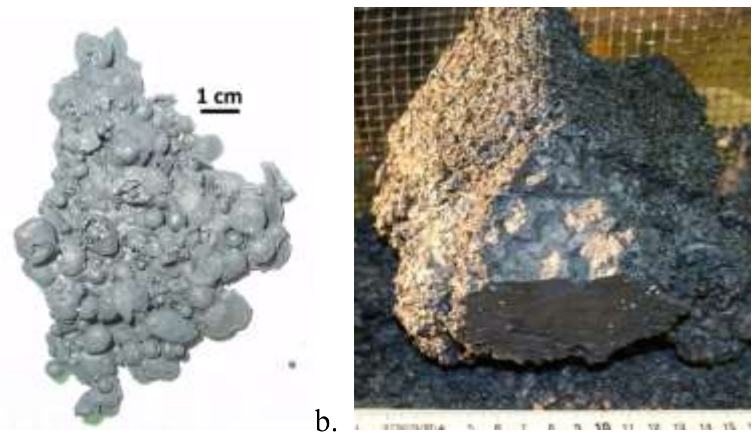

a. b.

Figure 3-80. Agglomerated debris (DEFOR-A2) (a); a cake (DEFOR-A6) (b)

Table 3-8: Ranges of the experimental parameters in DEFOR-A tests.

Parameters	A1	A2	A3	A4	A5	A6	A7	A8	A9	A10	A11	A12	A13	A14	A15	A16	A17	A18	A19	A20	A21
Melt temperature, K	1253	1246	1483	1221	1245	1279	1349	1255	1343	1644	1606	1618	1566	1740	1603	1621	1735	1693	1818	1791	1790

Melt superheat, K	110	103	*-	78	102	136	206	112	200	150	102	114	62	196	100	117	231	189	314	287	286
Melt jet initial diameter, mm	10	20	20	20	10	12	25	25	20	20	20	20	10	15	20	15	2x20	2x20	30	30	30
Elevation of nozzle outlet, m	1.7	1.7	1.7	1.7	1.7	1.7	1.62	1.62	1.7	1.72	1.8	1.85	1.85	1.75	1.8	1.65	1.65	1.65	1.44	1.65	1.5
Jet free fall height, m	0.18	0.18	0.18	0.2	0.18	0.18	0.2	0.2	0.18	0.2	0.7	0.13	0.13	0.2	0.2	0.2	0	0	0	0	0
Duration of melt release, s	38	11	-	11	38	20	10	10	11	13	12	23	6.3	-	9.6	22	10	13	10	15	13
Melt volume, l	3	3	3	3	3	3	3	3	3	3	3	3	3	3	2	4	5	5	5	5	5
Average flow rate, l/s	0.079	0.273	-	0.273	0.079	0.15	0.3	0.3	0.273	0.19	0.16	0.097	0.155	-	0.208	0.125	0.354	0.254	0.44	0.25	0.333
Initial average melt jet velocity, m/s	1.01	0.87	-	0.87	1.01	1.33	0.61	0.61	0.87	0	0	0	0	-	1.01	-	-	-	-	-	-
Water pool depth, m	1.52	1.52	1.52	1.5	1.52	1.52	1.42	1.42	1.52	1.52	1.1	1.85	1.85	1.75	1.8	1.65	1.65	1.65	1.44	1.65	1.5
Water initial temperature, K	346	366	345	346	364	346	356	355	355	348	348	348	348	354	354	345	355	354	359	353	358
Water subcooling, K	27	7	28	27	9	27	17	18	18	25	25	25	25	19	19	28	18	19	14	20	15

Table 3-9: DEFOR tests experimental conditions.

Parameters	A23	A24	A25	A26
Mixture	Bi_2O_3-WO_3	Bi_2O_3-WO_3	Bi_2O_3-WO_3	Bi_2O_3-WO_3
Composition	Eutectic	Eutectic	Eutectic	Eutectic
Melt density, kg/l	7.811	7.811	7.811	7.811
Melting temperature, K	1143	1143	1143	1143
Melt temperature in the funnel, K	1280	1248	1216	1299
Melt superheat in the funnel, K	137	105	73	156
Melt jet initial diameter, mm	25	34	34	34
Elevation of nozzle outlet, m	1.72	1.77	1.77	1.77
Jet free fall height, m	0.205	0.17	0.17	0.17
Duration of melt release, s	5.8	5.3	5.7	5.5
Melt volume, l	3.5	3.5	3.5	3.5
Average flow rate, l/s	0.54	0.62	0.59	0.59
Initial average melt jet velocity, m/s	-	-	-	-
Water pool depth, m	1.515	1.6	1.6	1.6
Water initial temperature, K	332	346	363	346
Water subcooling, K	41	27	10	27

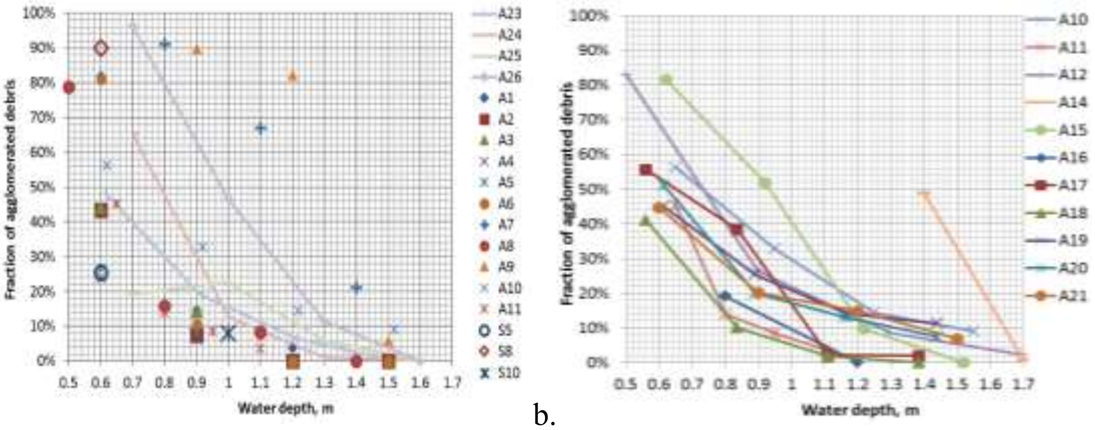

a. b.

Figure 3-81. Debris bed agglomeration fraction as function of water pool depth for A1-A9, S8, S10, A23-26 (a) and A10-A21 (b) tests.

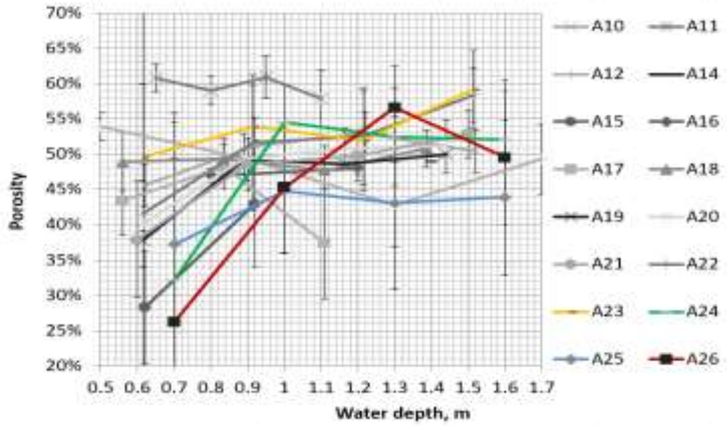

Figure 3-82: Comparison of the debris beds porosity.

Analysis of experimental data suggests that fraction of agglomerated debris decreases rapidly with the depth of the coolant as noticeable in Figure 3-81 for the whole set of experiments (A1-A26). Data on fraction of agglomerated debris from the new DEFOR-A tests agrees well with previously obtained results in the DEFOR-A and DEFOR-S experiments where smaller amount of melt (about 1.0 liter) was used [166]. We found that water subcooling is of minor importance until thermal stresses start to induce solid particle fracture.

On average, larger particles were obtained with ZrO_2-WO_3 melt than with Bi_2O_3-WO_3. Particle size distributions obtained in DEFOR-A overlap with the size distributions observed in FARO tests. The effect of jet free fall height was not noticeable. However, there is a tendency to generate larger particles in the tests with melt release under water. Initial jet velocity seems to have no noticeable effect on the fraction of agglomerated debris. Estimated porosity of the bed is on average about 45-50%, which is also similar to the previous tests. On average higher fraction of agglomerated debris and lower porosity are obtained at lower pool depth. As seen in Figure 3-82, high superheat (as in DEFOR-A26 test) leads to higher agglomeration fraction and lower porosity of the debris bed.

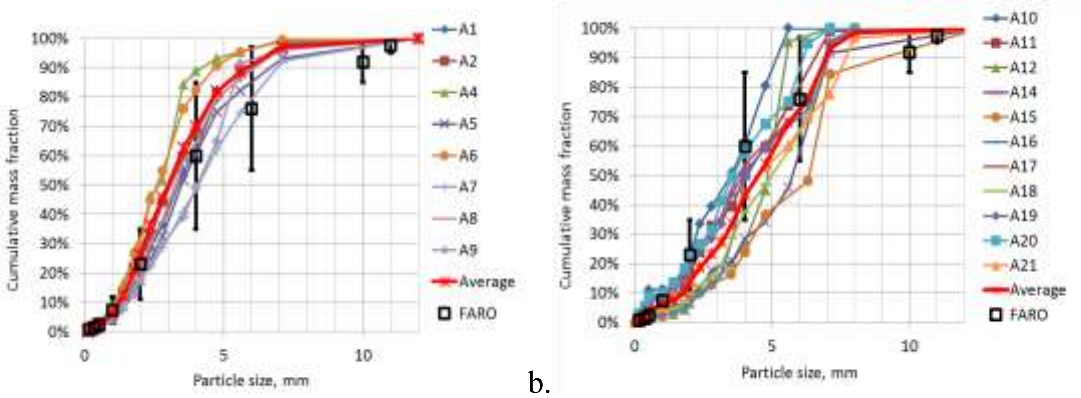

a. b.

Figure 3-83. Cumulative mass fraction for the debris in DEFOR-A1-A9 (a) and DEOFR-A10-A21 (b) tests. For comparison, the data from FARO tests and averaged DEFOR curves for corresponding series of tests are provided.

The particle size distributions (Figure 3-83) were obtained by sieving the debris. For comparison, the previously obtained result from DEFOR-A1-A9 test series [169], [168], [258] is provided in Figure 3-83a. Distributions from the tests with higher melt superheat are located slightly below the average, corresponding to larger particles. Some variations in the data due to the inherent uncertainties in high temperature melt-coolant interaction experiments can be expected. The data from A10-A21 tests (Figure 3-83b) show on average larger particles obtained with ZrO_2-WO_3 in comparison with the previous tests with Bi_2O_3-WO_3. Both series are within the ranges of FARO [185] data.

The small scale DEFOR tests have been carried out in order to clarify the influence of water subcooling on particle morphology [166]. The changes of particle morphology from mostly round shape to a fractured products at relatively small changes of water subcooling (~10-20 K) were explained in [171], [172] by the effect of particle cooling rate change at transition from film to nucleate boiling on the thermal stress of crystallized material. Experimental observations [166] and predictions [171], [172] also suggested that smaller particles (below 1 mm) would have higher chances to avoid fracturing. Experiments were conducted at the MISTEE (micro interactions in steam explosion energetic) small scale facility without steam explosion triggering. For a detailed description of the facility see [189], [190]. The first series of experiments were performed with WO_3-Bi_2O_3 in eutectic composition (74:27 mol%, T_{liq}=870°C) with an initial melt superheat (ΔT_{sup}) of ~130°C. The second series of experiments were performed with WO_3-ZrO_2 in eutectic composition (73:26 mol%, T_{liq}=1231°C) with an initial melt superheat (ΔT_{sup}) of ~130 to 160°C. A set of 3 experiments were performed for each water subcooling (at equal intervals of ~10k) for confirmation of data repeatability. Experimental observations confirmed that at high subcooling, the solidification is faster compared to low subcooling of water. Film boiling conditions (highly dependent on water temperature) dictates the fragmentation process. A morphological transition i.e. from round shapes (smooth) to rock like shape with sharp edges is observed, especially for the WO_3-Bi_2O_3. The mass fraction of fractured particles increases with increased water subcooling. A sharp transition in debris particle size distribution is observed at ~ 50 K water subcooling for WO_3-Bi_2O_3 and ~ 60 to 70 K water subcooling for WO_3-ZrO_2. It is instructive to note that that the average particle size of

WO_3- ZrO_2 is predominantly larger, where at high subcooling conditions ~ 60 to 70% of the debris particles were above 3 mm and at low subcooling conditions ~ 90% of the debris particles were above 3 mm. WO_3- ZrO_2 consistently produced mostly round shaped particles at even high subcooling conditions.

3.7.1.3 Debris Agglomeration Surrogate Model

Hydraulic resistance is a limiting factor that determines maximum decay heat that can be removed from the bed. If decay heat exceeds this maximum value, it will lead to the bed dryout, reheating and remelting of the debris. If melt is not completely solidified prior to settlement on top of the debris bed, agglomeration of the debris and even "cake" formation is possible [184], [166], [126], [167], [168], [169], [160]. Formation of agglomerated debris can significantly increase hydraulic resistance and reduce maximum decay heat which can be removed without reaching dryout of the debris bed. Thus agglomeration is important factor which can inhibit effectiveness of ex-vessel debris coolability [316]. Although agglomeration of the debris and "cake" formation have been observed in previous fuel-coolant interaction (FCI) experiments with prototypic corium mixtures (e.g. in FARO [184], CWTI and CCM [256] tests) and with corium simulant materials (e.g. in DEFOR-E [126] and DEFOR-S [166] tests), the first systematic experimental data was provided in DEFOR-A [167], [168], [169], [160] tests.

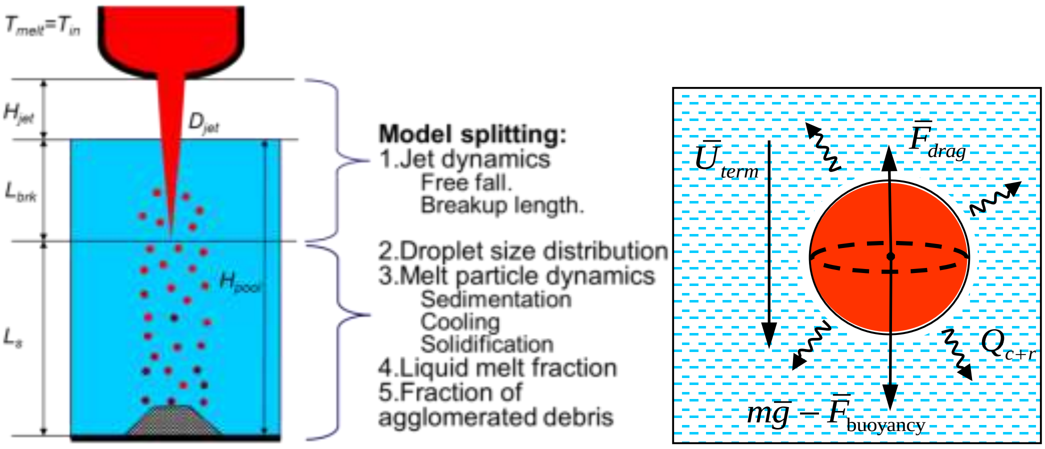

Figure 3-84. Splitting of physical processes for development of the SM.

The data obtained in DEFOR-A tests was used for development and validation of modeling approaches for prediction of agglomerated debris in various scenarios of melt ejection [144], [143], [145], [147], [148], [146], [153]. Proposed model for agglomeration is implemented in deterministic code VAPEX-P [51], [50] that simulates Fuel-Coolant-Interaction (FCI) phenomena including melt jet breakup, formation of liquid droplets, heat transfer between melt and coolant, sedimentation and solidification of the particles.

The goal of this work is to develop and validate a surrogate models for prediction of mass fraction of agglomerated debris. Physics based surrogate modeling approach is employed where computational efficiency and numerical stability are achieved by (i) considering only most important physical phenomena, and by (ii) decomposing tightly coupled problem into a set of loosely coupled ones with information exchange through initial and boundary conditions. The merits of physics based SM are (i) reduced number of the full model runs which are necessary for the calibration process; (ii) application of the SM beyond the domain covered with the original model. Physical phenomena and parameters important for assessment of agglomeration fraction are presented in Figure 3-84. The most important physical phenomena are modeled in the SM explicitly. Mutual feedbacks between such parameters as jet breakup length, coolant void fraction and velocity are taken into account as closures. Details of model implementation, calibration and verification are provided in [144], [143], [145], [147], [148], [146], [153]. Quite good agreement between FM and SM solutions is illustrated in Figure 3-85. It is instructive to note that in order to obtain one point on the agglomeration map (single combination of jet size and pool depth) with FM takes ~24 - 168 hours of computational time. Obtaining complete agglomeration map using SM takes about half an hour including post processing of the results.

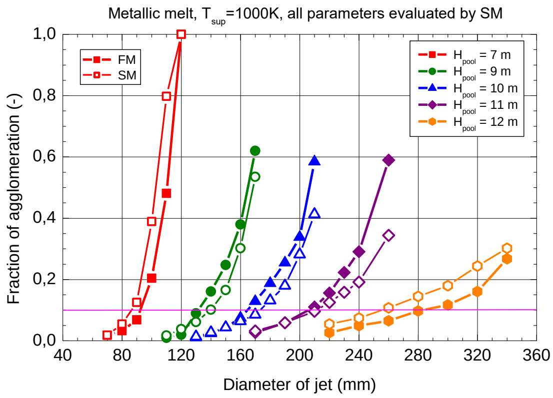

Figure 3-85. Comparison of predictions of mass fraction of agglomerated debris with full model and SM. Solid symbols – FM, half-filled symbols – SM.

Table 3-10: VAPEX SD model input parameters

Variable Name	Description	Units	Range
RHOP	Fuel density	kg/m3	[7500 ; 8500]
PHEAT	Fuel latent heat	J/kg	[2.6e5 ; 4.0e5]
CP	Fuel heat capacity	J/kg*K	[350 ; 650]
KFUEL	Fuel thermal conductivity	W/m*K	[2 ; 42]
Em	Emissivity	-	[0.1 ; 1.0]
TLIQSOL	Liquidus\Solidus Temperature	K	[1600 ; 2800]
Po	Containment pressure	Pa	[1e5 ; 4e5]
Tlo	Water pool temperature	K	[288 ; 368]

Table 3-11: Agglomeration SM Model input parameters

Variable Name	Description	Units	Range
DPARN	Jet diameter	m	[0.07 ; 0.6]
UPIN	Melt release velocity(initial)	m/s	[1 ; 8]
TSH	Melt superheat	K	[10 ; 1000]
xpw	Pool depth	m	[5 ; 9]
CBR $= C_{brk}$	Jet break up correlation coefficients		[0.0002 ; 0.001]
BBR $= B_L$			[0.0 ; 0.01]
AFCI $= A_{FCI}$	Pool void model;		[5 ; 15]

BFCI $= B_{FCI}$			[0.5 ; 3]
AVW $= A_{vw}$	Pool vertical velocity model;		[19.78 ; 19.78]
BVW $= B_{vw}$			[13.19 ; 19.78]
CVW $= C_{vw}$			[-0.35 ; -0.25]
AUW $= A_{uw}$	Pool lateral velocity model;		[10 ; 14]
BUW $= B_{uw}$			[-1.5 ; -0.5]
CUW $= C_{uw}$			[-0.1 ; -0.05]
UMIN $= U_{min}$			[0.0 ; 0.05]

Global sensitivity analysis was carried out [153] using Morris method [195], [236] and the physics based SM in order to identify the most influential parameters for debris agglomeration. In the analysis we considered both parameters of the melt release scenario and calibrated coefficients used in the SM closure parameters. The execution of the model is performed in two steps: (i) calculation of the data base of cooling histories of a single spherical particle falling through a fluid (VAPEX-SD), given properties of the melt, particles sizes and other parameters that can affect particle interaction with a fluid; (ii) calculation of the fraction of agglomerated debris, given single particle cooling histories, particle size distribution, jet properties (jet size, jet release velocity), pool conditions and closure parameters ranges, which are based on the results of models calibration.

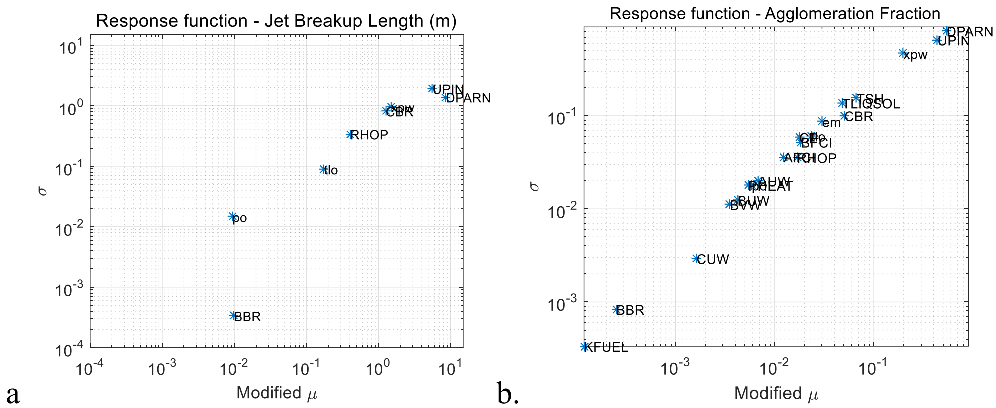

Figure 3-86: Morris Sensitivity results a) Jet Breakup Length; b) Debris agglomeration fraction.

Figure 3-86 presents the results of Morris sensitivity analysis. The results show that the fraction of agglomerated debris is mostly influenced by the parameters of the melt release scenarios DPARN (jet diameter), UPIN (initial melt release velocity) and XPW (pool depth). This is because the jet breakup length, which is one of the most important factors for debris bed agglomeration, is mostly influenced by DPARN, UPIN, XPW and closure coefficient CBR, however, the relative importance of CBR and XPW is significantly smaller compared to DPARN and UPIN for the selected ranges of the parameters. Further analysis is necessary, to determine the relative importance of jet break up model parameters on the results. This concerns mainly relatively small jet diameters (e.g. IGT failure), where uncertainty in the results due modelling parameters might be more important.

3.7.1.4 *Debris Bed Formation and Coolability Surrogate Models*

Full model (DECOSIM) simulation results were used as the basis for development of computationally efficient surrogate models for debris bed formation and coolability [307]. In the case of gradual melt release into a deep pool of saturated water the interaction of falling particles with the flow results in spreading of melt over the pool basemat, the smaller the particles and higher the decay heat power, the more effective is the spreading. In order to estimate the efficiency of particle spreading, a simple empirical model can be developed which generalizes the results of simulations [317]. Consider a droplet of diameter d_p falling in the water pool of depth H_P. A non-dimensional parameter χ was introduced $\tan\phi = f(\chi)$, $\chi = \frac{\Delta H_{ev}\rho_g}{\rho_p(1-\varepsilon)WH_P}\left(\frac{4gd_p}{3C_d}\frac{\rho_p-\rho_l}{\rho_l}\right)^{1/2}$ where droplet of diameter d_p falling in the water pool of depth H_P drag coefficient C_d is a function of particle Reynolds number, the vapor density must be evaluated at the pressure near the pool bottom, i.e., with the hydrostatic head taken into account: $\rho_g = \rho_g\left(P_{sys} + \rho_l g H_P\right)$, with P_{sys} being the system pressure in the gas space above the pool level. For each simulation [317], the final shape of debris bed was processed, and the characteristic tangent of slope angle determined. The solid line shows the best fit to the data. By the horizontal dashed line, the tangent of typical avalanche angle $\theta^0_{rep} = 35^{\circ}$ is plotted. Approximation (Figure 3-87), shows that for prototypic conditions particle spreading in the saturated pool is an effective mechanism for reducing the height of debris bed. The decay heat power can be expected to be in the range 100–150 W/kg. The largest mean particle diameter, can be expected in the range of 1–5 mm. The largest slope angle expected can be about 8 degrees, reached for the largest particle diameter and lowest decay heat power. Smaller particles are distributed almost evenly over the pool basemat.

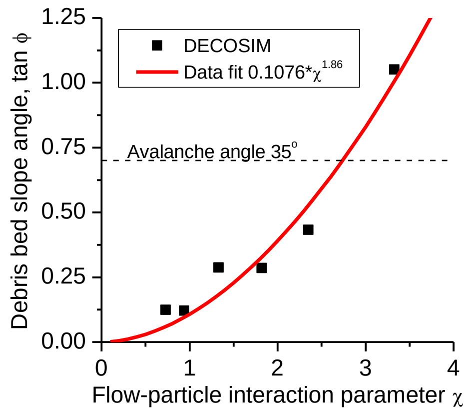

Figure 3-87: Slope angle for gradually formation bed in saturated water pool.

If the pool is subcooled it remains single-phase beyond the debris bed for a substantial period. Simulations of debris bed formation in a subcooled pool performed in [309] showed that temperature differences arising in the pool cause some natural circulation, but it is much weaker than that in a saturated pool and, therefore, the shape of debris bed at the initial stage is governed by particle avalanching only. However, gradual increase in the pool temperature due to latent and fusion heat transferred from hot melt particles, as well as decay heat released in corium results in boil-up of the pool after some delay time. The boil-up starts at the top layer of the pool where hot water plume from the debris bed reaches saturation conditions, while the rest of the pool remains subcooled. After the onset of boiling, intensive convection starts in the pool, so that the remaining part of melt interacts with the circulatory flow in the pool and is dispersed efficiently over the pool basemat. Thus the debris bed grows upwards mainly at the pre-boiling stage, while afterwards it mostly grows laterally, with the particle sedimentation flux distributed evenly over the pool bottom. This simple scheme can be used to set up the intermediate or final shape of the debris bed.

The time to boil-up of a pool having initial subcooling $\Delta T_w^0 = T_{sat}^0 - T_w^0$ (T_{sat}^0 is the saturation temperature at the pool pressure, T_w^0 is the initial water temperature) can be evaluated from a simple energy balance model offered in [309] and confirmed by numerical simulations at different subcoolings.

3.7.1.5 Surrogate model for post-dryout debris bed behavior

The numerical results obtained by DECOSIM indicate that in the cases where dryout occurs in the debris bed: dryout zone is located in the top part of the debris bed; vapor flows through the dry zone vertically upwards; temperatures of solid particles and vapor increase in the vertical direction almost linearly, the difference between them being few degrees; maximum temperatures of solid particles and vapor are attained in the top part of the dry zone; vapor cooling is capable of stabilizing the solid material temperature, provided that its flowrate through the dry zone is sufficient.

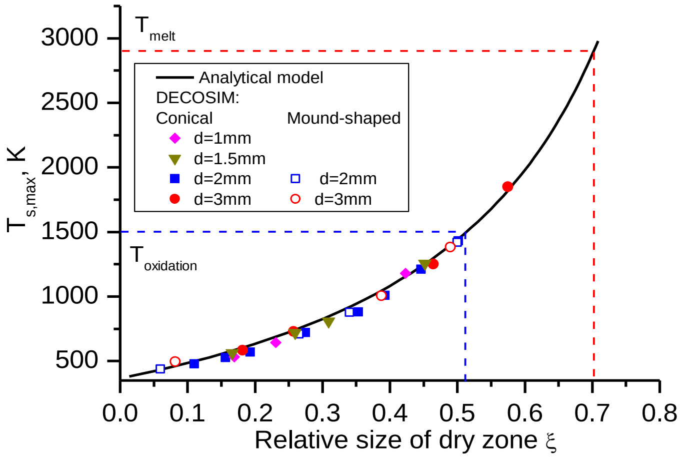

Figure 3-88: Maximum particle temperature vs relative size of dry zone.

These observations allowed an analytical model for the maximum temperature in the dry zone to be developed, laying the basis for post-dryout debris bed surrogate model [310]. The model was confirmed by further numerical simulations carried out by DECOSIM. In Figure 3-88, the maximum temperature of solid particles in the dry zone, $T_{s,max}$, is presented as a function of relative size of the dry zone with respect to debris bed height, ξ. The solid line corresponds to the analytical formula [310] $T_{s,max} = T_{sat} + \frac{\Lambda}{C_p}\frac{\xi}{1-\xi}$ Λ is the heat of evaporation, C_p is the heat capacity of vapor.

In order to apply the above formula in a surrogate model, it is necessary to define the relative size of dry zone ξ as a function of other problem parameters. DECOSIM simulations on post-dryout debris beds were processed in order to obtain a unified relationship for the dry zone size. It was shown that linear dependence exists between the dry zone size and the overheating parameter $\psi = (W - W_0)/W_0$, where W_0 as the dryout decay heat power. This is illustrated in Figure 3-89 where results of DECOSIM simulations are given in the "raw" form (a), as well as in the non-dimensional form (b).

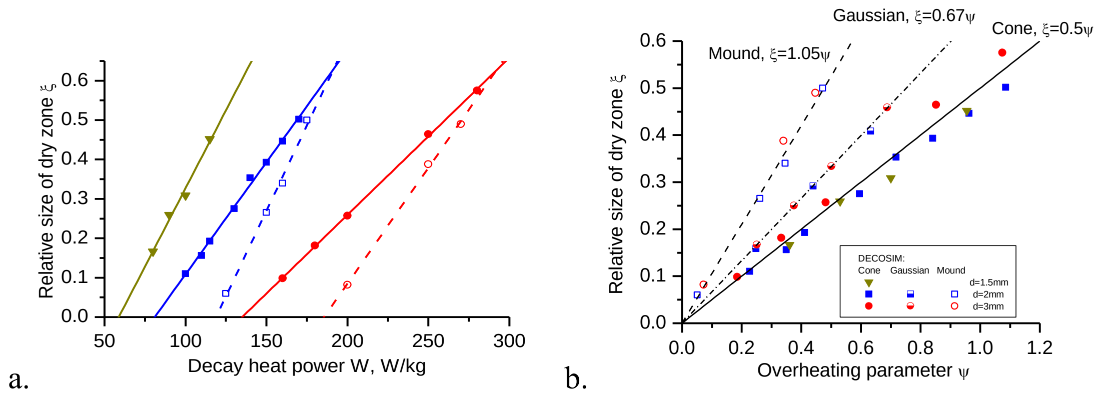

Figure 3-89: Dependence of the relative size of dry zone on decay heat power W (*a*) and overheating parameter ψ (*b*). The legend applies to both Figures.

Thus a surrogate model for the relative size of the dry zone in a post-dryout debris bed can be developed taking into account the debris bed properties (particle size and porosity), system conditions (system pressure, pool depth), and debris bed shape (geometry, aspect ratio, etc.). The model will require a shape-dependent factor $b(\Pi_{shape})$ for which further research is needed. Current results suggest that $b(\Pi_{shape})$ lies in the range between 0.5 and 1.05, see Figure 3-89 (b).

3.7.1.6 Effect of Melt Agglomeration on Debris Bed Coolability

Numerical and experimental studies demonstrate that presence of low-permeability zones (e.g. due to agglomeration) decreases the dryout heat flux [268]. In order to evaluate the effect of melt agglomeration on the coolability of debris bed, two main cases were considered: i) an impermeable "cake", and ii) a low-permeability zone (distributed agglomerates). Coolability of a debris bed with impermeable "cake" occupied the top $H_c = 10$ cm of a mound-shaped debris bed with height $H_{DB} = 2$ m was studied numerically in [311]. Cases with diameter of bed top $D_{\text{top}} = 0.5$, 1, 2, and 3 m are referred to as "Narrowest" (NN), "Narrow" (N), "Wide" (W), and "Widest" (WW) respectively. Vapor accumulates in a dry zone beneath the "cake". However, vapor flow through the dry zone provides some cooling. Time histories of maximum particle temperatures are presented in Figure 3-90. Beds with smaller "cakes" and larger particles are better coolable. The temperatures can either stabilize or escalate and lead to remelting.

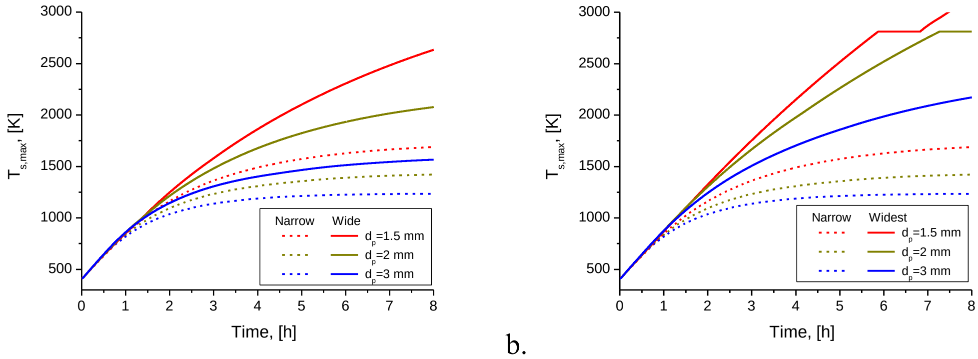

a. b.

Figure 3-90: Maximum temperatures of solid material for different debris bed geometries for decay heat power $W = 80$ W/kg.

Possible effect of vapor release through localized openings (e.g. a central hole) in the cake was studied using the same geometry as in [311]. Three cases were considered [312]: (i) a central hole, 0.2 m in diameter, which is equivalent to 1% opening area; (ii) a central hole, 0.5 m in diameter, which is equivalent to 6.25% opening area; (iii) a ring hole with the inner and outer diameters of 0.4 and 0.6 m respectively, equivalent to 20% opening by area. In Figure 3-91, the states of debris beds are presented at time 7 h. Time histories of the maximum temperature of solid material are shown in Figure 3-92. Even a small (by fraction of area) opening in the cake provides additional escape path for vapor from the dry zone. Larger opening provides better coolability, smaller vertical size of the dry zone and lower stabilization temperature.

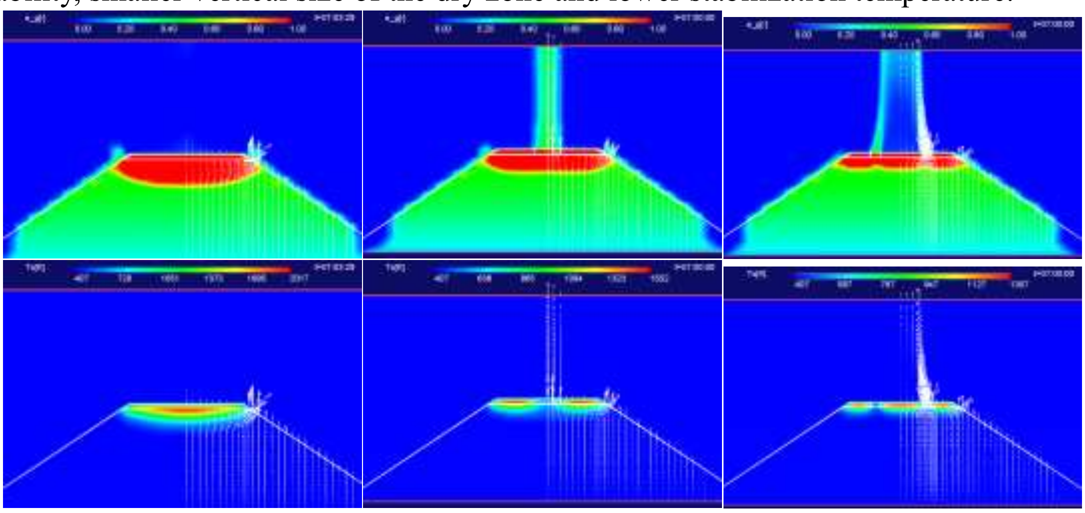

(a) (b) (c)

Figure 3-91: Void fraction (top row) and solid material temperature (bottom row) distributions at time 7 hours: (a) solid cake, (b) 0.5 m central hole, (c) ring hole. Vapor velocity is shown by arrows. Decay heat power $\boldsymbol{W} = \mathbf{80}$ W/kg

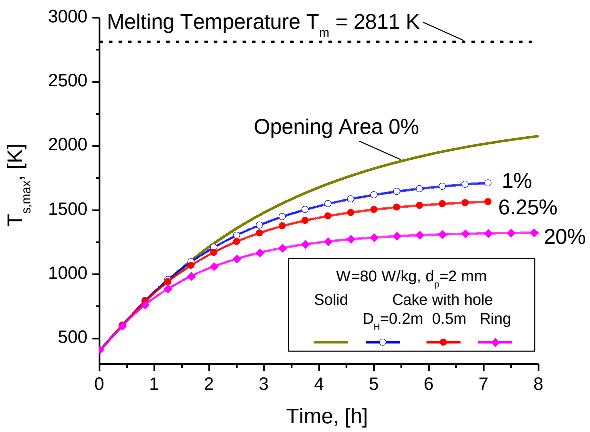

Figure 3-92: Time histories of maximum temperature of solid material for various openings in the cake.

Growth of the debris bed reduces the water pool depth above the debris bed top, so that at some point the depth of water becomes insufficient and melt particles reaching the debris bed form agglomerates. The taller the debris bed, the smaller is the effective pool depth, and the higher is the fraction of agglomerates. The vertical distribution of mass fraction of agglomerates, $\chi_{agg}(z)$, was determined from the surrogate model generalizing the results of numerical simulations. A relationship between the volume-averaged properties of debris (effective porosity, permeability, decay heat etc.) and mass fraction of agglomerates was obtained in [312]. To simplify the coupling of the agglomeration model with DECOSIM, a unified dependency was suggested. In (3-17) a the pool depth $H_{agg}(D_J)$ at which the mass fraction of agglomerates reaches 100% is plotted (this value corresponds to the distinct kink points dividing the plateau $\chi_{agg} = 1$ for $H < H_{agg}$ and rapidly decreasing curve for $H > H_{agg}$). In Figure 3-93b, the points from the decreasing parts of all curves in Figure 3-93a are replotted as a unified function of the reduced depth ζ found by fitting all curves by exponential functions. The following approximations were obtained (both D_J and H_{agg} are measured in meters):

$$H_{agg}(D_J) = 131.32 D_J^{0.02843} - 116.43, \quad \zeta = \frac{H - H_{agg}}{0.06 H_{agg}} \tag{3-17}$$

One can see in Figure 3-93b that with this scaling, all points collapse to a single curve which, within 5% accuracy, can be approximated by exponential function: $\chi_{agg} = \exp(-\zeta)$ for $\zeta \geq 0$, and $\chi_{agg} = 1$ for $\zeta < 0$. Note that both formulas can be combined in a single one:

$$\chi_{agg} = \min(\exp(-\zeta), 1.0) \tag{3-18}$$

Equations (3-17) and (3-18) provide an easy way to evaluate the mass fraction of agglomerates for a particular pool depth and melt jet diameter. It is assumed that the mass fraction $\chi_{agg}(\zeta(z))$

is the same at all radial positions for a given height, i.e., debris bed is stratified in horizontal layers with respect to fraction of agglomerates.

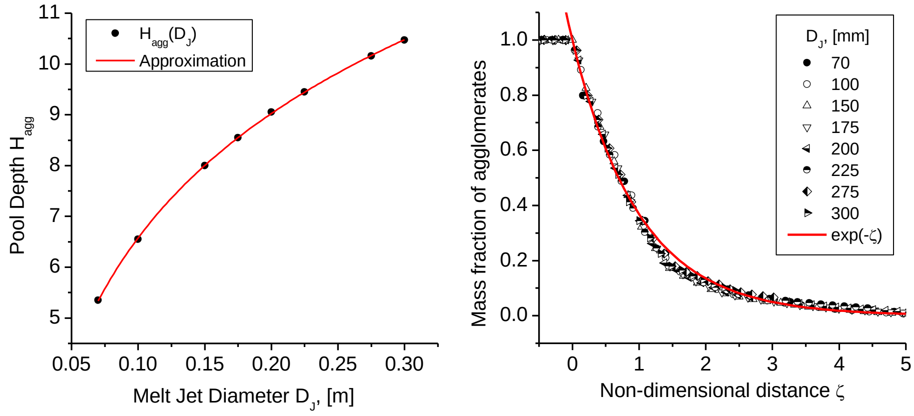

(a) (b)

Figure 3-93: Generalization of melt agglomeration results: (a) pool depth corresponding to onset of 100% agglomeration; (b) dependence of mass fraction of agglomerates on the reduced vertical distance ζ.

Using the above relationships, it is straightforward to evaluate the mass fraction of agglomerates on the debris bed top:

$$\chi_{top} = \min\left(\exp\left(-\zeta_{top}\right), 1.0\right),\ \zeta_{top} = 16.67\left(\hat{H} - 1\right),\ \hat{H} = \frac{H_P - H_{DB}}{H_{agg}(D_J)} \qquad (3\text{-}19)$$

after which the volume fraction of agglomerates and the effective porosity can be found. Note that the transition from with very little to complete agglomeration occurs in quite a narrow range of effective pool depths [162]. Simulations for distributed fraction of agglomerates were performed for the same debris bed geometry as for partially permeable cake. Note that in the absence of agglomerates selected debris beds are coolable. The cases for simulations were chosen such that the maximum agglomerate mass fraction χ_{top} was 10%, 20%, 50%, and 90%. The effective pool depth was assumed $H_P - H_{DB} = 7$ m. Results are summarized in Table 3-12. Cases with dryout are marked with "**Y**" symbol, and the maximum temperature obtained is given. In cases where temperature stabilization did not occur only the maximum temperature at time 4 hours is shown in bold italic, eventually material remelting is expected. The time histories of the maximum temperature of solid material in all the cases where dryout occurred are plotted in Figure 3-94. The distributions of void fractions and temperatures of solid material obtained for $W = 150$ W/kg, particle diameter $d_p = 1.5$ mm are presented in Figure 3-95. One can see that temperature stabilization occurs when the dry zone is of small vertical size, whereas large dry zone results in temperature escalation. Significant deterioration of debris bed coolability occurs when the fraction of agglomerates on the debris bed top is above 50%, with very noticeable effect observed for 90% fraction of agglomerates. Nevertheless, the effect of these agglomerates is still weaker than the effect of completely impermeable cake, or a cake with partial openings (holes).

Table 3-12: Results of simulations for vertically distributed agglomerates.

Decay heat power W, W/kg	**Particle Diameter d_p, mm**	**Melt Jet Diameter D_J, cm**	**Mass fraction of agglomerates on top of the bed, %**	**Dryout**	**Maximum Debris Temperature $T_{s,max}$, K**
80	2	8.9–10.5	10-50	N	410
		11.2	90	**Y**	703
100	2	8.9–10.5	10-50	N	410
		11.2	90	**Y**	929
120	2	8.9–10.5	10-50	N	410
		11.2	90	**Y**	1172
	1.5	8.9-9.5	10-20	N	410
		10.5	50	**Y**	538
		11.2	90	**Y**	***1933***
150	2	8.9-9.5	10-20	N	410
		10.5	50	**Y**	453
		11.2	90	**Y**	***1907***
	1.5	8.9	10	N	410
		9.5	20	**Y**	583
		10.5	50	**Y**	955
		11.2	90	**Y**	***3300***

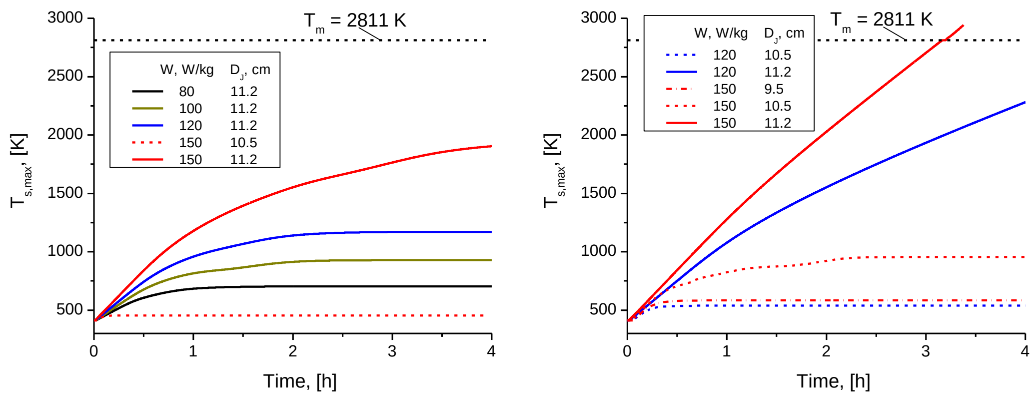

(a) (b)

Figure 3-94: Time histories of maximum temperature in the cases where dryout occurred: particle diameter $d_p = 2$ mm (a) and $d_p = 1.5$ mm (b).

Detailed analysis confirmed that coolability of debris bed can be deteriorated significantly in the presence of low-permeability zone (cake, distributed agglomerates). The effect of agglomerates on debris coolability becomes significant as soon as the mass fraction of agglomerates exceeds some 50% at the top of the bed. In this case, temperature escalation and remelting of material can be expected. Fraction of agglomerates in the top part of debris bed is very sensitive to melt jet diameter and pool depth.

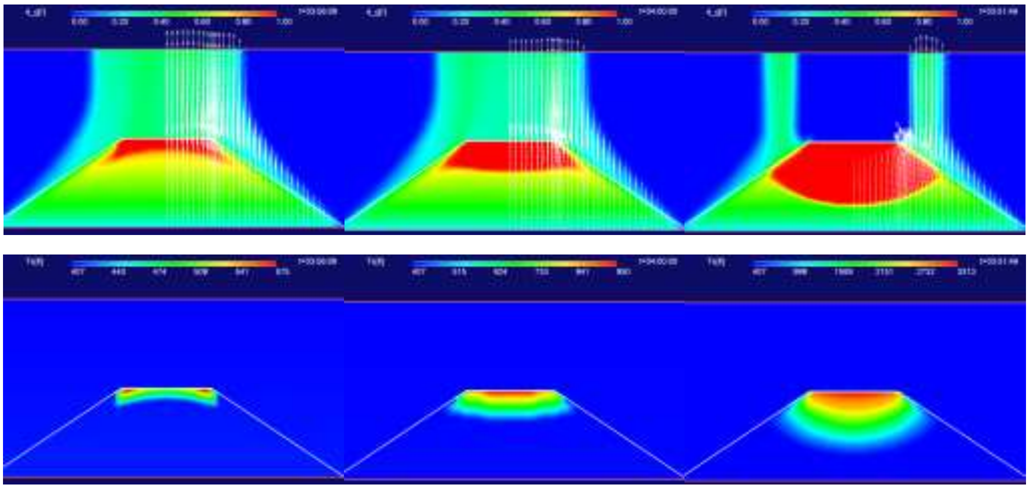

(a) (b) (c)

Figure 3-95: Void fraction (top row) and solid material temperature (bottom row) distributions at time 4 hours: (a) $\boldsymbol{D_J = 9.5}$ cm, (b) $\boldsymbol{D_J = 10.5}$ cm, (c) $\boldsymbol{D_J = 11.2}$ cm. Vapor velocity is shown by arrows.

3.7.1.7 Surrogate Model for Debris Bed Coolability in Presence of Agglomerates

Results of numerical simulations by DECOSIM code can be used as a database for development of a surrogate model (SM) for debris bed coolability taking into account the presence of agglomerates and providing a link between melt ejection mode (MEM) and debris coolability (DECO).

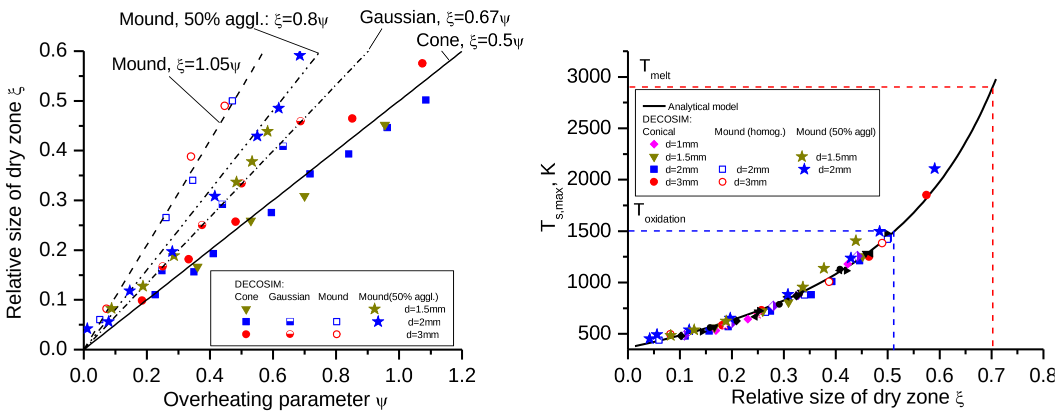

Figure 3-96: Relative size of dry zone vs overheating parameter (a), maximum temperature of particles as a function of dry zone size (b): stars correspond to debris bed with agglomerates, other points obtained for homogeneous bed.

The tentative surrogate model was developed by extending the approach which proved successful for homogeneous debris bed: Simulations performed for few values of decay heat power W; Relative size of dry zone $\xi(W)$ is determined; Extrapolation to $\xi = 0$ gives the dryout power W_{DHF}; Overheating parameter is determined as $\psi = (W - W_{DHF})/W_{DHF}$, dependence $\xi(\psi)$ is obtained; Maximum particle temperature is obtained as $T_{s,max}(\xi)$, compared with analytical model. So far, the surrogate model is based on simulations performed for 2 m-tall mound-shaped debris bed, with mass fraction of agglomerates on its top was 50%. Simulations were run until the particle temperature either stabilized, or reached the remelting temperature of corium. Results are presented in Figure 3-96 (points obtained for homogeneous beds are also plotted). One can see that results for 50% mass fraction agglomerates can be described pretty well by the surrogate model developed for homogeneous debris bed. Further simulations are necessary to establish the applicability boundaries in terms of the fraction of agglomerates.

1.1.1. DECO: Summary and Outlook

Significant progress has been achieved towards the main goal of DECO, i.e. development of the debris bed formation and coolability map. DECOSIM (Debris Coolability SIMulator) code capabilities were significantly extended in order to simulate (i) debris bed coolability in subcooled pool, (ii) post-dryout coolability of the debris bed, (iii) self-levelling of the debris bed, (iv) effect of agglomeration on coolability. However, no melt pool formation model is implemented yet. Several computationally efficient surrogate models have been developed and validated against DECOSIM (full model) predictions. Namely a surrogate model (SM) for prediction of the dryout, and a model for prediction of the maximum temperature in a bed with a dry zone with and without agglomerates, a surrogate model for prediction of debris spreading in the pool.

Particulate debris spreading in the pool and self-levelling of the debris bed have been investigated both experimentally and analytically. PDS-C (closures) experimental database was generalized and a universal non-dimensional closure has been proposed for determining particle flux as a function of the local slope angle and gas velocity. Developed closure has been used in a standalone 1D code for modeling of debris bed self-levelling in plant accident conditions and also implemented in DECOSIM code. The 1D debris spreading model has been used for extensive sensitivity and uncertainty analysis. Further reduction of uncertainty in extrapolation to prototypic accident conditions requires extension of the PDS-C database to particles of different properties, morphologies and size distributions. PDS-P (pool) facility was used to provide data for model validation relevant to particle spreading in a pool. New experimental techniques have been proposed for visualization of particle trajectories. Further work is necessary for obtaining velocity fields of the coolant flow.

The surrogate model for prediction of dryout coupled with self-levelling model has been used in extensive sensitivity, uncertainty and risk analysis by evaluating the conditional dryout probabilities. Sensitivity analyses suggest that the PDFs of the effective particle diameter and porosity are the main contributors to the uncertainty in the conditional containment failure probability (CCFP) and should be prioritized for future research. Clarification of the combination of the possible initial temperatures and heat-up rates would be also beneficial. It was found that the self-leveling phenomenon reduces the effect of initial angle factor on the CCFP. Nevertheless, the development of a model to predict the initial shape of the debris bed (initial angle factor) after spreading in the pool would be useful in the scenarios where the efficacy of self-leveling is small (i.e. due to high initial temperature). Further studies on the morphology of prototypic debris particles and angle of repose are necessary as well as new sets of PDS-C experiments with extend ranges of θ_{rep}^{0} in order to extend the validity ranges of the full and surrogate models.

Analysis of post dryout debris coolability with DECOSIM suggest that in all the cases with particle diameters of 3 mm, temperature stabilization occurred, while for the smallest particles (1 mm) steady temperature rise is observed at a rate proportional to specific power W. DECOSIM simulations have been carried in order to investigate the effect of lateral debris bed spreading on coolability. It has been shown that (i) for 1 mm particles, debris bed remains non-coolable, temperature escalation is observed with or without particle spreading; (ii) for 1.5 mm particles temperature stabilization is observed, for spreading debris bed; (iii) for 2 mm particles, debris bed is coolable, regardless of particle spreading.

Agglomeration surrogate model has been developed and validated. The model is based on problem decomposition into a set of loosely coupled models (i.e. jet breakup, particle sedimentation, cooling and solidification, agglomeration) that can be linked together through initial and boundary conditions. Several parameters in the SM model are calibrated, using analytical assessments and data from the full model in order to take into account phenomena and dependencies, which are not modeled explicitly in the SM. Comparison of the results predicted with the full and calibrated SM suggest that SM provides acceptable accuracy obtained with about hundred times smaller computational effort. Sensitivity analysis of the model suggest that jet diameter water pool depth and initial velocity of the melt are the major contributor dot the uncertainty in prediction.

A new series of DEFOR-A experiments has been carried out with increased sizes of the jet and wider ranges of water subcooling. The data on particle size distribution, debris bed porosity and agglomeration is in good agreement with the previous DEFOR-S, DEFOR-A and FARO tests. On average, larger particles were obtained with ZrO_2-WO_3 melt than with Bi_2O_3-WO_3, size distributions for both melt simulant materials are within the ranges of size distributions observed in FARO tests. The difference between particle sizes in the tests with free falling jets was found to be insignificant. There is a tendency to form slightly larger particles only in the tests with submerged nozzles where melt is released under water with initially small jet velocity. Initial jet velocity also seems to have no visible effect on the fraction of agglomerated debris. Increased size jet had no significant effect on particle size distributions and fractions of agglomerates. Small-scale DEFOR experiments were carried out for clarification and confirmation of previous DEFOR-S data, analytical results hypotheses. In general, results of this experimental program are in good agreement with the previous data.

The results presented in this section demonstrate coupling of the agglomeration model developed with the model for debris bed coolability. Simple formulas are offered for the spatial distribution of mass fraction of agglomerates allowing setup of debris bed properties as functions of height for different melt jet diameters and effective pool height. Numerical simulations are carried out demonstrating the effect of low-permeability zoned in the top part of porous debris bed on its coolability, including solid cake with some openings, as well as distributed agglomerates. An approach to development of the surrogate model that can take into account the effect of debris agglomeration on the coolability has been proposed.

3.8 Ex-vessel Steam Explosion SM

The ex-vessel steam explosion framework connects melt ejection mode with steam explosion loads on the containment structures to estimate containment failure probability. Development of the SM relies on a database of solutions generated by a 1D FCI code.

Multidimensional fuel-coolant-interaction (FCI) codes can help to identify information which is missing in 1D FCI codes. However, 2D/3D FCI codes are too computationally expensive to provide even sensitivity analysis, given large number of uncertain scenario and modeling parameters. Application of 1D code requires an additional method for calculating loads on containment structures. There is a need to resolve the link between ex-vessel coolability and steam explosion. Even a mild steam explosion might lead to degradation of debris bed cooling function. However, small size particles generated in steam explosion have little chance to settle on the bed as long as there is intensive coolant circulation in the pool.

Steam Explosion Impact Map probabilistic framework is demonstrated in the Figure 3-97. Melt Ejection Mode is defined as a number of vessel failure scenarios each characterized by a specific set of modelled and stochastic parameters. Pool Characteristics are determined by the accident scenario progression and plant damage state Pdfs. Steam Explosion Load analysis is performed with NRC approved 1D code TEXAS-V and complemented by MC3D 2D calculations for resolving spatial effects that are not captured by 1D code but required as an input and for cross-code comparison. Cumulative density function cdf3.2 requires both (i) addressing bounding failure criteria and (ii) deterministic analysis of failure mechanisms.

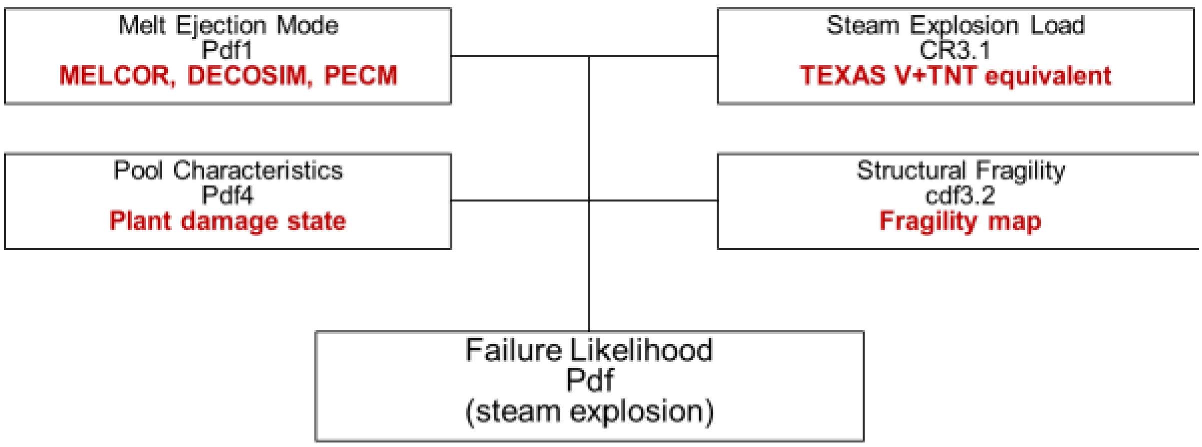

Figure 3-97: SEIM framework.

3.8.1 Approach

The employed here process of development and validation of a surrogate model is illustrated in Figure 3-98. Initial conditions come from the analysis at the previous stages of the deterministic framework (details of which are beyond the scope of this paper). Experimental and other evidences provide a knowledge base for calibration and validation of the models. Full Model (FM) is used to provide a database of solutions and better understanding of basic physical processes and typical behavior of the target parameters. Simplified modeling approaches and data mining techniques are used in order to develop a surrogate model. Surrogate model (SM) is an approximation of the FM model prediction of the target parameters. SM employs simplified physical modeling, calibratable closures, or approximations to the response surface of FM.

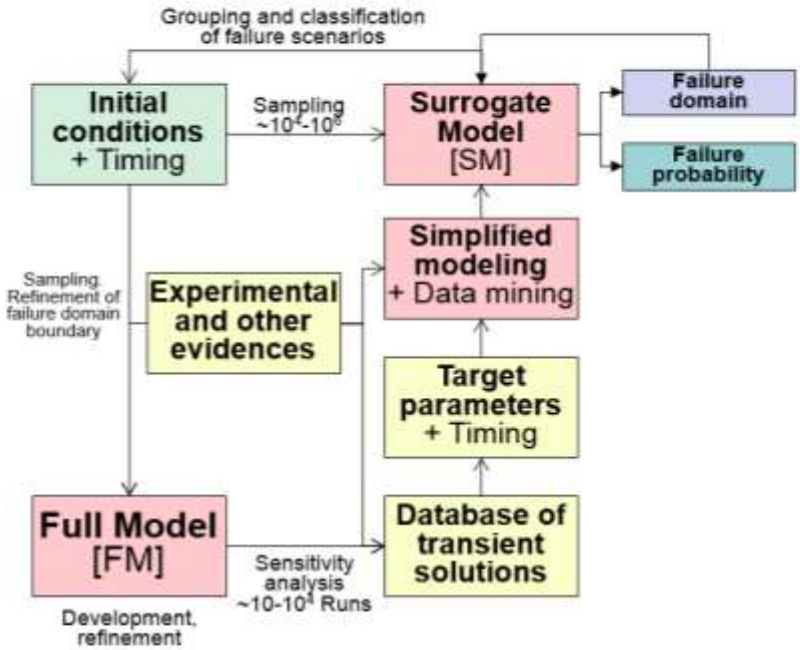

Figure 3-98: Full and Surrogate model development, integration with evidences, refinement, prediction of failure probability and failure domain identification.

In Section 3.8.2 we start with choice of the Fuel Coolant Interaction (FCI) code and detailed review of the modeling approaches in order to (i) select the most suited modeling options provided by the code for the calculation of premixing and steam explosion and (ii) define the list of relevant input and output model parameters. Implementation of the Full Model is detailed in the second paragraph of the Section 3.8.2 and followed by the definition of the relevant target functions, introduction of a simplified method for impulse propagation and approach for statistical treatment of the triggering time. A comprehensive sensitivity study to screen out non-influential parameters from the FM input is carried out in last paragraph of the Section 3.8.2. Development of the database of the FM solutions and its verification is undertaken in Section 3.8.3. Section 3.8.4 provide details on the development of the SM and comprehensive comparison of different characteristics of the full and surrogate models.

3.8.2 Steam Explosion Full Model

3.8.2.1 Review of TEXAS-V

TEXAS-V was chosen as a physics model to calculate premixing and steam explosion in Nordic type BWRs [75]. The choice was motivated by (i) TEXAS-V relatively high computational efficiency, (ii) extensive validation database.

Texas-V is a 1D 3-field transient code with Eulerian fields for gas and liquid and a Lagrangian field for fuel particles. It is comprised of two modules for calculation of premixing and steam explosion.

The premixing model is based on (i) two constitutive relations: the *fragmentation model for mixing* and the *phase change model;* (ii) two alternative modes of melt release: in the form of a coherent jet and in the form of discreet master particles; and (iii) two alternative mechanistic approaches for jet front breakup: *leading edge* and *trailing edge*.

The *fragmentation model for mixing* is comprised of three mechanisms: Kelvin-Helmholtz instability, boundary layer stripping and Rayleigh-Taylor instability. The former two are considered to have minor effect with vapor film present and are reduced rapidly with rise of void fraction. The Rayleigh-Tailor instability is thus the key mechanism describing fuel fragmentation in TEXAS. The model considers the fuel particles to be deformed and dynamically fragmented into a discrete number of particles from its initial diameter to smaller size [38], [39]:

$$D_f^{n+1} = D_f^n \cdot \left[1 - C_0 \Delta T^+ \cdot \left(\frac{\rho_c U_{rel}^2 D_f^n}{\sigma_f}\right)^{0.25}\right]$$

$$\Delta T^+ = \frac{U_{rel} \cdot (t^{n+1} - t^n)}{D_f^n} \cdot \left(\frac{\rho_c}{\rho_f}\right)^{0.5}$$

$$C_0 = 0.1093 - 0.0785 \cdot \left(\rho_c / \rho_f\right)^{0.5}$$

where $n, n+1$ designate old and new time step values; D_f is fuel particle diameter; ΔT^+ is a dimensionless time step; C_0 is the constant; U_{rel} is relative velocity; t is time; σ_f is fuel surface tension; ρ_f, ρ_c are densities of fuel and coolant respectively.

Therefore, the primary breakup is dominated by the existence of the jet front, the moment the jet front reaches the bottom of the domain primary breakup sharply reduces. It is further assumed that coherent fuel jet will not breakup until the fuel particle at the leading edge, exposed to the oncoming coolant, is fragmented (and swept away from the interface). This means that only master particles included in the leading edge of the jet can be subject to fragmentation.

The onset of master particle fragmentation is driven by one of the mechanistic approaches for jet front breakup. The *trailing edge* algorithm forces the leading master particle to fragment at the tail of the fragmented debris, i.e. at the beginning of the premixing region. The *leading edge* algorithm implies the start of the leading master particle fragmentation at the leading front of the fragmented debris, i.e. at the end of the premixing region.

The phase change model (in continuous liquid field) is comprised of two primary equations that define:

1. Heat loss from fuel particles $\dot{q}_{fuel}$:

$$-\dot{q}_{fuel} = \pi D_f^2 h_{film}\left(T_f - T_{sat}\right) + \pi D_f^2 \sigma F\left(T_f^4 - T_{sat}^4\right),$$

where the first term on r.h.s. describes convection heat transfer rate from the fuel particle to the liquid vapor interface, and the second term is the radiation heat transfer rate from the fuel particle to the saturated liquid-vapor interface; T_f and T_{sat} are fuel and saturation temperatures respectively; h_{film} is convection heat transfer coefficient; σ is Stefan-Boltzmann constant and F is the view factor between fuel particle surface and liquid-vapor interface. The temperature profile inside a particle is assumed constant in the bulk and linearly decreasing within a thin thermal layer δ.

The corresponding steam generation rate $\dot{\mathrm{M}}_{\mathrm{s,p}}$ is than derived from:

$$-\dot{q}_{fuel} = \pi\left(D_f + 2\delta_{film}\right)^2 h_{lg}\left(T_f - T_{sat}\right) + C_{rad}\pi D_f^2 \sigma F\left(T_f^4 - T_{sat}^4\right) + \dot{\mathrm{M}}_{\mathrm{s,p}} h_{fg},$$

where the first term on the r.h.s. is convection heat transfer rate from the liquid-vapor interface around the fuel particle to bulk liquid field and the second term is the fraction C_{rad} of radiation heat flux that is absorbed in the subcooled liquid; h_{fg} is the latent heat of evaporation; δ_{film} is the thickness of the steam film surrounding the fuel particle; $\dot{\mathrm{M}}_{\mathrm{s,p}}$ is ; h_{lg} is heat transfer coefficient from vapor to bulk liquid.

2. Heat flux balance around steam bubbles and resulting steam generation rate $\dot{\mathrm{M}}_{\mathrm{s,b}}$:

$$A_{gL} K_g \frac{\left(T_g - T_{sat}\right)}{\delta_g} = A_{gL} h_{L.sL}\left(T_{sat} - T_L\right) + \dot{\mathrm{M}}_{\mathrm{s,b}} h_{fg}$$

where the term on the l.h.s. is the vapor bubble-side heat transfer rate; the first term on the r.h.s. is the bulk liquid-side heat transfer rate; A_{gL} is the surface area of the interface between the liquid field and the vapor field as determined from the vapor bubble radius and the flow regime; K_g is effective thermal conductivity of the vapor film; δ_g is the vapor thermal thickness in the vapor bubble (taken in the range from 1 to 20% of the bubble size); $h_{L.sL}$ is heat transfer coefficient in the bulk liquid; T_L is liquid temperature; T_g is the temperature of the vapor bubble.

The net rate of steam generation $\dot{m}_s$ per unit volume is thus expressed in terms of the net heat flux $\dot{q}_{net,f}$

$$\dot{m}_s = \frac{\dot{q}_{net,f}}{h_{fg}V_{cell}} \tag{3-20}$$

$$\dot{q}_{net,f} = \dot{q}_{fuel} - \dot{q}_l - \dot{q}_v$$

where $\dot{q}_l$ and $\dot{q}_v$ are the heat received by coolant liquid and coolant vapor respectively, which becomes the internal energy of the coolant; and V_{cell} is cell volume.

The **fine fuel fragmentation** (upon steam explosion) is a computed using Tang and Corradini model [260] which is based on the original Kim's work [127]. It takes into account a combination of thermal and hydrodynamic fragmentation phenomena:

1. Film boiling around a molten fuel particle.
2. Film collapse by external pressure pulse.
3. Coolant micro-jets impingement on the surface of fuel droplet.
4. Rapid coolant expansion and fragmentation of the fuel into droplets.

The model is implemented in TEXAS with a semi-empirical equation where fine fragmentation rate $\dot{m}_f$ is expressed as:

$$\dot{m}_f = Cm_p \cdot \left(\frac{P - P_{th}}{\rho_c R_p^2}\right)^{0.5} F(\alpha)g(\tau) \tag{3-21}$$

where m_p is mass of the initial particle; R_p is radius of the initial particle; P_{th} is the threshold pressure necessary to cause film collapse; P is ambient pressure; $F(\alpha)$ is the compensation factor for coolant void fraction; and $g(\tau)$ is the factor for available fragmentation time.

The factor $F(\alpha)$ decrease from 1 to 0 at $\alpha = 0.5$ in order to take into account that coolant jet impingement become less likely to occur as vapor fraction increases. In the TEXAS input file this limit is named ALPHAS.

The threshold pressure P_{th} is evaluated based on theoretical work by Kim and experimental data. At ambient pressure 1 Bar the threshold pressure is in the range from 2 to 4 Bars. As the ambient pressure increases the threshold pressure also increases, however no quantitative values are suggested in the code manual. In the TEXAS input file this parameter is designated as POLD.

The integral fragmentation mass depends on the duration of the fragmentation process. The factor $g(\tau)$ is introduced as an empirical approach to account for the characteristic fragmentation time τ during which the above mechanism is considered to be active. The factor $g(\tau)$ decreases from 1 to 0 as this characteristic time is exceeded. At ambient pressure (1 Bar) the recommended value for it is 1-4 ms [39]. It is indicated that as ambient pressure increases the fragmentation limit time decreases.

The heat generated due to dynamic fine fragmentation is expressed in TEXAS as:

$$\dot{q}_{frag} = \dot{m}_f \cdot (C_{pf} \cdot (T_f - T_{sat}) + i_f) \tag{3-22}$$

where i_f is fuel latent heat; T_f is fuel temperature; C_{pf} is specific heat for the fuel. Due to extremely fine fragmentation of the fuel the rate of heat transfer is very fast. It is assumed that steam generation rate $\dot{m}_s$ per unit volume can be estimated as:

$$\dot{m}_s = \frac{\dot{q}_{net,f} + \dot{q}_{frag}}{h_{fg} V_{cell}} \tag{3-23}$$

Further details on the implemented models in TEXAS-V can be found in the thesis by Chu [39] for premixing model, by Tang [260] for propagation model and by Murphy for hydrogen generation [200], or in the TEXAS-V manual [44].

3.8.2.2 Modelling of steam explosion in Nordic type BWRs with TEXAS-V

The height of the computational domain, from the point of melt release to the bottom of the water pool, is set to 13.0 m in accord with design of Nordic type BWRs. The computational domain is divided onto 26 cells, each 0.5 m high with the same cross section area A_{cell}.

The study of the effect of the mesh cell height on TEXAS-V calculations suggests that with the decrease of the cell height from 0.4 to 0.2 m explosion impulses get weaker and the number of failed calculations increases; explosion impulses and statistics of numerically failed calculations were not sensitive to the variation of cell height in the range from 0.4 to 0.6 m.

The mesh cell cross-section area A_{cell} appeared to have a profound effect on the dynamic pressure and consequently on the explosion pressure impulse I_p:

$$\frac{\Delta I_p}{I_p} \cong \frac{A_{cell}}{\Delta A_{cell}} \tag{3-24}$$

We found that for chosen ranges of input parameters the product of the pressure impulse [Pa·s] and the cell cross section area [m^2] (a measure of the total released energy) remains practically independent from the mesh cell cross-section area (see Figure 3-99). Therefore we set the ratio of the jet radius (R_{jet}) to cell radius (R_{cell}) approximately the same as in KROTOS experiments (against which the TEXAS-V code was extensively validated). In this work the following relation has been used:

$$R_{cell} = 11.162 \cdot R_{jet} + 0.0014 \qquad (3\text{-}25)$$

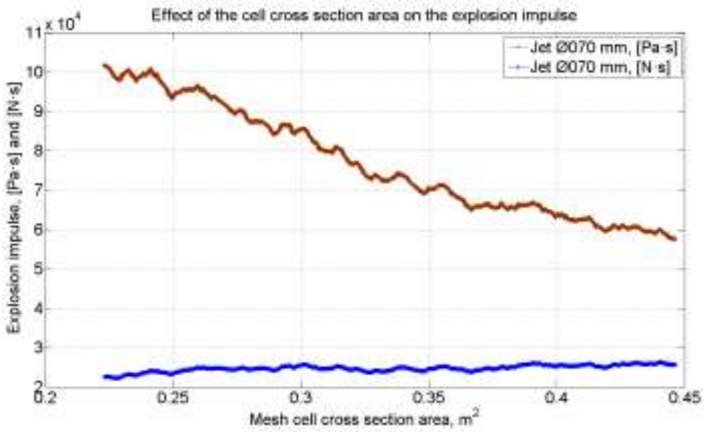

Figure 3-99: Effect of the mesh cell cross section area on the explosion impulse (blue) and the explosion pressure impulse (brown).

Reduced time steps were chosen to decrease the number of failed calculations (crashed due to problems with achieving numerical convergence), specifically, the maximum time step for premixing calculations was set to 10^{-6} s and the maximum time step for explosion was $0.5 \cdot 10^{-6}$ s.

The threshold pressure for film collapse in eq.(3-21) was set to be twice the system pressure: $P_{th} = 2 \cdot P$. The alternative formulation $P_{th} = P + 1Bar$ resulted in twice larger number of failed calculations.

A comparative calculation using trailing edge and leading edge algorithms (see Figure 3-100) suggests that the trailing edge algorithm provides slower jet propagation in water, enhanced primary breakup and higher steam generation rates. Supposedly, it is intended to reproduce fragmentation of small jets, i.e. jets prone to sinusoidal instability. Given characteristic scales of melt release in the reactor case and by comparison with the jet front propagation velocity in water predicted using MC3D [193] we have chosen the leading edge algorithm for modelling of jet fragmentation.

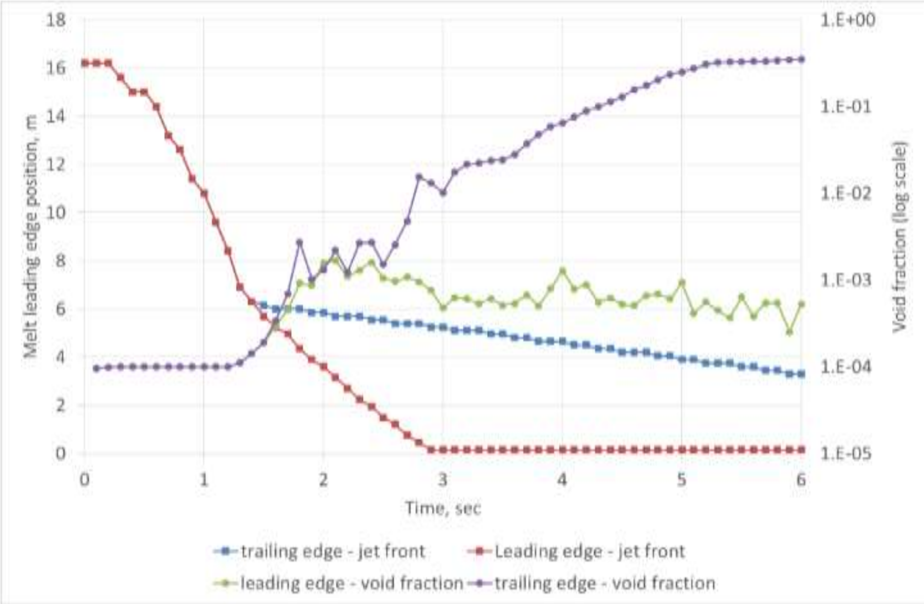

Figure 3-100: Trailing edge breakup vs leading edge breakup mechanisms.

Two more assumptions were made: (i) the model for hydrogen generation was not used and (ii) effects of the crust on explosion propagation were not modelled.

3.8.2.3 Processing of the Full Model output

Output functions

Two functions were derived to characterize a single TEXAS-V calculation: one for the characterization of the steam explosion energetics, i.e. explosion impulse (F_{expl}); and one for the characterization of the potential explosivity of premixture, i.e. total surface area of liquid melt droplets in water (F_{prmx}). Note that in TEXAS-V the rate of fine fragmentation, as defined in eq.(3-21), is proportional to the surface area of liquid melt. This means that F_{prmx} characterizes amount of melt available for explosion.

Explosion impulse was integrated from the dynamic pressure history for every cell separately; the maximum impulse was then taken:

$$F_{expl} = \max\left(\sum_{i}(P_{ij} - P_{0j})\delta t_i\right) \cdot A_{cell}, \quad [N \cdot s] \tag{3-26}$$

where P_{ij} is pressure in the cell j at the time instance i; P_{0j} is pressure in the cell j at time 0; δt_i is the time step at the time instance i, A_{cell} – mesh cell cross section area.

The total surface area of liquid melt droplets in water was approximated as:

$$F_{prmx} = 4\pi \sum_k \begin{cases} n_k R_k^2, & [Vs_{i(k)} < 0.5, \quad T_k > T_{melt}] \\ 0, & otherwise \end{cases}, \quad [m^2] \qquad (3\text{-}27)$$

where k is Lagrangian particle group number; R_k is particle radius in the k particle group; n_k is the number of particles in the k particle group; T_k is particle bulk temperature in the k particle group; T_{melt} is melting temperature of the fuel; $Vs_{i(k)}$ is steam fraction in the cell i where k particle group is located.

Impulse propagation

The explosion impulse in eq. (3-26) is a result of 1D solution taken from a single cell. It can be considered as a point like source. In order to estimate the explosion impulse at different locations in the containment an appropriate impulse propagation method must be used. For demonstration purposes it is assumed that explosion pressure impulse I [Pa·s] (similar to pressure distribution in a propagating spherical shock wave) is a decaying function of the distance r from the center of the explosion:

$$I = \tilde{c} \cdot r^{\nu}, \nu \cong -1, \tilde{c} = const \qquad (3\text{-}28)$$

The constant $\tilde{c}$ in eq.(3-28) is estimated assuming (i) explosion impulse F_{expl} to be distributed over the complete area of the containment base A_b and (ii) the point source of the explosion to be located in the center of the corresponding cell in TEXAS:

$$I_b = F_{expl}/A_b \qquad (3\text{-}29)$$

$$I_b = \frac{2}{r_b^2}\int_0^{r_b} \frac{\tilde{c}}{(h_c^2 + r^2)^{0.5}} \cdot r dr \qquad (3\text{-}30)$$

$$I(r) = I_b \cdot \frac{r_b^2}{2 \cdot ((r_b^2 + h_c^2)^{0.5} - h_c)} \cdot \frac{1}{r} \qquad (3\text{-}31)$$

where r_b is the radius of the containment; h_c is elevation of the computational cell above the bottom of the domain.

The impulse at the center of the containment floor is estimated substituting in eq.(3-31) $r = h_c$; the impulse at the wall of the containment is estimated assuming melt jet release at the side of the lower head, i.e. $r = 3\ m$ away from the wall.

Probabilistic treatment of the triggering time

During melt water interaction premixing conditions may vary rapidly in time [91]. This makes energetics of steam explosion sensitive to the triggering time.

To address the importance of this phenomena the dependence of normalized F_{prmx} and F_{expl} functions on the triggering time was investigated [92]. The data was obtained in two steps. First, premixing was calculated starting from melt release till the jet front arrival to the bottom of the domain and instantaneous premixing configurations were saved with 1 ms time step. Second, steam explosion calculations were carried out for every instantaneous premixing configuration. According to the Figure 3-101 during melt water interaction (t > 1.4 s) the normalized F_{prmx} and F_{expl} functions demonstrate quasi periodic and apparently correlated behavior. However, the correlation between the functions is not strong enough to use F_{prmx} for prediction of potential premixture explosivity: in the considered case the largest impulse is obtained at only about 40% of the maximum values of F_{prmx}.

The results in the Figure 3-101 indicate that *small variations in the triggering time may lead to large changes in the explosion energetics*: for example, between 1.90 and 2.01 s, i.e. within 110 ms time window, the explosion impulse changes almost 50 times from 377 kPa·s to 8 kPa·s.

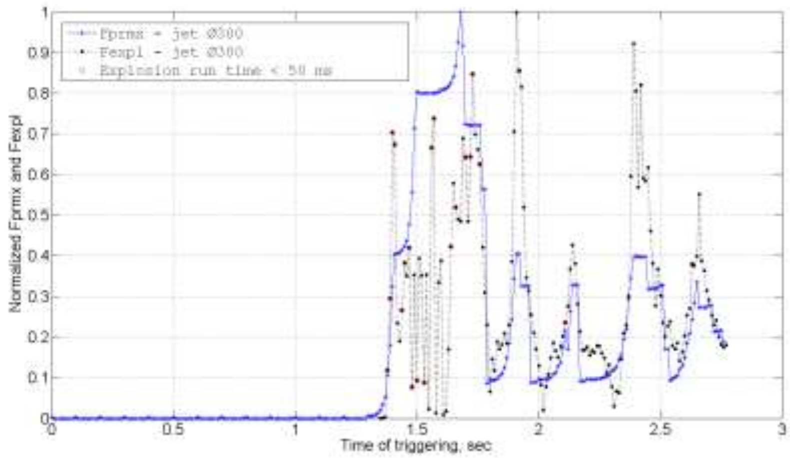

Figure 3-101: The dependence of normalized premixing F_{prmx} and explosion F_{expl} functions on the triggering time (release of oxidic corium melt with jet Ø300 mm into a 7 m deep water pool).

The high sensitivity of the explosion impulse to the triggering time is an intrinsic characteristic of the steam explosion.

In FCI calculations, the chaotic behavior of the steam explosion impulse with respect to the discreet triggering time makes the problem of prediction of steam explosion impulse ill-posed and, consequently, interpretation of FCI codes results highly uncertain. This is one of the main reasons for the large spread of (i) predictions with different FCI codes, and (ii) predictions with the same FCI code obtained by different users (see, for example, SERENA-II benchmark exercise [188] and [187], [186] for SERENA-I results). It is instructive to note that previous studies with the TEXAS code [215], [251], [33] or other codes were not able to identify and address the effect of the triggering time and resulting ill-posedness of the problem due the limited number of computations. The most robust approach to the treatment was attempted in [198], [199]. From risk perspective, the choice of the triggering time can change prediction of containment failure from physically unreasonable (at ~8 kPa·s) to unavoidable (at ~377 of kPa·s). Therefore, we advocate statistical treatment of the triggering time effect in both cross code comparisons and risk analysis.

In FCI experiments, the chaotic nature of steam explosion is expected to manifest itself through stochastic variations of explosion characteristics due to aleatory variability of (i) the triggering time and (ii) melt release conditions. Considering possible variation of the impulse (e.g. see Figure 3-102), the effect of the triggering time on the measurement of steam explosion energetics may exceed the effect of the other experimental parameters. Thus only statistical treatment using data from many repeatability tests can be used to reveal the influence of different factors.

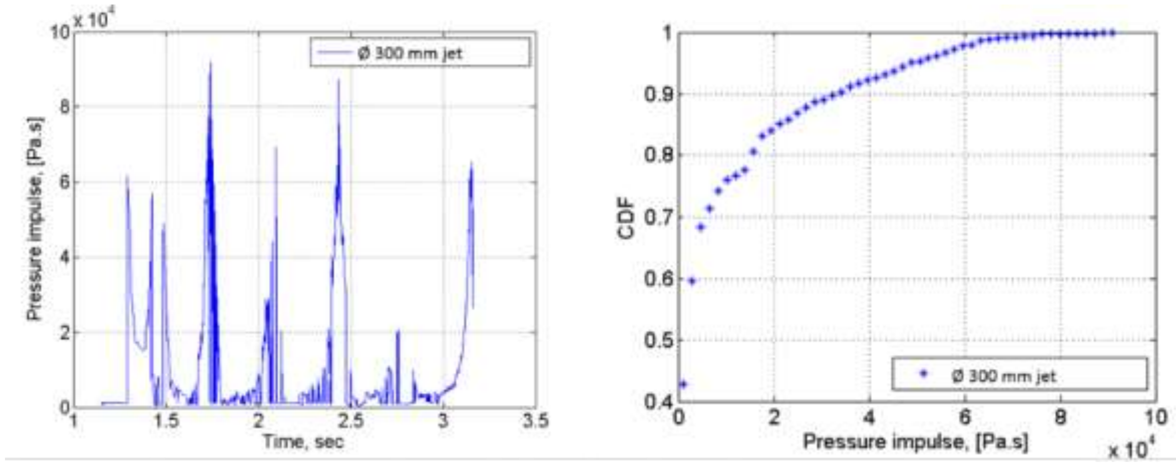

a b

Figure 3-102: Evolution of the explosion pressure impulse at pedestal wall as a function of triggering time (a) and resulting distribution of the explosion pressure impulse (b).

The ill-posedness and resulting chaotic behavior of the explosion impulse can be also addressed by considering statistical distributions of the impulses obtained at all the same conditions except for the triggering time. For example, evolution of the explosion impulse in Figure 3-102a can be characterized by a cumulative density function (CDF) of the predicted impulses as shown in Figure 3-102b. According to the data in the Figure 3-102b the percentile of explosion impulses that do not exceed, say, 80 kPa·s is 99.75%.

In order to make model output well-posed and independent from the choice of the triggering time we introduced statistical treatment of explosion impulse. For every melt release scenario, we estimate the values of the impulses that correspond to 50, 75, 95, 99 and 100 percentiles of the CDF. For example, for the cumulative distribution function (CDF) reported in Figure 3-102b, we can infer that for 95% of all possible triggering times the explosion impulse at the pedestal wall (plotted in Figure 3-102a) will not exceed 50 kPa·s.

3.8.2.4 Choice of important input parameters

Out of about 160 TEXAS-V input parameters 23 were selected for further analysis. The complete list is provided in Table 3-13. Ranges of parameters used in the sensitivity study were defined for typical scenario of oxidic melt release in Nordic BWR [93], [92]. Parameters not mentioned in the Table 3-13 were set in accord with default values defined in the TEXAS-V manual [44].

Table 3-13: Selected TEXAS-V parameters and their ranges

Parameter	**Units**	**Range**	**Description**
PO	**Bar**	**1÷4**	**Initial pressure**
TLO	**K**	**288-366**	**Water temperature**
XPW	**m**	**3.2-8.2**	**Water level in the containment**
TGO	K	TLO	Cover gas temperature
TWO	K	TLO	Wall temperature
RPARN	m	0.07	Fuel injection radius
		0.15	
CP	**J/kg·K**	**400÷570**	**Fuel capacity**
RHOP	**kg/m3**	**7600-8600**	**Fuel density**
PHEAT	**kJ/kg**	**260÷360**	**Fuel latent heat**
TMELT	K	2850	Fuel melting temperature
TPIN	**K**	**2850÷3150**	**Fuel injection temperature**
UPIN	**m/sec**	**1.5÷2.5**	**Fuel injection velocity**
KFUEL	**W/m·K**	**2÷11**	**Fuel thermal conductivity**
C(32)	**J/m^2**	**0.4÷0.6**	**Fuel surface tension**
C(18)	**-**	**0.6÷0.9**	**Fuel emissivity**
DXI	m	0.5	Cell height
ARIY	**m^2**	**0.7÷1.8**	**Cell cross-section area**
		3.8÷8	
TMAX	sec	-	Premixing time
CFR	**-**	**2.0÷2.7 E-03**	**Proportionality constant for the rate of fuel fine fragmentation**
RFRAG	**m**	**8÷1.2 E-05**	**Initial size of fragmented particles**
POLD	Pa	2×PO	Threshold pressure for film collapse
TFRAGLIMT	**s**	**0.0005÷0.0030**	**Fuel fragmentation time interval**
PTRIG	Bar	3	Trigger pressure

The sensitivity study used extended Morris method [235], [1], [32] and addressed 16 independent input parameters (printed in bold in the Table 3-13). The mean pressure impulse ($\bar{F}_{expl}/A_{cell}$, [Pa·s]) has been used as the response function. The results in Figure 3-103 are provided for the scenario with 140 mm jet diameter. The elements in the legend are sorted in descending order of Morris modified mean μ^* value. The spread of the results established in

3 consecutive sensitivity studies that used different number of trajectories is also illustrated in the figure. Two input parameters were screened out: RFRAG and C(18).

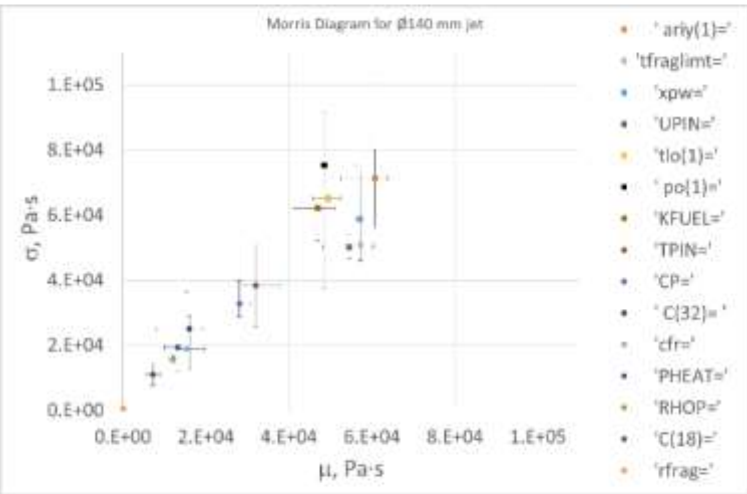

Figure 3-103: Morris diagram for mean pressure impulse.

3.8.3 Database of full model solutions

3.8.3.1 Database generation approach

The database consists of 1500 premixing sets and 455,386 explosion calculations. The list of input parameters and respective ranges is provided in the Table 3-14. Note that the ranges were extended compared to those used in the sensitivity study to include scenarios of metallic melt releases.

Table 3-14: Ranges of input parameters used for generation of the database of FM solutions

#	Parameter	Units	Range		Explanation
			min	max	
1	XPW	M	5	9	Water level
2	PO	Bar	1	4	System pressure
3	TLO	K	288	368	Water temperature
4	RPARN	m	0.035	0.3	Initial jet radius
5	CP	J/kg·K	350	650	Fuel heat capacity
6	RHOP	kg/m3	7500	8500	Fuel density
7	PHEAT	J/kg	260 000	400 000	Fuel heat capacity
8	TMELT	K	1600	2800	Fuel melting point
9	TPIN	K	1620	3150	Melt superheat
10	UPIN	m/s	-8	-1	Melt release velocity
11	KFUEL	W/m·K	2	42	Fuel thermal conductivity
12	CFR	-	0.002	0.0027	Proportionality constant for the rate of fuel fine fragmentation
13	TFRAGLIMT	ms	0.5	2.5	Fragmentation time

Parameters were considered as independent, except for TPIN > TMELT. Halton method [101] was used for the generation of the input. Explosion calculations were performed with 4 ms time step starting from melt contact with water and till melt contact with the bottom of the water pool.

3.8.4 Steam explosion Surrogate Model

3.8.4.1 Implementation of the Surrogate Model

The surrogate model has been developed using Artificial Neural Networks (ANNs). In this work a feedforward neural network with Bayesian regularization and backpropagation was implemented. The ANN structure obtained after training consists of two hidden layers formed by 3 sigmoid neurons and 5 sigmoid neuron respectively, followed by the output layer with 4 linear neurons (see Figure 3-104).

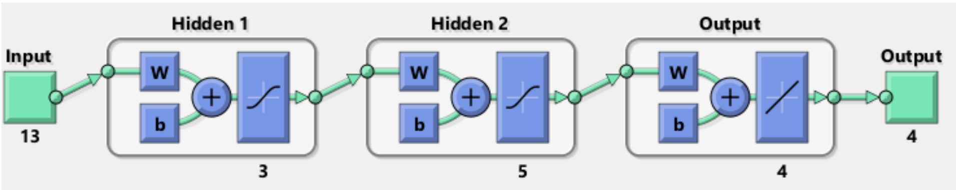

Figure 3-104: ANN structure.

The network is trained according to Levenberg-Marquardt optimization algorithm, applying internally Bayesian regularization. The filtered database (see Chapter 3.8) was used for the training of the ANN. The ANN predicts the mean and standard deviation of the impulse $\bar{I}_0$ at the center of the containment floor and at the wall (4 outputs) given 13 TEXAS-V parameters in the input: XPW, PO, TLO, RPARN, CP, RHOP, PHEAT, TMELT, TPIN, UPIN, KFUEL, CFR, and TFRAGLIMT.

3.8.5 Steam explosion surrogate model uncertainty

The uncertainty of SM in approximation of the FM can be characterized as a difference between FM and SM predictions ($Err_i = \ R_{FM,i} - R_{SM,i}$). The respective error histograms for steam explosion SM are plotted in the Figure 3-105a-d for explosion impulse at the containment base and at the pedestal wall. While error histograms expressed in terms of explosion pressure impulse have bell-like shape, those expressed in percentiles of the explosion impulse show increased frequencies at the tails of the distributions. The effect is due to the dependence of the error on the value of the impulse. This is further demonstrated in the Figure 3-105e and f. In the plots the *error* is estimated using:

$$2\frac{R_{FM,i} - R_{SM,i}}{R_{FM,i} + R_{SM,i}} \cdot 100\%$$

At low values of the explosion impulse (~1 kPa·s) the error may exceed ±200%; for large values of the explosion impulse (80-200 kPa·s) it stays within ±40%. The expected values of the error are around zero for the most part of the SM output. Exception occurs around small pressure impulses for which error exceeds ±100% shifting expected value of the error towards positive numbers (FM and SM can only predict positive pressure impulses).

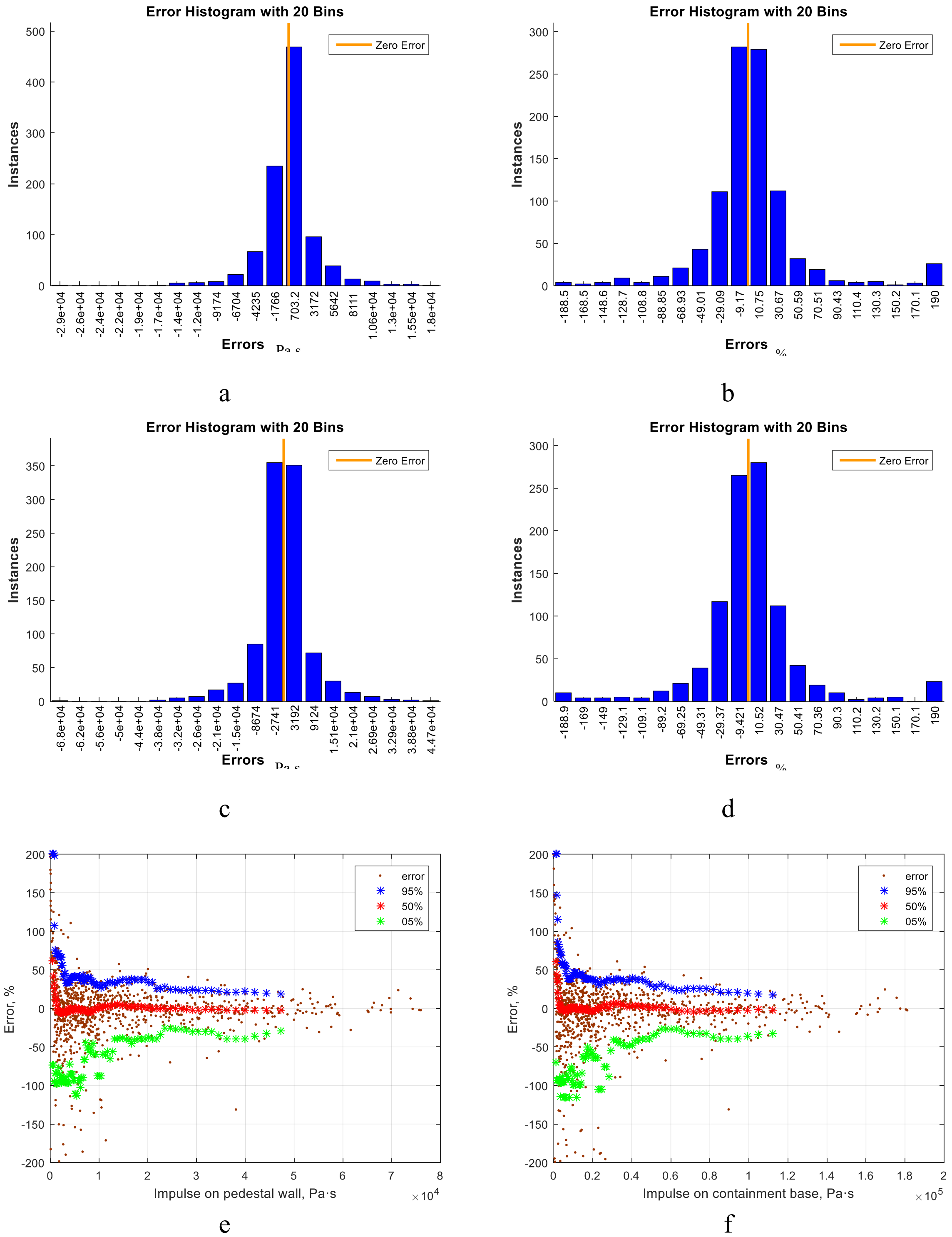

Figure 3-105: Histograms of SM error for the explosion pressure impulse at the pedestal wall (a,b), containment base (c,d) and error distribution as a function of the SM output (e and f).

3.8.5.1 Quantification of the uncertainty due to SM approximation of FM

Given single vector value of scenario parameters s_i, modelled input parameters ($p_{k-1,i}$) and intangible and deterministic parameters (d_{ki}, i_{ki}), a SM (CR_k – causal relation) predicts a single output value (or vector) ($R_{SM,i}$), see Figure 3-106a. The solution then should be complemented with the appropriate CDF of the SM error. In such case the output of the SM becomes a distribution that quantifies the SM uncertainty in approximating the FM output for given value of SM prediction, see Figure 3-106b.

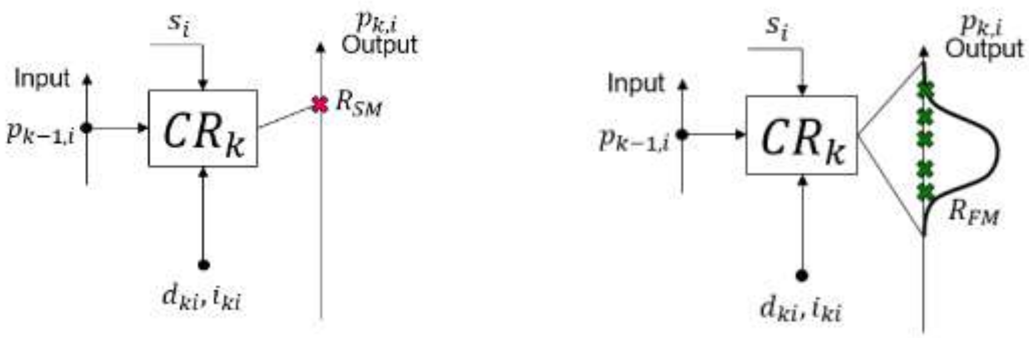

a b

Figure 3-106: SM (or CR – causal relation) output without (a) and with error quantification

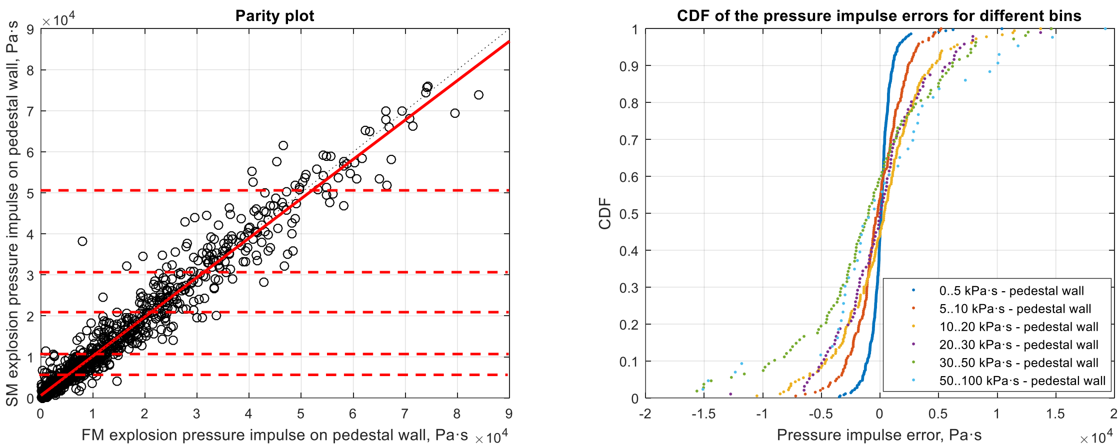

a b

Figure 3-107: Example binning of the SM output space (a) and respective CDFs of the SM errors (b)

Data in Figure 3-107 suggests that the error is a function of the output. Quantification of the error can be done by binning the SM output space (Figure 3-107a) and providing a distribution of the SM error for every bin (Figure 3-107b). Alternative approach would be to use the data on the SM error ($Err_i = R_{FM,i} - R_{SM,i}$) in the vicinity of predicted by SM output and construct respective CDF (see Figure 3-108a). Result of complementing a SM solution with a CDF of the SM error is demonstrated in Figure 3-108b.

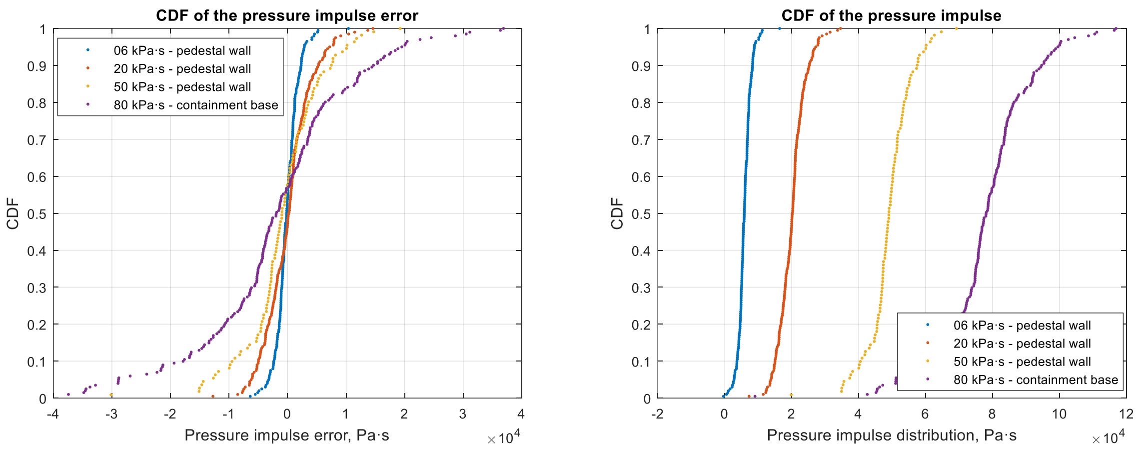

a b

Figure 3-108: CDF of explosion pressure impulse error (a) and SM output with the error (b) for selected values of impulses on the pedestal wall and containment base.

3.8.5.2 SM sensitivity study

The magnitude of the error (40-200%) established during comparison of the FM and SM predictions is quite high. Therefore we study the sensitivity of the SM model output to the error magnitude (parameter c_{err}) in comparison with the other model input parameters. Morris method was used; the range for the parameter c_{err} was set from -1 to 1. The results provided in the Figure 3-109 suggest that c_{err} is among the influential parameters, though it is much less important than initial jet diameter. Therefore, further reduction of the SM uncertainty may not be beneficial as long as the large uncertainty remains with respect to the initial jet diameter.

Besides SM input parameters, the diagram also includes the model sensitivity to the rate of enthalpy supply (dH/dt), which is computed using the following expression:

$$\frac{dH}{dt} = -\pi R^2 \rho \left(C_p \Delta T_{sup} + H_f \right) \mathrm{U}$$

where R is initial jet radius; ρ is melt density; C_p is melt heat capacity ΔT_{sup} is melt superheat, H_f is melt enthalpy and U is melt initial inlet velocity. High sensitivity of the model output to the enthalpy rate (which is a combination of SM input parameters) further indicates that uncertainty in the SM output is dominated by the input parameters and not by the SM error in approximation of the FM.

The results of the sensitivity study must be taken with caution. The c_{err} is not an epistemic parameter that may change depending on the melt release scenario from minimum to the maximum of its range as it occurs for other model input parameters. In this sense the sensitivity of the SM output to the change in c_{err} is only indicative that a more rigorous treatment is necessary.

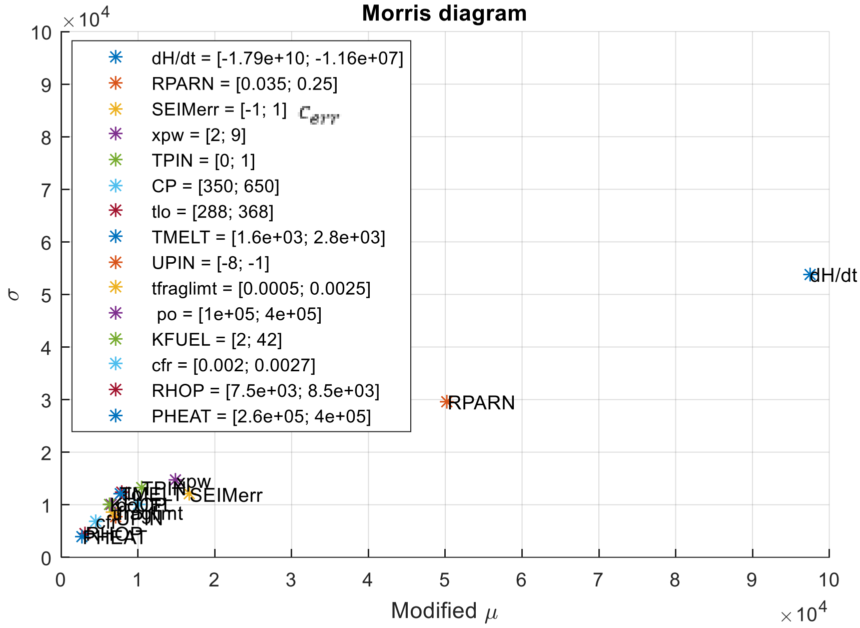

Figure 3-109: Modified Morris diagram for the 95% of the explosion pressure impulse on the pedestal wall. Parameters in the legend are sorted in descending order of importance.

3.8.6 Approaches to reduction of SM uncertainty

The above results indicated somewhat high SM uncertainty with respect to FM:

- ±66% at low values of impulses
- ±13% at high values of impulses

In addition, ANN was found to predict negative explosion impulses at high jet radiuses. Even though negative values are very rare < 1/10 000, they could give rise to reduced explosion impulses and may affect the risk assessments. Therefore, it is necessary to develop an approach that will improve the accuracy of SM.

Three approaches are currently being considered and implemented:

- Single ANN:
  - Find optimum model of a single ANN including:
    - Training methods.
    - ANN selection criteria.
    - Architecture (number of hidden layers and neurons).
- Bootstrap ANN:
  - Use selected optimum ANN structure and training
  - Train large number of ANNs by bootstrapping the data.
  - Use ensemble average of the neural networks for prediction
    - BANN was shown to perform better than a single best ANN in different applications.
- Dimensionality reduction of SM input:
  - Combine FM input parameters into groups to reduce
    - SM output variance.

- Computational costs.
- Complexity of interpretation of the results.

3.8.6.1 Single ANN development

The main sources of ANN Uncertainty include:

- Non exhaustive (insufficient or noisy) FM data.
- ANN architecture.
- Failure in obtaining global minimum when minimizing the difference between training data and ANN predictions.

The first item can only be resolved by modification or extension of the FM solution database and have not been applied. The last two are subject to optimization: a sensitivity analysis has been performed on the ANN architecture and training methods, in order to find the best fit to the data. The best performance belongs to a 2 hidden layer network with 8 by 11 architecture.

In order to reduce the possibility of negative impulses and in addition to improve the ANN selection process several simultaneous selection criteria has been implemented:

- Root-Mean-Square Error (RMSE).
- Goodness of fit (R^2).
- Validation error.
- Probability of non-physical (negative impulses) output.

Their combined application proved to be very beneficial in reducing the uncertainty of a single ANN.

3.8.6.2 Bootstrap ANN development

A number (B) of bootstrap samples is drawn at random with replacement from the original training set of n_p input/output patterns, $D \equiv \{\boldsymbol{x}, y\}$. The generic b^{th} sample is constituted by the same number of input/output patterns drawn among those in D. Each bootstrap sample D_b is then used as data set for training a different ANN. An ensemble of best ANNs is then selected from the pool of trained ANNs containing 100 000 bootstrapping. Number of ANNs in the ensemble is a subject of statistical analysis (computational performance vs accuracy). 4 Filter approach (similar to a single ANN) is used for the selection of each individual ANN. The obtained bootstrap ANN have generally higher accuracy then a single ANN, though at the expense of the ANN performance.

3.8.7 SEIM Failure Domain analysis

Failure domains enable us to investigate the effect of scenario parameters on the confidence in estimated containment conditional failure probability. They provide a more comprehensive view on the possible outcomes of steam explosion and effect of the SM error. We have considered three cases of melt release: one oxidic and two metallic (with low and high melt superheat). The ranges of the input parameters for each case are given in Table 4-3.

Following results of the sensitivity study we have chosen jet radius, water pool depth and melt release velocity as scenario parameters in terms of which failure domain maps were computed and plotted. The results of the calculations are provided in the Figure 3-110. Assessments were done for the failure of the non-reinforced and reinforced hatch door given c_{err}=0 and c_{err}=[-1;1], uniform distribution. The maps were estimated taking 95% of the explosion impulse, using 0.001 as the screening failure probability. The color map used in the failure domain maps is explained in the Table 3-16. It is instructive to note that SM error enlarges the failure and reduces the safe domains.

Table 3-15: Classification and ranges of model input parameters used for estimation of failure domain maps

#	Parameter	Units	Oxidic		Metallic (Case 01 / Case 02)	
Name	Meaning		min	Max	min	max
Scenario parameters						
RPARN	Initial jet radius	m	0.035	0.150	0.035	0.150
UPIN	Melt release velocity	m/s	1	8	1	8
XPW	Water level	m	2	9	2	9
Intangible parameters						
PO	System pressure	Bar	100000	400000	100000	400000
CP	Fuel heat capacity	J/kg·K	490	650	350	490
RHOP	Fuel density	kg/m3	7900	8500	7500	7900
PHEAT	Fuel latent heat	J/kg	300000	400000	250000	300000
TMELT	Fuel melting point	K	2800	2800	1650	1650
TPIN	Melt temperature	K	2810	3150	1660	2800/1966
TLO	Water temperature	K	288	368	288	368
KFUEL	Fuel therm. conduct.	W/m·K	2	6	6	32
CFR	Fuel fragmentation rate coefficient of proportionality	-	0.00200	0.00270	0.00200	0.00270
TFRAGLIMT	Fragmentation time	ms	0.00050	0.00250	0.00050	0.00250
Deterministic parameters						
c_{err}	SM error	-	-1	1	-1	1

Table 3-16: Color mapping of failure domains

Color	Definition	Comment
Red	$CCDF(P_f > 10^{-3}) > 95\%$	Failure probability is larger than 10^{-3} for at least 95% of all distributions of intangible parameters.
Green	$CCDF(P_f > 10^{-3}) < 5\%$	Failure probability is smaller than 10^{-3} for at least 95% of distributions of intangible parameters.
Blue	$5 \leq CCDF(P_f > 10^{-3}) < 50\%$	Failure probability is larger than 10^{-3} in 5-50% of distributions of intangible parameters.
Purple	$50 \leq CCDF(P_f > 10^{-3}) \leq 95\%$	Failure probability is larger than 10^{-3} in 50-95% of distributions of intangible parameters.

Results suggest that in case of non-reinforced hatch door (fragility limit 6 kPa·s), the failure of the containment is imminent (red domain) in a wide range of scenario parameters (RPARN, XPW and UPIN). Comparison of Case 01 vs Case 02 (see Table 4-3), suggests that with increase of melt superheat size of the failure domain increases. Failure domain is larger for the oxidic melt than for the metallic. This is attributed to the (i) lack of modelling of the effect of crust formation on the explosion energetics in TEXAS-V and (ii) higher absolute enthalpy of oxidic melt vs metallic due to difference in absolute melt temperatures.

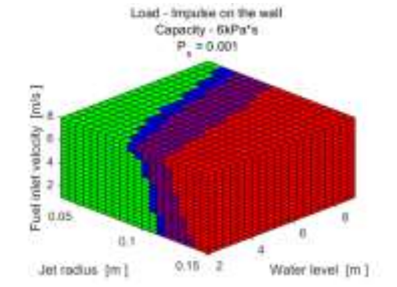	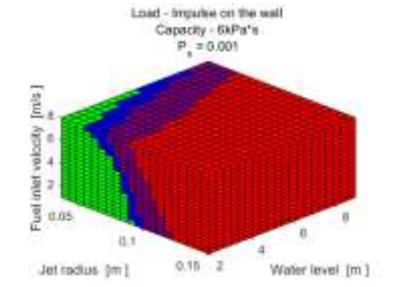	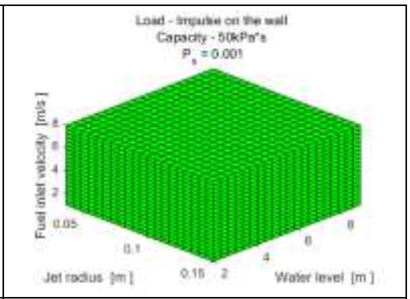
c_{err}= 0; 6 kPa·s; metallic release case #1	c_{err}=[-1;1]; 6 kPa·s; metallic release case #1	c_{err}=[-1;1]; 50 kPa·s; metallic release case #1
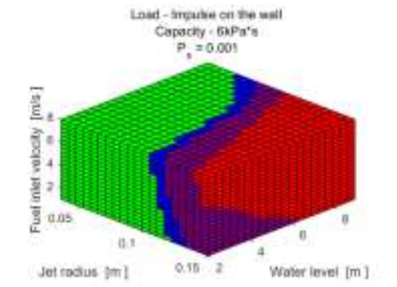	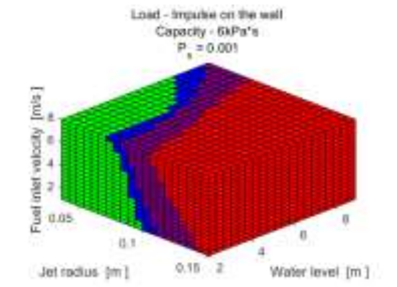	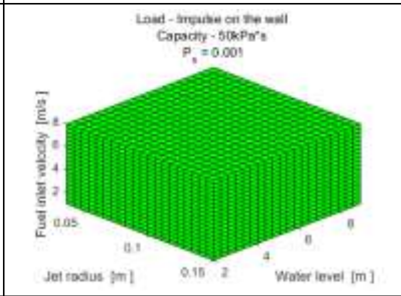
c_{err}= 0; 6 kPa·s; metallic release case #2	c_{err}=[-1;1]; 6 kPa·s; metallic release case #2	c_{err}=[-1;1]; 50 kPa·s; metallic release case #2
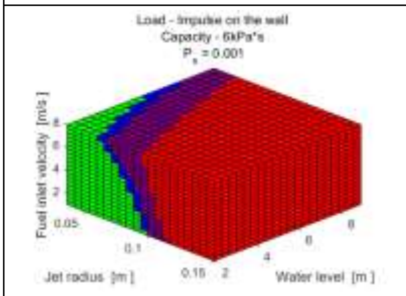	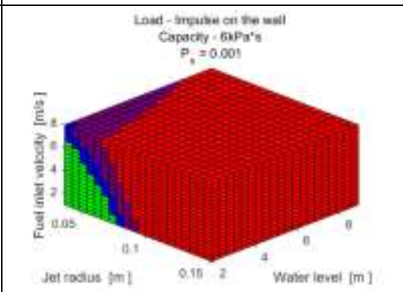	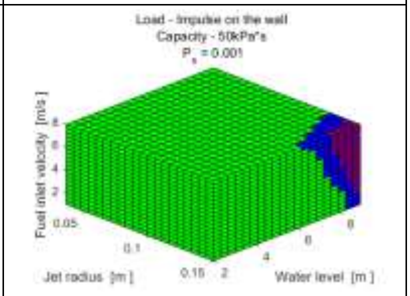
c_{err}= 0; 6 kPa·s; oxidic release	c_{err}=[-1;1]; 6 kPa·s; oxidic release	c_{err}=[-1;1]; 50 kPa·s; oxidic release

Figure 3-110: Failure domain maps for containments with reinforced and non-reinforced hatch door.

In the case of reinforced (50 kPa·s) hatch door the risk of containment failure is significantly reduced. Only in the case of oxidic melt release and incorporation of the SM error some uncertainty on the outcome of the steam explosion reappears. Note that in this analysis the jet diameter is limited to Ø300 mm. For larger size jets, the risk of containment failure will be larger.

The fact that failure domain reduces as a result of the reinforcement of the hatch is merely an indication that such reinforcement could be beneficial. There are two additional aspects to be considered. First, it is uncertain whether melt release scenarios that lead to the failure of the non-reinforced hatch door can occur in case of a sever accident. Indeed, if the size of the vessel breach would be limited to the size of IGT (Ø0.07 m) even in case of deep water pools (>8 m) containment will withstand the explosion. Second, once range of relevant scenarios and respective frequencies is identified, a decision model is required to justify or reject the modification. A criterion must be formulated based on the costs of modification, potential financial losses in case of a SAM failure, frequency of considered scenarios, number of reactors in question and modelling results. A simple approach to the formulation of the criterion can be made based on the following considerations

Decision / Outcome	Failure of SAM	Success of SAM	Utility
Not to reinforce	$P_{f_1}U_f$	$(1-P_1)\cdot 0$	$P_{f_1}U_f$
To reinforce	$P_{f_2}(U_r+U_f)$	$(1-P_{f_2})U_r$	$P_{f_2}U_f+U_r$

where P_{f_1} and P_{f_2} are conditional containment failure probabilities with non-reinforced and reinforced hatch respectively; $U_r = 10^5 \frac{€}{reactor} \cdot n_r = 10^6$ € is cost of hatch door reinforcement; $U_f = -10^{10}€ \cdot n_r n_y f_s = -10^{10} \cdot 10 \cdot 40 \cdot 10^{-5} = 4e^7€/\text{reactior} - \text{year}$ is the negative utility of a large release; $n_r = 10$ is number of reactors in question; $n_y = 40$ remaining years of operation $f_s = 10^{-5}\frac{1}{r\cdot y}$ is scenario frequency.

Equating the two utility costs one can show that modification can be justified when $(P_{f_2}U_f + U_r)/P_{f_1}U_f > 1$. Given above numbers the modification is justified if the change in conditional failure probability $(P_{f_1} - P_{f_2})$ exceeds 2.5%. When a number of scenarios is considered, a threshold could be set to the desired fraction of scenarios that would justify the modification.

3.8.8 Summary and conclusions

The goal of this work was development of a fast numerical tool (surrogate model) that can be used for the assessment of the risk of containment failure in Nordic type BWR due to steam explosion. Three primary tasks have been accomplished: (i) development of the Full Model, (ii) generation of the Full Model solution database, and (iii) development of the surrogate model.

We utilized TEXAS-V to build the Full Model (FM) for the assessment of the steam explosion energetics in Nordic type BWRs and combine it with a simplified impulse propagation approach.

Extensive simulations using the TEXAS-V revealed that explosion impulse is a chaotic function of the triggering time – phenomena that has an important impact on both risk analysis and interpretation of experimental results. Specifically, it was found that explosion impulse can change 50 times within just a 110 ms time window. It is instructive to note that in the steam explosion experiments the aleatory uncertainty due to the influence of the triggering time is also expected to be significant. Proper statistical treatment with multiple repletion of the tests at the same melt release conditions is necessary in order to measure the effects of the other experimental parameters.

We have further, implemented an approach to encompass the chaotic nature of the explosion impulse by characterizing its statistical distribution. The objective is double fold, first it imposes well-posedness on the response function and second allows characterization of the explosion impulse in terms of confidence intervals and confidence levels – approach highly beneficial for risk assessment.

After ensuring model physical well-posedness we proceed with detailed sensitivity study followed by parameter screening leaving 13 most important parameters. The model was then sampled to generate a large database of solutions (1500 premixing sets comprised of 455K of premixing/explosion calculations). Numerically failed calculations were filtered from the database. Physical sensibility of the FM model response to variation of the input parameters was verified in a statistical sense. The database was used for the development of the surrogate model. The surrogate model was implemented using ANN. SM and FM were then systematically compared and results were found to be in a satisfactory agreement.

An approach for quantification of the SM uncertainty is proposed and implemented in the ROAAM+ framework. We found that uncertainty in the containment failure is still dominated by the enthalpy rate of the jet and jet diameter even if the SM uncertainty can be in the range from ~13% to 66% (for small impulses).

Taking into account SM uncertainty leads to increased size of the failure domain. Analysis of the failure domains suggest that reinforcement of the hatch-door might be beneficial as it significantly reduces the risk of the containment failure. SM uncertainty does not affect the conclusion on the benefit of the hatch door reinforcement.

New approaches are currently under development for improved SMs:

- Reduced error.
- Faster performance.

There are several issues that still should be addressed:

1. Melt releases with multiple jets.
2. Multiple consecutive steam explosions.
3. Effect of crust formation around melt particles on the energetics of the steam explosions.
4. Generation of non-condensable gases during premixing.
5. Validation of the explosion propagation model.

Chapter 4. UNCERTAINTY QUANTIFICATION AND RISK ANALYSIS RESULTS

This section presents discussion of the preliminary risk analysis using the surrogate models and framework discussed in detail in previous sections. Results are preliminary as they are determined by current set of assumptions and simplifications employed in modeling.

ROAAM+ aim is to provide assessment of failure probability to enable robust decision making. Decision is robust if it is insensitive to uncertainty, while uncertainty still can be large.

The goal of ROAAM+ preliminary risk analysis is to identify

– ***Main contributors*** to the uncertainty in failure probability Pf.
– ***Importance*** of the ***dependencies*** between different accident stages and respective models
    • in different accident progression scenarios.
– The needs for ***further refinement*** of the knowledge and tools.
    • Models / experiments / frameworks.

Thus the main objective is to identify potential importance of the modeling assumptions on the risk assessment and pave the way to clarification of identified issues in the remaining part of the project following the iterative refinement approach discussed in the previous sections.

The reverse analysis starts with sensitivity analysis of load, capacity and P_f predicted by the framework in order to identify the most influential parameters. Additional knowledge about the other uncertain parameters will not reduce significantly uncertainty in P_f. Thus research can be focused in the next iteration on clarification of the main sources of uncertainty for the risk assessment and decision making.

Next step in the reverse analysis is identification of failure domains. The space of the most influential parameters identified in the sensitivity analysis is used for failure domain visualization. The ranges of the most important parameters where the influence of the other parameters might become important can be also identified as a matter of future research necessary to reduce uncertainty and achieve a robust risk assessment.

4.1 Results using ROAAM+ Framework

The goal of this section is to illustrate comprehensive uncertainty analysis for identification and clarification of (i) main contributors to the uncertainty and risk; (ii) importance of the dependencies between different accident stages in different accident progression scenarios; (iii) the needs for further refinement of the knowledge and tools (models, experimental data, etc.)

We discuss key elements of the reverse analysis with the failure domain (FD) identification and forward analysis with estimation of failure probability (FP) for ex-vessel steam explosion and coolability.

4.1.1 Description of the framework

The surrogate models implemented in the framework (see Figure 3-1) and their role is detailed in the Table 4-1. Four techniques were used for implementation of the SMs: (i) mapping (based on mapping of the FM solution to a grid in the space of the input parameters); (ii) polynomial (scaling analysis and data fitting); (iii) physics based uses simplified modelling of the phenomena; (iv) Artificial Neural Networks (ANN is based on complex regression analysis). Failure criteria are determined for SEIM and DECO.

Table 4-1: Surrogate models of the ROAAM+ framework.

SM	Type	Role
CORE	Mapping	Given timings of ADS and ECCS recovery provides time, composition and mass of core relocation and conditions in the lower drywall: pressure, pool temperature and depth
Vessel failure	Polynomial	Given mass and composition of the debris in the lower head computes timings of the IGT, CRGT and vessel failures and corresponding mass and composition of liquid melt available for release
Melt release	Physics based	Given timings and mode of lower head failure computes conditions of melt release, i.e. ablation of the breach, rate and duration of the release, thermal properties of the melt
SEIM	ANN	Given conditions of melt release and LDW characteristics, returns three explosion impulses and three values of containment capacity
DECO	Physics based	Given conditions of melt release and LDW characteristics, returns dryout heat flux and max debris bed heat flux

At given melt release conditions SEIM surrogate model estimates characterizes loads by mean and standard deviation of the explosion impulses predicted by TEXAS-V for different triggering times. The SEIM failure domain is determined for three fragility limits: 6, 50 and 80 kPa·s. These roughly correspond to the order of magnitudes of fragility limits for non-reinforced hatch door, reinforced hatch door and reactor vessel pedestal respectively.

Current implementation of DECO is a combination of two surrogate models: (i) spreading of particles during sedimentation in the pool which estimates the slope angle of the formed debris bed; (ii) debris bed coolability (returning actual and critical heat flux for given debris bed configuration). Forward and reverse analysis (see Figure 3-1) is performed.

The failure domain is constructed in the space of the input parameters (input space) partitioned into a finite number of cells. Every cell is characterized by a unique combination of the input parameters ranges. The output of the SM is sampled in each cell (by varying deterministic and intangible parameters). The framework compares loads against capacity and renders every computed case to a failure or success. The number of "fail" and "success" cases is counted in each cell, weighted by corresponding probability density functions of deterministic and intangible parameters and normalized to provide conditional failure probability which is compared to the screening probability. The cells where conditional failure probability exceed screening level are grouped into a "failure domain" indicating conditions at which the mitigation strategy fails. For visualization we introduce four-colored failure domain map (see Figure 4-1) where color-code is defined as in Table 4-2

Table 4-2: Definition of failure domains.

Failure domain	Definition	Comments
Red	$CCDF(P_f > 10^{-3}) > 95\%$	Failure probability is larger than 10^{-3} for 95% of possible distributions of the intangible parameters.
Green	$CCDF(P_f > 10^{-3}) < 5\%$	Failure probability is larger than 10^{-3} for only 5% of possible distributions of the intangible parameters.
Blue	$5 \le CCDF(P_f > 10^{-3}) < 50\%$	Failure probability is larger than 10^{-3} in 5-50% of possible distributions of the intangible parameters.
Purple	$50 \le CCDF(P_f > 10^{-3}) \le 95\%$	Failure probability is larger than 10^{-3} in 50-95% of possible distributions of the intangible parameters.

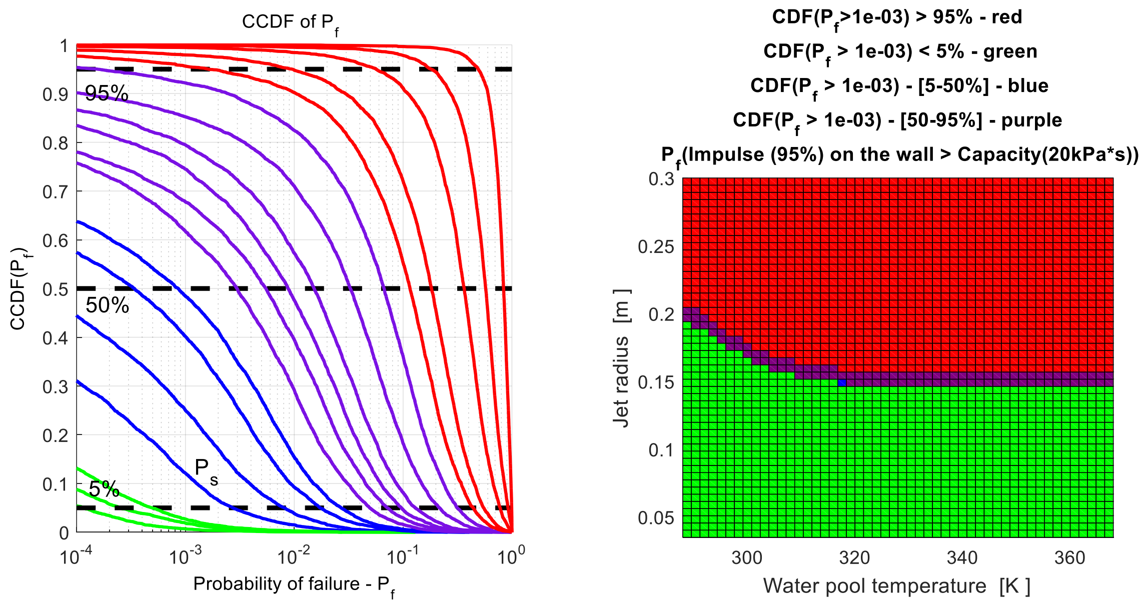

a b

Figure 4-1: Example of the CCDFs of failure probability (a) taken from the first vertical line in failure domain map (b).

The green domain represent the area where SAM is successful and containment failure (due to ex-vessel steam explosion or ex-vessel debris coolability) is physically unreasonable [270] with 95% confidence level, the red domain represents the area where within 95% confidence level the failure imminent (i.e. failure probability exceed physically unreasonable threshold). The domains colored purple and blue represent the area of scenario space where the outcome depends on uncertainty coming from model deterministic and intangible parameters and their distributions.

4.2 Reverse Analysis for Steam Explosion using SEIM Surrogate Model

Different scenarios of melt release have been considered in the analysis. The failure domain is determined in the space of the SEIM input parameters: XPW – water pool depth, UPIN – melt jet release velocity; RPARN – Jet radius.
Results suggest that in case of non-reinforced hatch door (fragility limit 6 kPa·s), the failure of the containment is imminent (red domain) for most of possible combinations of scenario parameters (RPARN, XPW and UPIN). If the hatch door is reinforced (50 kPa·s) there is no risk of containment failure (see Figure 4-2b,d,e and Figure 4-3b,d,e). Note that the jet diameter is limited to Ø300 mm in this analysis. For larger size jets, the risk of containment failure will be larger.
For assessment of the risk of containment failure in Swedish type BWRs we employ failure domains approach. Two scenarios of melt release are considered: release of oxidic or metallic melt. Release of metallic melt was further split into two subcases: Case 01 with up to 1150 K melt superheat and Case 02 with maximum melt superheat of 300 K (the same as for oxidic melt).

Classification of the parameters and their ranges are provided in the Table 4-3. Estimated failure domain maps are given in the Figure 4-2 and Figure 4-3. The maps were estimated taking 95% of the explosion impulse, 0.001 as the screening probability. The color map used in the failure domain maps is explained in the Figure 4-1.

Table 4-3: Classification and ranges of model input parameters used for estimation of failure domain maps.

#	Parameter	Units	Oxidic		Metallic (Case 01 / Case 02)	
Name	Meaning		min	Max	min	max
Scenario parameters						
RPARN	Initial jet radius	m	0.035	0.150	0.035	0.150
UPIN	Melt release velocity	m/s	-8	-1	-8	-1
XPW	Water level	m	5	9	5	9
Deterministic and intangible parameters						
PO	System pressure	Bar	100000	400000	100000	400000
CP	Fuel heat capacity	J/kg·K	490	650	350	490
RHOP	Fuel density	kg/m3	7900	8500	7500	7900
PHEAT	Fuel heat capacity	J/kg	300000	400000	250000	300000
TMELT	Fuel melting point	K	2800	2800	1650	1650
TPIN	Melt temperature	K	2810	3150	1660	2800 / 1966
TLO	Water temperature	K	288	368	288	368
KFUEL	Fuel thermal conductivity	W/m·K	2	6	6	32
CFR	Proportionality constant for the rate of fuel fine fragmentation	-	0.00200	0.00270	0.00200	0.00270
TFRAGLIMT	Fragmentation time	ms	0.00050	0.00250	0.00050	0.00250

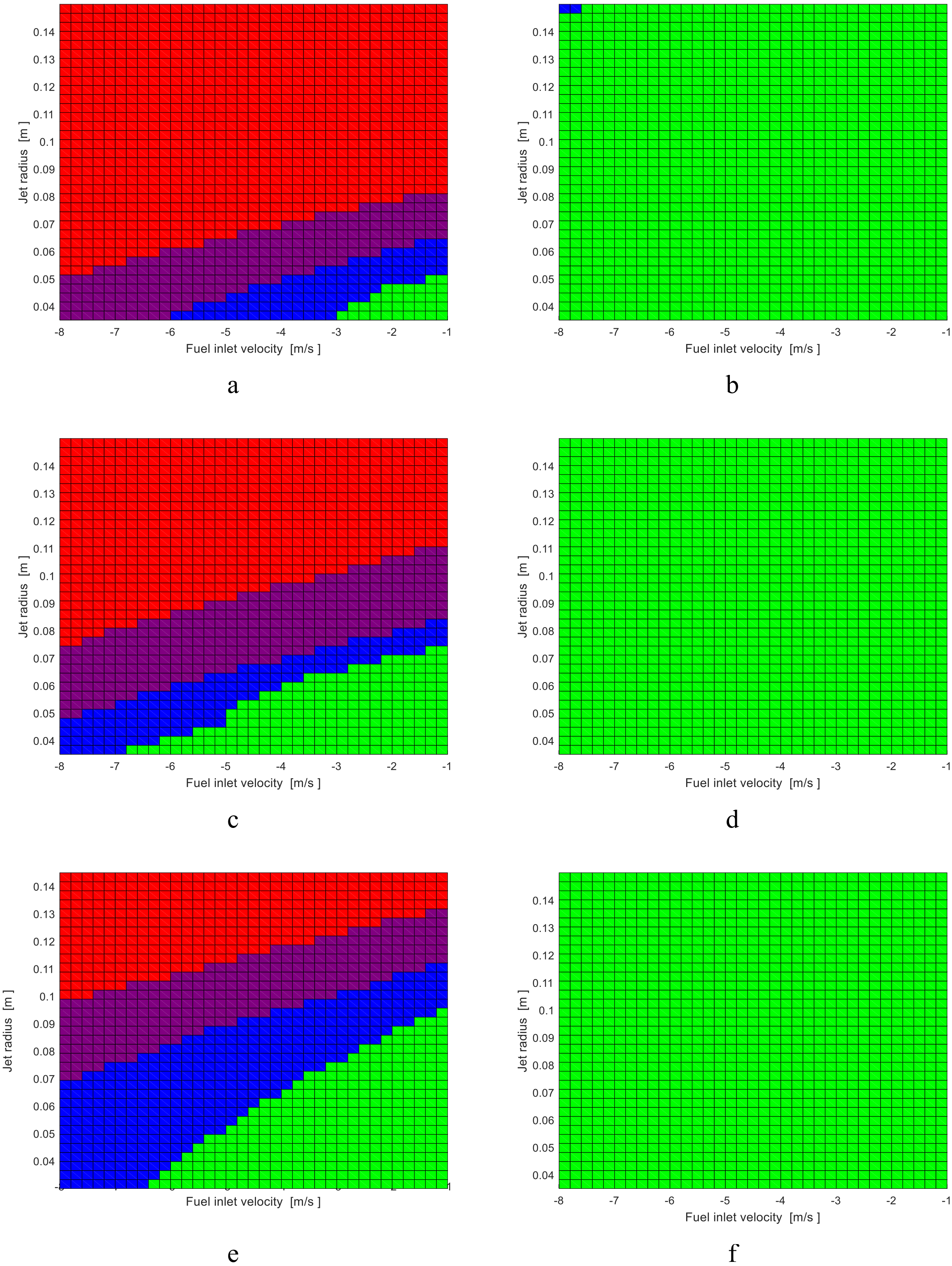

Figure 4-2: Failure domain maps in terms of melt release velocity and jet radius.
(a and b – scenario of oxidic melt release for 6 kPa·s and 50 kPa·s fragility limit;
c and d – scenario of metallic melt release Case 01 for 6 kPa·s and 50 kPa·s fragility limit;
e and f – scenario of metallic melt release Case 02 for 6 kPa·s and 50 kPa·s fragility limit)

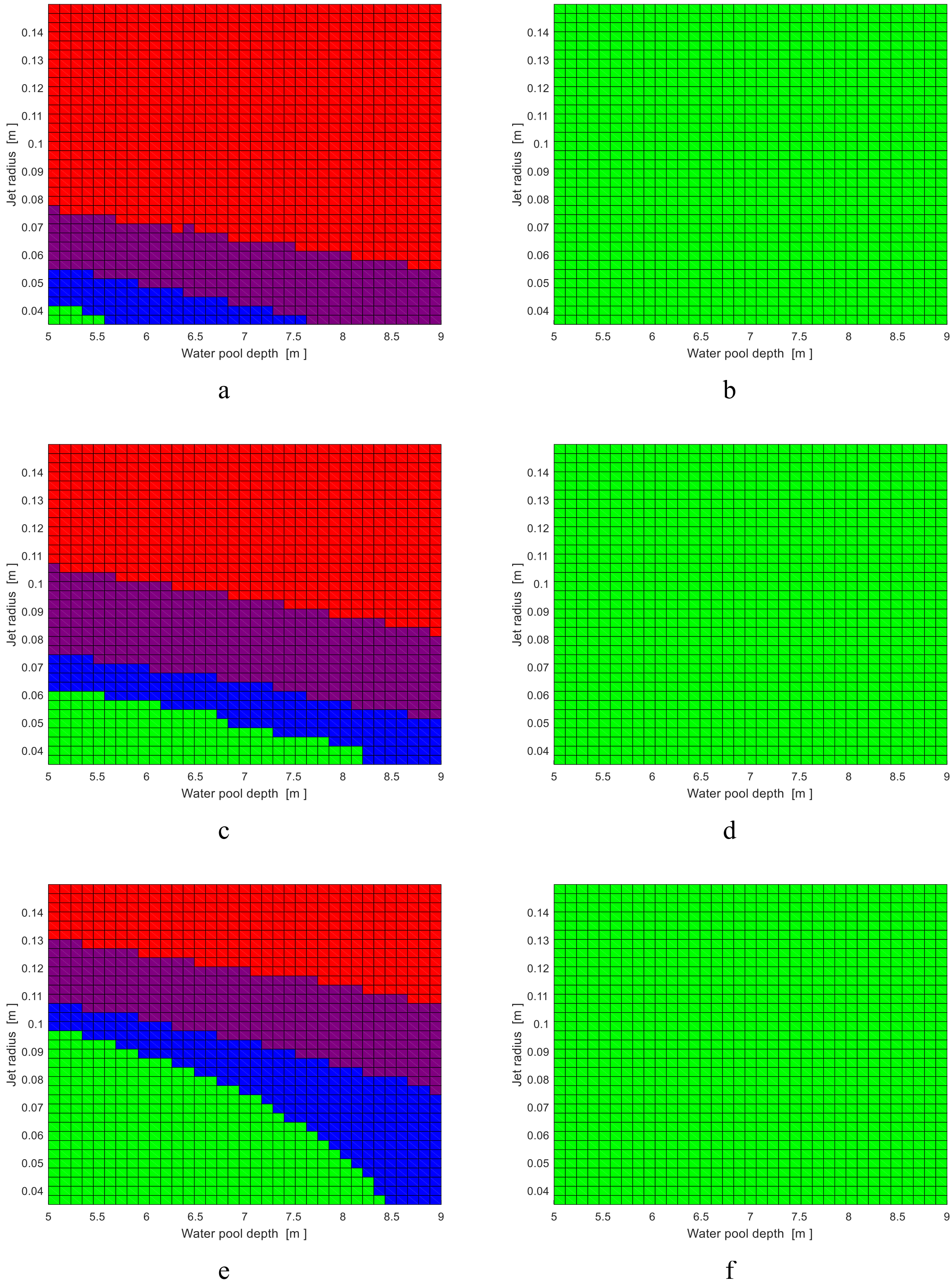

Figure 4-3: Failure domain maps in terms of water level and jet radius
(a and b – scenario of oxidic melt release for 6 kPa·s and 50 kPa·s fragility limit;
c and d – scenario of metallic melt release Case 01 for 6 kPa·s and 50 kPa·s fragility limit;
e and f – scenario of metallic melt release Case 02 for 6 kPa·s and 50 kPa·s fragility limit)

Comparison of Case 01 vs Case 02 (see Table 4-3), i.e. Figure 4-2c vs Figure 4-2d and Figure 4-3c vs Figure 4-3d, suggests as expected that with increase of melt superheat failure domain increases. Current version of the TEXAS-V SM predicts larger failure domain for the oxidic melt than for the metallic one (compare Figure 4-2a vs Figure 4-2c and Figure 4-3a vs Figure 4-3c). It is instructive to note that there is no modelling of crust formation effect on the explosion energetics in TEXAS-V, and melt emissivity was not considered in development of the current SM (because it was identified as less important parameter in the preliminary sensitivity analysis [93]).

4.3 Results of Analysis for Debris Bed Coolability

4.3.1 Sensitivity Analysis for Debris Coolability and Spreading in the Pool

According to the general approach for reverse analysis in ROAAM+ framework, failure domain identification starts with model sensitivity analysis to identify the most influential parameters for both standalone and coupled through the framework models.

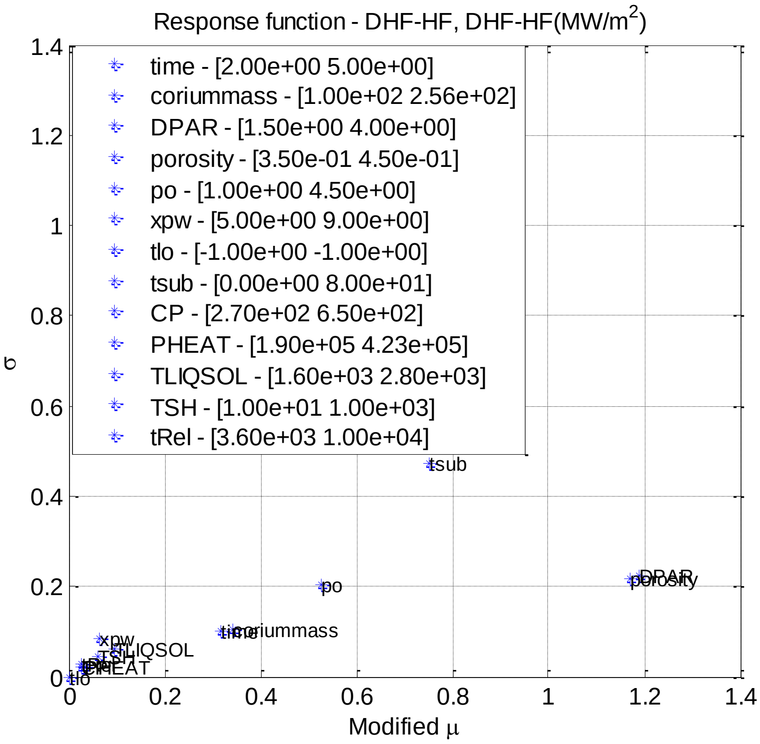

Figure 4-4: Morris diagram for Debris bed coolability input parameters (Base Case)

In this section we discuss sensitivity analysis for Debris Bed Coolability SM that has been carried out in order to evaluate the importance of the DECO SM input parameters and their ranges on the output. Figure 4-4 represents the results of sensitivity analysis using Morris method for the DECO SM output HF-DHF (MW/m^2) (the difference between heat flux and dryout heat flux) for the "Base Case" scenario and ranges (see Table 4-4). The results indicate the dominant effect of DPAR and porosity (particle diameter and porosity) together with tsub (water subcooling) on the results. Initial water subcooling affects time delay for onset of the debris bed spreading and thus height of the debris bed.

4.3.2 Failure Domain Analysis for Debris Coolability and Spreading in the Pool

Figure 4-5 presents the results of failure domain analysis for DECO SM. The figure illustrates the effect of the screening probability in the space of water subcooling and debris porosity. Note that only spreading in the pool is considered in this model currently.

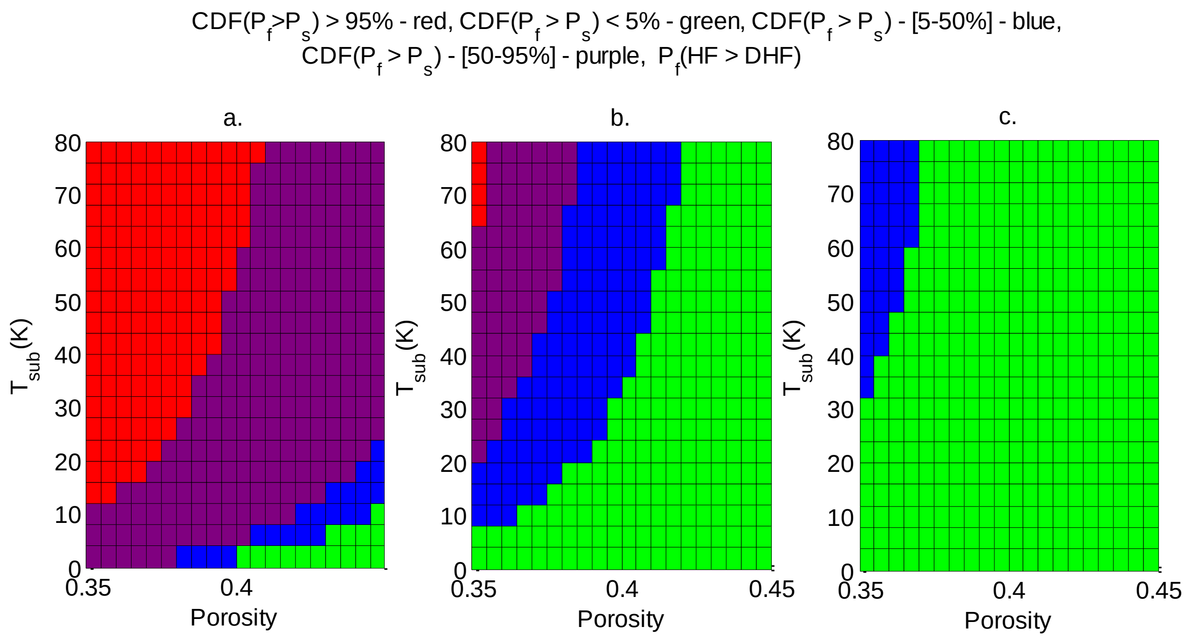

Figure 4-5: Failure domain analysis for DECO SM with different values of screening probability P_s, a. $P_s = 10^{-3}$; b. $P_s = 0.5$; c. $P_s = 0.99$

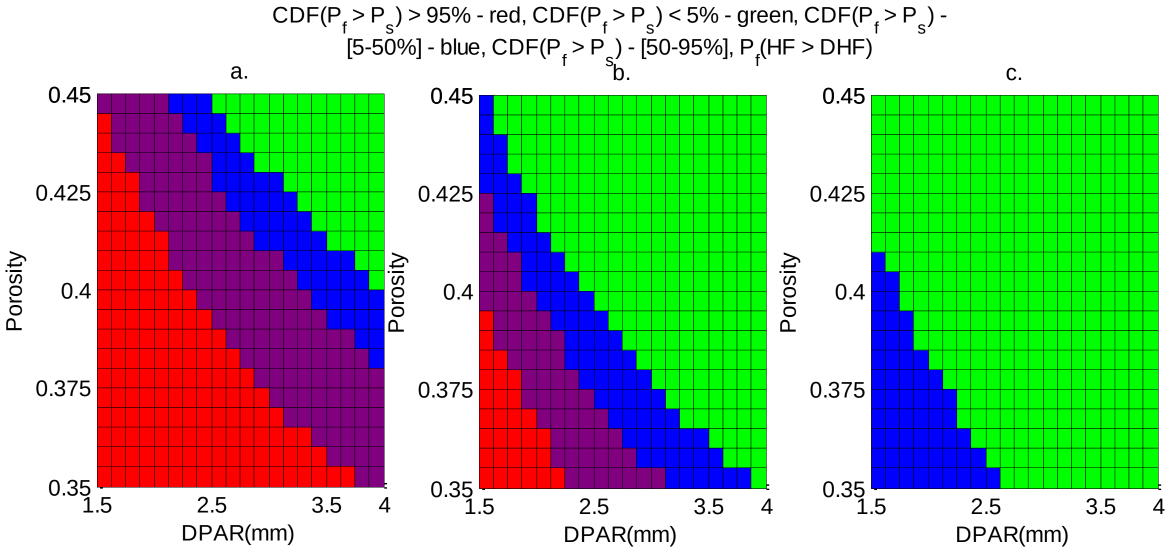

Figure 4-6: Failure domain analysis for DECO SM with different values of screening probability P_s, a. $P_s = 10^{-3}$; b. $P_s = 0.5$; c. $P_s = 0.99$

The Figure 4-5a can be interpreted as follows: the failure (HF>DHF) probability P_f does not exceed screening frequency $P_f \leq P_s = 10^{-3}$ only for scenarios high debris porosity (>40%) and low water pool subcooling (<5-10 K) for more than 95% possible combinations of distributions of uncertain parameters. In other words, green domain in Figure 4-5a can be considered as “safe” where “possibility” of failure is extremely small. The necessity of failure is illustrated in Figure 4-5c. With small debris porosity (<38%) and high water subcooling (>30K) probability of failure exceed $P_s = 0.99$ in approximately 5-50% of possible combinations of the distributions of the uncertain parameters.

Figure 4-6 presents similar results but in the space of particle size and porosity. Formation of a non-coolable debris bed is of low possibility for porosity >0.4 and effective particle size >2.5 mm (Figure 4-6a). High necessity of failure is observed for smaller particles and porosity Figure 4-6b,c.

Table 4-4: DECO SM ranges for the “Base Case”

Name	Description	Range	Units
Time	Time after SCRAM	[2-5]	Hours
coriummass	Debris mass in LP	[100-256]	Tons
DPAR	Particle diameter	[1.5-4]	Mm
Porosity	Debris porosity	[0.35-0.45]	-
PO	System pressure	[1-4.5]	Bar
XPW	LDW water pool depth	[5-9]	M
Tsub	Water pool subcooling	[0-80]	K
CP	Fuel heat capacity	[270-650]	J/kg·K
PHEAT	Fuel latent heat	[1.9e5-4.23e5]	J/kg
TLIQSOL	Temperature of Liquidus\Solidus	[1600-2800]	K
TSH		[10-1000]	K
tRel	Duration of melt release	[3600-10000]	sec

Better knowledge about particle size and porosity would be the most effective means for reduction of the uncertainty in coolability. Further experimental studies can be carried out using corium simulant materials in DEFOR-S type experiments to assess the ranges of porosity for debris of prototypic morphology.

Uncertainty in water subcooling depends on the accident scenario and its ranges can be quantified through modeling of different possible sequences. The effect of water subcooling on debris bed height is an epistemic uncertainty that can be reduced through

- further development of DCOSIM models and extensive validation and against PDS-P experiments;
- analysis of the accident sequences and possible ranges of water subcooling.

Combining the modeling of particle spreading in the pool and particulate debris bed spreading after debris settling due to self-leveling phenomenon might be the most effective approach to reduction of the uncertainty in the assessment of the risks associated with porous debris bed coolability.

Among the other parameters only system pressure, mass of debris and time after SCRAM can noticeably affect selected failure criteria. Uncertainty in mass of debris and time after SCRAM can be reduced through improved modeling of the melt release mode in MEM. Employment of less conservative failure criteria (e.g. post dryout temperature stabilization) can further help to clarify the safety margins.

4.3.3 Reverse and Failure Domain Analysis using Combined SM on Debris Bed Coolability and Particulate Debris Spreading

4.3.3.1 Main results

The developed ANN-based SM of the coolability of debris bed with taking into account effect of bed self-leveling (particulate debris spreading) has been has been used in reverse analysis to identify the failure domain. The input parameters and their varied ranges used in both, sensitivity study and FD identification, are provided in Table 4-5. The final results, namely the Morris diagram and identified FDs are shown respectively in Figure 4-4 and set of plots from Figure 4-8 till Figure 4-10.

There is an easily observable link between the Morris diagram and FD plots. Three most influencing input parameters identified from Morris diagram are (in the order of most influential first):

- Particle diameter (DPAR)
- Bed porosity (porosity)
- Initial bed heat-up rate (trat)

The failure domains are shown for any two combinations of the above listed parameters: porosity-DPAR (Figure 4-8); TRAT-DPAR (Figure 4-9) and TRAT-porosity (Figure 4-10). It is natural that highly porous debris bed composed of large particles should have higher probability to be coolable. Indeed, Figure 4-8 demonstrate this.

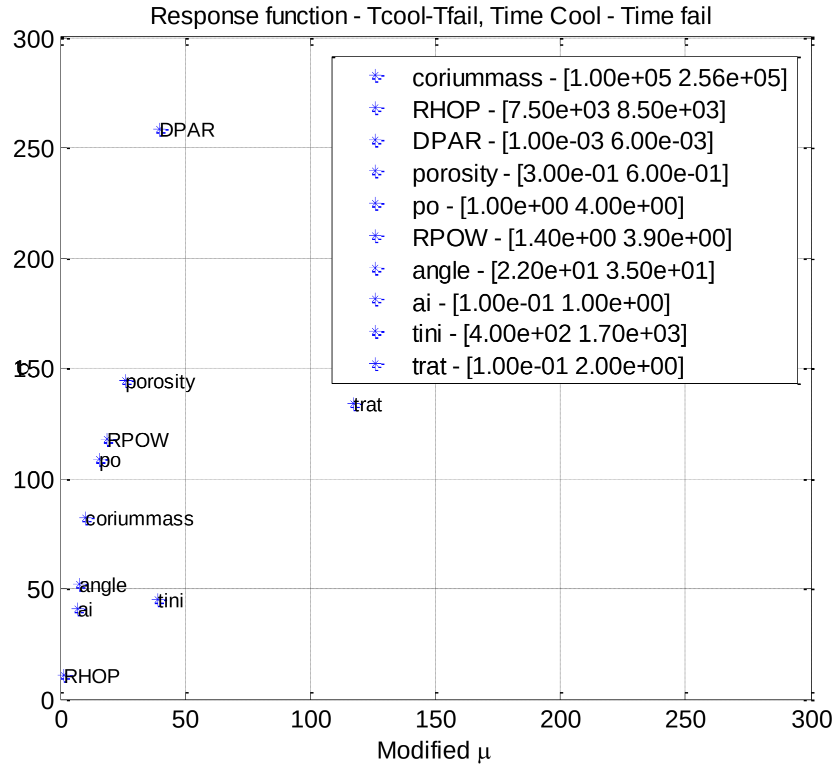

Figure 4-7: Morris diagram for coolability and self-leveling.

Table 4-5: SM ranges for the input parameters

	Name	Range		Description	Units
1	coriummass	1e5	2.5e5	Debris mass	Kg
2	RHOP	7500	8500	Fuel density	JKg/m3
3	DPAR	1e-3	6e-3	Particle diameter	m
4	porosity	0.3	0.6	Porosity	-
5	PO	1	4	LDW Pressure	bar
6	RPOW	1.4	3.9	Reactor Thermal Power	GW
7	angle	22	35	Critical angle or repose	degrees
8	ai	0.1	1.0	Initial angle factor	-
9	tini	400	1700	Initial temperature of settled particles	K
10	trat	0.1	2.0	Initial heat up rate	K

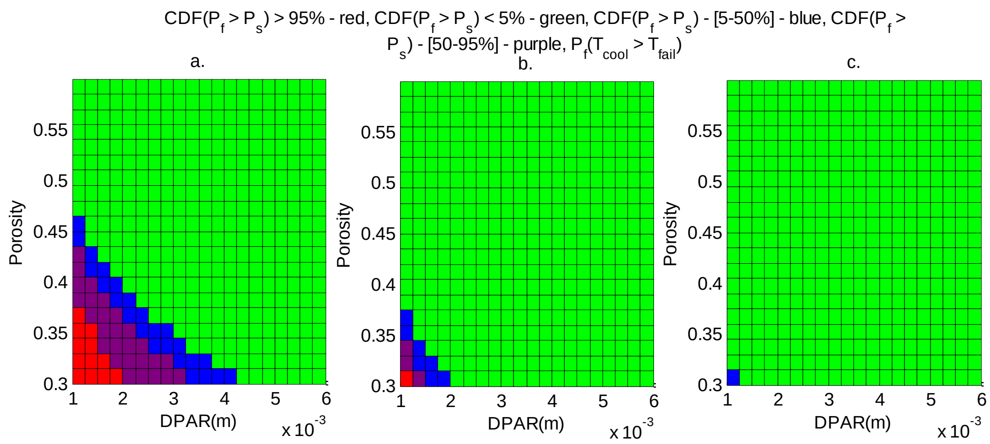

Figure 4-8: Failure domain analysis for PDS SM with different values of screening probability P_s, a. $P_s = 10^{-3}$; b. $P_s = 0.5$; c. $P_s = 0.99$

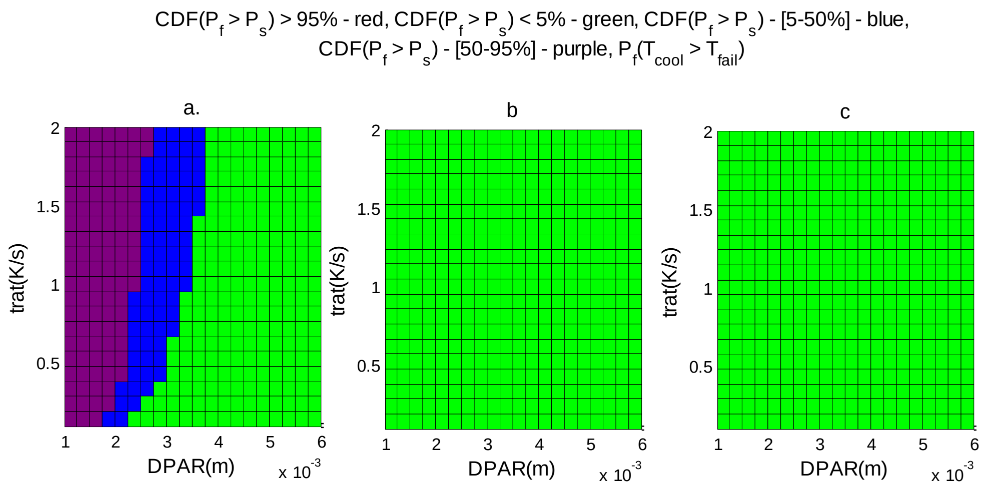

Figure 4-9: Failure domain analysis for PDS SM with different values of screening probability P_s, a. $P_s = 10^{-3}$; b. $P_s = 0.5$; c. $P_s = 0.99$

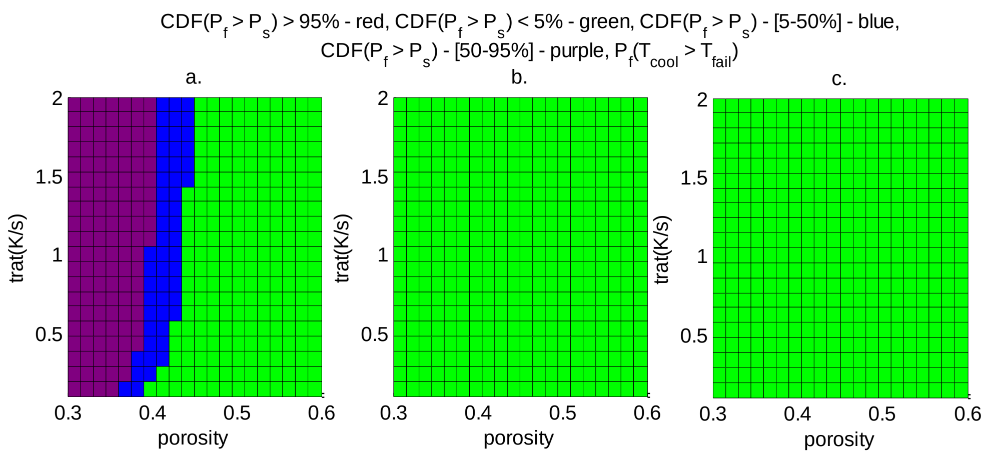

Figure 4-10: Failure domain analysis for PDS SM with different values of screening probability P_s, a. $P_s = 10^{-3}$; b. $P_s = 0.5$; c. $P_s = 0.99$

4.3.4 Debris Agglomeration Failure Domain Analysis

In order to understand better how influential factors affect the risks we employ failure domain approach. Failure domain is a domain in the space of the input parameters where probability of "failure" can exceed a certain limit (screening probability P_S). The failure can be considered, for instance, as an exceedance of safety important parameter over a critical threshold. It is instructive to note that failure probability can be calculated for a given set of probability distributions of the uncertain input parameters. However, the information about the distributions is rarely available. In this work we use second order probability analysis where uncertain distributions are also varied. As a result, a set of possible failure probability values are obtained and characterized by cumulative distribution function (CDF) of the failure probability (P_F).

Results of failure domain analysis performed for Debris Agglomeration SM are presented in Figure 4-11 and Figure 4-12 . Different colors correspond to the different values of the $\boldsymbol{CDF(P_F)}$. The value of $\boldsymbol{CDF(P_F)}$ correspond to the percentile of possible combinations of the distributions of uncertain parameters that result in $\boldsymbol{P_F > P_S}$. Different safety thresholds (5 and 10%) were used for the fraction of agglomerated debris. In Figure 4-11 the results for screening probability $\boldsymbol{P_S = 10^{-3}}$ are presented. Apparently a green domain which correspond to $\boldsymbol{CDF(P_F > 10^{-3}) < 5\%}$ occupies only a small part that correspond to deep pool, small jet diameters and small velocities of melt release. Figure 4-12 show that the exceedance of the safety threshold for the fraction of agglomerates is practically imminent with $\boldsymbol{P_S = 0.99}$ in case of relatively shallow pools, large jets and large melt release velocities.

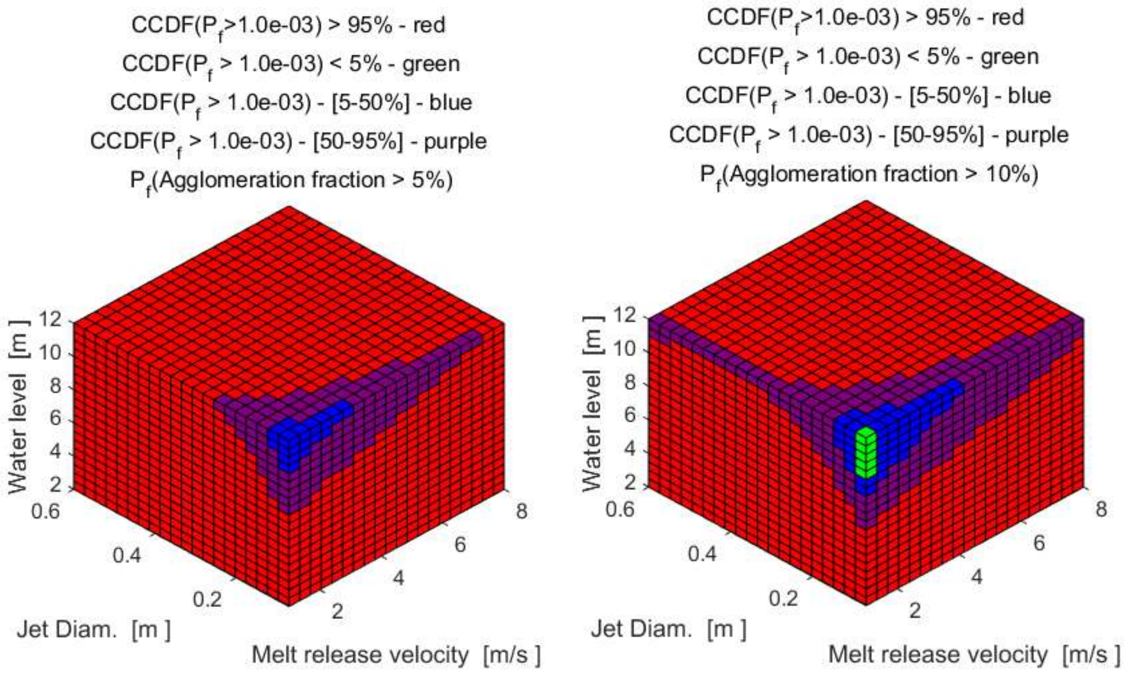

a) b)

Figure 4-11: Failure domain analysis for Debris Agglomeration SM (P_S=0.001) in terms of Jet Diameter (m), Melt release velocity(m/s) and LWD water level (m), with different values of debris agglomeration fraction threshold a) 5%; b) 10%.

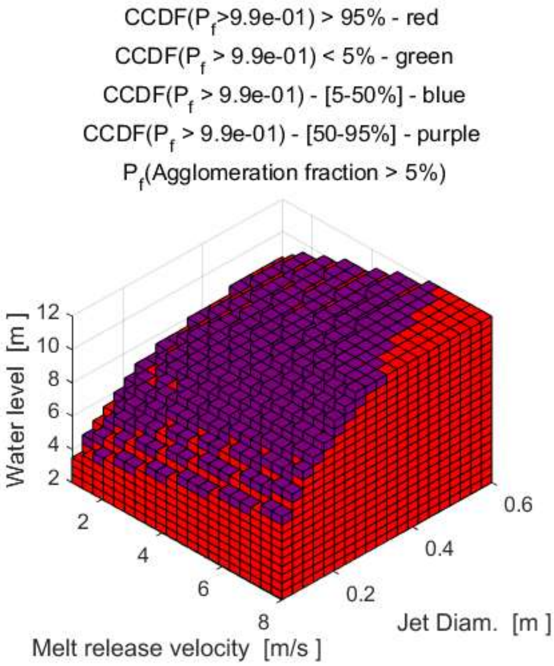

a)

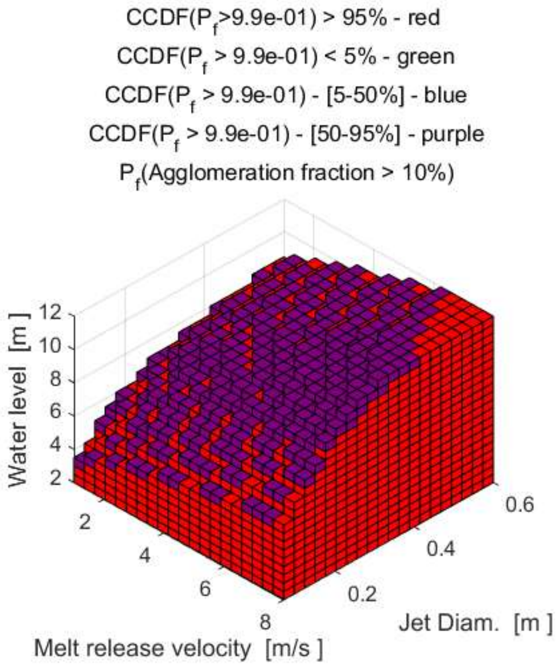

b)

Figure 4-12: Failure domain analysis for Debris Agglomeration SM (P_s=0.99) in terms of Jet Diameter (m), Melt release velocity(m/s) and LDW water level (m), with different values of debris agglomeration fraction threshold a) 5%; b) 10%. Only domain with $\mathrm{CDF}(P_f > P_s) > 50\%$ are shown.

Figure 4-13 illustrate failure domain analysis results for Debris Agglomeration as a function of Jet Diameter, LDW Pool Temperature and Pool depth. The results show that debris agglomeration is currently one of the major contributor to the uncertainty in debris bed coolability. Current model suggest that agglomeration can be avoided only in dripping mode of melt release (very small jet, deep pool). Yet, it is believed that there is significant degree of conservatism in current modeling of agglomeration, especially jet breakup length; Modeling of the effect of agglomeration on coolability (see results obtained with DECOSIM). Thus possible ways to reduce the uncertainty in prediction of coolability are:

- Significant reduction of the uncertainty in the melt release.
- Reduction of uncertainty in
    - Effect of jet breakup on agglomeration modeling
    - Coolability analysis.

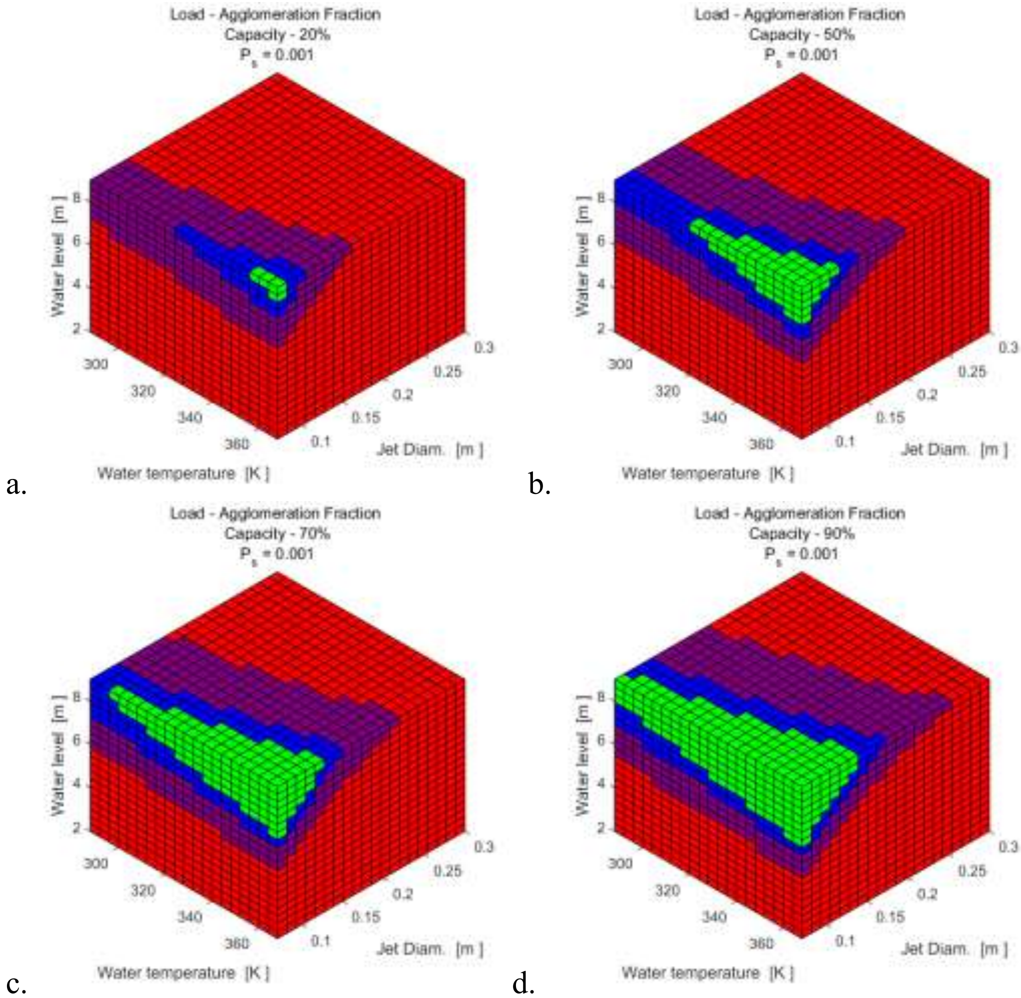

Figure 4-13: Failure domain analysis for Debris Agglomeration SM (P_S=0.001) in terms of Jet Diameter (m), Melt release velocity(m/s) and LDW water level (m), with different values of debris agglomeration fraction threshold a) 20%; b) 50% c) 70%. d) 90%.

4.3.5 Failure Domain Analysis for the Whole ROAAM+ Framework

In this section we show the results of failure domain analysis for the whole ROAAM+ framework, considering different severe accident scenarios. In-vessel accident progression and melt release conditions are predicted by Core Relocation SM (see section 3.3), ex-vessel accident progression, debris agglomeration and steam-explosion loads are evaluated using debris agglomeration and ex-vessel steam explosion surrogated models. In the analysis we considered a metallic release (see sections 3.8), since the temperature of ejected debris was predicted below 2900K and the mass of stailess steel oxide is small, according to MELCOR predictions.

Failure domain analysis was performed for melt release conditions, predicted by Core relocation SM, with penetration failure modelling and solid debris ejection mode ON and OFF (IDEJ0 and 1). Furthermore, we considered median values of the distribution of prediction of melt release conditions by core relocation SM (see section 3.3.6 for details).

4.3.5.1 Failure Domain Analysis with Core relocation SM Predictions for Penetration Failure without Solid Debris Ejection.

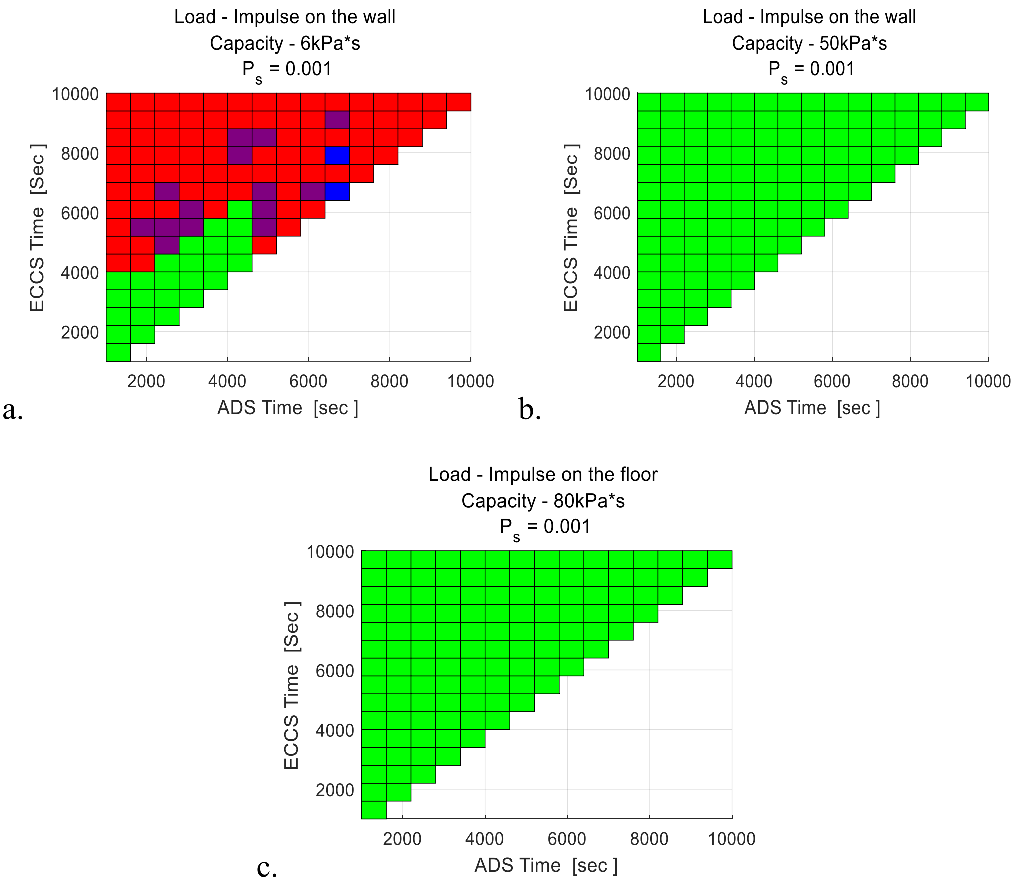

Figure 4-14: Failure domain analysis for SEIM SM (P_s=0.001) in terms of severe accident scenario (ADS and ECCS Timings) with different fragility limits for a) LDW hatch door; b) Reinforced LDW hatch door. c) LDW floor.

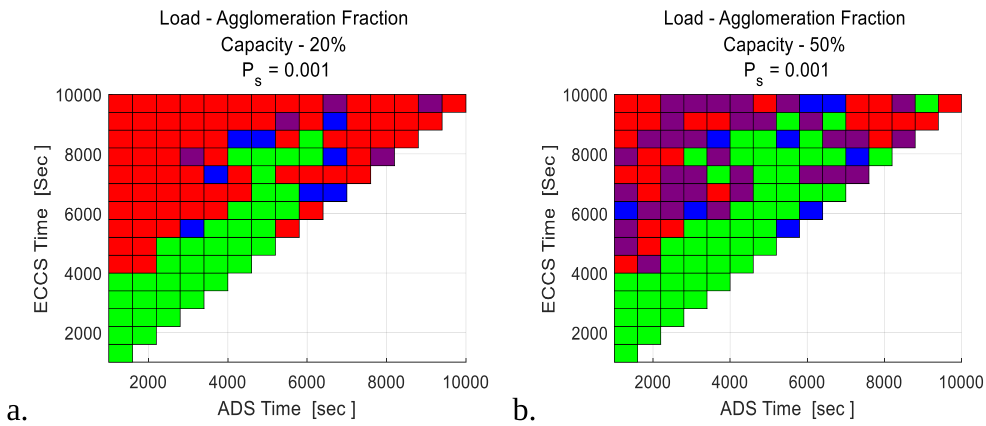

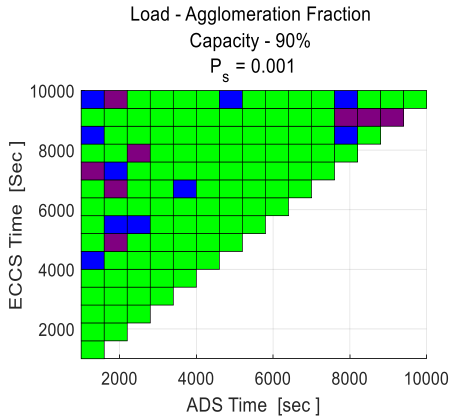

c.

Figure 4-15: Failure domain analysis for Debris Agglomeration SM (P_s=0.001) in terms of severe accident scenario (ADS and ECCS Timings) with different debris agglomeration fraction threshold a) 20%; b) 50% c) 90%.

4.3.5.2 Failure Domain Analysis with Core relocation SM Predictions for Penetration Failure with Solid Debris Ejection.

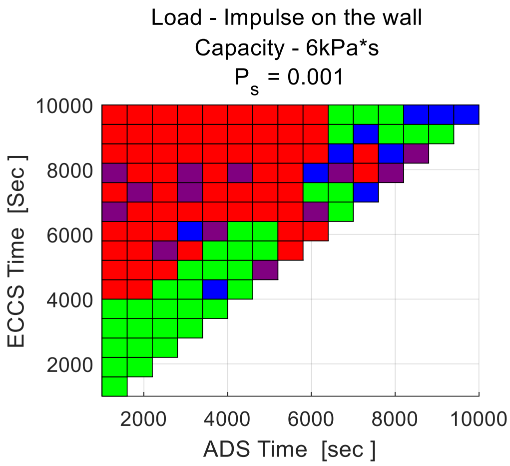

a.

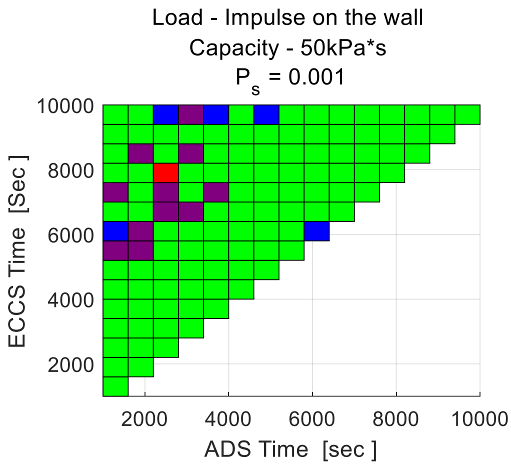

b.

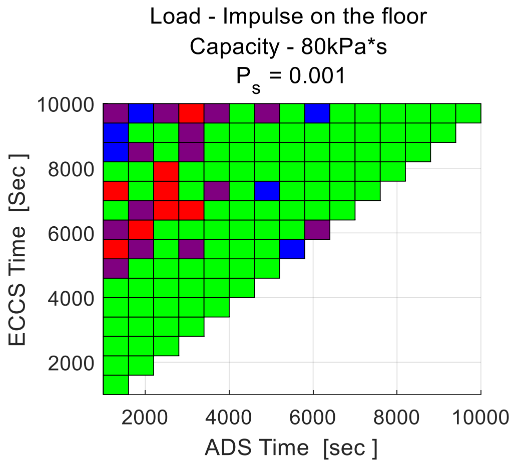

c.

Figure 4-16: Failure domain analysis for SEIM SM (P_s=0.001) in terms of severe accident scenario (ADS and ECCS Timings) with different fragility limits for a) LDW hatch door; b) Reinforced LDW hatch door. c) LDW floor.

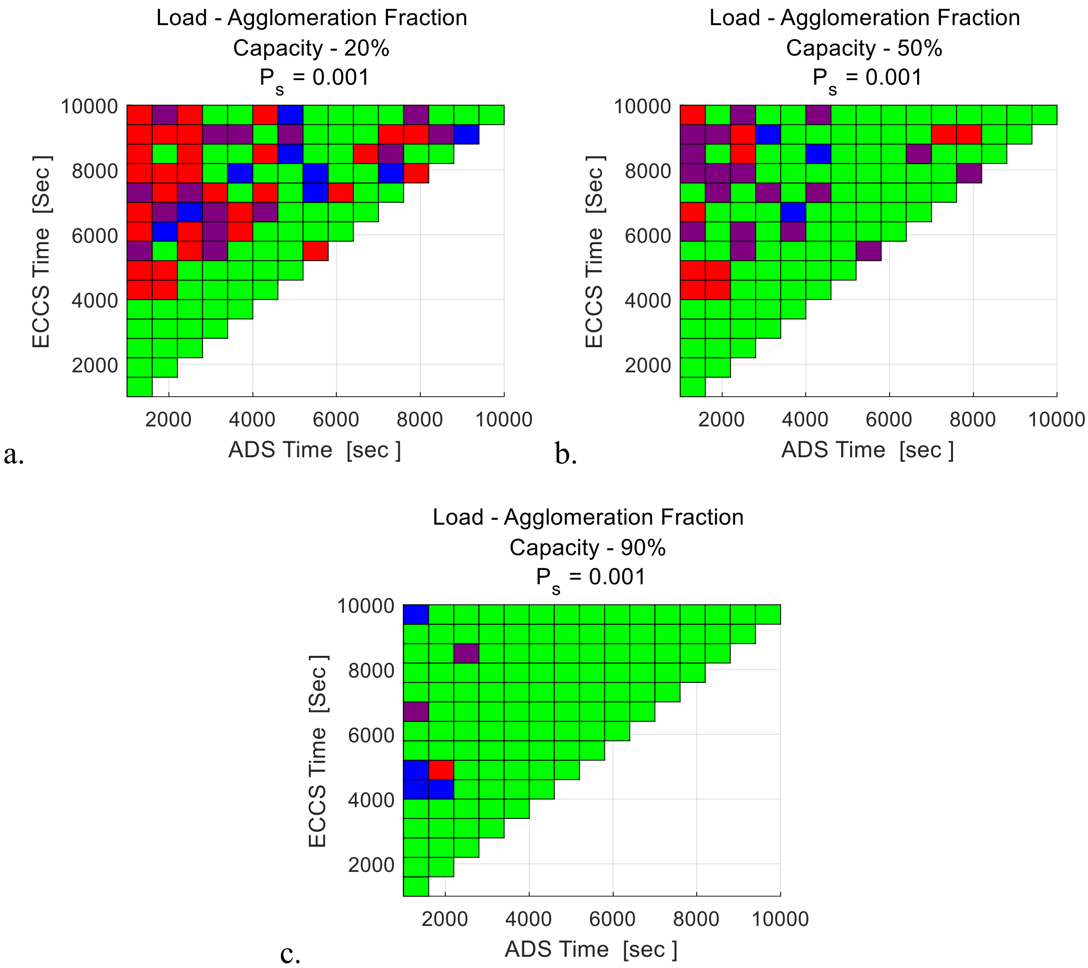

Figure 4-17: Failure domain analysis for Debris Agglomeration SM (P_S=0.001) in terms of severe accident scenario (ADS and ECCS Timings) with different debris agglomeration fraction threshold a) 20%; b) 50% c) 90%.

4.3.5.3 Discussion

The results presented in the sections 4.3.5.1 and 4.3.5.2 illustrate the effect of the accident scenario (in terms of ADS and ECCS timings) on the risk of containment failure due to ex-vessel steam explosion and debris coolability (formation of non-coolable debris configuration). The results show that the containment failure due to containment phenomena in Nordic BWR can be avoided in scenarios with early ADS and ECCS activation. Delay in depressurization, up to 5000sec, followed by the water injection within approximately 1000sec can results in in-core/in-vessel accident termination, and no threat to containment integrity (see Figure 4-18 and *4-19*).

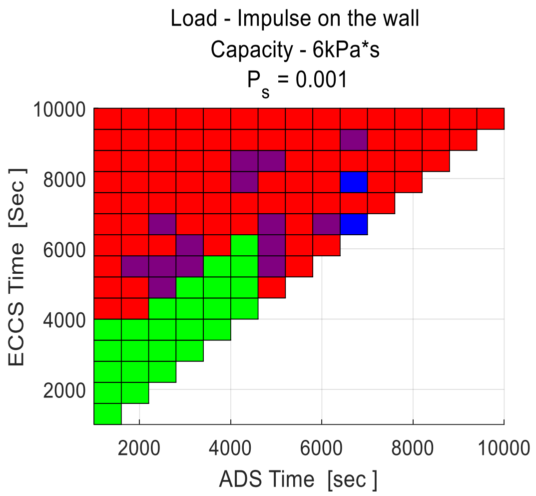

a.

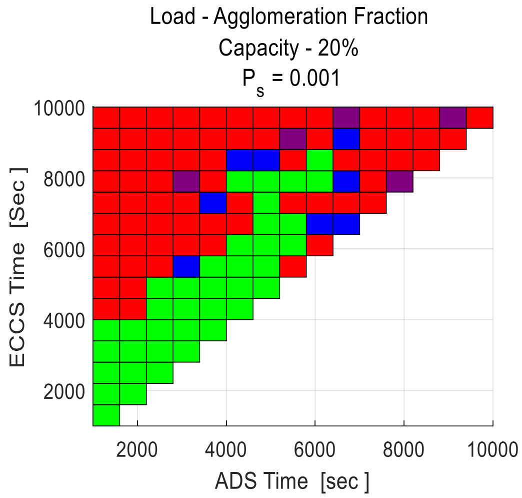

b.

Figure 4-18: Failure domain analysis with (P_s=0.001) for a) Ex-vessel steam explosion load on the hatch door (6kPa*s); b) Debris Agglomeration with agglomeration fraction threshold of 20%.

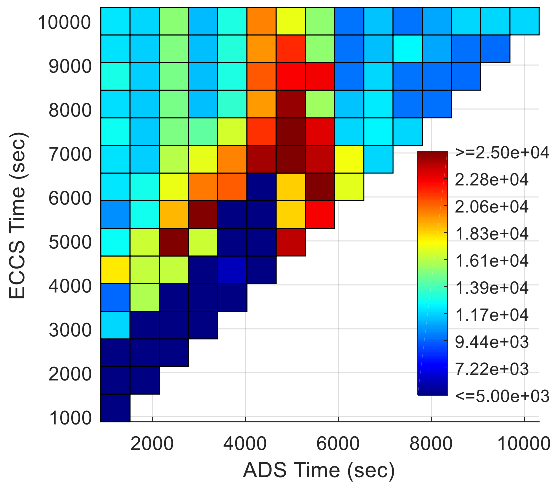

Figure 4-19: The time of vessel lower head breach due to penetration failure, as a function of severe accidentscenario (ADS and ECCS Timing).

Severe accident scenarios with vessel breach in most of the cases result in high loads on the containment hatch door due to ex-vessel steam explosion, and formation of non-coolable debris configuration.

Reinforcement of the containment hatch door to 50kPa*s can significantly reduce the risk of containement failure due to ex-vessel steam explosion, as shown in Figure 4-14a vs. *4-14*b and Figure 4-16a vs. *4-16*b.

Furhtermore, the results show that there is significant effect of the modelling of debris behavior and melt release option used in MELCOR (Core relocation SM). It is assumed in MELCOR code that in case of penetration failure, all debris can be ejeted regardless of its state (solid debris ejection ON – IDEJ0), only molten debris plus some fraction of solid debris can be ejected, based on the solid material transport model (solid debris ejection OFF- IDEJ1). This results in larger debris ejection rates predicted by MELCOR code in case of solid debris ejection on (IDEJ0) compared to solid debris ejection off (IDEJ1), but on the other hand it results in smaller values of the temperature of the ejected debris (TPIN).

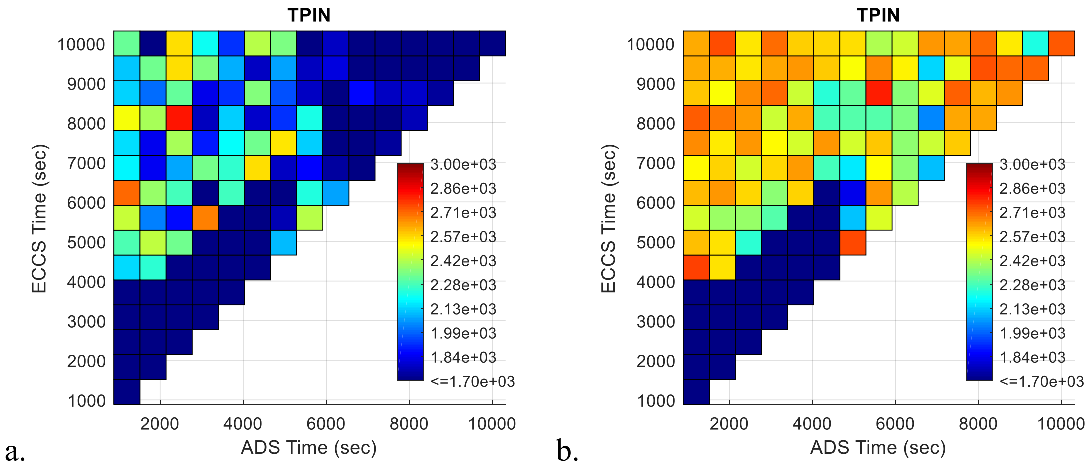

Figure 4-20: The median value of the temperature (K) of the debris ejected from the vessel at max. debris ejection rate, as a function of severe accident scenario (ADS, ECCS Timing) for a) Solid debris ejection ON (IDEJ0) b) Solid debris ejection OFF (IDEJ1).

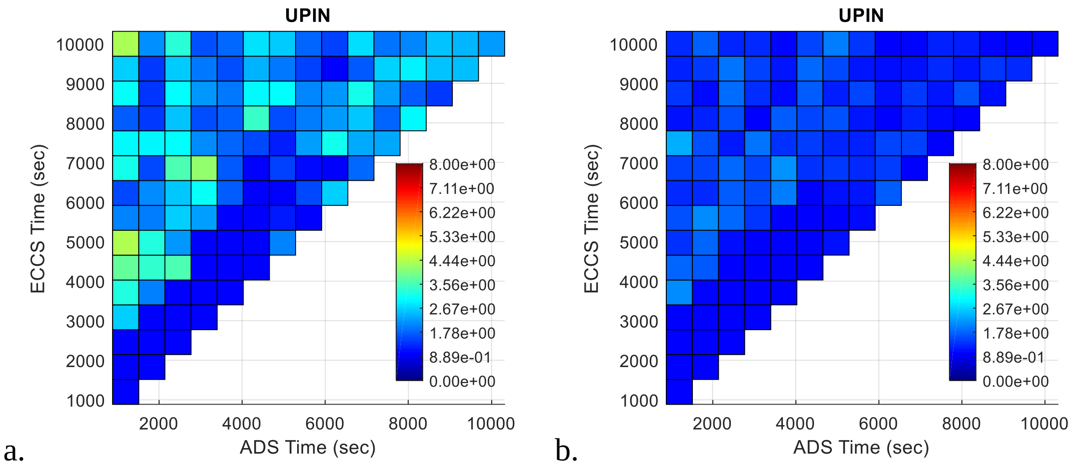

Figure 4-21: The median value of the jet speed (m/s) at max. debris ejection rate, as a function of severe accident scenario (ADS, ECCS Timing) for a) Solid debris ejection ON (IDEJ0) b) Solid debris ejection OFF (IDEJ1).

Additionally, it is assumed in MELCOR that particulate debris will sink into a molten pool, displacing the molten pool volume. Once solid debris components with lower melting point (such as stainless steel) start to melt, the volume occupied by solid debris decreases, the molten materials will occupy empty volume within the solid debris (reducing solid debris porosity). The remaining part will form a molten pool on top of the particulate debris, which will be displaced by the particulate debris from the cell located above, which eventually can result in stainless steel-rich layer on top of the solid debris, and, on the other hand it results in limited availability of molten materials to be released from the vessel. This behavior can result in formation of significant amounts of molten materials with significant superheat on the top of the solid particulate debris, which results in large debris ejection rates, ablation of the failure opening later in time.

4.4 Decision Support and Connection to PSA with ROAAM+ Results

Top layer of ROAAM+ framework for Nordic BWR is comprised of a set of coupled modular frameworks connecting initial plant damage states with respective containment failure modes. The results of ROAAM+ framework are presented as failure domain maps constructed in the space of the input/scenario parameters (input space) partitioned into a finite number of cells. Every cell is characterized by a unique combination of the input parameters ranges. The output of the SM is sampled in each cell (by varying deterministic and intangible parameters). The framework compares loads against capacity and renders every computed case to a failure or success. The number of "fail" and "success" cases is counted in each cell, weighted by corresponding probability density functions of deterministic and intangible parameters and normalized to provide conditional failure probability which is compared to the screening probability. The cells where conditional failure probability exceed screening level are grouped into a "failure domain" indicating conditions at which the mitigation strategy fails.

Information about severe accident scenario s_i and its frequency f_i - is necessary input to ROAAM+ framework and it can be provided from the PSA-L1.

4.4.1 Decision Support

The aim of the ROAAM+ framework is to provide an assessment in support of the decision whether or not the risk associated with current SAM strategy is acceptable. The risk in each scenarios is presented as a triplet $R_i = \{s_i, f_i, pdf(P_{Fi})\}$, where scenario s_i has frequency f_i and uncertainty in the failure is characterized by distribution probability of failure probability $pdf(P_{Fi})$. Such approach keeps separation between frequencies of scenarios (s_i, f_i) that characterize statistical data about frequencies of failures of systems and components etc. that can be obtained from PSA-L1, and confidence in prediction of the phenomena determining containment failure ($pdf(P_{Fi})$) that is obtained from the uncertainty analysis using deterministic models. As we will demonstrate, this separation is important for an adequate approach to interpretation of the risk and respective decision making process.

Scenario frequencies are the inputs to ROAAM+ framework provided from PSA L1 analysis results, i.e. frequencies of correspondent plant damage states (PDSs). Conditional containment failure probability (or probability distribution of conditional containment failure probability) for each scenario is a main outcome of ROAAM+ framework analysis. Figure 4-22a presents decision criteria as a function of accident scenario frequency (CDF) and Conditional Containment Failure Probability (CCFP) or Conditional Probability of Unacceptable Release (CPUR), and Figure 4-22b illustrates ROAAM+ results of $pdf(P_{Fi})$ as box and whiskers plots for scenario s_i, with frequency f_i). Based on the results it is possible to judge, whether or not current SAM strategy is effective for a given severe accident scenario s_i, and the likelihood that there are some combinations of modelling parameters (i.e. deterministic, intangible parameters and correspondent probability distributions) that can cause failure for the given scenario.

a.

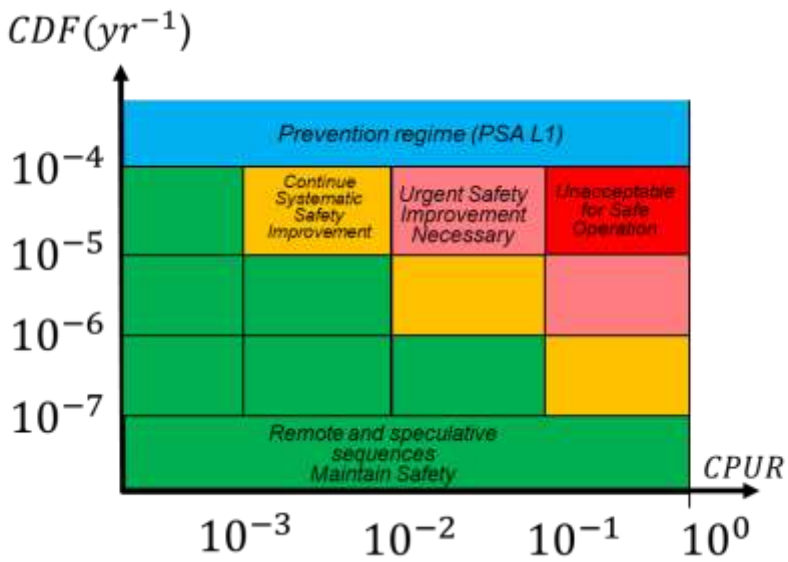

b.

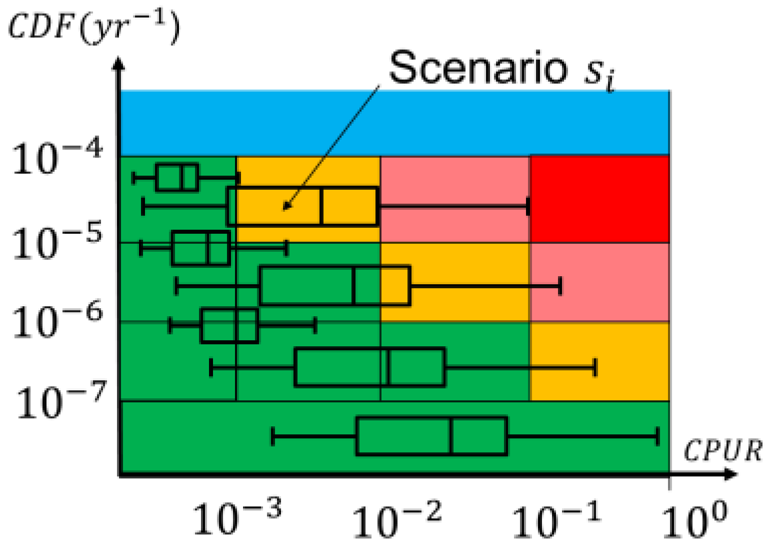

Figure 4-22: Decision support with ROAAM+.

4.4.2 Improvement of Sequence Modelling with ROAAM+ Data

From the initial sequences in the PSA Level 1, all events that are leading to a certain PDS are then treated in the same manner in the continued sequence (however, dependencies are treated logically correct if the failure should affect systems in PSA Level 2). It is however obvious that it will be different scenarios from a deterministic stand point if there is an initial loss of offsite power and no start of the diesels, compared to a scenario where the diesels would stop after some hours.

The purpose with the improved integrated link between the PSA and deterministic analyses is hence to be able to judge if, for example, these scenarios need to be treated differently in the PSA context.

The approach chosen in this report was to identify some sequences from the PSA Level 1 and to use ROAAM+ framework to evaluate the progress of these sequences and correspondent conditional containment failure probability for different severe accident scenario.

To illustrate an approach for improvement of sequence modelling in PSA L1 (L1+) let's assume the following failure domain maps obtained with ROAAM+ framework for ex-vessel steam explosion as a function of lower drywell water pool depth and release size (jet diameter), see Figure 4-23.

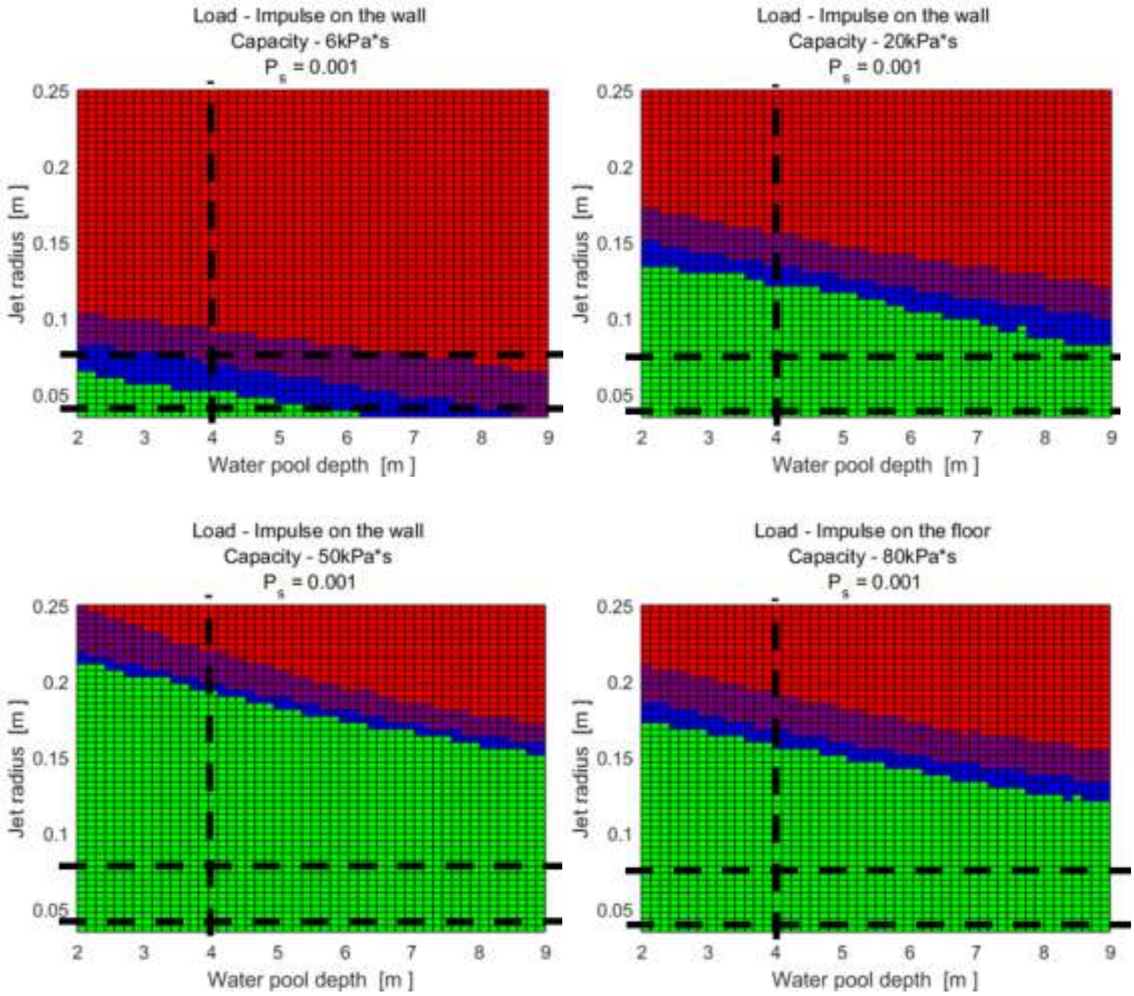

Figure 4-23: SEIM Failure Domain Maps.

Taking the lowest fragility limit (which roughly corresponds to the non-reinforced hatch door) and assuming the following:

- Lower Drywell Pool Depth:
    - "Deep" if pool depth > 4m
    - "Shallow" otherwise.
- Release Size (Jet diameter (Djet))
    - Djet <75.e-3m – Dripping Mode (corresponds to IGT failure)

- 75.e-3m <= Djet <150.e-3m – Medium release (ablated IGT)
- Djet >= 150.e-3m – CRGT failure + ablated CRGT.

The failure domain map can be represented by 6 modes:

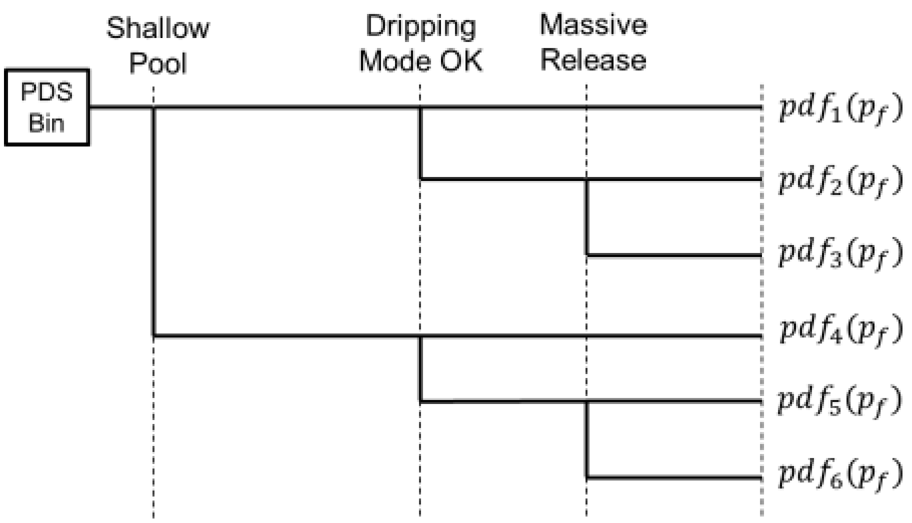

Figure 4-24: Refined Containment Event Tree Example.

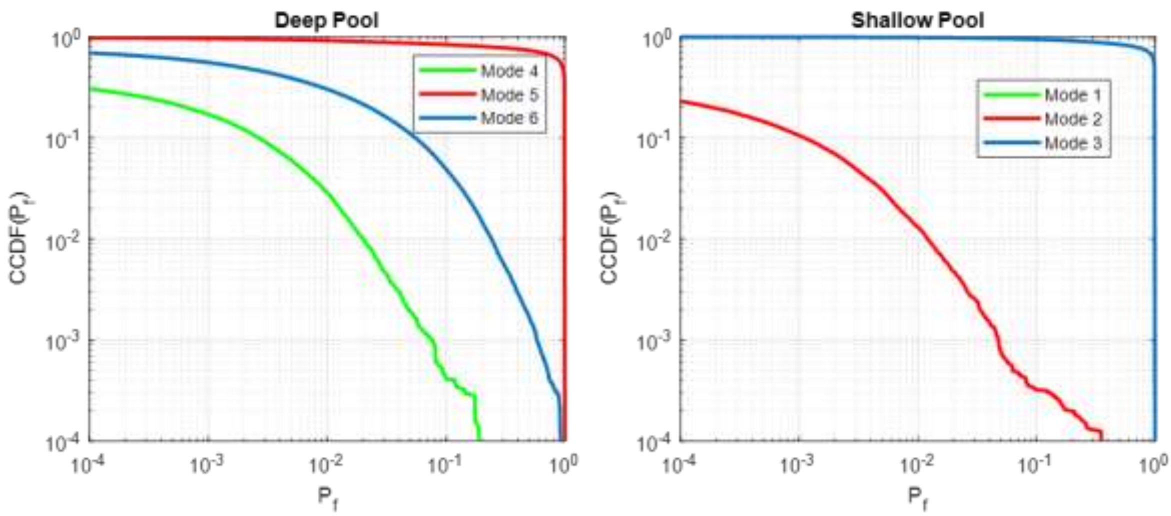

a) b)

Figure 4-25: Complimentary Cumulative Distribution Function of Conditional Containment Failure Probability due to Ex-Vessel Steam Explosion with Non-reinforced Hatch Door: (a) for Deep Pool (b) Shallow Pool.

In Mode 1 ("Shallow Pool" and "Dripping Mode"), based on ROAAM+ results (see Figure 4-23), maximum conditional containment failure probability is 0 for all fragility limits, meaning that whatever uncertainty is in modelling of ex-vessel steam explosion (SEIM), containment failure due to ex-vessel steam explosion is physically unreasonable, and SAM strategy is effective even with non-reinforced LDW hatch door.

On the other hand, in case of “deep pool” (i.e. LDW pool depth > 4m), probability of failure in case of non-reinforced door ranges from [0,0.729] (see Figure 4-25), depending on water pool depth within this range and deterministic, intangible parameters used in modelling of ex-vessel steam explosion.

Figure 4-25a,b show the CCDF of conditional containment failure probability due to ex-vessel steam explosion in case of medium release and shallow (Figure 4-25a) / deep (Figure 4-25b) pool. These results clearly indicate that there’s significant difference in CCFP depending on the LDW water pool depth.
Presented results of ROAAM+ framework analysis clearly shows that there are sequences that affect the phenomena that can occur, e.g. in presented example, depending on the water pool depth, the conditional containment failure probability due to ex-vessel steam explosion can change significantly and result in consequences of risk significance. Moreover, reverse analysis with ROAAM+ can provide insights regarding under what conditions each phenomenon is relevant. Thus, based on ROAAM+ results we can judge if these sequences need to be treated differently in PSA context, and result in refinement of plant damage states in PSA L1.

This example is studied further in section 5.3, where its results are integrated with the PSA model.

Chapter 5. Improvements in PSA modelling to integrate dynamic features.

Section 5.1 provides a general introduction to a common approach for modelling of severe accident progression sequences in Probabilistic Safety Assessment (PSA) developed in [155]. Section 5.2-5.4 discusses possible methodological enhancements of PSA using a dynamic approach as well as a feasibility study performed for a large scale PSA model, which continues the example discussed in section 4.4.2.

5.1 Sequence Modelling in PSA Level 2

5.1.1 Assumptions and Limitations in PSA

PSA is used to systematically identify, evaluate and rank the sequence of events that can lead to core damage and radioactive release to the environment. Identification and hence opportunities for improvement in risk dominant feature of the facility is one of the overall objectives. The analysis is probabilistic, i.e. it is based on probability and reliability calculations and the result is an estimate of the frequency of detected events.

Some key assumptions and limitations in PSA level 1 (L1) analysis are:

- Implemented deterministic analyses are correct.
- Blow-down paths and building structures can withstand emerging loads at rupture.
- Studied transient time is normally 1 day, i.e., objective function is required during this time (Level 1 analysis includes 20-24 hours from initiating event, sequences that have not led to the core overheating within this time are not considered as core damage sequences and excluded from Level 2 analysis).
- Aggravating manual interventions are not considered.
- Restricted modeling of manual interventions during transients (only when clear instructions are provided and there is sufficient time available).
- System requirements should be established either via thermal-hydraulic calculations or through references in the SAR.
- Timing within sequences is represented simplified (conservative).

5.1.2 Phases during severe accidents

The first phase of an accident is studied in PSA L1 and the result is a number of sequences ending with either success or core damage.

For those sequences ending with core damage the following accident progression is studied in PSA level 2 (L2). The accident progression is often divided in the following parts:

- **In-vessel** – Describes the heat up and meltdown of the core.
- **Vessel melt through**– Describes the phenomena occurring at vessel melt through.
- **Ex-vessel** – Describes the long term progression of the plant after melt through.

Related phenomena suitable for further study with deterministic methods can be found both in PSA L1 and in the different phases of PSA L2.

5.1.2.1 Core Damage States in PSA L1

The basic set of core damage states in PSA L1 is generated by simply differing between core damage and success. Usually, the core damage states are also separated into generic categories with respect to the cause of the core damage. A possible grouping of such generic reasons of damage is given by:

- HS1: Failure to shut down the reactor.
- HS2: Failure to make up water to the reactor.
- HS3: Failure to remove residual heat from the reactor.
- HS4: Overpressure of the primary system.
-

Typically, failure of core cooling or residual heat removal gives the major contributions to core damage, but this varies from plant to plant.

Failure to shut down the reactor usually gives a low contribution to the total core damage frequency. Reactivity control is however a very complex process to model since an incomplete or delayed shutdown puts higher demands on the other functions such as core cooling, pressure relief of the primary system etc. It may therefore be interesting to study this in more detail since the core damage frequency due to failure of shutdown may be underestimated in the existing PSA studies.

5.1.2.2 Plant Damage States Classification in PSA L2

In PSA L1 for the Nordic BWR reference plant design, the core damage states are grouped into 4 categories: HS1 (ATWS), HS2 (Loss of core cooling), HS3 (Failure to remove decay heat) and HS4 (Primary system overpressure). The categories (HS1, HS2, and HS4) correspond to early core damage scenarios, HS3 – corresponds to late core damage.

In addressing ex-vessel behavior and consequences, the following physical phenomena can challenge containment integrity: direct containment heating (DCH), ex-vessel steam explosions (EVE) and insufficient ex-vessel debris coolability (DECO).

A quantitative perspective on these phenomena should be derived from the PSA L1. Direct containment heating (DCH) correspond to high pressure (HP) melt-through processes, steam explosion (EVE) corresponds to low pressure (LP) melt-through and, finally, both consequences will lead to large amounts of core debris relocated to the lower drywell which can challenge its' floor and penetrations integrity, i.e. ex-vessel debris bed coolability is an all-pervasive issue.

Initial conditions and correspondenting frequencies for the sequences that will lead to the different core degradation, in-vessel debris bed formation and vessel failure scenarios can be identified from PSA L1 data.

In conclusion, the core damage sequencescan be grouped based on the aforementioned challenges to containment integrity as shown in Figure 5-1.

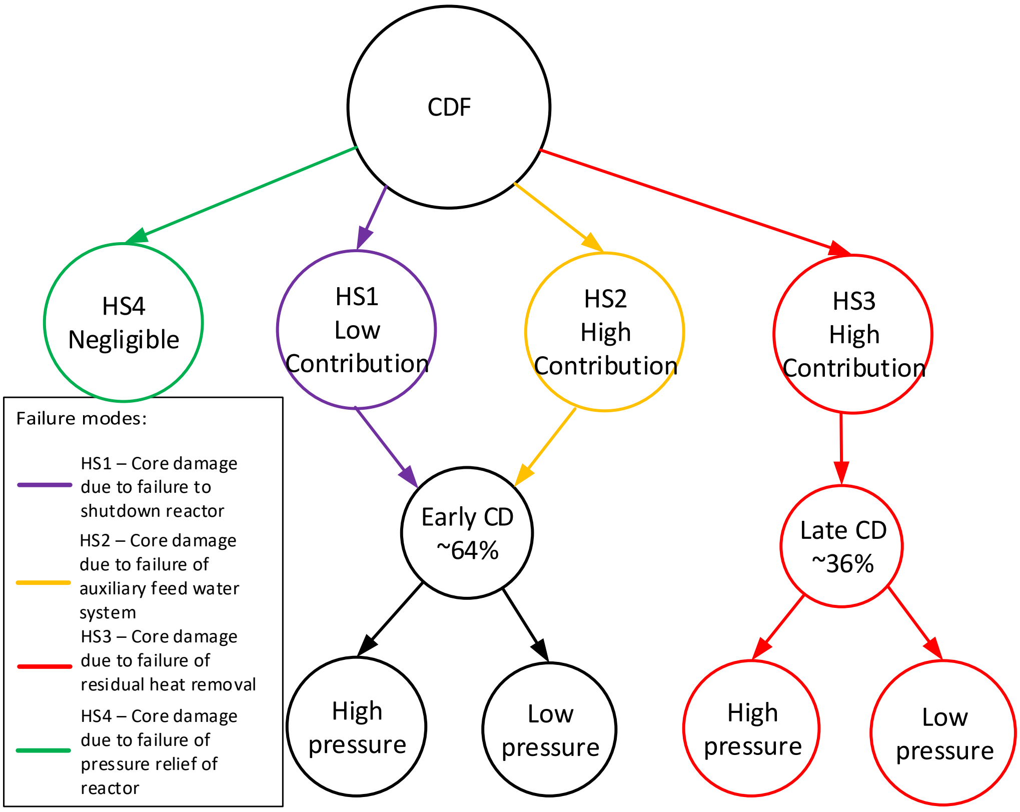

Figure 5-1: Core Damage States Classification.

5.1.2.3 Level 2 PSA

In a standard PSA, the output of PSA Level 1 is typically core damage (possibly separated in a few sub-categories). These core damage sequences are then divided into a number of sub-categories representing the important features for Level 2 progression.

The link between PSA L1 and L2 is the plant damage states. The plant damage states describe not only the core damage state but also the conditions of the primary system and the containment. There are normally around 20-40 Plant Damage States (PDS) defined in the interface between Level 1 and 2.

For the generic Nordic BWR studied here, there are 27 PDSs for power operation and low power operating modes. The attributes that are considered relevant for modelling of the continued process are:

- Core damage state (failure of shutdown, core cooling or residual heat removal).
- Initiating event (transient or LOCA).
- Time of core melt (early, late).
- Reactor pressure (low, high).

- Containment atmosphere (inert, air).
- Containment spray system status.
- Containment pressure relief status.
- Filtered containment venting status (activated, not yet activated, failed).
- Bypass of containment (bypass, intact).
- Suppression pool temperature (warm if pool cooling fails, else cool).

The events that are represented in a PSA Level 2 are those tha tmay change the conditions for retaining of releases within the RPV or the containment. Hence, if the coolability in the RPV is different in different scenarios – then this is vital information. If the sequences are affecting the phenomena that can occur, then this is also vital information. For each of the PDS, a subsequent containment event tree (CET) is defined, modelling the continued accident progression.

The accident progression sequences are influenced by various physical phenomena. The types of phenomena that are usually accounted for in a PSA are:

- Re-criticality (in the core, in lower plenum, in containment).
- Hydrogen burn (deflagration and detonation).
- In-vessel steam explosion.
- Ex-vessel steam explosion.
- Direct containment heating.
- Rocket mode.
- Melt concrete interaction (basemat penetration).
- Steam generator tube rupture (only for PWR).

The effect of the phenomena can be:

- Containment rupture.
- Different types of containment bypass.
- Activation of filtered containment venting.

The effect most focused on in the following is containment rupture.
The sequences in the CET end at the release categories (RC) and there are normally around 15-40 of such. The RCs can be defined in different ways, for example by release size or type of sequence. The normal approach is to use the sequence type, because then only a limited amount of verifying deterministic calculations are considered to be required. For the sequence type approach, the characterization is for example based on;

- Release path (containment bypass, containment rupture, filtered release, leakage).
- Timing of release (early, late).
- Initiator (pipe rupture, transient).
- Sprinkling of containment established (yes/no).

5.2 Methodological enhancement – DSA and PSA integration

All possible failure combinations should be covered by the PSA and the PSA model therefore includes a large number of possible failures and possible severe accident progression sequences. Current PSA models are static and grouping of sequences (failure combinations that have similar effect) as well as simplified treatment of timing of failure combinations are needed.

Ideally, a risk analysis would, at all points, consider all challenges that can occur at that particular point in time. The process could be thought of like a dynamic event tree covering all possible failures (aleatory) and uncertainties associated with the lack of knowledge about system response (epistemic uncertainty). As muchas this is an appealing approach, the state space that would need to be analyzed to cover all possible scenarios and epistemic uncertainties is enormous and it will not be feasible to perform this analysis with a brute force approach.

A limited dynamic approach to PSA would give enhanced information about which scenarios that should be studied separately and information about timing of events of importance. One important aim of a dynamic approach to PSA is to quantify and eventually reduce epistemic uncertainties. The deterministic analysis can provide important insights to which parameters that are of relevance and should be included in the definition of the sequences and the modelling of physical phenomena.

One major advantage with a dynamic approach to PSA is the possibility to address different types of parameters, dependencies and uncertainties that are not taken into account in a static PSA. It is important to distinguish between different types of parameters influencing the severe accident progression:

- Scenario parameters: Parameters describing various aspects of systems response.
- Physical parameters: Parameters describing well-posed physical problems or “causal relations”.
- Intangible parameters: Other aspects which uncertainty can only be bounded.

The static PSA is built on choosing the correct scenario parameters to describe the accident progression and typically uses a pre-set choice of physical parameters in the underlying deterministic analysis. It is however difficult to handle both intangible parameters and physical parameters influencing more than one sequence of events. Such parameters may for example influence more than one phenomenaon. The benefit of the dynamic approach within the ROAAM+ framework is the possibility to address all of the three types of parameters listed above.

As it will be practically impossible to consider all possible combinations, there is still a need to find which of these parameters, and in which combination (scenario, physical and intangible), that may have a large influence on the risk analysis.

The enhanced information from a dynamic approach can be used in the PSA in several ways. Examples of possible gains are:

- Improved sequence definitions when phenomena can be relevant (improved PDS definitions and sequences in the containment event tree), see section 5.2.1. This corresponds to improvement in the definition of scenario parameters.
- Estimation of probabilities for phenomena, see section 5.2.2. This follows from the improved definition of scenario parameters which also results in improved understanding of how the physical and intangible parameters affect phenomena.
- Improved knowledge of timing in sequences (see also bullet 1 above) which can be another base for improved realism in PSA quantification. Improvements in PSA quantification methods would for example enable correct consideration of repair and mission time during the sequence. See section 5.2.3. This corresponds to better definition of scenario parameters.

It shall be mentioned that a dynamic approach to PSA is expected to be especially relevant regarding PSA-L2 since physical phenomena and grouping of events here have higher influence on the analyzed scenarios. The improvement of dynamic behavior of especially timing in sequences may also be relevant for increased realism when a PSA is developed to reach "safe state" – as the transient time studied will be long and hence would call for better treatment of repair.

5.2.1 Improved Sequence Definitions

The binning of accident sequences from PSA level 1 into plant damage states, as well as the modelling of accident progression scenarios in PSA level 2 are based on factors such as type of initiating event, time from initiating event and pressure in the reactor. These factors, scenario parameters and physical parameters, are normally based on a finite amount of analyses, where engineering judgements are necessary.

An IDPSA approach can provide valuable information regarding these scenario parameters and influence the definition of sequences in PSA, since the IDPSA approach is informed by a significantly larger number of calculations. Several key elements in the level 2 sequences and phenomena handling and their boundaries can be analyzed at each stage of the modelling of accident progression via for example a reverse analysis in the ROAAM+ methodology.

The scenario parameters can be considered in the PSA by improveding the definition of the attributes of the sequence from PSA L1. The definition of the scenario parameters should not be limited to definition of the plant state at onset of core damage, but reflect the plant state (with regard to system availability) for the complete sequence also including systems relevant for the containment event trees. This leads to a significant increase of plant damage states, compared to normal practice.

The analysis of the phenomena will then include all relevant information about scenario parameters, and the quantification of the phenomena can then focus on a correct and consistent quantification (considering the dependency between phenomenona as well as how the physical and intangible parameters affect them in the specific scenario). This is further discussed in section 4.4.2.

Example of improved sequence definition

One example that have been studied with reverse analysis in the ROAAM+ approach is how recovery of emergency cooling system (ECCS) and ADS should inform the scenario parameters (and therefore the definition of plant damage states). These safety systems are, for some reason, assumed to fail during PSA level 1 and a possibility of system recovery to avoid more severe consequences is modelled in PSA level 2. A successful recovery early in the sequence would allow the core to be arrested in the reactor pressure vessel (RPV) and hence provide the best possibility to limit the releases.

Aarresting the core in the RPV is based on the assumption that coolability is possible given successful recovery of the ECCS and ADS. Low pressure scenarios can for example be considered successful if reflooding is activated within three hours after core melt. This modelling is supported by a few MAAP analyses.

The human reliability analysis regarding recovery actions is based on the available time for operator action. It can be noted that the dominating sequences for loss of feed water from PSA level 1 are due to loss of external power supply and failure of back-up power systems. The time for possibility of manual recovery of back-up power systems and the time for possibility of return of off-site power are therefore very important for the quantitative results.

The result of the reverse analysis using the ROAAM+ approach is graphically shown in the decision tree indicates the "safe" timespans, i.e. when recovery of ECCS and ADS leads to coolability of the debris, and the "failed" timespans, i.e. when there is a possibility, even with recovery, that the debris may not be coolable. The reverse analysis using the ROAAM+ approach indicates that the current assumptions regarding available time for recovery needs to be updated, since the successful states in the IDPSA indicates that the systems needs to be activated earlier to ensure a successful cooling.

It can be noticed that the "safe" state in the decision tree is given by a threshold. The word "Safe" means, in the ROAAM+ approach, that the conditional containment failure probability for debris coolability is lower than 1E-3, which indicates, in the arbitrary scale of probability, a "physically unreasonable" level of likelihood.

When likelihoods used in ROAAM+ are translated into PSA probabilities, the arbitrary scale of probability should be applied in reverse in order to achieve the same meaning between "physically unreasonable" level in ROAAM and screening frequency in PSA. The reason is that a threshold should preferably be set so that the conditional probability would be insignificant with regard to the target value (frequency of <1E-7) for releases. The target value for PSA Level 1 is often set to 1E-5. A conditional failure probability for level 2 less than 1E-4 would hence fulfil the condition to be insignificant (two orders of magnitude below the acceptable threshold). This means that all “safe” scenarios can be disregarded in the PSA if 1E-4 is used as a threshold value in the analysis.

The studied example provides a possibility to identify how the scenario parameter “timing of recoveriesy” affects the possibility to obtain coolability. The results can be used to improve sequence definition by:

- Giveing more accurate and refined definition of available times for different operating actions and thus provide a better basis material for the HRA.
- Identifying the sequences where the debris may not be coolable after re-flooding.
- Provideing failure probabilities for the identified sequences. Coolability may need to be modelled with a failure probability that is dependent on the timing of the sequence. Time dependent failure probabilities can be considered since the plant damage states are binned with time after initiating event as one factor. The binning of the plant damage states may therefore be updated with regards to the findings from the deterministic analysis.

The dynamic approach used in this project has provided interesting information regarding scenario parameters that can be used to improve the sequence definitions and to reduce the epistemic uncertainty. The inverse ROAAM+ approach has also provided very interesting results for the treatment of phenomena in the sequence following melt through. An example of how this information can be used to improve sequence definition is shown in the feasibility study in section 5.3.

5.2.2 Estimation of Probabilities of Phenomena and Consequences

In addition to a better understanding of the sequences and their causes, it has to be recognized that we will neither have full understanding nor the possibility to represent all possible realistic situations in a risk analysis. Hence it will also be of vital importance that, in addition to a better representation of the sequences, we improve our ability to estimate the probability that a certain phenomenon with risk significant consequences can occur.

The analysis of physical phenomena requires extensive understanding of complex interactions and feedbacks between scenarios of accident progression and phenomenological processes. Physical phenomena are of high importance for the PSA level 2 results since they influence the severity of the consequences.

The analysis includes identification of relevant phenomena, identification of relevant sequences where phenomena can occur as well as estimating the probability on of iries. The available data for phenomena is often based on scarce data, which typically leads to conservative assumptions. Better support and basis material for the analysis of probabilities for phenomena, given scenario conditions, would therefore substantially increase the level of accuracy and credibility.

The phenomena are often seen as independent in the PSA. The physical and intangible parameters influencing the phenomena are therefore not taken fully into account. A dynamic approach to PSA can therefore provide valuable insights influencing the modeling of phenomena.

The analysis with ROAAM+ provides insights regarding the conditions for which each phenomenon is relevant. The backward analysis regarding steam explosion, for instance, provides information regarding at what conditions a steam explosion can give consequences of risk significance. The analysis provides a possibility to handle scenario, physical and intangible parameters and identify the parameters of high importance. The scenario parameters can thereby be improved and the epistemic uncertainty can be reduced. There are however still epistemic uncertainty remaining through the physical parameters (which cannot be addressed by improved scenario definition) and the intangible parameters. The dynamic analysis should properly consider how the intangible and physical parameters affect the different phenomena. Since the phenomena share parameters, the phenomena are dependent and thereby it is not correct to estimate them separately.

An example of how a dynamic approach, considering both improvements in scenario parameters and also considering the most important dependencies in physical and intangible parameters, can influence the modelling of phenomena and the estimation of probabilities are shown in the feasibility study of section 5.3.

5.2.3 Improved Knowledge of Timing in Sequences

From the PSA, cut set lists are produced (or rather minimal cut set (MCS) lists). Improvements in timing in sequences could be implemented in different ways. Here we discuss two ways:

- Improved definition of scenario parameters including timing of systems.
- Improvements in mathematical models for inclusion of dynamic features into the cut set list calculation.

These two ways are discussed below.

Improved definition of scenario parameters including timing of systems

Let us assume that we have an MCS list. This list will include basic events representing phenomena (as well as component failures and human actions – but these are not of interest in this context). These phenomena are treated as individual events – and there is no information on timing. Now, let us assume that we have a decision tree describing the success and failure cases (the scenario parameters).

The combination of the MCS list and the information in the decision tree could be merged. Conceptually, this could be done in an automated way, but currently the information is needed to inform the sequence definition – and allow for a refined set up of the sequence.

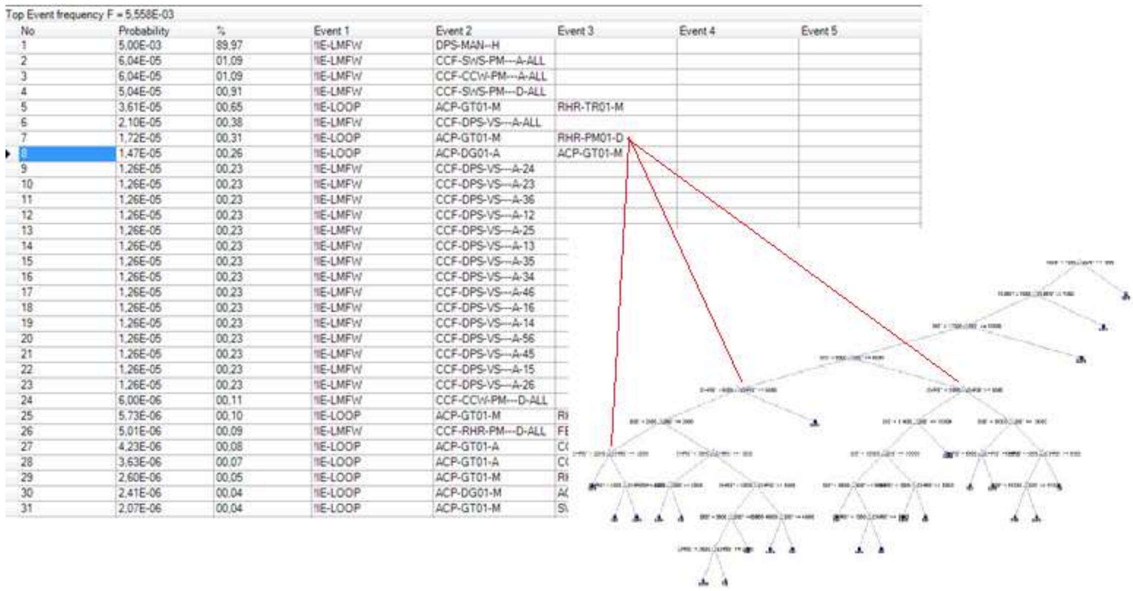

Figure 5-2: The conceptual idea of having the decision tree as input for the quantification of an MCS list. The figure is intended to illustrate that one event may have different failure probability in different cases.

In [152] an example is given, presenting a decision tree where the ROAAM+ approach is used to develop the timing information that should be considered when the failure domains for debris coolability (with regard to restart of ECCS and activation of ADS) in a high pressure core damage sequence is studied.

Improvements in mathematical models for inclusion of dynamic features into the cut set list calculation

Large PSA studies analyze failure combinations or failure scenarios leading to failures in a static way. Timed dependencies between systems are either disregarded or approximated by discretization of time and convolution. The static character of PSA models offers no natural way of modelling repairs either.

Certain scenarios in Level 2 (and Level 3) analyses for nuclear power plants require longer time horizon, e.g., reaching a cooled and stable situation in a scenario with the core melt arrested in the reactor pressure vessel, The Fukushima accident gives analyses of longer scenarios additional importance.

As an example, the probability of each individual pump system failing in operation grows with growing mission time for each pump. However, one does not need each pump to operate over the entire time horizon.

For very small systems, it is possible to build Markov Chains to better represent timing. However, for the problem size of PSA models of nuclear stations – it will not be feasible to build a model as a Markov Chain.

A recently developed formalism, Static and Dynamic FT, is presented in [348]. The method improves the calculation of large PSA models, using the cut set list and using Continuous Time Markov Chains (CTMCs) to include time into the calculation. The dependency between basic events is defined by triggers, see figure below.

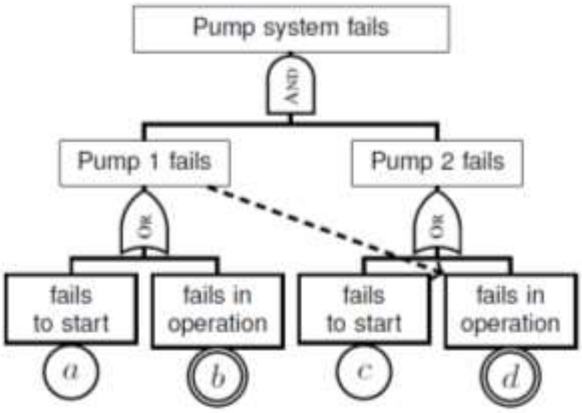

Figure 5-3: Pump 2 mission time event is dependent on a trigger – failure of pump 1. This allows for more realistic consideration of time in operation for pump 2.

The approach described in [348] develops a set of Markov Chains, using the MCS list and the information about triggers from the PSA model.

This way of including time into a dynamic calculation is not addressing exactly the same type of dynamic behavior as discussed in previous section – even though the approach definitely can be used to improve the accuracy in the frequency of the scenarios. The improvement in this algorithm is focusing on improved accuracy in the reliability calculation itself (and not the appropriate setup of the scenario parameter).

5.3 Example of a Dynamic Approach in a Large Scale PSA Model

The dynamic approach to PSA can, as described in section 5.2, be used to enhance the PSA in several aspects. A feasibility study is presented here as an example of how a dynamic approach can be used in a large scale PSA. The feasibility study is aiming at studying, at a higher level of detail, the attributes that are of interest for the core relocation, melt through of the reactor pressure vessel (RPV) and the following effects on phenomena.

A generic PSA for Nordic BWR is used as reference case. In the reference model, each phenomenon, for example steam explosion or debris bed coolability, is modelled with fixed probabilities independent of the accident progression sequence in which they are used. The reference case provides information to the deterministic analysis about which phenomena and parameters that are currently analyzed and is used in the binning of sequences and consequences.

Two important phenomena occurring at or after reactor vessel melt-through are steam explosion and debris bed coolability. To be able to study how these phenomena depend on different parameters, a dynamic approach is used. The parameters that may influence the phenomena are physical parameters such as pressure, temperature and water depth in different parts of the plant, scenario specific parameters such as size of the melt-through as well as intangible parameters.

5.3.1 Dynamic Approach

The ROAAM+ framework has been used to study the containment phenomena steam explosion and debris bed coolability. The deterministic study has analyzed a large number of parameters and the analysis shows that the probabilities for the studied phenomena are highly dependent of the following parameters:

- The mass flow of core melt at reactor vessel melt through.
- The depth of the water pool under the reactor vessel.
- The temperature of the water pool.

In this feasibility study, a reference large scale PSA model is modified to consider the depth of the water pool and the mass flow of corium at vessel melt through.

The information from the deterministic analysis is used to improve the sequence definition and the estimation of probabilities of phenomena, thereby creating an enhanced PSA model with updated containment event trees (CET) and scenario specific phenomena probabilities. The study aims at indicating the effect of taking the enhanced information about phenomena into account when calculating the large release frequency for transients and CCI for a selection of PDS.

The analysis is performed for a few selected plant damage states (PDS) named HS2-TH1 and HS2-TL4, see Chapter 5.3.2 for description. The motivation for this selection is that these PDS together contribute with around 70 % of the large releases in PSA level 2.

5.3.2 Description of Reference Case PSA model

The reference PSA model is a generic full scale PSA for a Nordic BWR.

In the reference PSA model the accident progression for PSA level 2 is modeled in a containment event tree, CET. In the CET there is no explicit modeling of phenomena. Instead, there is a function event where all the phenomena are treated in a common fault tree.
The probabilities for steam explosion resulting in containment failure are:

- 1E-3 for low pressure melt through.
- 3E-3 for high pressure melt through.

These values are always applied even if the lower drywell (LDW) flooding system fails. The rationale for this modeling is that no positive credit should be taken for system failures. Furthermore, there may be enough water for a steam explosion to occur but not enough to avoid melt through of the penetrations in the LDW floor. The probabilities for melt through of the penetrations in the LDW floor are:

- 1E-3 for successful LDW flooding.
- 1.0 for failure of the LDW flooding system.

The studied PDS in this feasibility study are:

- HS2-TH1. This is a plant damage state where the initiating event is a transient or a CCI, core cooling has failed and the reactor vessel pressure is still high (the automatic depressurization system, ADS, has failed).
- HS2-TL4. This is a plant damage state where the initiating event is a transient or a CCI, core cooling has failed and the reactor vessel pressure is low.

5.3.3 Description of Enhanced PSA Model

5.3.3.1 Containment Event Tree

The containment event trees for the plant damage states HS2-TH1 and HS2-TL4 are here modified to consider the depth of the water pool in lower drywell (LDW) and the mass flow of corium at vessel melt through.

The water depth alternatives are:

- Deep water pool in LDW.
- Shallow water pool in LDW.
- No water in LDW.

The melt flow alternatives are:

- Dripping.
- Medium.
- Large.

For each combination of water depth and melt flow there are unique probabilities for steam explosion and not coolable debris bed in LDW. This is explicitly modeled in the CET.

The water temperature in lower drywell is scenario specific and set to constant for the modelled plant damage states. This has therefore no influence on the improvement of sequence definitions in the CET.

Figure 5-4 shows the part of the CET influenced by the updated modelling. In the complete CET there are also function events and sequences for isolation, long term residual heat removal etc. As seen in Figure 5-4 there is one common function event for steam explosion and one common function event for coolability. For each sequence, however there is a unique basic event used for each phenomenon depending on the sequence (i.e. the combination of depth and melt flow).

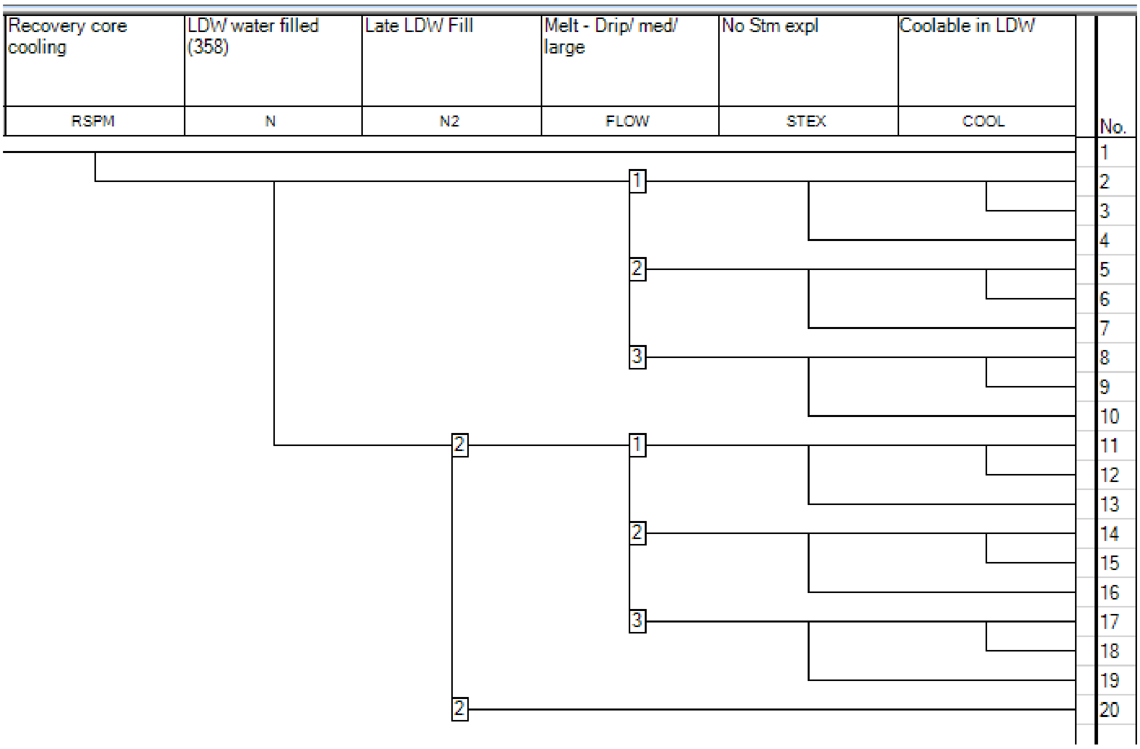

Figure 5-4: Containment Event Tree with explicit modeling of steam explosion and coolability.

5.3.3.2 Deterministic input

The deterministic analysis described in section 0 yields probability distributions for steam explosion and coolability given a certain combination of temperature, water depth and melt flow.

The melt flow is expressed as the corresponding diameter of the melt jet. The parameters vary from:

- LDW water temperature 290 - 366 K, 20 different values
- LDW water depth 2,21 - 8,8 m, 20 different values
- Melt jet diameter 0,07575 - 0,2945 m, 20 different values

For each phenomenon there are 4 different sets of data as described above.
For steam explosion there are data for containment fragility of:

- 6 kPa*s
- 20 kPa*s
- 50 kPa*s
- 80 kPa*s

For debris bed coolability there are data for different fractions of agglomeration:

- 20% agglomeration.
- 50% agglomeration.
- 70% agglomeration.
- 90% agglomeration.

5.3.3.3 *Assumptions and limitations*

Temperature in LDW

The temperature is assumed to be 322 K for all cases. This is according to MAAP calculations of HS2-TH1 and HS2-TL4 sequences. The LDW water temperature has been observed to have only a minor effect on the phenomena studied here.

Fragility

- For steam explosion, the non-reinforced door (6 kPa*s) probabilities are used. This gives the highest probabilities for the steam explosion damage of the containment structures.
- For coolability, the debris is -assumed to be non-coolable if the agglomeration fraction reaches 90 %. This gives the lowest probabilities for non-coolable debris bed.

Deep pool – 7.8 m

After successful automatic opening of the LDW flooding system it is assumed that the LDW water level will be 7.8 m at reactor vessel melt through. This is according to MAAP calculations of HS2-TH1 and HS2-TL4 sequences.

The probability for opening of LDW flooding is modelled in Risk Spectrum.

Shallow pool – 3.9 m

If automatic opening of LDW flooding fails, it is assumed that the operators can manually take actions to fill the LDW. Possible actions are:

- Manual opening of LDW flooding.
- Manual start of the drywell spray system.
- Manual start of the independent spray system.

Successful manual start of LDW flooding is assumed to lead to shallow pool in LDW at reactor vessel melt through. The level for shallow pool is assumed to be 3.9 m. The probability for failure of manual flooding is assumed to be 0.1.

Failure of LDW flooding

If LDW flooding fails completely, the following probabilities are assumed:

- Steam explosion 0.0.
- Debris bed not coolable 1.0.

Melt flow at reactor vessel melt through

The melt flow at reactor vessel melt through is divided in dripping, medium and large. These melt flow sizes are defined by the following diameters of the melt jet:

- $d_{jet} < 0.075$ m Dripping flow.
- $0,075 < d_{jet} < 0.150$ m Medium Flow.
- $d_{jet} > 0.150$ m Large Flow.

In the deterministic input data, there are individual probability distributions for steam explosion and coolability for 20 different melt flows ranging from 0.07575 m to 0.2945 m. In this case it is assumed that d_{jet} = 0.7575 gives dripping flow. (Otherwise, there are no data for dripping flow.)

- Dripping flow Based on d_{jet} = 0.7575.
- Medium flow Based on 6 different d_{jet} between 0.08725 and 0.14475.
- Large flow Based on 13 different d_{jet} between 0.15625 and 0.29425.

At present there are no probability distributions for the different melt flow sizes. Furthermore, the correlation between steam explosion and non-coolable debris bed has not been taken into account using the current data compilation from ROAAM+. This is due to the fact that the output from ROAAM+ and the current test case model built in RiskSpectrum has not fully taken all the data (the correlation) in consideration when the unacceptable release frequency is estimated. When performing an uncertainty analysis, samples will be taken from the individual probability distributions for steam explosion and coolability, disregarding any correlation between the two. In order to correctly account for this effect, it is therefore necessary that the data compilation from ROAAM+ is extended to include these correlation data. The possible treatment of such data in RiskSpectrum is described further in section 5.3.3.5.

In the analyses presented earlier, the probabilities for dripping, medium and large melt flows were set to 1/3 each with uniform distributions and the uncertainty analysis was performed without taking the correlations described above into account. In the current analysis, the uncertainty analysis is instead replaced by a study covering the following three cases:

- Bounding pessimistic, with probabilities for dripping/medium/large flow set to 0/0/100 %.
- Bounding optimistic, with probabilities for dripping /medium/large flow set to 100/0/0 %.
- A sensitivity study, with probabilities for dripping /medium/large flow set to 0/100/0 %.

5.3.3.4 -Probabilities of phenomena

The individual probabilities for steam explosion and non-coolability are calculated as the average value of different melt flows in each size respectively, given the depth and the temperature described above. This results in the following probabilities for steam explosion and non coolable debris bed in LDW:

	Steam explosion	Non-coolable
• Deep pool, dripping flow	0	3.61E-02
• Deep pool, medium flow	1.55E-02	2.83E-01
• Deep pool, large flow	6.36E-01	8.52E-01
• Shallow pool, dripping flow	0	1.0
• Shallow pool, medium flow	3.60E-04	1.0
• Shallow pool, large flow	3.78E-01	1.0

5.3.3.5 Uncertainties of phenomena

In the deterministic analysis of the physical phenomena described in section 0, a set of simulations are performed depending on a number of parameters. The output of the analysis is probabilities for physical phenomena with associated uncertainty distributions. These uncertainty distributions for the different phenomena are therefore not independent since the underlying calculations are based on variations of the same deterministic and intangible parameters. To be able to use this information correctly, a non-standard interface, allowing use of externally developed simulation data, should be used in RiskSpectrum to enable the uncertainty distribution for the phenomena to be consistently treated. Furthermore, the simulations should not use a Monte-Carlo approach on the probabilistic distributions for each phenomenon independently, but simulate on the deterministic and intangible parameters.

5.3.4 --Analysis and Comparison between Reference Case Model and Enhanced Model

All transients and CCIs leading to the plant damage states HS2-TH1 and HS2-TL4 are analyzed for all analyzed level 2 release categories. Release categories leading to release frequencies over 0.1% of the core inventory of an 1800 MW BWR are grouped as non-acceptable. Furthermore, Iin the analyses presented in earlier phases of the SPARC project, the release category “basemat meltthrough” was, according to industry standard, presented individually, i.e. excluded from the group of non-acceptable releases. It can however be argued that basemat meltthrough cases could represent large releases e.g. after the standard analysis period of 72 h. To account for this possibility, the former non-acceptable release group is, in the current analysis, merged with the basemat meltthrough group to form a group named “non-contained release”.

The normalized results for non-contained release per type of initiating event are shown in Figures 7-5 to 7-7 and Tables 7-1 to 7-3. The normalization is done with respect to the frequency for non-contained release due to Loss of offsite power.

The analysis shows that the non-contained release frequency increases significantly in the enhanced model, partly due to the inclusion of basemat meltthrough in the grouping, partly due to the ROAAM+ methodology itself.

It can be noted that the initiating event group spurious M isolation is much more affected by the enhanced modelling than the other initating event types studied. To explain the reason for this, it can first be noted that the group of non-acceptable releases, for a BWR, to a relatively large extent contains so-called bypass sequences, in which closure (isolation) of the containment fails and the release path occurs through e.g. through open steamlines. Such sequences will not be affected by the ROAAM+ approach since they are not created by the studied containment rupture phenomena. M isolation, or IM isolation, refers to a specific function of the reactor protection system, which initiates closing of isolation valves in the feedwater lines. The effect of the initiating event is thereby at first sight similar to that of the loss of feedwater transient. However, in the generic Nordic BWR plant design represented by the PSA model used in this study, M isolation automatically activates another isolation function that initiates closure of the steam lines. This implies that for sequences starting with spurious M isolation, bypass sequences through open steam lines are directly excluded (apart from cases with mechanical errors in the MSIVs) and this category of initiating events becomes the only category where the ROAAM+ methodology will influence all the resulting accident sequences. In contrast, e.g. the loss of feedwater initiating event category has a relatively low frequency, which implies that together with the event probabilities prescribed by the ROAAM+ methodology, sequences affected by ROAAM+ to a large extent end up below the cut-off frequency of the PSA analysis, leaving almost only bypass sequences above it. In summary, loss of feedwater sequences will in this model be minimally affected by ROAAM+ while the inverse is true for spurious M-isolation sequences, thereby creating a large difference between these seemingly similar initiating event families. When the results are adjusted for bypass cases, the impact of the ROAAM+ approach increases and the differences between e.g. loss of feedwater and spurious M isolation are reduced, even reversed as seen in Figures 7-8 and 7-9 and Tables 7-4 and 7-5.

It is clear from these results that the sensitivity of the non-contained release frequency to the size of the vessel melt jet, and thereby to correlation between steam explosion and debris coolability, is very large. The sensitivity analysis however shows identical results for 100 % medium flow and 100 % dripping flow.

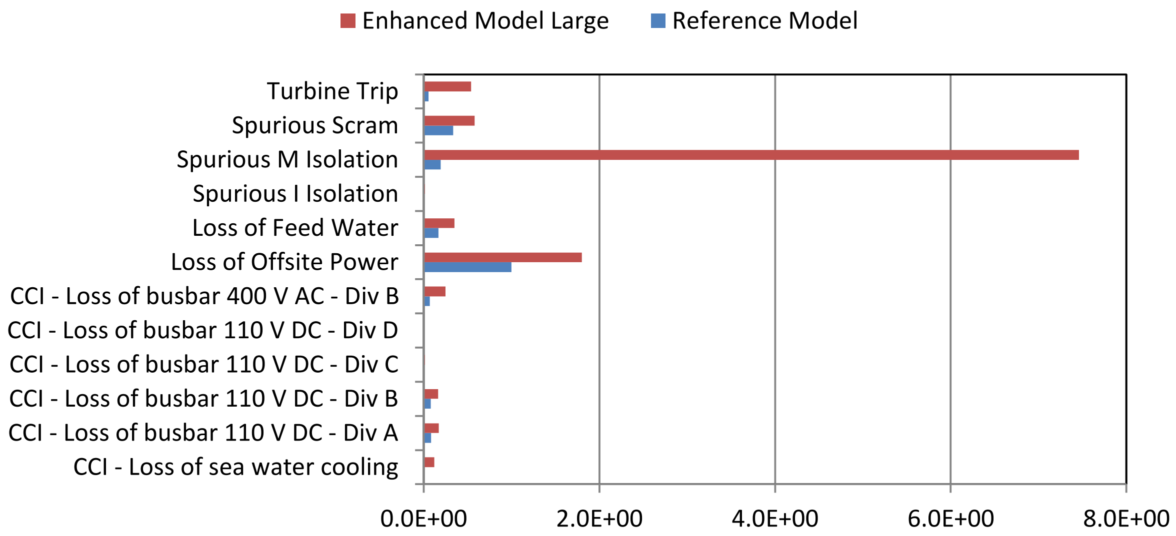

Figure 5-5: Comparison of normalized frequencies for non-contained release between the reference case and the enhanced model -using large flow at melt-through.

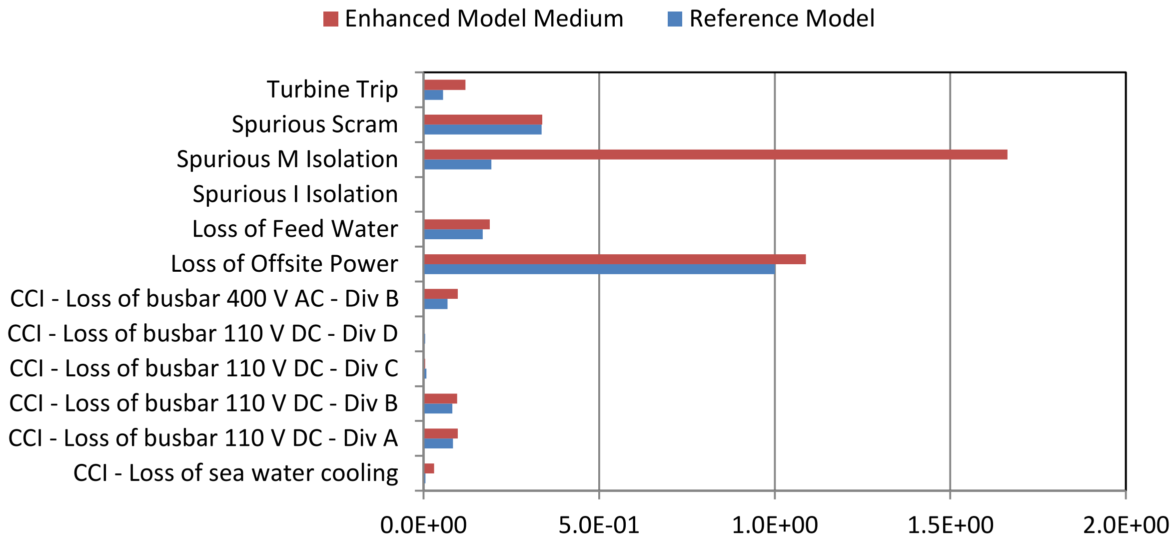

Figure 5-6: Comparison of normalized non-contained release frequencies between the reference case and the enhanced model using medium flow at melt-through.

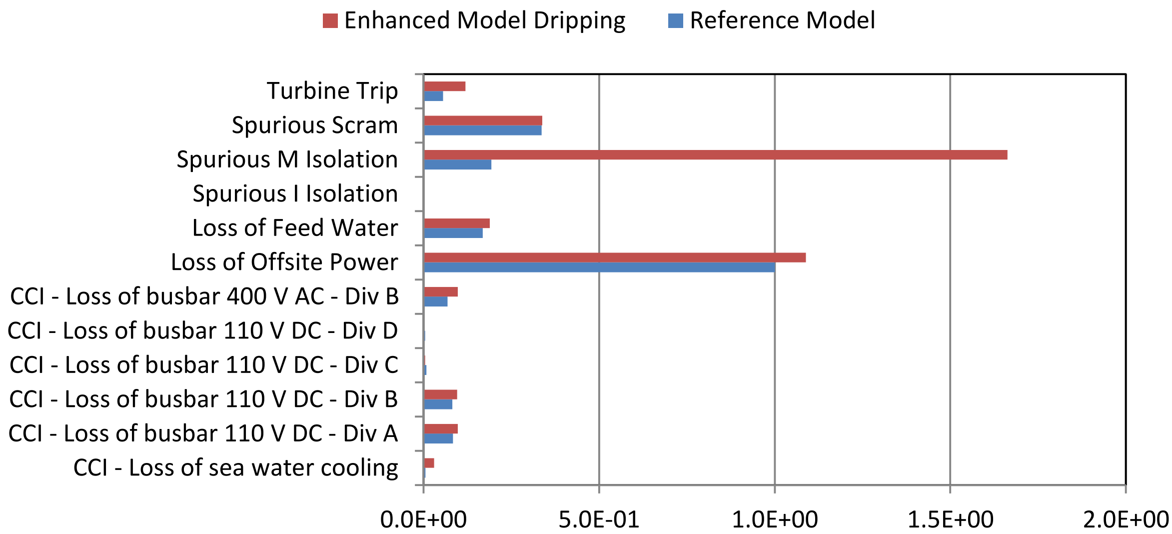

Figure 5-7: Comparison of normalized non-contained release frequencies between the reference case and the enhanced model using dripping flow at melt-through.

Table 5-1: Comparison of normalized frequencies for non-contained release between the reference case and the enhanced model -using large flow at melt-through.

Initiating event	**Reference Case**	**Enhanced Model**	**Difference**
CCI - Loss of sea water cooling	5.9E-03-	1.2E-01-	1947%
CCI - Loss of busbar 110 V DC - Div A	8.4E-02-	1.7E-01-	104%
CCI - Loss of busbar 110 V DC - Div B	8.2E-02-	1.6E-01-	99%
CCI - Loss of busbar 110 V DC - Div C	8.6E-03-	1.5E-02-	79%
CCI - Loss of busbar 110 V DC - Div D	5.0E-03-	6.3E-03-	25%-
CCI - Loss of busbar 400 V AC - Div B	6.9E-02-	2.5E-01-	261%
Loss of Offsite Power	1.0E+00	1.8E+00	80%
Loss of Feed Water	1.7E-01-	3.5E-01-	107%
Spurious I Isolation	9.1E-04-	1.6E-02-	1615%
Spurious M Isolation	1.9E-01-	7.5E+00	3768%
Spurious Scram	3.4E-01-	5.8E-01-	73%
Turbine Trip	5.5E-02-	5.4E-01-	878%
Total result	**2.0E+00**	**1.1E+01**	**471%**

Table 5-2: Comparison of normalized frequencies for non-contained release between the reference case and the enhanced model using medium flow at melt-through.

Initiating event	**Reference Case**	**Enhanced Model**	**Difference**
CCI - Loss of sea water cooling	5.9E-03	3.0E-02	410%
CCI - Loss of busbar 110 V DC - Div A	8.4E-02	9.7E-02	16%
CCI - Loss of busbar 110 V DC - Div B	8.2E-02	9.6E-02	17%
CCI - Loss of busbar 110 V DC - Div C	8.6E-03	4.4E-03	-49%
CCI - Loss of busbar 110 V DC - Div D	5.0E-03	1.1E-03	-78%
CCI - Loss of busbar 400 V AC - Div B	6.9E-02	9.7E-02	42%
Loss of Offsite Power	1.0E+00	1.1E+00	9%
Loss of Feed Water	1.7E-01	1.9E-01	11%
Spurious I Isolation	9.1E-04	1.6E-03	78%
Spurious M Isolation	1.9E-01	1.7E+00	762%
Spurious Scram	3.4E-01	3.4E-01	1%
Turbine Trip	5.5E-02	1.2E-01	116%
Total result	**2.0E+00**	**3.7E+00**	**86%**

Table 5-3: Comparison of normalized frequencies for non-contained release between the reference case and the enhanced model using dripping flow at melt-through.

Initiating event	**Reference Case**	**Enhanced Model**	**Difference**
CCI - Loss of sea water cooling	5.9E-03	3.0E-02	410%
CCI - Loss of busbar 110 V DC - Div A	8.4E-02	9.7E-02	16%
CCI - Loss of busbar 110 V DC - Div B	8.2E-02	9.6E-02	17%
CCI - Loss of busbar 110 V DC - Div C	8.6E-03	4.4E-03	-49%
CCI - Loss of busbar 110 V DC - Div D	5.0E-03	1.1E-03	-78%
CCI - Loss of busbar 400 V AC - Div B	6.9E-02	9.7E-02	42%
Loss of Offsite Power	1.0E+00	1.1E+00	9%
Loss of Feed Water	1.7E-01	1.9E-01	11%
Spurious I Isolation	9.1E-04	1.6E-03	78%
Spurious M Isolation	1.9E-01	1.7E+00	762%
Spurious Scram	3.4E-01	3.4E-01	1%
Turbine Trip	5.5E-02	1.2E-01	116%
Total result	**2.0E+00**	**3.7E+00**	**86%**

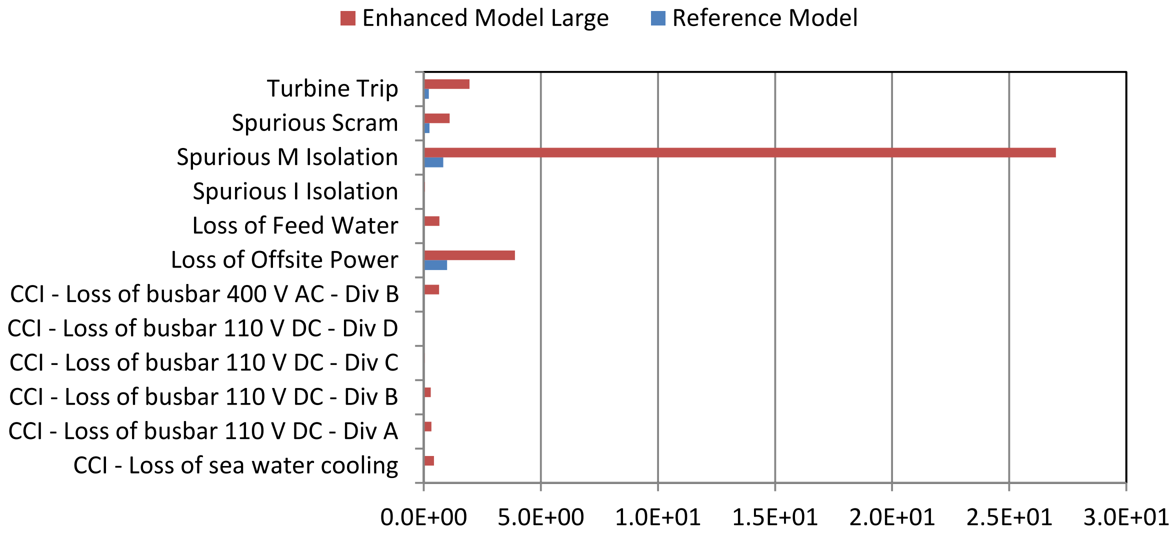

Figure 5-8: Comparison of normalized non-contained release frequencies excluding bypass between the reference case and the enhanced model using large flow at melt-through.

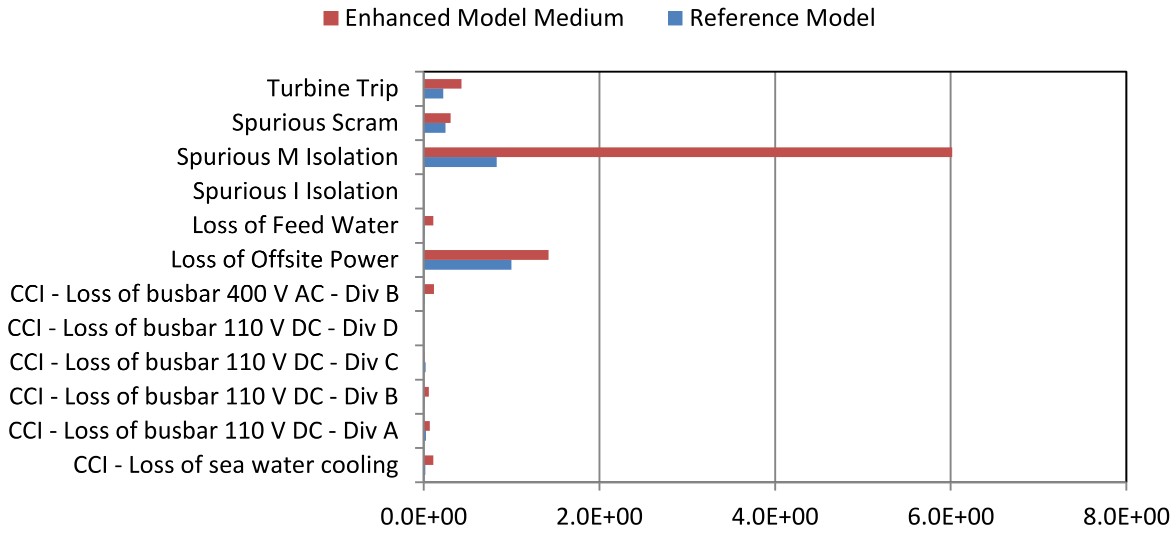

Figure 5-9: Comparison of normalized non-contained release frequencies excluding bypass between the reference case and the enhanced model using medium flow at melt-through.

Table 5-4: Comparison of normalized frequencies for non-contained release excluding bypass between the reference case and the enhanced model using large flow at melt-through.

Initiating event	**Reference Case**	**Enhanced Model**	**Difference**
CCI - Loss of sea water cooling	2.0E-02	4.4E-01	2055%
CCI - Loss of busbar 110 V DC - Div A	2.7E-02	3.3E-01	1158%
CCI - Loss of busbar 110 V DC - Div B	1.0E-02	3.0E-01	2926%
CCI - Loss of busbar 110 V DC - Div C	2.2E-02	3.8E-02	70%
CCI - Loss of busbar 110 V DC - Div D	1.8E-03	6.3E-03	245%
CCI - Loss of busbar 400 V AC - Div B	1.0E-02	6.6E-01	6346%
Loss of Offsite Power	1.0E+00	3.9E+00	290%
Loss of Feed Water	1.2E-02	6.7E-01	5243%
Spurious I Isolation	3.7E-03	5.6E-02	1445%
Spurious M Isolation	8.3E-01	2.7E+01	3141%
Spurious Scram	2.5E-01	1.1E+00	350%
Turbine Trip	2.2E-01	2.0E+00	774%
Total result	**2.4E+00**	**3.6E+01**	**1412%**

Table 5-5: Comparison of normalized frequencies for non-contained release excluding bypass between the reference case and the enhanced model using medium flow at melt-through.

Initiating event	**Reference Case**	**Enhanced Model**	**Difference**
CCI - Loss of sea water cooling	2.0E-02	1.1E-01	439%
CCI - Loss of busbar 110 V DC - Div A	2.7E-02	7.0E-02	164%
CCI - Loss of busbar 110 V DC - Div B	1.0E-02	6.0E-02	497%
CCI - Loss of busbar 110 V DC - Div C	2.2E-02	1.1E-02	-50%
CCI - Loss of busbar 110 V DC - Div D	1.8E-03	2.4E-04	-113%
CCI - Loss of busbar 400 V AC - Div B	1.0E-02	1.2E-01	1056%
Loss of Offsite Power	1.0E+00	1.4E+00	42%
Loss of Feed Water	1.2E-02	1.1E-01	766%
Spurious I Isolation	3.7E-03	5.7E-03	55%
Spurious M Isolation	8.3E-01	6.0E+00	622%
Spurious Scram	2.5E-01	3.1E-01	24%
Turbine Trip	2.2E-01	4.3E-01	93%
Total result	**2.4E+00**	**8.7E+00**	**259%**

5.3.5 Uncertainty analysis

Due to the reasons explained in section 5.3.3.3, no new uncertainty analysis of PSA level 2 results has been performed in the current phase of the SPARC project. The uncertainty analysis performed in the previous project phase (i.e. not taking correlation between phenomena into account) is repeated below for easy reference.

The -results of the uncertainty analysis for non-acceptable release (excluding basemat meltthrough) are shown in Table 5-6. The results show that the uncertainty ranges from roughly half the point estimate frequency up to about 1.5 of the point estimate frequency. This is a reasonably narrow interval, which is positive – as the uncertainty is an important factor in PSA-L2. It could be relevant to further study the cases where the uncertainty range is greater – to understand if the uncertainty can be reduced.

Table 5-6: Uncertainty analysis for non-acceptable release (All the median values are normalized.)

Initiating event	**5%**	**median**	**95%**
CCI - Loss of sea water cooling	56%	100%	158%
CCI - Loss of busbar 110 V DC - Div A	91%	100%	112%
CCI - Loss of busbar 110 V DC - Div B	91%	100%	112%
CCI - Loss of busbar 110 V DC - Div C	95%	100%	107%
CCI - Loss of busbar 110 V DC - Div D	100%	100%	100%
CCI - Loss of busbar 400 V AC - Div B	84%	100%	123%
Loss of Offsite Power	93%	100%	109%
Loss of Feed Water	91%	100%	112%
Spurious I Isolation	58%	100%	163%
Spurious M Isolation	54%	100%	161%
Spurious Scram	95%	100%	107%
Turbine Trip	66%	100%	147%

5.3.6 Influence of Limitations in Enhanced PSA model

There are a number of assumptions and limitations in the implementation in the enhance PSA model that influence the result. Some comments regarding the importance of different parameters and modeling aspects are:

- Melt jet diameter - dripping, medium, large: This parameter is crucial for the results since steam explosion at dripping melt flow has a probability of zero. A more realistic modeling needs to take physical properties into account when determining the probabilities of the melt jet diameter.
- Failure criteria: The data from ROAAM+ for steam explosion and debris bed non-coolability are obtained according to different failure criteria. For both parameters the criteria yielding the highest phenomena probabilities were chosen. For steam explosion this is realistic since the doors are not yet reinforced. For debris bed non-coolability it

is optimistic since we assume that debris is non-coolable when agglomeration fraction reaches 0.9.

- Water depth for deep/shallow pool: The water depth at "deep pool" is related to system functionality and can be calculated with MAAP or even with simple hand calculations. If the LDW flooding system works, there will always be about 8 m of water in LDW. The water depth for shallow pool is much more uncertain since this completely depends on the sequence. A more realistic modeling could take different water depth for shallow pool in different sequences.
- Water temp in LDW at vessel melt through: This parameter is not very uncertain. The temperature is assumed to be 322 K for all cases (This is according to MAAP calculations of HS2-TH1 and HS2-TL4 sequences.) It is also seen in the data from ROAAM+ that the LDW water temperature has a small effect on the phenomena studied here.

There is a need to make the feasibility study more realistic regarding some of the related parameters discussed above. The quantitative results should therefore be seen as indicative.

5.4 Discussion - Dynamic Approach to PSA

A dynamic approach to PSA can, as discussed in section 5.2 and shown in section 5.3, influence the analysis is several ways. The feasibility study has shown an example of a dynamic approach where the PSA is used as a basis to select important initiating events and sequences in the severe accident progression. These scenarios are then analyzed with a dynamic deterministic model yielding information about which parameters that are of high importance for the development of the accident progression. The results from the deterministic analysis are used in the PSA to improve sequence definition as well as improve the estimation of phenomena depending on the sequence and the varied parameters.

The dynamic approach used in the project requires extensive work regarding building the deterministic model. Once built, this model can however be modified to evaluate different initiating events and sequences. The changes in the enhanced PSA-model on the other hand are limited and easy to implement.

The integrated approach requires improvement in especially scenario definition, which practically leads to more plant damage states. The PDS should consider all necessary scenario parameters, that may affect the calculation of phenomena and hence consider also the system availability normally represented within CETs.

The implementation of the dynamic approach in the feasibility study in a large scale PSA model shows that the integration of the ROAAM+ results and the PSA model is not only feasible, but could potentially lead to a considerable change of the frequency for non-acceptable release. The results show that the parameters indicated by the dynamic approach as being of high importance to the results are indeed of high importance to the quantitative results. It also emphasizes the need to distinguish between different probabilities of phenomena depending on different scenario, physical and intangible parameters.

The integrated approach will also have the ability to give a more comprehensive estimation of the uncertainty compared to the standard approach. The uncertainty related to phenomena will consider the interdependency between phenomena (all the way back to relevant intangible and physical parameters, and of course scenario parameters).

Chapter 6. Conclusions and Suggestions

This report presents research progress towards development of risk oriented accident analysis frameworks for quantifying conditional threats to containment integrity for a reference plant design of Nordic type BWRs. Further extension of the Risk Oriented Accident Analysis Methodology (ROAAM+) has been proposed and implemented in order to address the challenges presented by the Nordic BWR severe accident management strategy for risk analysis. Namely, the importance of uncertainty in both scenarios and phenomena and the complex multistage accident progression.

The key element of ROAAM+ is a two-level coarse-fine adaptive iterative refinement process of the development of risk assessment framework and necessary knowledge. The top level of the risk assessment framework is based on computationally efficient surrogate models (SMs) that can be used for extensive sensitivity and uncertainty analysis in order to guide identification of the main sources of uncertainty, failure domains in the space of uncertain scenarios and modeling parameters, and ultimate risk assessment. The bottom layer of the framework consists of detailed computationally expensive full models (FMs) and databases of their solutions as well as experimental data and evidences, which are used in the development of the SMs.

In this project detailed mechanistic full models (FM) have been further developed for deterministic analysis of steam explosion and coolability phenomena. When necessary and feasible, new experimental data was produced in order to create new models or reduce uncertainty in existing models. Databases of the full model solutions were obtained. A set of computationally efficient surrogate models (SM) has been developed using the databases of FM solutions. The SMs were used in extensive sensitivity and uncertainty analysis implemented in the ROAAM+ framework. The reverse analysis in the ROAAM+ helped to identify failure domains in the space of the accident scenario parameters. Uncertainty in the containment failure probability has been quantified according to the state-of-the-art knowledge using the forward analysis. An approach has been developed and demonstrated for using obtained in ROPAAM+ data on the failure probability for different combinations of scenario parameters in a large scale PSA model. Results of the pilot study show clear benefits for PSA improvement in more realistic understanding and modeling of the risks.

Main highlights and findings from the development of ROAAM+ methodology, full and surrogate models for different stages of the accident progression and phenomena are summarized below.

<u>ROAAM+ methodology</u>: Methodological guidelines and approaches to development of the full surrogate models, supporting experiments and risk assessment frameworks have been developed, implemented and demonstrated. Advanced methods for quantification of uncertainty in the assessment of the overall failure probability and identification of failure domains in the space of scenario parameters have been proven crucial for adequate representation of uncertainty. A framework has been implemented as a set of customizable tools and interfaces using MATLAB. Approaches to consideration of the FM and SM uncertainty in

the risk assessment have been implemented. Connection of the ROAAM+ data to different decision making approaches and tools including PSA have been suggested. ROAAM+ provides a variety of techniques, including expensive sensitivity analysis, that enable identification of the major contributors to uncertainty bot for risk assessment and for guiding research programs that aim to reduce the uncertainty in assessment of effectiveness of a severe accident management strategy. Extensive analysis for quantification of risks of steam explosion and formation of non-coolable debris has been carried out. It has been shown that the major source of uncertainty is the melt release conditions. Results suggest that the failure of containment due to steam explosion or formation of non-coolable debris can be considered as physically unreasonable only if the melt is released in a dripping mode by a small size (<100 mm) jet. It has been also demonstrated that system resilience with respect to steam explosion threat can be significantly improved by reinforcing the week elements of the containment (e.g. hatch doors) by increasing their fragility levels up to ~50 kPa*s. The major negative factor for formation of non-coolable debris bed is agglomeration, which can be mitigated by decreasing melt jet size below 100 mm.

<u>Core degradation and relocation to the lower head</u>: Extensive study of the scenarios of core degradation and relocation to the reactor vessel lower head has been undertaken. The goals were to quantify the properties of debris in the lower head and characteristics of the vessel failure and melt release as an input to analysis of the ex-vessel accident progression. Different version of the MELCOR code (1,.86, 2.1, 2.2) were employed. Sensitivity analysis suggests importance of the modeling uncertainty (between different codes that use different models and in the same code using different values for the model closure parameters). An effort to quantify the uncertainty due to modeling and scenario factors has been made and a large database of MELCOR simulations (~thousands scenarios) has been generated. Two major modes of core degradation were observed depending on the timing of recovery of the core cooling system: (i) retention of debris in the damaged core region with only small (up to ~20 tons) relocation of mostly metallic debris to the lower head; (ii) relocation of large faction of the core (>150 tons). Significant effect of delay of vessel depressurization on the properties of the debris in the lower plenum was identified. Vessel failure and melt release analysis was carried out using different assumptions (e.g. about possibility of ejection of solid/liquid debris upon vessel failure). The results suggest that neither dripping nor massive release conditions cannot be positively excluded. A possibility of release of highly superheated metallic melt (up to ~1200 K) was observed in significant fraction of scenarios. Failure of penetrations was observed on average earlier than vessel wall.

<u>In Vessel Debris Coolability and Vessel Failure</u>: DECOSIM code was further developed in order to address in-vessel coolability phenomena in case when debris bed is porous. Extensive parametric studies suggested that it is not possible to exclude neither formation of a large melt pool (when water present in the vessel can temporary protect vessel wall and penetration, in scenarios with relatively large (> 2mm) debris size) neither early failure of the penetrations and melt release in the dripping mode (in case when a dry hot zone is located near the vessel wall, in scenarios with relatively small size of debris <1.5 mm).

Melt release: A set of models has been developed to study potential limiting mechanisms in the melt release, breach ablation and plugging phenomena. Importance of the multicomponent debris remelting phenomena and respective possibility of melt accumulation have been demonstrated. Domains of melt release parameter were plugging and ablation are expected have been quantified. It is demonstrated that neither plugging (leading to formation of a melt pool) nor ablation (leading to increase of the jet diameter and melt mass flow rate) cannot be positively excluded. Release of the melt in the dripping mode (without plugging or significant ablation) cannot be excluded either according to the analysis results, however the range of melt release parameters where whole core can be released in a dripping mode is relatively narrow.

Ex-vessel debris bed formation and coolability: A comprehensive research program has been carried out to address major phenomena that can affect formation of a non-coolable debris bed. Full (SDECOSIM) and surrogate model have been developed for prediction of dryout and pot-dryout debris bed behavior. Particulate debris spreading and bed self-leveling phenomena have been studied experimental and a set of analytical models have been developed and validated. It has been shown that the debris bed spreading mechanisms are quite effective in prevention of formation of a tall non-coolable debris bed. Further validation of the codes and models would be necessary on order to reduce uncertainty on predictions and extend the domain of model applicability.

Debris agglomeration is currently the major factor that can lead to formation of non-coolable debris bed. Full and surrogate models have been developed in order to quantify the phenomena of agglomeration and the impact of these phenomena on the coolability. DECOSIM model was further developed in order to adequately represent domains in the bed with variable mass fraction of agglomerated debris. The DECOSIM simulations were carried out using data on spatial distribution of agglomerates using the surrogate model for agglomeration. Results suggest that coolability can be significantly impaired when fraction of agglomerated reaches >20~50% (depending on the particle size). This corresponds top jet diameters of >100 mm. Further model development and validation would be necessary in order to reduce and quantify associated phenomenological uncertainty.

Steam explosion: A surrogate model has been developed using the database of TEXAS-V code (FM) simulations (in total 455000 cases of premixing/explosion calculations) for Nordic type BWRs. A statistical treatment for the chaotic response of the explosion impulse to small variations in the triggering time has been proposed. Most important parameters where identified using sensitivity analysis. The surrogate model was implemented using different artificial neural network (ANN) approaches. An approach for quantification of the SM uncertainty was implemented. We found that uncertainty in the containment failure is still dominated by the enthalpy rate of the jet and jet diameter even if the SM uncertainty can be relatively large for single comparisons of SM vs FM predictions. Consideration of SM uncertainty lead to increased size of the failure domain. New approaches are currently under development for improved SM for reduced error and faster performance. For more comprehensive risk assessment there are several issues that can be addressed in the future such as melt releases with multiple jets; multiple consecutive steam explosions; effect of crust formation around melt particles on the energetics of the steam explosions; generation of non-condensable gases during premixing etc.

Pilot application of the ROAAM+ generated data for improvement of a large scale PSA model provided following insights. The feasibility study has shown an example of coupling PSA with ROAAM+. The results from the deterministic analysis are used in the PSA to improve sequence definition as well as improve the estimation of frequency of unacceptable release due to phenomena depending on the sequence. The changes in the enhanced PSA-model are limited and easy to implement.

ROAAM+ results can be used to refine and improve the PSA in several ways. The integrated approach requires improvement in scenario definition, which practically leads to larger number of plant damage states (PDS). The PDS should consider all necessary scenario parameters, that may affect the calculation of phenomena and hence consider also the system availability normally represented within containment event trees (CETs). One example is the analysis of recovery of core cooling, where ROAAM+ has provided usable information regarding the timing and possibility of core coolability (re-flooding). This information can be used as a basis material for the HRA, to re-define the binning of plant damage states as well as provide probabilities for failure of coolability.

The implementation in a large scale PSA model shows that the integration of the ROAAM+ results and the PSA model is not only feasible, but could potentially lead to a considerable change of the frequency for non-acceptable release. The results show that the parameters indicated by the ROAAM+ approach as being of high importance to the quantitative results. It also emphasizes the need to distinguish between different probabilities of phenomena depending on different scenario, physical and intangible parameters.

The approach has demonstrated that the vision, to develop the sequence from core melting, and to understand what are the important factors, is possible to meet. The integrated approach will have the ability to give a more comprehensive estimation of the uncertainty compared to the standard approach. The uncertainty related to phenomena will consider the interdependency between phenomena (all the way back to relevant intangible and physical parameters, and of course scenario parameters).

Acknowledgements

The work is supported by the Swedish Nuclear Radiation Protection Authority (SSM), Swedish Power Companies, Nordic Nuclear Safety Research (NKS), and Swiss Federal Nuclear Safety Inspectorate (ENSI) under the APRI-MSWI program at the Royal Institute of Technology (KTH), Stockholm, Sweden.
The simulations were performed on resources provided by the Swedish National Infrastructure for Computing (SNIC) at PDC Centre for High Performance Computing (PDC-HPC).

REFERENCES

[1] Adams, B. M., “DAKOTA, A Multilevel Parallel Object-Oriented Framework for Design Optimization, Parameter Estimation, Uncertainty Quantification, and Sensitivity Analysis. Version 5.2 User’s manual,” Sandia National Laboratories P.O. Box 5800 Albuquerque, New Mexico 87185, SAND2010-2183, 2011.

[2] Adams, B.M., et al., Dakota, A Multilevel Parallel Object-Oriented Framework for Design Optimization, Parameter Estimation, Uncertainty Quantification, and Sensitivity Analysis: Version 6.0 Reference Manual, Sandia National Laboratories, 2014.

[3] Ahna, K.-I., et al., The plant-specific uncertainty analysis for an ex-vessel steam explosion-induced pressure load using a TEXAS–SAUNA coupled system. Nuclear Engineering and Design, 249, pp. 400-412. 2012.

[4] Alsmeyer, H., Review on Experiments on Dry Corium Concrete Interaction in: Molten Corium/Concrete Interaction and Corium Coolability – A State of the Art Report - Directoriate-General XII Science, Research and Development, EUR 16649EN, 1995.

[5] Alvarez, D., Amblard, M., 1982. Fuel Leveling. In: Proc. 5th Information Exchange Mtg. on Post-Accident Debris Cooling, Karlsruhe, Germany, July 28–30, 1982.

[6] Apostolakis G., Cunningham M., Lui C., Pangburn G., Reckley W., “A Proposed Risk Management Regulatory Framework,” U.S. Nuclear Regulatory Commission, NUREG-2150, Washington, DC, April 2012.

[7] Apostolakis, G., “The concept of probability in safety assessments of technological systems,” Science 250, 1359–1364. doi:10.1126/science.2255906, 1990.

[8] Asmolov, V. V., “RASPLAV Project Major Activities and Results,” RASPLAV Seminar, Program Review Meeting of OECD RASPLAV Project, Nov. 2000, Munich.

[9] Asmolov, V. V., Abalin, S. S., Merzliakov, A. V., Zagryazkin, V. N., Astakhova, Ye. V., Daragan, I. D., Daragan, V. D., D’yakov, Ye. K., Kotov, A. Yu., Maskaev, A. S., Rakitskaja, Ye. M., Repnikov, V. M., Vishnevsky, V. Yu., Volko, V. V., Popkov, A. G., Strizhov, V. F., “RASPLAV Final Report: Properties Studies: Methodology and Results,” Kurchatov Institute, Moscow, 2000.

[10] Basso S., Konovalenko A. and Kudinov P., “Development of scalable empirical closures for self-leveling of particulate debris bed”, In Proceedings of ICAPP-2014, Charlotte NC, USA, April 6-9, Paper 14330, 2014.

[11] Basso S., Konovalenko A. and Kudinov P., “Sensitivity and Uncertainty Analysis for Predication of Particulate Debris Bed Self-Leveling in Prototypic SA conditions”, In Proceedings of ICAPP-2014, Charlotte NC, USA, April 6-9, paper 14329, 2014.

[12] Basso S., Konovalenko A. and Kudinov P., “Scaling Approaches to Experimental studies of Debris Bed Self-Leveling,” Nuclear Engineering and Design, Submitted, 2015.

[13] Basso, S., Konovalenko, A., Kudinov, P. “Empirical Closures for Particulate Debris Bed Spreading Induced by Gas-Liquid Flow”, Nuclear Engineering and Design, 297, 19-25, (2016).

[14] Basso S., Konovalenko A., Yakush S. E. and Kudinov P., "Effectiveness of the debris bed self-leveling under severe accident conditions," Annals of Nuclear Energy, Volume 95, September 2016, Pages 75-85, 2016.
[15] Basso S., Konovalenko A., Yakush S. E. and Kudinov P., "The Effect of Self-Leveling on Debris Bed Coolability Under Severe Accident Conditions," Nuclear Engineering and Design, Volume 305, 246-259, 2016.
[16] Beale, M., Hagan, M., Demuth, H., 2014. Neural Network Toolbox Version: 8.2.1, User's Guide.
[17] Bergman, T. L., Lavine, A. S., Incropera, F. P., DeWitt D. P., Fundamentals of Heat and Mass Transfer, 6th edition, John Wiley and Sons, 2011.
[18] Berthoud, G., "Vapor explosions," Annual Review of Fluid Mechanics, 32, pp.573-611, 2000.
[19] Bittermann D., Fischer, M., "Development and Design of the EPR™ Core Catcher" in the book "Advances in Light Water Reactor Technologies," Springer New York, pp.119-142, (2011).
[20] Brayer, C., "Modelisation de l'explosion de vapeur en geometrie stratifiee, in Laboratoire de Modélisation et de Développement des Logiciels," Commissariat à I'Energie Atomique - Centre d'Etudes Nucléaires de Grenoble. p.204, (1994).
[21] Breeding, R.., Helton, J.., Gorham, E.., Harper, F. "Summary description of the methods used in the probabilistic risk assessments for NUREG-1150." Nucl. Eng. Des. 135, 1–27. (1992).
[22] Brito, P.B., Fabiao, F., Staubyn A., "Euler, Lambert, and the Lambert W-function today", Applied Probability Trust (9 January 2008).
[23] Britter R. E., "The spread of a negatively buoyant plume in a calm environment", Atmospheric Environment, 13, pp. 1241-1247, (1979).
[24] Brosi, S., Duijvestijn, G., Hirschmann, H., Jäckel, B.S., Nakada, K., Patorski, J.A., Rösel, R., Seifert, H.P., Tipping, Ph., "CORVIS. Investigation of light water reactor lower head failure modes", Nuclear Engineering and Design, 168, pp.77-104 (1997).
[25] Budu, A., "Debris Bed Formation at Low Temperature (DEFOR-LT experiment): Coolant flow influence on debris packing," SARNET mobility research report, Division of Nuclear Power Safety KTH, Stockholm, 2008.
[26] Buck, M., Burger, M., Rahman, S., Pohlner, G., "Validation of the MEWA Model for Quenching of a Severely Damaged Reactor Core." In-Vessel Coolability Workshop Proceedings, 12-14 October 2009, NEA headquarters, Issy-les-Moulineaux, France, NEA/CSNI/R(2010)11, pp.337-355. (2009).
[27] Bürger M., Buck M., Schmidt W., and Widmann W., "Validation and Application of the WABE code: Investigations of Constitutive Laws and 2D effects on Debris Coolability," Nuclear Engineering and Design, Vol. 236, pp. 2164–2188 (2006).
[28] Bürger, M., Cho, S.H., Berg, E.V., Schatz, A., "Breakup of melt jets as pre-condition for premixing: Modeling and experimental verification," Nuclear Engineering and Design, Volume 155, Issues 1–2, 2 April 1995, Pages 215-251.
[29] Cacuci, D.G., Ionescu-Bujor, M., 2004. A comparative review of sensitivity and uncertainty analysis of large-scale systems. II: statistical methods. Nucl. Sci. Eng. 204–217.

[30] Cadinu, F., Tran, C.-T., and Kudinov, P., “Analysis of In-Vessel Coolability and Retention with Control Rod Guide Tube Cooling in Boiling Water Reactors”, Joint OECD/NEA – EC/SARNET2 Workshop, In-Vessel Coolability, NEA Headquarters, Issy-les-Moulineaux, France, October 12 - 14, 2009.
[31] Carniglia, S. C., and Barna, G. L., “Handbook of Industrial Refractories Technology: Principles, Types, Properties and Applications,” Carniglia and Barna, Noyes Publications, Park Ridge, NJ. 1992.
[32] Campolongo, F., J. Cariboni, and A. Saltelli, An effective screening design for sensitivity analysis of large models. Environmental Modelling & Software, 22, pp. 1509-1518, 2007.
[33] Chen, R.H., Corradini M. L., Su G. H., and Qiu S. Z., “Analysis of KROTOS Steam Explosion Experiments Using the Improved Fuel-Coolant–Interaction Code TEXAS-VI,” Nuclear Science and Engineering, 2013. 174: p. 46-59.
[34] Cheng, S., Tanaka, Y., Gondai, Y., Kai, T., Zhang B., Matsumoto, T., Yamano, H., Suzuki, T., Tobita Y. “Experimental studies and empirical models for the transient self-leveling behavior in debris bed”, Journal of Nuclear Science and Technology, 48(10), pp. 1327-36, (2011).
[35] Cheng, S., Yamano, H., Suzuki, T., Tobita, Y., Gonda, Y., Nakamura, Y., Zhang, B., Matsumoto, T., Morita, K., “An experimental investigation on self-leveling behavior of debris beds using gas-injection”, Experimental Thermal and Fluid Science, 48, 110-121, 2013.
[36] Cheng, S., Tagami, H., Yamano, H., Suzuki, T., Tobita, Y., Zhang, B., Matsumoto, T., Morita, K., “Evaluation of debris bed self-leveling behavior: A simple empirical approach and its validations”, Annals of Nuclear Energy, 63, 188-198, 2014.
[37] Christie, M., Glimm, J., Grove, J.W., Higdon, D.M., Sharp, D.H., Wood-Schultz, M.M., “Error Analysis and Simulations of Complex Phenomena.” Los Alamos Sci. 6–25, (2005).
[38] Chu, C.C. and D. Corradini, “A Dynamic Model for Droplet Fragmentation,” Transactions of American Nuclear Society, 47p. 1984.
[39] Chu, C.C., “One dimensional transient fluid model for fuel-coolant interaction,” university of Wisconsin-Madison. 1986.
[40] Chu, T. Y., Pilch, M. M., Bentz, J. H., Ludwigsen, J. S., Lu, W.Y. and Humphries, L. L., “Lower Head Failure Experiment and Analyses”, NUREG/CR-5582, SAND98-2047, (1999).
[41] Chu, C.C., Sienicki, J.J., Spencer, B.W., Frid, W., Löwenhielm, G., “Ex-vessel melt-coolant interactions in deep water pool: studies and accident management for Swedish BWRs,” Nuclear Engineering and Design, Volume 155, Issues 1–2, 2 April 1995, Pages 159-213.
[42] “CORCON-MOD2 User's Manual”, NUREG/CR-3920, SAND84-1246, Rev. 3, August 1984.
[43] Corradini, M., “Analysis and Modelling of Steam Explosion Experiments,” NUREG/CR2072, SAND 80-2131, Sandia National Laboratories, Alberquerque, NM, p.112, 1981.
[44] Corradini, M.L., et al., Users’ manual for Texas-V: One dimensional transient fluid model for fuel-coolant interaction analysis. 2002, University of Wisconsin-Madison: Madison WI 53706.

[45] Cripps, R.C., Hirschmann, H., Jackel, B.S., Patorski, J.A. and Seifert, H.P., "CORVIS Project – State of Progress CORVIS Report", PSI Technical Report TM-49-95-03 (1995).
[46] CSNI, Proceedings of the Committee on the Safety of Nuclear Instalations (CSNI) Specialists' Meeting on Core Debris-Concrete Interactions (Sep.1986), EPRI NP-5054-SR, Feb 1987., 1986.
[47] CSNI, Proceedings of the Committee on the Safety of Nuclear Instalations (CSNI) Specialists' Meeting on Core Debris-Concrete Interactions (Apr. 1992), KfK-5108, NEA/CSNI/R(92)10, 1992.
[48] Cullen, A., Frey, C. "Probabilistic Techniques in Exposure Assessment," Plenum Press: New York. Springer, (1999).
[49] Dardenne, A., van Lamsweerde, A. and Fickas, S. 'Goal-Directed Requirements Acquisition', Science of Computer Programming 20 (1993).
[50] Davydov, M.V., "Mathematical modeling of the process of interaction between high temperature melt and coolant in severe accident at NPP with water cooled reactor installation," PhD thesis: 05.14.03. 2010. 197p. (in Russian)
[51] Davydov, M.V., Melikhov, V.I., Melikhov, O.I., "Numerical Analysis of Multiphase Premixing of Steam Explosions," In: Proceedings of 3rd Int. Conf. Multiphase Flow (ICMF-98), 1998 8-12 June, Lyon, France.
[52] Dempster, A.P., "Upper and Lower Probabilities Induced by a Mulitvalued Mapping," Annals of Mathematical Statistics, 38, 325–339. (1967.)
[53] Dempster, A.P., Upper and lower probability inferences based on a sample from a finite univariate population. Biometrika 54, 515–28. doi:10.1093/biomet/54.3-4.515 (1967b.)
[54] Dinh, T.-N. "Validation Data to Support Advanced Code Development", 15th International Topical Meeting on Nuclear Reactor Thermal Hydraulics, NURETH-14, paper 676, Pisa, Italy, May 2013.
[55] Dinh, T.N., Bui V.A., Nourgaliev R.R., Green J.A., Sehgal B.R., "Experimental and analytical studies of melt jet-coolant interactions: a synthesis," Nuclear Engineering and Design, Volume 189, Issues 1–3, 11 May 1999, Pages 299-327.
[56] Dinh, T. N., Dong, W. G., Green, J. A., Nourgaliev, R. R., and Sehgal, B. R., "Melt Jet Attack of Reactor Vessel Lower Plenum: Phenomena and Prediction Method," Proc. of the Eighth International Topical Meeting on "Nuclear Reactor Thermal Hydraulics, NURETH-8", Kyoto, Japan, Sep 1997, 2, pp. 612–619.
[57] Dinh, T.N., Konovalikhin, M., Paladino, D., Green, J. A., Gubaidulin, A., and Sehgal B.R., "Experimental Simulation of Core Melt Spreading on a LWR Containment Floor in a Severe Accident," 6th International Conference on Nuclear Engineering (ICONE-6), San Diego, California, May 10-15, 1998.
[58] Dinh, T.N., Konovalikhin, M.J., Sehgal, B.R., "Core melt spreading on a reactor containment floor," Progress in Nuclear Energy, 36 (4), pp. 405-468, 2000.
[59] Dinh, T.N., Salmassi, J.Tu, T., and Theofanous, T.G., "Limits of coolability in the AP1000-related ULPU 2400, configuration V facility", NURETH-10, October 5-9, Seoul, Korea, 2003.
[60] Dinh T.N., and Theofanous T.G., "Ex-Vessel Melt Coolability", CRSS-Research Report 02/03 prepared for the U.S. Nuclear Regulatory Commission, University of California, Santa Barbara, 150p., March 12, 2002.

[61] Dombrovsky, L.A., Davydov, M.V., Kudinov, P., “Thermal radiation modeling in numerical simulation of melt-coolant interaction,” Comp. Therm. Sci. 1 (1) 2009, pp. 1-35.

[62] Dombrovsky, L.A., Davydov, M.V., and Kudinov, P., Thermal radiation modeling in numerical simulation of melt-coolant interaction, Proc. Int. Symp. Adv. Comput. Heat Transfer (CHT-08), May 11–16, 2008, paper 155.

[63] Dombrovsky, L.A. and Dinh, T.-N. “The Effect of Thermal Radiation on the Solidification Dynamics of Metal Oxide Melt Droplets”, Nuclear Engineering and Design, 236(6), pp. 1421–1429, (2008).

[64] Doppler, D., Gondret, P., Loiseleux, T., Meyer, and S., Rabaud, M., “Relaxation dynamics of water-immersed granular avalanches”, J. Fluid Mech., 577, pp. 161-181, (2007).

[65] Dubois, D. “Possibility theory: qualitative and quantitative aspects.” (1998).

[66] Dubois, D., Prade, H. “Possibility theory and its applications: a retrospective and prospective view.” The 12th IEEE International Conference on Fuzzy Systems, 5–11. doi:10.1109/FUZZ.2003.1209314 (2003).

[67] Eames, I., Gilbertson, M., “Aerated granular flow over a horizontal rigid surface”, *J. Fluid Mech*. **424**, 169-195, 2000.

[68] Eldred, M.S., Swiler, L.P., Tang, G. “Mixed aleatory-epistemic uncertainty quantification with stochastic expansions and optimization-based interval estimation.” Reliab. Eng. Syst. Saf. 96, 1092–1113. doi:10.1016/j.ress.2010.11.010 (2011).

[69] S. E. Elghobashi, T. W. Abou-Arab, “A Two-equation Turbulence Model for Two-phase Flows,” *Phys. Fluids*, **26**, pp. 931–937 (1982).

[70] Ergün S., “Fluid Flow through Packed Columns,” Chemical Engineering Progress, Vol. 48, 2, pp. 89-94 (1952).

[71] Epstein, M. and Fauske, H.K., “Applications of the Turbulent Entrainment Assumption to Immiscible Gas-Liquid and Liquid-Liquid Systems,” Chemical Engineering Research and Design, Volume 79, Issue 4, May 2001, Pages 453-462, (2001).

[72] Farmer, M.T., Kilsdonk, D.J., Aeschlimann, R.W., “Corium Coolability under Ex-Vessel Accident Conditions for LWRs, Nucl. Eng. and Tech., June 2009, pp.41–45.

[73] Fletcher, D.F. and Anderson, R.P., “A review of pressure-induced propagation models of the vapour explosion process,” Progress in Nuclear Energy, 23(2): pp.137-179, 1990.

[74] Frid, W. and Kudinov, P., “Ex-Vessel Melt Coolability Issue in BWRs with Deep Water Pool in Lower Drywell,” OECD/NEA MCCI Seminar 2010, Cadarache, France, 15th - 17th November, (2010).

[75] Frid, W., et al., Severe Accident Research and Management in Nordic Countries: A Status Report, W. Frid, Editor. 2002.

[76] Friedman, S. P., and D. A. Robinson, Particle shape characterization using angle of repose measurements for predicting the effective permittivity and electrical conductivity of saturated granular media, Water Resour. Res., 38(11), 1236, doi:10.1029/2001WR000746, 2002.

[77] Frost, D.L., Bruckert, B., and Ciccarelli, G., “Effect of boundary conditions on the propagation of a vapor explosion in stratified molten tin/water systems,” Nuclear Engineering and Design, 155, pp.311-333 (1995).

[78] Frählich G., “Interaction experiments between water and hot melts in entrapment and stratification configurations”, Chemical Geology, 62, pp. 137-147, (1986).

[79] Gabor, J.D., Simulation Experiments for Internal Heat Generation, Reactor Development Program Progress Report ANL-RDP-32, Argonne National Laboratory, Argonne, USA,1974.
[80] Gabor, J.D., Purviance, R.T., Cassulo, J.C., and Spencer, B.W., "Molten aluminum alloy fuel fragmentation experiments," Nuclear Engineering and Design, Volume 146, Issues 1–3, February 1994, Pages 195-206.
[81] I. Gallego-Marcos, W. Villanueva, P. Kudinov, "Possibility of Air Ingress into a BWR Containment during a LOCA in case of Activation of Containment Venting System," The 10th International Topical Meeting on Nuclear Ther-mal-Hydraulics, Operation and Safety (NUTHOS-10), Okinawa, Japan, De-cember 14-18, Paper 1292, 2014.
[82] Galushin S., and Kudinov P., "An Approach to Grouping and Classification of Scenarios in Integrated Deterministic-Probabilistic Safety Analysis," Probabilistic Safety Assessment and Management PSAM 12, June 22-27, 2014, Honolulu, Hawaii, Paper 330, 2014.
[83] Galushin S. and Kudinov P., "Analysis of Core Degradation and Relocation Phenomena and Scenarios in a Nordic-type BWR," Nuclear Engineering and Design, Volume 310, 15 December 2016, Pages 125–141, 2016.
[84] Galushin S. and Kudinov P., "An Approach to Grouping and Classification of Scenarios in Integrated Deterministic-Probabilistic Safety Analysis," Science and Technology of Nuclear Installations, Article ID 278638, 13 pages, 2015.
[85] Galushin S., Villanueva W., Grishchenko D., Kudinov P., "Development of core relocation surrogate model for prediction of debris properties in lower plenum of a Nordic BWR", NUTHOS-11: The 11th International Topical Meeting on Nuclear Reactor Thermal Hydraulics, Operation and Safety, Gyeongju, Korea, October 9-13, (2016).
[86] Galushin S., Kudinov P., "Comparison of MELCOR code versions predictions of the properties of relocated debris in lower plenum of Nordic BWR" 17th International Topical Meeting on Nuclear Reactor Thermal Hydraulics, Xi'an, Shaanxi, China, Sept. 3-8, (2017)
[87] Galushin S., Kudinov P., "Effect of Severe Accident Scenario and Modeling Options in MELCOR on the Properties of Relocated Debris in Nordic BWR Lower Plenum" 17th International Topical Meeting on Nuclear Reactor Thermal Hydraulics, Xi'an, Shaanxi, China, Sept. 3-8, (2017).
[88] Gauntt, R. O. and Humphries, L. L., "Final Results of the XR2-1 BWR Metallic Melt Relocation Experiment", NUREG/CR-6527, SAND97-1039, (1997).
[89] Randall Gauntt, Donald Kalinich, Jeff Cardoni, Jesse Phillips, Andrew Goldmann, Susan Pickering, Matthew Francis, Kevin Robb, Larry Ott, Dean Wang, Curtis Smith, Shawn St.Germain, David Schwieder, Cherie Phelan, "Fukushima Daiichi Accident Study", SAND2012-6173, Sandia Report, SNL, 2012.
[90] Greene, S.R., Hodge, S.A., Hyman, C.R., Tobias, M.L., "The Response of BWR Mark II Containment to Station Blackout Severe Accident Sequences", NUREG/CR-5565, ORNL/TM-11548, May 1991.
[91] Grishchenko, D., et al., KROTOS KS-4 test data report 2011, CEA: France, Cadarache.
[92] Grishchenko, D., Basso, S., Galushin, S., Kudinov P., "Development of TEXAS-V Code Surrogate Model for Assessment of Steam Explosion Impact in Nordic BWR," The 16th

International Topical Meeting on Nuclear Reactor Thermal Hydraulics (NURETH-16), Chicago, IL, USA, August 30-September 4, paper 13937, 2015.

[93] Grishchenko D., Basso S., Kudinov P., and Bechta S. "Sensitivity Study of Steam Explosion Characteristics to Uncertain Input Parameters Using TEXAS-V Code," The 10th International Topical Meeting on Nuclear Thermal-Hydraulics, Operation and Safety (NUTHOS-10), Okinawa, Japan, December 14-18, 2014, Paper 1293, 2014.

[94] Grishchenko, D., Konovalenko, A., Karbojian, A., Kudinova, V., Bechta, S., and Kudinov, P., "Insight into steam explosion in stratified melt-coolant configuration," 15th International Topical Meeting on Nuclear Reactor Thermal Hydraulics, NURETH 15, May 12 to 17, 2013, Pisa, Italy, Paper 599. (Best paper award).

[95] Grishchenko D., Basso S., Kudinov P., "Development of a surrogate model for analysis of ex-vessel steam explosion in Nordic type BWRs," Nuclear Engineering and Design, Volume 310, 15 December 2016, Pages 311-327, 2016.

[96] Goronovski A., Villanueva W., Kudinov P., Tran C.-T. "Effect of Corium Non-Homogeneity on Nordic BWR Vessel Failure Mode and Timing," Proceedings of ICAPP 2015, May 03-06, Nice, France, Paper 15160, 2015.

[97] Goronovski, A., Villanueva, W., Tran, C.-T., and Kudinov, P., "The Effect of Internal Pressure and Debris Bed Thermal Properties on BWR Vessel Lower Head Failure and Timing," 15th International Topical Meeting on Nuclear Reactor Thermal Hydraulics, NURETH 15, May 12 to 17, 2013, Pisa, Italy, Paper 500.

[98] "GSN community standard version 1" 2011 Origin Consulting (York) Limited.

[99] Han J., Cheng H., Xin D., and Yan X., "Frequent pattern mining: current status and future directions," Data Mining and Knowledge Discovery, vol. 15, no. 1, pp. 55–86, 2007.

[100] Halton J. H., Numerische Mathematik 2, 84-90 (1960); see also B. Vandewoestyne and R. Cools Computational and Applied Mathematics 189, 1&2, 341-361 (2006).

[101] Halton, J., Smith, G. "Algorithm 247: Radical-Inverse Quasi-Random Point Sequence." Commun. ACM 7, 701–702. (1964).

[102] Hammersley R. J. and Henry R. E., "Experiments to Address Lower Plenum Response under Severe Accident Conditions", EPRI Report TR-103389-V2P1, Vol. 1&2 (1994).

[103] Harlow, F.H., Ruppel, H.M., "Propagation of a liquid-liquid explosion," Los Alamos National Laboratory, Report LA 8971 MS, p.11 (1981).

[104] Helton, J.C., Johnson, J.D., Oberkampf, W.L., Sallaberry, C.J., "Representation of analysis results involving aleatory and epistemic uncertainty," International Journal of General Systems, Vol.39(6),pp.605-646, (2010).

[105] Helton, J.C. Quantification of margins and uncertainties: Conceptual and computational basis. Reliab. Eng. Syst. Saf. 96, 976–1013. doi:10.1016/j.ress.2011.03.017. (2011).

[106] Helton, J.C. Uncertainty and sensitivity analysis in the presence of stochastic and subjective uncertainty, Journal of Statistical Computation and Simulation. doi:10.1080/00949659708811803. 57 (1–4) 3–76, (1997).

[107] Helton, J.C., Breeding, R.J. Calculation of reactor accident safety goals. Reliab. Eng. Syst. Saf. 39, 129–158. doi:10.1016/0951-8320(93)90038-Z. (1993).

[108] Helton, J.C., Johnson, J.D., Sallaberry, C.J., Storlie, C.B. Survey of sampling-based methods for uncertainty and sensitivity analysis. Reliab. Eng. Syst. Saf. 91, 1175–1209. doi:10.1016/j.ress.2005.11.017. (2006).

[109] Hesson, J.C., Sevy, R.H., Marciniak, T.J., Post-Accident Heat Removal in LMFBRs. In: Vessel Considerations, ANL-7859, Argonne National Laboratory, Argonne, USA.,1971
[110] Hofmann G., "On the location and mechanisms of dryout in top-fed and bottom-fed", Nuclear Technology, 65, (1984).
[111] Hofmann, P. "Current knowledge on core degradation phenomena, a review." J. Nucl. Mater. 270, 194–211. doi:10.1016/S0022-3115(98)00899-X, (1999).
[112] Howson, C., Urbach, P., "Scientific Reasoning the Bayesian Approach", 2nd edition Chicago, 52-55, (1997).
[113] Hu K. and Theofanous, T.G., "On the Measurement and Mechanism of Dryout in Volumetrically Heated Coarse Particle Beds," Int. J. Multiphase Flow, Vol. 17, No. 4, pp. 519–532 (1991).
[114] Humphries, L.L., Chu, T.Y., Bentz, J., Simpson, R., Hanks, C., Lu, W., Antoun, B., Robino, C., Puskar, J., Mongabure, P., "OECD Lower Head Failure Project Final Report", CSNI-R2002-27 (2002).
[115] Huppert H. E., "The propagation of two-dimensional and axisymmetric viscous gravity currents over a rigid horizontal surface", J. Fluid Mech., 121, pp. 43-58, (1982).
[116] Huppert H., "Flow and instability of a viscous current down a slope," Nature, 300, pp. 427-429, 1982.
[117] IAPWS, The International Association for the Properties of Water and Steam, http://www.iapws.org.
[118] Inselberg, A. "Parallel Coordinates: Visual Multidimensional Geometry and Its Applications", Springer, (2009).
[119] Ishii M., Mishima K., "Two-Fluid Model and Hydrodynamic Constitutive Relations," Nuclear Engineering and Design, 82, pp. 107-126 (1984).
[120] Journeau, C., Boccaccio, E., Brayer, C., Cognet, G., Haquet, J.-F., Jégou, C., Piluso, P., Monerris, J., "Ex-vessel corium spreading: Results from the VULCANO spreading tests", Nuclear Engineering and Design, 223(1), pp. 75-102, 2003.
[121] Kallenberg, O. "Foundations of Modern Probability." Springer, New York. (1997).
[122] Kang, K. H., Park, R. J., Kim, J. T., Lee, K. Y. and Kim, S. B., "Thermal Behavior of the Reactor Vessel Penetration under External Vessel Cooling during a Severe Accident", Nuclear Technology, 145 (2004).
[123] Kaplan S. and Garrick, B. J., "*On The Quantitative Definition of Risk*," Risk Analysis, 1: pp.11–27, (1981).
[124] Kaplan, S. Formalisms for handling phenomenological uncertainties: the concepts of probability, frequency, variability, and probability of frequency. Nucl. React. Saf. 137–142. (1992).
[125] Karbojian, A., Ma, W.M., Kudinov, P., Davydov, M., Dinh, N., "A scoping study of debris formation in DEFOR experimental facility", 15th International Conference on Nuclear Engineering, Nagoya, Japan, April 22-26, 2007, Paper number ICON15-10620.
[126] Karbojian, A., Ma, W., Kudinov, P., and Dinh, T.-N., "A Scoping Study of Debris Bed Formation in the DEFOR Test Facility", Nuclear Engineering and Design, 239, 2009, 1653-1659.
[127] Kim, B.J., "Heat transfer and fluid flow aspect of small-scale single droplet fuel-coolant interaction," University of Wisconsin-Madison. 1985.

[128] Kim E., J. H. Park, M. H. Kim and H. S. Park, "The influence of two-phase flow on pore clogging by fine particle settlement during ex-vessel debris bed formation in severe accident," in Proceedings of the 2014 22nd International Conference on Nuclear Engineering (ICONE22), Prague, Czech Republic, July 7-11, (2014).

[129] Kelly, T.: 'Arguing Safety: A Systematic Approach to Managing Safety Cases', D.Phil Thesis, University of York (1998). Available for download from http://wwwusers.cs.york.ac.uk/~tpk.

[130] L.A. Klinkova, V.I. Nikolaichik, N.V. Barkovskii and V.K. Fedotov, "Thermal Stability of Bi2O3", Russian journal of inorganic chemistry, vol 52, no:12, pp.1822-1829, 2007.

[131] Koide, K., Yasuda, T., Iwamoto, S., Fukuda, E.," Critical gas velocity required for complete suspension of solid particles in solid-suspended bubble columns". *J. Chem. Eng*. Jpn. 16 (1), 7–12, 1983.

[132] Koide, K., Horibe, K., Kawabata, H., Ito, S., "Critical gas velocity required for complete suspension of solid particles in solid-suspended bubble column with draught tube". *J. Chem. Eng*. Jpn. 17 (4), 368–374. 1984.

[133] Konovalenko, A., Basso, S., Karbojian, A., and Kudinov, P., "Experimental and Analytical Study of the Particulate Debris Bed Self-leveling," Proceedings of The 9th International Topical Meeting on Nuclear Thermal-Hydraulics, Operation and Safety (NUTHOS-9), Kaohsiung, Taiwan, September 9-13, N9P0305, 2012.

[134] Konovalenko A., Basso S., and Kudinov P. "Experiments and Characterization of the Two-Phase Flow Driven Particulate Debris Spreading in the Pool," The 10th International Topical Meeting on Nuclear Thermal-Hydraulics, Operation and Safety (NUTHOS-10), Okinawa, Japan, December 14-18, 2014, Paper 1257, 2014.

[135] Konovalenko A., Basso S., Kudinov P., Yakush S. E., "Experimental Investigation of Particulate Debris Spreading in a Pool", Nuclear Engineering and Design, Volume 297, pp208-219, 2016.

[136] Konovalenko A., Basso S., Kudinov P., Yakush S. E., "Experiments and Modeling of Particulate Debris Spreading in a Pool," The 16th International Topical Meeting on Nuclear Reactor Thermal Hydraulics (NURETH-16), Chicago, IL, USA, August 30-September 4, paper 14221, 2015.

[137] Konovalenko, A., Karbojian, A., and Kudinov, P., "Experimental Results on Pouring and Underwater Liquid Melt Spreading and Energetic Melt-coolant Interaction," Proceedings of The 9th International Topical Meeting on Nuclear Thermal-Hydraulics, Operation and Safety (NUTHOS-9), Kaohsiung, Taiwan, September 9-13, N9P0303, 2012.

[138] Konovalenko, A. and Kudinov, P., "Development of Scaling Approach for Prediction of Terminal Spread Thickness of Melt Poured into a Pool of Water," Proceedings of The 9th International Topical Meeting on Nuclear Thermal-Hydraulics, Operation and Safety (NUTHOS-9), Kaohsiung, Taiwan, September 9-13, N9P0302, 2012. (Best paper award).

[139] Konovalikhin M. J., "Investigation on melt spreading and coolability in a LWR severe accident", doctoral thesis, Royal Institute of Technology, ISSN 1403-1701, ISRN KTH/NPS/CSC-0011-SE, 2001.

[140] Kolev N., Multiphase Flow Dynamics, Vol. 2, Ch. 2, Springer, Berlin, Heidelberg, NY (2005).

[141] Kudinov, P., "Decomposition, Validation and Synthesis in Multiscale Problems of Severe Accident Analysis," Verification and Validation for Nuclear Systems Analysis Workshop, Center for Higher Education, Idaho Falls, ID, July 21 - July 25, 2008.
[142] Kudinov, P. and Davydov M., "Development of Surrogate Model for Prediction of Corium Debris Agglomeration," In Proceedings of ICAPP-2014, Charlotte, USA, April 6-9, Paper 14366, 2014.
[143] Kudinov, P. and Davydov, M., "Approach to Prediction of Melt Debris Agglomeration Modes in a LWR Severe Accident," Proceedings of ISAMM-2009, Böttstein, Switzerland, October 26 - 28, 2009.
[144] Kudinov, P. and Davydov, M., "Development of Ex-Vessel Debris Agglomeration Mode Map for a LWR Severe Accident Conditions," Proceedings of the 17th International Conference on Nuclear Engineering, July 12-16, 2009, Brussels, Belgium, Paper ICONE17-75080.
[145] Kudinov, P. and Davydov, M., "Development and Validation of the Approach to Prediction of Mass Fraction of Agglomerated Debris," The 8th International Topical Meeting on Nuclear Thermal-Hydraulics, Operation and Safety (NUTHOS-8), Shanghai, China, October 10-14, N8P0298, 2010.
[146] Kudinov P., Davydov M.V., "Development and validation of conservative-mechanistic and best estimate approaches to quantifying mass fractions of agglomerated debris," Nuclear Engineering and Design, 262, September 2013, pp. 452-461.
[147] Kudinov and Davydov M., "Prediction of Mass Fraction of Agglomerated Debris in a LWR Severe Accident," The 14th International Topical Meeting on Nuclear Reactor Thermal Hydraulics (NURETH-14), Toronto, Ontario, Canada, September 25-29, 2011.
[148] Kudinov, P., Davydov, M., Pohlner G., Bürger M., Buck M., and Meignen R., "Validation of the FCI codes against DEFOR-A data on the mass fraction of agglomerated debris," 5th European Review Meeting on Severe Accident Research (ERMSAR-2012) Cologne (Germany), March 21-23, 2012.
[149] Kudinov, P. and Dinh, T.-N., "An analytical study of mechanisms that govern debris packing in a LWR severe accident", The 12th International Topical Meeting on Nuclear Reactor Thermal Hydraulics (NURETH-12), Sheraton Station Square, Pittsburgh, Pennsylvania, U.S.A. September 30-October 4, 2007. Paper 247.
[150] Kudinov, P. and Dinh, T.-N., "A Computational Study of Debris Bed Formation," ANS Transactions, 2008, paper 193463.
[151] Kudinov P., Galushin S., Goronovski A., and Villanueva W., "RES1: Definition of a Reference Nordic BWR Plant Design and Plant Damage States for Application of ROAAM to Resolution of Severe Accident Issues," Research Report, The Eighth Framework of Accident Phenomena of Risk Importance (APRI-8), Division of Nuclear Power Safety, Royal Institute of Technology (KTH), Stockholm, Sweden, April 04, 2014.
[152] Kudinov P, Galushin S., Grishchenko D., Yakush S., Adolfsson Y., Ranlöf L., Bäckström O., Enerholm A., Krcal P., Tuvelid A., "Deterministic-Probabilistic Safety Analysis Methodology for Analysis of Core Degradation, Ex-vessel Steam Explosion and Debris Coolability", NKS-345, ISBN 978-87-7893-427-7. Jul 2015.
[153] Kudinov P., Galushin S., Davydov M., "Analysis of the Risk of Formation of Agglomerated Debris in Nordic BWRs," NUTHOS-11:The 11th International Topical

Meeting on Nuclear Reactor Thermal Hydraulics, Operation and Safety, Gyeongju, Korea, October 9-13, N11P0592, 2016.

[154] Kudinov P., Galushin S., Raub S., Phung V.-A., Kööp K., Karanta I., Silvonen T., Adolfsson Y., Bäckström O., Enerholm A., Krcal P., Sunnevik K., "Feasibility Study for Connection Between IDPSA and conventional PSA Approach to Analysis of Nordic type BWR's," NKS-DPSA Project, NKS-R, Report: NKS-315, 2014.

[155] Pavel Kudinov, Sergey Galushin, Dmitry Grishchenko, Sergey Yakush, Yvonne Adolfsson, Lisa Ranlöf, Ola Bäckström, Anders Enerholm, "Scenarios and Phenomena Affecting Risk of Containment Failure and Release Characteristics," SPARC Project, NKS-395 22 Aug 2017, 2017.

[156] Pavel Kudinov, Sergey Galushin, Dmitry Grishchenko, Sergey Yakush, Simone Basso, Alexander Konovalenko, Mikhail Davydov, "Application of Integrated Deterministic-Probabilistic Safety Analysis to Assessment of Severe Accident Management Effectiveness in Nordic BWRs," The 17th International Topical Meeting on Nuclear Reactor Thermal Hydraulics (NURETH-17) Paper: 21590, Qujiang Int'l Conference Center, Xi'an, China， September 3-8, 2017.

[157] Kudinov P., Galushin S., Yakush S., Villanueva W., Phung V.-A., Grishchenko D., Dinh N., "A Framework for Assessment of Severe Accident Management Effectiveness in Nordic BWR Plants," Probabilistic Safety Assessment and Management PSAM 12, June 22-27, 2014, Honolulu, Hawaii, Paper 154, 2014.

[158] Kudinov P., Grishchenko D., Konovalenko A., Karbojian A. "Premixing and Steam Explosion Phenomena in the Tests with Stratified Melt-Coolant Configuration and Binary Oxdic Melt Simulant Materials," Nuclear Engineering and Design, Volume 314, Pages 1-338 (1 April 2017).

[159] Kudinov P., Grishchenko D., Karbojian A., Villanueva W., "Design and development of experiments for validation of debris remelting and interactions with structures," Accident Phenomena of Risk Importance (APRI-8), Report MEM1, Rev.2, January 10, 2015.

[160] Kudinov P., Grishchenko D., Konovalenko A., Karbojian A., "Experimental Investigation of Debris Bed Agglomeration and Particle Size Distribution Using WO3-ZrO2 Melt," The 16th International Topical Meeting on Nuclear Reactor Thermal Hydraulics (NURETH-16), Chicago, IL, USA, August 30-September 4, paper 14220, 2015.

[161] Kudinov P., Grishchenko D., Konovalenko A., Karbojian A., Bechta S. "Investigation of Steam Explosion in Stratified Melt-Coolant Configuration," The 10th International Topical Meeting on Nuclear Thermal-Hydraulics, Operation and Safety (NUTHOS-10), Okinawa, Japan, December 14-18, 2014, Paper 1316, 2014.

[162] Kudinov P., Grishchenko D., Galushin S., Yakush S., Konovalenko A., Basso S., Davydov M., Thakre S., Villanueva W., Ma W., Yu P., Manickam L., "Integrated ROAAM+ Development and Analysis Results for Nordic BWRs". Accident Phenomena of Risk Importance (APRI-9) Report, January 2017.

[163] Kudinov P., Grishchenko D., Galushin S., Yakush S., Konovalenko A., Basso S., Davydov M., Villanueva W., Goronovski A., "RES3: Preliminary Analysis of Conditional Containment Failure Probabilities Using ROAAM+ Frameworks." Risk Oriented Framework for Safety Analysis of Severe Accident Issues in Nordic BWRs. Accident Phenomena of Risk Importance (APRI-8), January 2016.

[164] Kudinov, P., Karbojian, A., Ma, W.M., Davydov, M., and Dinh, T.-N., "A Study of Ex-Vessel Debris Formation in a LWR Severe Accident", Proceedings of ICAPP 2007, Nice, France, May 13-18, 2007, Paper 7512.

[165] Kudinov, P., Karbojian, A., Ma, W.M., and Dinh, T.-N., "An experimental study on debris formation with corium simulant materials," Proc. ICAPP'08, Anaheim, CA USA, June 8–12, 2008, paper 8390.

[166] Kudinov, P., Karbojian, A., Ma, W., and Dinh, T.-N. "The DEFOR-S Experimental Study of Debris Formation with Corium Simulant Materials," Nuclear Technology, 170(1), April 2010, pp. 219-230, 2010.

[167] Kudinov, P., Karbojian, A., and Tran, C.-T., "Experimental Investigation of Melt Debris Agglomeration with High Melting Temperature Simulant Materials," Proceedings of ISAMM-2009, Böttstein, Switzerland, October 26 - 28, 2009.

[168] Kudinov, P., Karbojian, A., Tran, C.-T., and Villanueva, W., "The DEFOR-A Experiment on Fraction of Agglomerated Debris as a Function of Water Pool Depth," The 8th International Topical Meeting on Nuclear Thermal-Hydraulics, Operation and Safety (NUTHOS-8), Shanghai, China, October 10-14, N8P0296, 2010.

[169] Kudinov, P., Karbojian, A., Tran, C.-T., Villanueva, W., "Experimental Data on Fraction of Agglomerated Debris Obtained in the DEFOR-A Melt-Coolant Interaction Tests with High Melting Temperature Simulant Materials," Nuclear Engineering and Design, 263, October 2013, Pages 284-295, 2013.

[170] Kudinov, P., Ma, W.M., Tran, C.-T., Hansson, R., Karbojian, A., and Dinh, T.-N. "Multiscale Phenomena of Severe Accident," NKS-R and NKS-B Joint Summary Seminar, Armémuseum, Stockholm, 26th - 27th March 2009.

[171] Kudinov, P. and Kudinova, V., "Influence of Water Subcooling on Fracture of Melt Debris Particle," ANS Transactions, 2009, paper 210646.

[172] Kudinov, P., Kudinova, V., and Dinh, T.-N., "Molten Oxidic Particle Fracture during Quenching in Water," 7th International Conference on Multiphase Flow ICMF 2010, Tampa, FL USA, May 30-June 4, 2010.

[173] Kudinov P., Vorobyev Y., Sánchez-Perea M., Queral C., Jiménez Varas G., Rebollo M. J., Mena L., Gómez-Magán J., "Integrated Deterministic-Probabilistic Safety Assessment Methodologies", Nuclear España, 347, Enero, pp.32-38, 2014.

[174] Kymäläinen, O., Tuomisto, H., Hongisto, O., and Theofanous, T. G., "Heat Flux Distribution from a Volumetrically Heated Pool with High Rayleigh Number," Nucl. Eng. Des. 149, 401–408, 1994.

[175] Kymäläinen, O., Tuomisto, H., and Theofanous, T. G., "In-Vessel Retention of Corium at the Loviisa Plant," Nucl. Eng. Des. 169, 109–130, 1997.

[176] Lahey R. T., Drew Jr, D. A., "The Analysis of Two-Phase Flow and Heat Transfer Using a Multidimensional, Four Field, Two-Fluid Model," Nuclear Engineering and Design, 204, pp. 29-44 (2001).

[177] Lakehal D., "On the Modelling of Multiphase Turbulent Flows for Environmental and Hydrodynamic Applications," Int. J. Multiphase Flow, 28, pp. 823-863 (2002).

[178] Launder B. E., Spalding D. B., Mathematical Models of Turbulence, Academic Press, London, 1972.

[179] Li L., Karbojian A., Kudinov P., Ma W., "An Experimental Study on Dryout Heat Flux of Particulate Beds Packed with Irregular Particles," Proceedings of ICAPP 2011, Nice, France, May 2-5, 2011, Paper 11185. 2011.

[180] Liao, W.-K., Liu, Y., and Choudhary, A.. "A Grid-based Clustering Algorithm using Adaptive Mesh Refinement," In proceedings of the 7thWorkshop on Mining Scientific and Engineering Datasets, 2004.

[181] Lindholm, I., Nilsson, L., Pekkarinen, E., Sjövall, H., "Coolability of degraded core under reflooding conditions in Nordic boiling water reactors", Nordic nuclear safety research, NKS-2(95), September, (1995).

[182] Lipinski, R.J., "A one dimensional particle bed dryout model," ANS Trans. 38, pp, 386–387, 1981.

[183] Lucas A, Arnaldos J, Casal J, Puigjaner L, "Improved equation for the calculation of minimum fluidization velocity*", Ind Eng Chem Process Des Dev,* **25**, 426-429 (1986).

[184] Magallon, D., Huhtiniemi, I., Hohmann, H., "Lessons Learnt from FARO/TERMOS Corium Melt Quenching Experiments," In: Proceedings of the OECD/CSNI Specialists Meeting on Fuel-Coolant Interactions, Tokai-Mura, Japan, NEA/CSNI/R(97)26, Part II, 1997, pp.431-446.

[185] Magallon, D., "Characteristics of corium debris bed generated in large-scale fuel-coolant interaction experiments," Nuclear Engineering and Design, 236, 2006, pp.1998–2009.

[186] Magallon, D., et al., OECD research programme on fuel-coolant interaction. Steam explosion resolution for nuclear applications - SERENA. 2007.

[187] Magallon, D., et al. Results of phase 1 of OECD programme SERENA on fuel-coolant interaction. in ERMSAR 2005. 2005. Aix-en-Provence.

[188] Magallon, D., SERENA Programme Reactor exercise: Synthesis of calculations. 20 p., 2012.

[189] Manickam L., Kudinov P, Bechta S., "On the Influence of Water Subcooling and Melt Jet Parameters on Debris Formation," 15th International Topical Meeting on Nuclear Reactor Thermal Hydraulics, NURETH 15, May 12 to 17, 2013, Pisa, Italy, Paper 512.

[190] Manickam, L., Kudinov, P., Ma, W., Bechta, S., Grishchenko, D., 2016. "On the influence of water subcooling and melt jet parameters on debris formation," Nucl. Eng. Des. 309, 265–276, 2016.

[191] Marsland, S., "Machine Learning: an algorithmic perspective", Chapman and Hall (2009).

[192] Matsuo E., Abe Y., Chitose K., Koyama K., Itoh K., "Study on jet breakup behavior at core disruptive accident for fast breeder reactor," Nuclear Engineering and Design, Volume 238, Issue 8, August 2008, Pages 1996-2004.

[193] Meignen, R. "Status of the Qualification Program of the Multiphase Flow Code MC3D," in Proceedings of ICAPP '05. 2005. Seoul, KOREA, May 15-19, 2005.

[194] Meignen R., Raverdy B., Buck M., Pohlner G., Kudinov P., Ma W., Brayer C., Piluso P., Hong S.-W., Leskovar M., Uršič M., Albrecht G., Lindholm I., Ivanov I., "Status of steam explosion understanding and modelling," Annals of Nuclear Energy, Article in Press, Available online 23 August 2014.

[195] Morris M. D., "Factorial sampling plans for preliminary computational experiments", Technometrics, 33, (2), pp. 161–174, 1991.

[196] Moore, R.E.. Interval Analysis. Prentice Hall. (1966).
[197] Moore, R.E., Kearfott, R., Cloud, M.. Introduction to Interval Analysis, Mathematics of Computation. Society for Industrial and Applied Mathematics. doi:10.2307/2004792. (2009).
[198] Moriyama, K., et al., Evaluation of Containment Failure Probability by Ex-Vessel Steam Explosion in Japanese LWR Plants. Journal of Nuclear Science and Technology, 2012. 43(7): p. 774-784.
[199] Moriyama, K. and H.S. Park, Probability distribution of ex-vessel steam explosion loads considering influences of water level and trigger timing. Nuclear Engineering and Design, 2015. 293: p. 292-303.
[200] Murphy, J., A Hydrogen Generation Model for TEXAS. 1992, University of Wisconsin.
[201] Namiech J., Berthoud G., Coutris N., “Fragmentation of a molten corium jet falling into water,” Nuclear Engineering and Design, Volume 229, Issues 2–3, April 2004, Pages 265-287.
[202] National-Research-Council, 2008. Evaluation of Quantification of Margins and Uncertainties methodology for assessing and certifying the reliability of the nuclear stockpile. National Academy of Sciences. doi:10.1016/j.ress.2011.03.015
[203] National-Research-Council, 1990. Implentatation of the safety goals.
[204] Nigmatulin, B.I., Melikhov, V.I., Melikhov, O.I., VAPEX Code for Analysis of Steam Explosions under Severe Accidents. Heat and Mass Transfer in Severe Nuclear Reactor Accidents, New York, Wallingford (UK), Begell House, 1995, pp. 540-551.
[205] Nourgaliev, R. R., and Dinh, T. N., “The Investigation of Turbulence Characteristics in an Internally Heated Unstably Stratified Fluid Layers,” Nucl. Eng. Des. 178(1), 235–259, 1997.
[206] Novak Z., Gary E.W., Mamoru I., Wolfgang W., Boyack B.E, Dukler A.E., Griffith P, Healzer J.M, Henry R.E, Lehner J.R, Levy S, Moody F.J, Pilch M, Sehgal B.R, Spencer B.W, Theofanous T.G, Valente J, “An integrated structure and scaling methodology for severe accident technical issue resolution: Development of methodology,” Nuclear Engineering and Design, Volume 186, Issues 1–2, 1 November 1998, Pages 1-21.
[207] Oliveira, P. J., Issa, R. I., “Numerical aspects of an algorithm for the Eulerian simulation of two-phase flows,” Int. J. Numer. Meth. Fluids, 43, pp. 1177–1198 (2003).
[208] ONR Nuclear Safety Technical Assessment Guide, “The purpose, scope and content of nuclear safety cases,” NS-TAST-GD-051 (Rev 3) July 2013. http://www.onr.org.uk/operational/tech_asst_guides/ns-tast-gd-051.pdf
[209] Rahman, S., 2013. Coolability of Corium Debris under Severe Accident Conditions in Light Water Reactors. Universität Stuttgart.
[210] Rechard, R.P., 2000. Historical background on performance assessment for the Waste Isolation Pilot Plant. Reliab. Eng. Syst. Saf. 69, 5–46. doi:10.1016/S0951-8320(00)00023-5
[211] Rechard, R.P., 1999. Historical relationship between performance assessment for radioactive waste disposal and other types of risk assessment. Risk Anal. 19, 763–807.
[212] Rocquigny, E. de, Devictor, N., Tarantola, S., 2008. Uncertainty in Industrial Practice: A Guide to Quantitative Uncertainty Management. John Wiley & Sons Ltd.

[213] Palagin A., Miassoedov A., Gaus-Liu X., Muscher H., Buck M., Tran C.T., Kudinov P., Carenini L., Koellein C., Luther W., Chudanov V., “Analysis and interpretation of the LIVE-L6 experiment,” 5th European Review Meeting on Severe Accident Research (ERMSAR-2012), Cologne (Germany), March 21-23, 2012.

[214] Park, R. J., Kang, K. H., Kim, J. T., Lee, K. Y., and Kim, S. B., “Experimental and Analytical Studies on the Penetration Integrity under External Vessel Cooling”, Nuclear Technology, 145 (2004).

[215] Park, I.K., Kim D.H., and Song J.H. “Steam explosion module development for the MELCOR code using TEXAS-V,” Journal of Korean Nuclear Society, 2003. 32(4): pp.286-298, 2003.

[216] Parry, G.W., Winter, P., “Charaterization and evaluation of uncertainty in probabilistic risk analysis,” Nucl. Saf. 22, 28–42. (1981).

[217] Pianosi, F., Sarrazin, F., Wagener, T., 2015. A Matlab toolbox for Global Sensitivity Analysis. Environ. Model. Softw. 70, 80–85. doi:10.1016/j.envsoft.2015.04.009.

[218] Philippe P. and Richard. T., “Start and stop of an avalanche in a granular medium subjected to an inner water flow”, Phys. Rev. E, 77, pp. 041306, (2008).

[219] Phung, V. -A., Grishchenko, D., Galushin, S., Kudinov, P., “Prediction of In-Vessel Debris Bed Properties in BWR Severe Accident Scenarios using MELCOR and Neural Networks,” Journal of Annals of Nuclear Energy, submitted January 2017.

[220] Phung, V.-A. Galushin, S. Raub, S. Goronovski, A., Villanueva, W., Kööp, K., Grishchenko, D., Kudinov, P., “Characteristics of debris in the lower head of a BWR in different severe accident scenarios,” NED, Volume 305, 15, August 2016, pages 359-370, 2016.

[221] Phung V. A. and Kudinov P., “Relaxation Time Concept for Flow Regime Transition in Two-Phase Flow Simulations,” ANS Transactions, 2009, paper 210649.

[222] Phung V. A., Kozlowski T., Kudinov P., Rohde M., "Simulation of Two-Phase Flow Instability in CIRCUS Facility Using RELAP5" ANS Transactions, 2008, paper 197733.

[223] Phung V.-A. and Kudinov P., “Identification of Two-Phase Flow Regimes in Unstable Natural Circulation Using TRACE and RELAP5,” Proceedings of The 9th International Topical Meeting on Nuclear Thermal-Hydraulics, Operation and Safety (NUTHOS-9), Kaohsiung, Taiwan, September 9-13, , N9P0062, 2012.

[224] Phung V. A., Kudinov P., and Rohde M., “Validation of RELAP5 with Sensitivity Analysis for Uncertainty Assessment for Natural Circulation Two-Phase Flow Instability,” Proc. The 13th International Topical Meeting on Nuclear Reactor Thermal Hydraulics (NURETH-13), September 27-October 2, 2009. Kanazawa City, Ishikawa Prefecture, Japan, Paper N13P1248.

[225] Pohlner G., Buck M., Meignen R., Kudinov P., Ma W., Polidoro F., Takasuo E., “Analyses on Ex-Vessel Debris Formation and Coolability Performed in the Frame of WP5.3-EXCOOL Sub Work Package of SARNET,” ERMSAR 2013, Avignon (France), Palais des Papes, 2-4 October, 2013.

[226] Pohlner G., Buck M., Meignen R., Kudinov P., Ma W., Polidoro F., Takasuo E., “Analyses on ex-vessel debris formation and coolability in SARNET frame,” Annals of Nuclear Energy, Volume 74, December 2014, Pages 50-57, 2014.

[227] Pohlner, G., Buck, M., Rahman, S., 2013. Modeling and Validation Basis of the JEMI Code, Institut für Kernenergetik und Energiesysteme, Universität Stuttgart, Bericht IKE 2-161, September 2013.

[228] Reed A.W., "The Effect of Channelling on the Dryout of Heated Particulate Beds Immersed in a Liquid Pool," Ph.D. Thesis, Massachusetts Institute of Technology, Cambridge, 1982.

[229] Rempe, J. L. et. al., "BWR Lower Head Failure Head Failure Assessment for CSNI Comparison Exercise", EGG-EAST-9609, April 1991.

[230] Rempe, J.L., Chavez, S.A., Thinnes, G.L., Allison, C.M., Korth, G.E., Witt, R.J., Sienicki, J.J., Wang, S.K., Stickler, L.A., Heath, C.H., and Snow, S.D., "Light Water Reactor Lower Head Failure," Report NUREG/CR-5642, Idaho Falls (1993).

[231] Robb K., Corradini M., "Melt eruption modeling for MCCI simulations", The 14th International Topical Meeting on Nuclear Reactor Thermalhydraulics, NURETH-14 290, Toronto, Ontario, Canada, September 25-30, 2011.

[232] Robinson, D., Friedman, S., "Observations of the effects of particle shape and particle size distribution on avalanching of granular media", *Physica A: Statistical Mechanics and its Applications*, **311**, *1*, 97-110, 2002.

[233] Saito, M., Sato, K., Furutani, A., Isosaki, M., Imahori, S., and Hattori, Y., "Melting Attack of Solid Plate by a High-Temperature Liquid Jet- Effect of Crust Formation," Nucl. Eng. Des. 121, 11–23. 1990.

[234] Saito, M., Sato, K., Imahori, S., "Experimental study on penetration behaviors of water jet into freon-11 and liquid nitrogen," In: Proceedings of ANS National Heat Transfer Conference, Houston, U.S., Vol. 3, 1988, pp. 173–183.

[235] Saltelli A., Tarantola S., Campolongo F., Ratto M., Sensitivity Analysis in Practice, John Wiley & Sons Ltd, p. 94, 2004.

[236] Saltelli, A., Ratto, M., Andres, T., Campolongo, F., Cariboni, J., Gatelli, D., Saisan, M., Tarantola, S., 2008. Global Sensitivity Analysis: The Primer. John Wiley & Sons Ltd., (2008).

[237] Samarasinghe, S., "Neural Networks for Applied Sciences and Engineering", Taylor and Francis Group, doi:10.1017/CBO9781107415324.004, (2007).

[238] Sato T., Matsumoto K., Kurosaki T., Taguchi, K., "ABWR1 - A Generation III.7 Reactor after the Fukushima Daiichi accident," Proceedings of ICONE-23, 23rd International Conference on Nuclear Engineering, May 17-21, 2015, Chiba, Japan, ICONE-1693, 2015.

[239] SCDAP/RELAP5/MOD3.1 Code Manual, Volume IV: MATPRO -- A Library of Materials, Properties for Light-Water-Reactor Accident, Analysis. NUREG/CR-6150 EGG-2720, Vol. 4. (1993).

[240] Schneider, J.P., Marciniak, M., Jones, B.G., "Breakup of Metal Jets Penetrating a Volatile Liquid," Proc. 5th International Topical Meeting on Reactor Thermal Hydraulics (NURETH-5), vol. 2. Salt Lake City, USA, 1992. pp. 437–449.

[241] Schulenberg, T., Müller, U., "An improved model for two-phase flow through beds of coarse particles," Int. J. Multiphase Flow, 13, pp. 87–97, 1987.

[242] Schmidt W., "Interfacial drag of two-phase flow in porous media," Int. J. Multiphase Flow, Vol. 33, pp. 638–657 (2007).

[243] Scobel, J.., Theofanous, T.., Sorrell, S.., 1998. Application of the risk oriented accident analysis methodology (ROAAM) to severe accident management in the AP600 advanced light water reactor. Reliab. Eng. Syst. Saf. 62, 51–58. doi:10.1016/S0951-8320(97)00170-1.

[244] Sehgal, B.R., H.O. Haraldsson, and Z.L. Yang, A Review of Steam Explosions with Special Emphasis on the Swedish and Finnish BWRs. Sehgal Konsult. 2002.

[245] Sehgal, B.R. et al., Final report for the "Melt-Vessel Interaction (MVI)" project, SKI 00:53, 2000.

[246] Shackelford, J.F., et al., In: Shackelford, J.F., Alexander, W. (Eds.), Frontmatter Materials Science and Engineering Handbook. CRC Press LLC, Boca Raton. 2001.

[247] Shafer, G., 1976. A mathematical theory of evidence. Princeton University Press.

[248] Shamsuzzaman M., B. Zhang, T. Horie, F. Fuke, T. Matsumoto, K. Morita, H. Tagami, T. Suzuki and Y. Tobita, "Numerical study on sedimentation behavior of solid particles used as simulant fuel debris," Journal of Nuclear Science and Technology, vol. 51, no. 5, pp. 681-699, (2014).

[249] Sobol, I.M., "The distribution of points in a cube and the approximate evaluation of integrals," U.S.S.R. Comput. Math. and Math. Phys., 7, pp. 86-112. (1976).

[250] Song, J.H., Kim, J.H., Hong, S.W., Min, B.T. and Kim, H.D., "The Effect of Corium Composition and Interaction Vessel Geometry on the Prototypic Steam Explosion," Annals of Nuclear Energy, 33(17-18), pp. 1437-1451 (2006).

[251] Song, J.H., I.K. Park, and J.H. Kim, A coherent methodology for evalluation of a steam explosion load using TEXAS-V. Journal of Korean Nuclear Society, 2004. 36(6): p. 571-581.

[252] Speranskaya, E.I., 1970. The Bi2O3-WO3 System. Inorganic Materials (Engl.Transl.), 6, pp.127–129.

[253] Spencer, B.W., Gabor, J.D., Cassulo, J.C., "Effect of Boiling Regime on Melt Stream Breakup in Water." In: T.N. Veziroglu (Ed.), Particulate Phenomena and Multiphase Transport, vol. 3. Hemisphere. 1987.

[254] Spencer, B.W., Sienicki, J.J., McUmber, L.M., "Hydrodynamics and Heat Transfer Aspects of Corium/Water Interactions," EPRI NP-5127, Electric Power Research Institute, Palo Alto, CA. 1987.

[255] Spencer, B. W., Wang, K., Blomquist, C. A., Mcumber, L. M., and Schneider, J. P., "Fragmentation and Quench Behaviour of Corium Melt Streams in Water," NUREG/CR-6133, ANL-93/32, Argonne National Laboratory, 1994.

[256] Spencer, B.W., Wang K., Blomquist, C.A., McUmber, L.M., and Schneider, J.P., "Fragmentation and Quench Behaviour of Corium Melt Streams in Water," NUREG/CR-6133 ANL-93/32, Argonne National Laboratory. 1994.

[257] Stapelberg R. F. "Handbook of Reliability, Availability, Maintainability and Safety in Engineering Design," Springer, London, 2009, Chap. 3.

[258] Strålsäkerhetsmyndigheten, "APRI-7 Accident Phenomena of Risk Importance", En lägesrapport om forskningen inom svåra havarier under åren 2009-2011, rapportnummer 2012:12, ISSN:2000-0456, 2012.

[259] Sudha A.J, Murthy S. S., Kumaresan M., Lydia G., Nashine B. K. and Chellapandi P., "Experimental analysis of heaping and self-levelling phenomena in core debris using lead spheres," Experimental Thermal and Fluid Science, vol. 68, pp. 239-246, 2015.
[260] Tang, J., Modeling of the complete process of one-dimensional vapor explosions, University of Wisconsin-Madison, 1993.
[261] Takasuo, E., Kinnunen, T., Pankkoski, H., and Holmström, S., "Description of the COOLOCE test facility – Conical particle bed", VTT report VTT-R-08956-10 (2010).
[262] Takasuo, E., Kinnunen, T., Pankkoski, H., and Holmström, S., reports VTT-R-07097-11 and VTT-R-02427-11 on experiments on coolability of conical particle bed, VTT (2011).
[263] Takasuo, E., Kinnunen, T. Pankakoski, P.H., Holmström, S., "The COOLOCE particle bed coolability experiments with a cylindrical geometry: Test series 3–5," Research Report VTT-R-07099-11. Espoo, 2011. 27 p.
[264] Takasuo, E., Kinnunen, T. Pankakoski, P.H., Holmström, S., "The COOLOCE particle bed coolability experiments with a conical geometry: Test series 6–7," Research Report VTT-R-07097-11. Espoo, 2011. 26 p.
[265] Takasuo, E., Kinnunen, T., and Holmström, S., "COOLOCE particle bed coolability experiments with a cylindrical test bed: Test series 8–9," Research Report VTT-R-07224-12. Espoo, 2012. 44 p.
[266] Takasuo, E., Holmström, S., Kinnunen, T., and Pankakoski P.H., "The COOLOCE experiments investigating the dryout power in debris beds of heap-like and cylindrical geometries," Nuclear Engineering and Design 250 (2012), p. 687-700.
[267] Takasuo, E., "Debris Coolability Simulations with Different Particle Materials and Comparisons to COOLOCE Experiments," VTT report VTT0R-00257-13 (2013).
[268] Takasuo E., Kinnunen T., Lehtikuusi T. and Holmström S., "COOLOCE Debris Bed Coolability Experiments with an Agglomerate Simulant: Test Series 11," VTT Report VTT-R-03316-13 (2013).
[269] Taylor, G.I., "The dispersion of jets of metals at low melting point in water." In: Batchelor, G.K. (Ed.), The Scientific Paper of Sir Geoffrey Ingram Taylor, vol. 3., Cambridge University Press, 1963. 559 pp.
[270] Theofanous, T. G., "On Proper Formulation of Safety Goals and Assessment of Safety Margins for Rare and High-Consequence Hazards," Reliability Engineering and System Safety, 54, pp.243-257, (1996).
[271] Theofanous, T. G. and Dinh, T.-N., "Integration of multiphase Science and Technology with Risk Management in Nuclear Power reactors: Application of the Risk-Oriented Accident Analysis Methodology to the Economic, Simplified Boiling Water Reactor Design," Multiphase Science and Technology, V20(2), 2008, Pages 81-211.
[272] Theofanous, T. G., Liu, C., Additon, S., Angelini, S., Kymalainen O., and Salmassi, T., In-Vessel Coolability and Retention of a Core Melt, Nucl. Eng. Des. 169, 1–48, 1997.
[273] Theofanous, T. G., Liu, C., Additon, S., Angelini, S., Kymäläinen O., and Salmassi, T., In-Vessel Coolability and Retention of a Core Melt, DOE/ID-10460, Vols. 1-2, Oct. 1996.
[274] Theofanous, T.G. and Saito, M., An Assessment of Class-9 (Core-Melt) Accidents for PWR Dry-Containment Systems, Nuclear Engineering and Design, vol.66, pp.301-332., 1981.

[275] Theofanous, T. G., and Syri, S., "The Coolability Limits of a Reactor Pressure Vessel Lower Head," Nucl. Eng. Des. 169, 59–76, 1997.
[276] Torregrosa, C., Villanueva, W., Tran, C.-T., and Kudinov, P., "Coupled 3D Thermo-Mechanical Analysis of a Nordic BWR Vessel Failure and Timing," 15th International Topical Meeting on Nuclear Reactor Thermal Hydraulics, NURETH 15, May 12 to 17, 2013, Pisa, Italy, Paper 495.
[277] Torregrosa, M.C., "Coupled 3D Thermo-Mechanical Analysis of Nordic BWR Lower Head Failure in case of Core Melt Severe Accident" MSc Thesis, Royal Institute of Technology (KTH), 2013.
[278] Toulmin, S.: The Uses of Argument (1958; 2nd edn, 2003).
[279] Tran, C.T., and Dinh, T. N., "The Effective Convectivity Model for Simulation of Melt Pool Heat Transfer in a Light Water Reactor Pressure Vessel Lower Head. Part I: Physical Processes, Modeling and Model Implementation", pp.849-859, 2009. "Part II: Model Assessment and Application", Progress in Nuclear Energy, Vol.51, N.8, pp.860-871, 2009.
[280] Tran, C.-T. and Kudinov P., "Local Heat Transfer From The Corium Melt Pool to the BWR Vessel Wall," The 14th International Topical Meeting on Nuclear Reactor Thermal Hydraulics (NURETH-14), Toronto, Ontario, Canada, September 25-29, 2011.
[281] Tran, C.-T. and Kudinov P., "A Synergistic use of CFD, Experiments and Effective Convectivity Model to Reduce Uncertainty in BWR Severe Accident Analysis," CFD4NRS-3 Workshop, Bethesda, MD, USA, September 14-16, 2010.
[282] Tran, C.-T. and Kudinov, P., "The effective convectivity model for simulation of molten metal layer heat transfer in a boiling water reactor lower head," Proceedings of ICAPP '09, Tokyo, Japan, May 10-14, 2009 Paper 9114.
[283] Tran, C. T., Kudinov P., and Dinh, T. N. "An approach to numerical simulation and analysis of molten corium coolability in a BWR lower head," XCFD4NRS Workshop, Grenoble, France, September 10-12, 2008.
[284] Tran, C. T., Kudinov, P., and Dinh, T. N., "An approach to numerical simulation and analysis of molten corium coolability in a BWR lower head," Nuclear Engineering and Design, 240, 2010, 2148–2159.
[285] Tran, C.-T., Villanueva, W., and Kudinov, P., "A Study on the Integral Effect of Corium Material Properties on Melt Pool Heat Transfer in a Boiling Water Reactor," Proceedings of The 9th International Topical Meeting on Nuclear Thermal-Hydraulics, Operation and Safety (NUTHOS-9), Kaohsiung, Taiwan, September 9-13, , N9P0289, 2012.
[286] Tung, V.X. and Dhir, V.K., "A hydrodynamic model for two-phase flow through porous media," Int. J. Multiphase Flow Vol. 14, No. 1, pp. 47–65 (1988).
[287] Tyrpekl V., "Material effect in the nuclear fuel-coolant interaction: Structural analysis of steam explosion debris and solidification mechanism," PhD thesis, Strasbourg University, Charles University in Prague, 2012.
[288] U.S. Nuclear Regulatory Commission and Regulatory Guide 1.203, "Transient and Accident Analysis Methods," Revision 0, December 2005
[289] U.S.-Government-Accountability-Office, 2006. Nuclear Weapons NNSA Needs to Refine and More Effectively Manage Its New Approach for Assessing and Certifying Nuclear Weapons.

[290] U.S.-Nuclear-Regulatory-Commission, 1975. Reactor safety study. An assessment of accident risks in U. S. commercial nuclear power plants. WASH-1400.
[291] U.S.-Nuclear-Regulatory-Commission, 2014. Probabilistic risk assessment and severe accident evaluation for new reactors.
[292] Vandewoestyne B. and Cools R. Computational and Applied Mathematics 189, 1&2, 341-361 (2006).
[293] Villanueva, W., Tran, C.-T., Kudinov, P., "Coupled thermo-mechanical creep analysis for boiling water reactor pressure vessel lower head," Nuclear Engineering and Design, 249, 2012, 146-153.
[294] Villanueva, W., Tran C.-T., and Kudinov P., "Analysis of Instrumentation Guide Tube Failure in a BWR Lower Head," Proceedings of The 9th International Topical Meeting on Nuclear Thermal-Hydraulics, Operation and Safety (NUTHOS-9), Kaohsiung, Taiwan, September 9-13, , N9P0268, 2012.
[295] Villanueva, W., Tran, C.-T., and Kudinov, P., "Effect of CRGT Cooling on Modes of Global Vessel Failure of a BWR Lower Head," Proceedings of the 20th International Conference on Nuclear Engineering (ICONE-20), Anaheim, CA, USA, July 30 - August 3, Paper 54955, 2012.
[296] Villanueva W., Tran C.-T., and Kudinov P., "A Computational Study On Instrumentation Guide Tube Failure During a Severe Accident in Boiling Water Reactors," The 14th International Topical Meeting on Nuclear Reactor Thermal Hydraulics (NURETH-14), Toronto, Ontario, Canada, September 25-29, 2011.
[297] Villanueva W., Tran C.-T., and Kudinov P., "Assessment with Coupled Thermo-Mechanical Creep Analysis of Combined CRGT and External Vessel Cooling Efficiency for a BWR," The 14th International Topical Meeting on Nuclear Reactor Thermal Hydraulics (NURETH-14), Toronto, Ontario, Canada, September 25-29, 2011.
[298] Villanueva W., Tran C.-T. and Kudinov P., "Coupled Thermo-Mechanical Creep Analysis for Boiling Water Reactor Pressure Vessel Lower Head" The 8th International Topical Meeting on Nuclear Thermal-Hydraulics, Operation and Safety (NUTHOS-8), Shanghai, China, October 10-14, N8P0248, 2010.
[299] Vorobyov, Y. and Dinh, T.N., A Genetic Algorithm-Based Approach to Dynamic PRA Simulation. in ANS PSA 2008 Topical Meeting - Challenges to PSA during the nuclear renaissance. 2008. Knoxville, Tennessee: American Nuclear Society, LaGrange Park, IL.
[300] Vorobyev Y., Kudinov P., Development and Application of a Genetic Algorithm Based Dynamic PRA Methodology to Plant Vulnerability Search, ANS PSA 2011 International Topical Meeting on Probabilistic Safety Assessment and Analysis, Wilmington, NC, March 13-17, 2011, on CD-ROM, American Nuclear Society, LaGrange Park, IL (2011).
[301] Vorobyev Yu.B., Kudinov P., Jeltsov M., Kööp K., Nhat T.V.K., "Applica-tion of information technologies (genetic algorithms, neural networks, parallel calculations) in safety analysis of Nuclear Power Plants," Proceedings of the Institute for System Programming of RAS, 26(2), pp.137-158, 2014.
[302] Wang, S.K., Blomquist, C.A., Spencer, B.W., McUmber, L.M., Schneider, Y.P., "Experimental Study of the Fragmentation and Quench Behavior of Corium Melts in Water, ANS Proceedings of the 25th National Heat Transfer Conference, HTC3, Houston, TX, 1988. pp. 120–153.

[303] Welty J. R.,Wicks C. E., Wilson R. E., Rorrer G. L., Fundamentals of Momentum, Heat and Mass transfer, 5th edition, John Wiley and Sons, 2007.

[304] WENRA Report on Safety of new NPP designs, Published by Western European Nuclear Regulators' Association (WENRA) Reactor Harmonisation Working Group (RHWG), Aug. 28, 2013. http://www.wenra.org/media/filer_public/2013/08/23/rhwg_safety_of_new_npp_designs.pdf

[305] Wilson, S. McDermid, J. Fenelon, P. and Kirkham, P. "No More Spineless safety Cases: A Structured Method and Comprehensive Tool Support for the Production of Safety Cases," presented at the 2nd International Conference on Control and Instrumentation in Nuclear Installations (INEC'95), Cambridge, UK 1995.

[306] Xiao Yan Liu, E. Specht, J. Mellmann, "Experimental study of the lower and upper angles of repose of granular materials in rotating drums," Powder Technology, Volume 154, Issues 2–3, 6 July 2005, Pages 125-131.

[307] Yakush S. E., Konovalenko A., Basso S. and Kudinov P., "Effect of Particle Spreading on Coolability of Ex-Vessel Debris Bed" The 16th International Topical Meeting on Nuclear Reactor Thermal Hydraulics (NURETH-16), Chicago, IL, USA, August 30-September 4, paper 14112, 13p, 2015.

[308] S. E. Yakush, A. Konovalenko, S. Basso, P. Kudinov, " Validation of DECOSIM Code Against Experiments on Particle Spreading by Two-Phase Flows in Water Pool", NUTHOS-11: The 11th International Topical Meeting on Nuclear Reactor Thermal Hydraulics, Operation and Safety, Gyeongju, Korea, October 9-13, 2016.

[309] Yakush, S, Kudinov, P. "Effects of Water Pool Subcooling on the Debris Bed Spreading by Coolant Flow," Proceedings of the 11th International Conference on Advanced Nuclear Power Plants (ICAPP 2011), Nice, France, May 2011, paper 11416, 14 p. 2011.

[310] Yakush S. and Kudinov P., "A Model for Prediction of Maximum Post-Dryout Temperature in Decay-Heated Debris Bed," Proceedings of the 2014 22nd International Conference on Nuclear Engineering, ICONE22, July 7-11, Prague, Czech Republic, ICONE22-31214. 2014.

[311] Yakush S. E., and Kudinov P., "Effect of Melt Agglomeration on Coolability of a Debris Bed". NUTHOS-11:The 11th International Topical Meeting on Nuclear Reactor Thermal Hydraulics, Operation and Safety, Gyeongju, Korea, October 9-13, 2016. N11A0590.

[312] Yakush S. E., and Kudinov P., "Melt Agglomeration Influence on Ex-vessel Debris Bed Coolability" The 17th International Topical Meeting on Nuclear Reactor Thermal Hydraulics (NURETH-17), Paper: 21455, Qujiang Int'l Conference Center, Xi'an, China，September 3-8, 2017.

[313] Yakush S., Kudinov P., "In-vessel debris bed coolability and implications for vessel failure mode" NUTHOS-11:The 11th International Topical Meeting on Nuclear Reactor Thermal Hydraulics, Operation and Safety, Gyeongju, Korea, October 9-13, N11P0532, 2016.

[314] Yakush, S. E., Kudinov, P., Villanueva, W., and Basso, S., "In-Vessel Debris Bed Coolability and its Influence on the Vessel Failure," 15th International Topical Meeting on Nuclear Reactor Thermal Hydraulics, NURETH 15, May 12 to 17, 2013, Pisa, Italy, Paper 464.

[315] Yakush, S. and Kudinov, P., "Transient Phenomena of Ex-vessel Debris Bed Formation in a LWR Severe Accident," ANS Transactions, 2009, paper 210830.
[316] Yakush, S. and Kudinov, P., "Simulation of Ex-Vessel Debris Bed Formation and Coolability in a LWR Severe Accident," Proceedings of ISAMM-2009, Böttstein, Switzerland, October 26 - 28, 2009.
[317] Yakush, S., Kudinov, P., and Dinh, T.-N., "Multiscale Simulations of Self-organization Phenomena in the Formation and Coolability of Corium Debris Bed," Proc. The 13th International Topical Meeting on Nuclear Reactor Thermal Hydraulics (NURETH-13), September 27-October 2, 2009. Kanazawa City, Ishikawa Prefecture, Japan, Paper N13P1143.
[318] Yakush, S., Kudinov, P., and Dinh, T.-N., "Modeling of Two-Phase Natural Convection Flows in a Water Pool with a Decay-Heated Debris Bed," Proc. ICAPP'08, Anaheim, CA USA, June 8–12, 2008, paper 8409.
[319] Yakush, S., Kudinov, P., and Lubchenko, N., "Coolability of heat-releasing debris bed. Part 1: Sensitivity analysis and model calibration," Annals of Nuclear Energy, 52, February 2013, pp. 59-71, 2013
[320] Yakush, S., Kudinov, P., and Lubchenko, N., "Coolability of heat-releasing debris bed. Part 2: Uncertainty of dryout heat flux," Annals of Nuclear Energy, 52, February 2013, pp. 72-79.
[321] Yakush, S., Lubchenko, N., and Kudinov, P., "Risk-Informed Approach to Debris Bed Coolability Issue," Proceedings of the 20th International Conference on Nuclear Engineering (ICONE-20), Anaheim, CA, USA, July 30 - August 3, Paper 55186, 2012.
[322] Yakush S. E., Lubchenko, N.T., and Kudinov P., "Surrogate Models for Debris Bed Dryout," 15th International Topical Meeting on Nuclear Reactor Thermal Hydraulics, NURETH 15, May 12 to 17, 2013, Pisa, Italy, Paper 278.
[323] Yakush, S. E., Lubchenko, N. T., and Kudinov, P., "Risk and Uncertainty Quantification in Debris Bed Coolability," 15th International Topical Meeting on Nuclear Reactor Thermal Hydraulics, NURETH 15, May 12 to 17, 2013, Pisa, Italy, Paper 283.
[324] Yakush S. E., Villanueva W., Basso S. and Kudinov P., "Simulation of In-vessel Debris Bed Coolability and Remelting," The 10th International Topical Meeting on Nuclear Thermal-Hydraulics, Operation and Safety (NUTHOS-10), Okinawa, Japan, December 14-18, 2014, Paper 1281, 2014.
[325] Yang, Wen-Ching, "Handbook of Fluidization and Fluid-Particle Systems", Taylor & Francis Group, ISBN 9780824702595, Chapter 26, p.712, 2003.
[326] Zhang, B., Harada., T., Hirahara, D., Matsumoto, T., Morita., K., Fukuda, K., Yamano, H., Suzuki, T., Tobita, Y., "Self-Leveling Onset Criteria in Debris Beds", *J. Nuclear Science and Technology,* **47,** 384-395, 2010.
[327] Zhang B., Harada T., Hirahara D., Matsumoto T., Morita K., Fukuda K., Yamano H., Suzuki T., Tobita Y. "Experimental investigation on self-leveling behavior in debris beds", Nuclear Engineering and Design, 241(1), pp. 366-377, (2011).
[328] Zhang J.-P., Epstein N., Grace J. R., "Minimum fluidization velocities for gas-liquid-solid three phase systems", Powder Technology, 100(2-3), pp. 113-1118, (1998).

[329] Zhang, B., Harada, T., Hirahara, D., Matsumoto, T., Morita, K., Fukuda, K., Yamano, H., Suzuki, T., Tobita, Y., 2010. Self-Leveling Onset Criteria in Debris Beds. J. Nucl. Sci. Technol. 47, 384–395. doi:10.1080/18811248.2010.9711969

[330] Zio, E., Pedroni, N., 2013. Literature review of methods for representing uncertainty. Toulouse, Franc.

[331] M. Belhadj, M. Hassan, and T. Aldemir, On the need for dynamic methodologies in risk and reliability studies. Reliability Engineering and System Safety, 1992. 38: p. pp.219-236.

[332] T. Aldemir, et al., NUREG/CR- 6942, Dynamic Reliability Modeling of Digital Instrumentation and Control Systems for Nuclear Reactor Probabilistic Risk Assessments. 2007b, US Nuclear Regulatory Commission, Washington, DC.

[333] C.D. Fletcher, and R.R. Schultz, RELAP5/MOD3 User Guidelines. NUREG/CR-5535. 1992, US Nuclear Regulatory Commission, Washington, DC.

[334] R.O. Gauntt, et al., MELCOR Computer Code Manuals. NUREG/CR-6119/SAND 2005-5713. 2005, US Nuclear Regulatory Commission, Washington, DC.

[335] CEA/NERA, Working Group on Operating Experience; "Status of OECD/NEA Country Regulatory Responses to the Forsmark-1 Event of 25 July 2006 and NEA/CSNI DiDELSYS Task Group Report Recommendations" (2010)

[336] VTT Research Report VTT-R-08589-12 Proceedings of the IDPSA-2012 Integrated Deterministic-Probabilistic Safety Analysis Workshop. November 2012.

[337] Nilsson, L. (2006). Development of an Input Model to MELCOR 1.8.5 for Oskarshamn 3 BWR. SKI Report 2007:05.

[338] L.L. Humphries, B.A. Beeny, F. Gelbard, D.L. Louie, J. Phillips, "MELCOR Computer Code Manuals", Vol. 1: Primer and Users' Guide Version 2.2.9541, SAND2017-0455 O, (2017).

[339] L.L. Humphries, B.A. Beeny, F. Gelbard, D.L. Louie, J. Phillips, "MELCOR Computer Code Manuals", Vol. 2: Reference Manual Version 2.2.9541, SAND2017-0876 O, (2017).

[340] Imtiaz K. Madni, Evaluation of MELCOR improvements: Peach Bottom Station Blackout Analyses, BNL-NUREG-49201. (1994).

[341] A. Tuvelid, "Comparison of MELCOR and MAAP calculations of core relocation phenomena in Nordic BWR's" – Master Thesis, KTH, Stockholm, Sweden, (2016).

[342] Kyle Ross, Jesse Phillips, Randall O. Gauntt, Kenneth C. Wagner, MELCOR Best Practices as Applied in the State-of-the-Art Reactor Consequence Analyses (SOARCA) Project, NUREG/CR-7008, (2014).

[343] Müller, C. Review of Debris Bed Cooling in TMI-2 Accident. Garching: GRS Forschungsinstitute, (2006).

[344] Makoto Akinaga, Hirohide Oikawa, Ryoichi Hamazaki, Ken-ichi Sato, Takashu Uemura. Probablistic Evaluation of In-vessel retention capability applying phenomenological event tree. (2004).

[345] R.O Gauntt, J. C. (2005). MELCOR Computer Code Manual Vol.2 Reference Manual Version 1.8.6. Albuquerque: Sandia National Laboratories.

[346] R.O Gauntt, J. C. (2005). MELCOR Computer Code Manuals Vol. 1 Primer and User's Guide Version 1.8.6 . Albuquerque: Sandia National Laboratories.

[347] "Fukushima Daiichi Unit 1 Accident Progression Uncertainty Analysis and Implications for Decommissioning of Fukushima Reactors – Volume I", Sandia National Laboratories, SAND2016-0232, (2016).
[348] Butkova, Y., Bäckström, O., Hermanns, H, Krcal, P., Wang, W. "Dynamic Features in Large PSA Studies", ESREL 2016.
[349] Brown, Douglas. "Tracker video analysis and modeling tool." October 3 (2009): 2013.

[350] Nield, D.A., Bejan, A., "Convection in Porous Media," Springer, 4th edition, 2013.
[351] Zadrazil, A., Stepanek, F., Matar, O. K. "Droplet spreading, imbibition and solidification on porous media," J. Fluid Mech. 2006, 562, pp. 1–33.
[352] Liu, Y., Zheng, Z., Stone, H. A. "The influence of capillary effects on the drainage of a viscous gravity current into a deep porous medium," J. Fluid Mech. 2017, 817, pp. 514-559.
[353] B. Efron and R. Tibshirani, "An Introduction to the Bootstrap," New york: Chapman and Hall, 1993.
[354] N. Pedroni, E. Zio and G. Apostolakis, "Comparison of bootstrapped artificial neural networks and quadratic response surfaces for the estimation of the functional failure probability of a thermal-hydraulic passive system," Reliability Engineering & System Safety, vol. 95, no. 4, p. 386–395, 2010.
[355] E. Zio, "A study of the bootstrap method for estimating the accuracy of artificial neural networks in predicting nuclear transient processes," IEEE Transactions on Nuclear Science, vol. 53, no. 3, p. 1460–78, 2006.
[356] E. Ferrario, N. Pedroni, E. Zio and F. Lopez-Caballero, "Bootstrapped Artificial Neural Networks for the seismic analysis of structural systems," Structural Safety, vol. 67, pp. 70-84, 2017.
[357] Z.-H. Zhou, J. Wu and W. Tang, "Ensembling neural networks: Many could be better than all," Artificial Intelligence, vol. 137, p. 239–263, 2002.
[358] Z. H. Zhou, "Ensemble methods: foundations and algorithms," CRC press, 2012.
[359] T. G. Dietterich, "An experimental comparison of three methods for constructing ensembles of decision trees: Bagging, boosting, and randomization," Machine Learning, vol. 40, pp. 139-157, 2000.

[360] Magallon, D. (2012). SERENA Programme Reactor exercise: Synthesis of calculations: 20.

[361] Hansson, R. C., Park, H.S., Dinh, T.N., "Dynamics and preconditioning in a single droplet vapor explosion", Nuclear Technology, Vol.167, pp.223-234, 2008.
[362] Hansson, R. C., Park, H.S., Dinh, T.N., "Simultaneous high speed digital cinematographic and X-ray radiographic imaging of a multi-fluid interaction with rapid phase changes", Experimental Thermal and Fluid Science, Vol.33, pp.754-763, 2009.
[363] Hansson, R.C., "Triggering and energetics of a single drop vapor explosion: The role of entrapped nob-condensable gases", Nuclear Engineering and Technology, Vol.41, pp.1215-1222, 2009.

[364] Hansson, R. C., Dinh, T. N., Manickam, L., “A study of the effect of binary oxide materials in a single droplet vapor explosion triggering”, Nuclear Engineering and Design, Vol 264, pp. 168-175, 2013.
[365] Huhtiniemi, I., Magallon, D., Hohmann, H., “Results of recent KROTOS FCI tests: alumina versus corium melts”, Nuclear Engineering and Design, 189, 379-389, 1999.
[366] Manickam, L., Thakre, S., Ma, W., Bechta, S., “Simultaneous visual acquisition of melt jet breakup in water by high speed videography and radiography”, Proc. of NUTHOS-10, Okinawa, Japan, December 14-18, 2014.
[367] Manickam, L., Thakre, S., Ma, W., “An experimental study on void generation around a hot metal particle quenched into water pool”, Proc. of NURETH-16, Chicago, U.S.A, Aug 30 –Sep4, 2015.
[368] Manickam, L., Bechta, S., Ma, W., “On the fragmentation characteristics of melt jets quenched in water”, International Journal of Multiphase Flow, Vol 91: pp. 262-275, 2017.
[369] Nelson, L.S., Duda, P.M., “Steam explosion experiments with single drops of iron oxide: PART II: parametric studies”, NUREG CR-2718, April, 1985.
[370] Trypekl, V., Piluso, P., S. Bakardijeva, S., Niznansky, D., Rehspringer, J., Bezdicka, P., Dugne, O., “Prototypic corium oxidation and hydrogen release during the Fuel–Coolant Interaction”, Annals of Nuclear Energy, 75: 210-218, 2015.
[371] Zambaux, J.A., Manickam, L., Meignen, R., Ma, W., Bechta, S., Picchi, S., “Study on thermal fragmentation characteristics of a superheated alumina droplet”, Proc. of ERMSAR-17, Warsaw, Poland, May 16-18, 2017.
[372] Severe Accident Management Guidance Technical Basis Report, Volume 1: Candidate High-Level Actions and Their Effects. EPRI, Palo Alto, CA: 2012. 1025295
[373] Larry L. Humphries, “Quicklook Overview of Modell Changes in MELCOR 2.2: Rev 6342 to Rev 9496” SANDIA REPORT SAND2017-5599, (2017)
[374] Sergey Galushin, Pavel Kudinov, “Sensitivity analysis of debris properties in lower plenum of a Nordic BWR”, Nuclear Engineering and Design, Volume 332, June 2018, Pages 374-382, ISSN 0029-5493, https://doi.org/10.1016/j.nucengdes.2018.03.029. (2018).
[375] M. Pilch and W. W. Tarbell, High Pressure Ejection of Melt from a Reactor Pressure Vessel—the Discharge Phase, NUREG/CR-4383, SAND85-0012 (September 1985).
[376] W. Hering and K. Muller, “Modelling of Eutectic Interactions in KESS-III (Module EUTECT),” International CORA Workshop 1992, Karlsruhe, FRG, October 5-8, 1992.
[377] Galushin S., Kudnov P., “Analysis of the Effect of Severe Accident Scenario on the Vessel Lower Head Failure in Nordic BWR using MELCOR code”, Probabilistic Safety Assessment and Management PSAM 14, September 2018, Los Angeles, CA.
[378] Galushin S., Kudnov P., “Sensitivity Analysis of the Vessel Lower Head Failure in Nordic BWR using MELCOR Code”, Probabilistic Safety Assessment and Management PSAM 14, September 2018, Los Angeles, CA.

Bibliographic Data Sheet **NKS-410**

Title	Scenarios and Phenomena Affecting Risk of Containment Failure and Release Characteristics
Author(s)	Pavel Kudinov[1], Sergey Galushin[1], Dmitry Grishchenko[1], Sergey Yakush[1] Anders Riber Marklund[2], Ola Bäckström[2]
Affiliation(s)	[1]Division of Nuclear Power Safety (NPS), Royal Institute of Technology (KTH); [2]Lloyd's Register Consulting – Energy AB
ISBN	978-87-7893-499-4
Date	October 2018
Project	NKS-R / SPARC
No. of pages	238
No. of tables	27
No. of illustrations	153
No. of references	378
Abstract max. 2000 characters	The report summarizes results of the NKS-SPARC project. The ROAAM+ framework addresses accident progression from initial plant damage states to ex-vessel melt-coolant interactions and debris coolability. Detailed mechanistic full models (FM) have been developed. A set of computationally efficient surrogate models (SM) has been developed using the databases of FM solutions. Uncertainty in the containment failure probability has been quantified according. An approach has been developed and demonstrated for using obtained in ROPAAM+ data on the failure probability for different combinations of scenario parameters in a large scale PSA model. Results of the pilot study show clear benefits for PSA improvement in more realistic understanding and modeling of the risks. Main findings of the analysis of effectiveness of SAM strategy in Nordic BWRs using ROAAM+ framework and main results are presented using failure domain maps. The project outcomes enhance completeness and consistency of safety analysis and modelling methods for level 2 PSA; presentation of results in level 2 PSA, and related risk criteria.
Key words	ROAAM+, IDPSA, PSA, DSA, BWR, Severe accident, MELCOR, core degradation, steam explosion, debris coolability.

Available on request from the NKS Secretariat, P.O.Box 49, DK-4000 Roskilde, Denmark.
Phone (+45) 4677 4041, e-mail nks@nks.org, www.nks.org